AD NUMBER

AD803781

LIMITATION CHANGES

TO:

Approved for public release; distribution is unlimited.

FROM:

**Distribution authorized to U.S. Gov't. agencies and their contractors;
Administrative/Operational Use; AUG 1966. Other requests shall be referred to Air Force Flight Dynamics Lab., Wright-Patterson AFB, OH 45433.**

AUTHORITY

AFFDL ltr 25 Apr 1972

AFFDL-TR-66-122

INVESTIGATION OF BOUNDARY LAYER TRANSITION IN HYPERSONIC FLOW AT ANGLE OF ATTACK

A. L. Nagel
R. T. Savage
R. Wanner
Appendix by R. W. Blank

TECHNICAL REPORT AFFDL-TR-66-122

August 1966

Air Force Flight Dynamics Laboratory
Research and Technology Division
Air Force Systems Command
Wright-Patterson Air Force Base, Ohio

NOTICES

When government drawings, specifications, or other data are used for any purpose other than in connection with a definitely related government procurement operation, the United States government thereby incurs no responsibility nor any obligation whatsoever; and the fact that the government may have formulated, furnished, or in any way supplied the said drawings, specifications, or other data, is not to be regarded by implication or otherwise as in any manner licensing the holder or any other person or corporation, or conveying any rights or permission to manufacture, use, or sell any patented invention that may in any way be related thereto.

Copies of this report should not be returned to the Research and Technology Division unless return is required by security considerations, contractual obligations, or notice on a specific document.

BLANK PAGE

INVESTIGATION OF BOUNDARY LAYER TRANSITION IN HYPERSONIC FLOW AT ANGLE OF ATTACK

A. L. Nagel
R. T. Savage
R. Wanner
Appendix by R. W. Blank

FOREWORD

This report was prepared by the Aerospace Group of The Boeing Company, Seattle, Washington, under USAF Contract AF33(615)-2011 through S.A. No. 2. The contract was initiated under Project 1366, Tasks 136606 and 136615, BPSN 4 (6199-62405334-136606-136615). The work was administered under the direction of the Air Force Flight Dynamics Laboratory, Research and Technology Division, Wright-Patterson Air Force Base, Ohio. Messrs. V. Dahlem III, E.D. McElderry, and R. Jenson, of the Gas Dynamics Branch acted as Air Force Project Engineers.

This report covers work conducted between July 1964 and June 1966.

The contributions of the following are acknowledged: ARO, Inc. (Von Karman Facility, Hypersonic Branch); Messrs. J.C. Sivells and H.T. Wood for supervisory activities, R.L. Palko for project engineer and coordination activities in connection with the wind-tunnel test program; and Barbara J. Barrett for exceptional effort, accuracy, and efficiency in calculation and report preparation.

The manuscript was released by the authors for publication as an RTD technical report in September 1966.

This technical report has been reviewed and is approved.

For PHILLIP P. ANTONATOS
Chief, Flight Mechanics Division
Air Force Flight Dynamics Laboratory

ABSTRACT

An analytical and experimental investigation has been made of boundary layer transition at angle of attack in hypersonic flow. A new method of calculating laminar flow stability has been developed that is more general than previous methods. The method employs the timewise integration of perturbation equations derived from the complete Navier-Stokes equations for two-dimensional flow of a compressible fluid with variable transport properties. The present calculations are for perturbations about a known steady flow. The perturbations are assumed to be sinusoidal in the streamwise direction, but no restriction is known that would prevent the streamwise wave form from being arbitrary, as are the vertical distributions and the time variations. The sinusoidal wave assumption greatly reduces the amount of computer time required and simplifies the interpretation of the results. Nonlinear terms are easily retained with the present method, but nonlinear calculations are not physically correct when perturbations are required to be sinusoidal. For this reason nonlinear terms were deleted for all calculations presented.

The experimental program was conducted in Arnold Center tunnels B and C at Mach numbers of 6, 8, and 10. The models included blunt and sharp flat plates and a 75-degree delta wing with sharp leading edges. The results are somewhat questionable due to probe interferences and leakages that are now known to have occurred during the tests. However, the results are self-consistent and consistent with the results of previous investigations. Natural transition data for the sharp flat plate at angles of attack up to 15 degrees agree with previous results for zero angle of attack when compared on the basis of local flow properties. Transition Reynolds numbers on the sharp flat plate were found to increase as the 0.4 power of the unit Reynolds number, but the effect on the sharp delta wing centerline data was much smaller. The independence of this effect of angle of attack, and the dependence on the model geometry suggest that the unit Reynolds number trend is not produced by model or wind tunnel disturbances, but is an authentic fluid mechanical effect that will occur in free flight as well. No explanation of the unit Reynolds number effect was found in the analytic studies, however.

When corrected to a common unit Reynolds number, the transition Reynolds number was found to increase exponentially with Mach number, for Mach numbers from 4 to 10.

Attempts were made to trip the boundary layer by mass injection to verify the analytic prediction that below a certain critical Reynolds number, the boundary layer could not be tripped. These attempts were successful to the extent that tripping did not occur below, nor even near the calculated critical Reynolds numbers. However, other tripping techniques should be investigated before any conclusions are formed.

CONTENTS

ILLUSTRATIONS

TABLES

SYMBOLS

A	Area
a	Speed of sound, $a = \sqrt{\gamma\ RT}$
c	Specific heat of model skin
c_p	Specific heat at constant pressure
c_v	Specific heat at constant volume
C_f	Skin friction coefficient, $\frac{2\ \tau_w}{(\rho\ u^2)_\infty}$
C_P	Pressure coefficient, $\frac{2\ (P - P_\infty)}{(\rho\ u^2)_\infty}$
D	Leading-edge diameter; nose diameter
e	Base of natural logarithms, 2.71828 ....
k	Thermal conductivity
L	Length
$\dot{m}_j$	Mass injection rate
M	Mach number
M_j	Nondimensional mass injection rate, $\frac{(\dot{m}/A)_j}{(\rho\ u)_\infty}$
n	Time level; exponent
$N_{Re,\infty}$	Free-stream Reynolds number
$N_{Re,e}$	Reynolds number based on boundary layer edge conditions
$N_{Re,Tr}$	Transition Reynolds number
P	Pressure; general polynomial
$\dot{q}$	Heating rate, Btu/ft^2-sec
Q	Any flow property (see Equation 2-4)
r	Recovery factor
R	Gas constant in equation of state; radius
t	Time
T	Temperature
u	Velocity component in x-direction
$\|u'\|$	Amplitude (see Equation 2-44)

SYMBOLS (Continued)

v	Velocity component in y-direction
$\|\|v'\|\|$	Amplitude (see Equation 2-44)
w	Velocity component in z-direction
x, y, z	Cartesian coordinates
x_T	Distance from leading edge to boundary layer trip
$\Delta x, \Delta y, \Delta t$	Increments in x, y, and t
α	Angle of attack; wave number, $\frac{2\pi}{\lambda}$
γ	Ratio of specific heats, $\frac{c_p}{c_v}$
δ	Boundary layer thickness
δ^*	Boundary layer displacement thickness
θ	Boundary layer momentum thickness
Λ	Sweep angle
λ	Wavelength
μ	Absolute viscosity
ρ	Density
τ	Dimensionless time, $\frac{\bar{u}t}{\delta^*}$; shear stress

Subscripts

adj	Adjusted to a unit Reynolds number of 2×10^5
aw	Adiabatic wall
CL	Centerline
D	Based on diameter
e	Boundary layer edge
j	Injection jet
L	Laminar; "left hand" (i.e., at $x = x_0$), see R (subscript)
LE	Leading edge
m	Mean; measured
match	Inner boundary of numerical "wave trap" (see Equation 2-51)
max	Maximum, outer boundary of y
min	Minimum
n	Normal

o	Wind tunnel or plenum total condition; initial value
p	Probe location
R	"Right hand" (i.e., at $x = x_o + \frac{\lambda}{4}$), see L (subscript)
T	Turbulent; pitot pressure
Tr	Transitional
v	Viscous
w	Wall
x_1	Evaluated at x_1
1	Evaluated in front of shock
2	Evaluated behind shock
∞	Free-stream condition

Superscripts

n	Exponent; time level (see Equation 2-17)
*	Aft of boundary layer trip
'	Prime — fluctuating component (see Equation 2-4); y derivatives
—	Bar — steady flow component (see Equation 2-4); averaged value
.	Dot — time derivative

BLANK PAGE

I

INTRODUCTION

It has long been recognized that fluid flows can exist in at least two distinct states. The first state is characterized by smooth, well-behaved streamlines with an absence of mixing; the term "laminar" derived from the latin word for layers is used to describe this type of flow. The second state is known as turbulent flow and is characterized by apparently random fluctuations of velocity, both in magnitude and direction. Although the fluctuations are generally much smaller than the average velocity of the flow, they lead to important changes in overall flow properties. For example, the amount of power required to transport fluid through a given pipe at a given rate may be an order of magnitude greater if the flow becomes turbulent than would be required if laminar flow could be retained. Experimentally, it is found that turbulent flow, if it exists at all, occurs downstream of the laminar region, which is now believed to always exist at the most upstream point in the flow field. The process wherein the laminar flow becomes turbulent is known as flow transition and has been observed in pipes, free jets, wakes, and boundary layers.

Boundary layer transition has taken on increased importance with the advent of hypersonic flight. As at lower speeds, transition can have a significant detrimental effect on flight performance by increasing friction drag. However, even more important are the large increases in aerodynamic heating rates that can occur as a result of boundary layer transition at hypersonic speeds. Associated with the increased heating are more severe requirements on materials, which often increase weights. It may be found that turbulent heating rates exceed values that can be tolerated by any known materials regardless of their weight, thus necessitating configuration compromises as well as weight penalties.

EARLY INVESTIGATIONS

Although the phenomena of flow transition and turbulence have undoubtedly been observed since earliest times, the first paper reporting a systematic investigation was apparently published by Osbourne Reynolds in 1883 (Ref. 1). Reynolds noted that traces of dye introduced into a low-velocity stream formed a well defined and continuous filament throughout the entire length of a pipe. However, when the velocity of the flow or the diameter of the pipe was increased, the filament persisted only for a short distance and thereafter became diffused across the entire pipe. This behavior indicated that the flow was not always parallel to the wall, but contained transverse velocity components as well. By examination of the flow-conservation equations, Reynolds identified the dimensionless grouping $(\rho uD/\mu)$ as being the critical parameter governing the onset of the diffusive type of flow, which we know today as turbulent flow. In honor of Reynolds' pioneering work, that dimensionless grouping has now become known as the Reynolds number.

Further investigation by Reynolds revealed that, while the Reynolds number was important in determining the type of flow, it was not the only factor. He found that, if the reservoir for his flow system were allowed to settle for long periods of time prior to the experiment, the length of laminar run was increased. He also found that the length of laminar flow could be further increased by carefully shaping the inlet to the pipe. As a result of these observations, Reynolds was led to surmise that, perhaps in the total absence of disturbing influences, laminar flow could be maintained infinitely far, but that the flow was unstable above a certain critical value of the Reynolds number. Above that critical value, small disturbances—once initiated—would derive energy from the main stream of the flow and increase.

Experimentally, it has since been found that, in pipe flows, the turbulent state cannot be produced below a Reynolds number of about 2000, whereas if every effort is made to avoid initial disturbances, laminar flow can be maintained to Reynolds numbers at least on the order of 100,000. There is every reason to believe that laminar flow can be maintained to even higher Reynolds numbers if more careful experimental techniques are used. These observations, together with the results obtained from flow stability theory, substantiate virtually beyond a doubt the correctness of Reynolds' original suggestion, although it was many years before convincing proof could be demonstrated.

It may be seen from the above discussion that experimental observations of transitional and turbulent flows are by no means new. Theoretical investigations also have a long history, but to date only modest success has been achieved. It is still not possible to calculate turbulent flow properties without incorporating empirical constants, and even then the calculations must neglect many effects known to exist.

The process of transition itself is little better understood. However, considerable progress has been made in analyzing initial phases of the breakdown of laminar flow, a phenomenon that is more easily treated. As long as the analysis is confined to small deviations from a basic laminar flow the governing differential equations are linear, and while their solution is not easy it is at least possible. In obtaining these solutions the disturbances are assumed to be sinusoidal traveling waves that may be either amplified or damped as a function of time. If the disturbances are found to be amplified, the flow is said to be unstable.

The results of the stability theory, first obtained by Tollmien in 1929 (Ref. 2), were surprising because they indicated that boundary layer flow is unstable with respect to a given wavelength of disturbance only in a narrow range of Reynolds numbers. It had been expected that all disturbance would be damped at very low Reynolds numbers; the theory indicated that damping would occur at high Reynolds numbers as well.

Of course many attempts were made to verify the analytic predictions of Tollmien, but it was not until 1943 that Schubauer and Scramstad (Ref. 3) were able to obtain experimental verification, and then only after a new low-turbulence wind tunnel was specially constructed for that specific purpose. The results obtained by Schubauer and Scramstad brilliantly confirmed the theoretical predictions, not only as to the existence of a lower critical Reynolds number, but also as to many of the details of the flow. The experiments showed that, for each specific wavelength, there existed only a small range of Reynolds numbers within which the disturbances would be amplified, confirming the theoretical predictions. The experimental minimum and maximum critical Reynolds numbers agreed well with the predicted values.

The theory also indicates that the disturbance must have a particular distribution through the boundary layer. The Schubauer and Scramstad experiments showed that, when a periodic disturbance was introduced near the wall by use of a vibrating ribbon, a disturbance profile of the type predicted by the theory did in fact occur.

LATER INVESTIGATIONS

Experimental and theoretical studies have progressed more recently into supersonic and hypersonic flows. As might be expected, both the experiments and the analyses have become more difficult. The stability theory has progressed along the lines of the incompressible theory, but in high-speed flows it is necessary to simultaneously solve four differential equations rather than the single equation that describes incompressible flow. A more detailed discussion of stability theory will be given in the next section.

Experimental investigations have been carried out at supersonic speeds by Low (Ref. 4), Moeckel (Ref. 5), Brinich (Refs. 6 through 10), Rogers (Ref. 11), and many others. Hypersonic investigations have been made by James (Ref. 12), Potter and Whitfield (Ref. 13 and 14), Deem, Erickson, and Murphy (Ref. 15), Korkegi (Ref. 16), and others. Of these, the data by James are particularly interesting because they are taken on small free-flying models rather than on wind-tunnel models, unlike most of the available data.

Although these data have established some general trends, there are also some questions raised that have not been answered. For example, one of the most consistent trends observed in the experimental results is an increase in transition Reynolds number with unit Reynolds number. The unit Reynolds number effect is particularly interesting because it involves a dimensional quantity, and as such no effect is to be expected. Rather, it would seem that the unit Reynolds number should be nondimensionalized by multiplication by some appropriate length factor, but there seems to be no suitable characteristic length not already reflected in some other test parameter. There is, however, little doubt that the unit Reynolds number effect does exist because it appears in the data from many sources.

PRESENT INVESTIGATION

The present investigation had two objectives:

1) Develop a new method of calculating flow stability based on the time integration of the Navier-Stokes equations.

2) Obtain additional experimental data that could be compared with the results of the analytic method.

The ultimately desired analytic result is a rational method of predicting transition in flight. It is to be expected that such a rational method would necessarily include the initial phase of transition, the amplification of small disturbances. However, the existing stability theory is a linearized theory and its limitation to small disturbances is fundamental to its development. Therefore, it does not seem suitable for extensions that encompass the nonlinear effects characterizing actual transition. Hence, the development of a rational analytic method for predicting transition would begin with the development of a less restricted stability theory.

The time integration method described in this report represents a considerable departure from the classical method, as may be seen from the description in the following sections. It was anticipated that considerable difficulty would be encountered in its development but that the new method, once developed, would be much more general than previous methods. In particular, the new method should encompass all speed ranges and include all terms in the equations for all parts of the flow field.* The time integration method should be applicable to arbitrary disturbances, which would allow calculating the behavior of the disturbances actually expected, rather than being restricted to the specific forms given by the stability theory. The new method would not be a priori restricted to small disturbances to allow linearization of the equations, so it would have the potential of calculating the nonlinear effects that occur in the transition region, although it was not expected that the method could be developed so far in the present study.

From the above discussion, it is seen that the analysis is more concerned with whether transition can occur than with whether it will occur. According to all previous theory, laminar flow can exist infinitely far if all disturbances can be eliminated. While complete elimination of all disturbances is of course not possible, the theory also indicates that the length of laminar flow can be increased without limit as the size of disturbances is reduced.

---

* The stability theory has often been applied in a reduced form, retaining only the most important terms in various subdivisions of the flow field. Also, many low-speed calculations neglect temperature and viscosity perturbations, so that the same equations could not be applied in hypersonic flow.

Of course, the designer is also more concerned with whether transition can occur rather than whether it will always occur. Even if the probability of transition is low, conservative design practice requires that it be taken into account in the design.

Unfortunately, in the existing spontaneous (natural) transition data the nature of the initial disturbance is usually not known. Thus there is no way to relate the occurrence of transition to amplification, and the theoretical results cannot be checked against such data. In the present study, therefore, the boundary layer was artifically tripped by mass injection to introduce a known initial disturbance. Mass injection was selected after an examination of several possible tripping methods because of its reported effectiveness and because the strength of the tripping disturbance (injection rate) could be varied without interrupting the test.

Artificial tripping has an added advantage in providing an empirical lower limit on transition, even in the absence of any analytic results.

As described in the following sections, the objectives of the analytic program were met, although the development was much more difficult than originally expected. The results presented are preliminary, but it is believed that the feasibility of the method has been demonstrated.

The experimental program was less successful, and most of the results are now known to be affected by probe interferences and leakages. However, the location of transition by the pitot probe techniques that were used depends on qualitative trends rather than absolute values, somewhat minimizing the effects of the pitot system deficiencies. The data obtained are self-consistent and agree with previous results where comparable data are available. The data obtained extend previous natural transition results to include angle of attack and delta wing planform effects, as well as the effects of mass injection.

II

ANALYTIC PROGRAM

INTRODUCTION

This introductory section gives a brief survey of the background for the present analytic study.

CLASSICAL METHOD

The classical theory of the stability of incompressible fluid flows is based on the complete Navier-Stokes equations including unsteady terms. These equations are more complete than those of boundary layer theory wherein many terms are neglected, particularly those concerned with momentum in the direction normal to the surface. The Navier-Stokes equations are then rewritten into a set of equations describing a steady flow with unsteady perturbations. No approximation is necessarily involved in the rewritten equations because every flow can be considered to be the sum of a steady-state flow plus an unsteady perturbation flow. However, at this point several approximations are incorporated into the classical stability theory. First, it is assumed that the laminar flow being analyzed satisfies all of the steady flow terms, and all terms involving only the steady flow are deleted. Then the remaining equations for the unsteady perturbations (which may involve some of the steady flow quantities, however) are linearized by neglecting all products of the small perturbations. Then it is assumed that there exists a solution of a particular form, namely:

$$Q(x, y, t) = f(y)\, e^{i(\alpha x - \beta t)} \tag{2-1}$$

Equation 2-1 is a general form in which Q represents any perturbation quantity. The function f depends on y only for any given perturbation quantity, but is not necessarily the same for all perturbations. When this equation is incorporated into the perturbation equations, the following equation is obtained:

$$(\bar{u} - c)\,(\varphi'' - \alpha^2 \varphi) - \bar{u}''\,\varphi = -\frac{i\,\nu}{\alpha\, R}\,(\varphi^{iv} - 2\alpha^2\,\varphi'' + \alpha^4 \varphi) \tag{2-2}$$

In Equation 2-2, known as the Orr-Sommerfeld equation after the physicists who derived it early this century, φ expresses the variation with respect to y of a perturbation stream function of the form of Equation 2-1 and so is related to f(y) in that equation. The primes (') denote y derivatives.

Equation 2-2 is exact only for parallel flows wherein the steady-state vertical velocity is everywhere zero. Also neglected in its derivation are all streamwise derivatives of the steady flow. For boundary layer flow, neither the vertical velocity nor the streamwise derivatives are exactly zero. However, both are

small if the Reynolds number is large, and Equation 2-1 is the basis of all of classical boundary layer stability calculations. Because of the smallness of the vertical velocity component, it is common in papers on flow stability to describe boundary layer flow as "nearly parallel." The effect of the steady state-vertical velocity has been examined by several authors with the conclusion that Equation 2-2 is adequate for boundary layer flow, provided

$$(\alpha R)^{1/3} \gg 1 \qquad (2-3)$$

Although the Equation 2-2 was obtained early this century by Orr and Sommerfeld, no solution was found until 1929, by Tollmien as already stated. His solution was not an exact solution of Equation 2-2, however. By careful examination of the individual terms in Equation 2-2, Tollmien was able to show that it was not necessary to solve the complete equation over the entire flow field. Accordingly, Tollmien then solved reduced equations involving only the most important terms over each of several different regions of the flow field. The complete solution was then formed by patching the resulting solutions together. Tollmien's solution is well described in the book, "Boundary Layer Theory," by Schlichting (Ref. 17).

Two comparatively recent analytic calculations are worthy of special note. In 1956 J. T. Stuart published a second-order stability calculation (Ref. 18) that includes the effect of the perturbations on the steady flow. The perturbations themselves were calculated by the linear theory. Stuart's calculations showed that the minimum critical Reynolds number decreases with the amplitude of the disturbance. As a part of his study, Stuart derived an equation for the mean distortion of the laminar flow by the unsteady perturbations. His expression allows calculation of the minimum critical Reynolds number by an algebraic operation on the integral of the disturbances over the boundary layer. Stuart's expression could be very useful in conjunction with the present method, but requires extensions that have not yet been made.

Another noteworthy development is presented in a paper by Keller and DeSanto (Ref. 19). Their method, very similar to the present method, is discussed later.

EXTENSION TO COMPRESSIBLE FLOW

Extension of the classical method to compressible flows has also been the subject of many years investigation, and has been even more difficult. The compressible perturbation equations cannot be reduced to a single ordinary differential equation as in the incompressible case; rather there exists a coupled system of four equations that must be solved simultaneously. Since the dependent variable in those equations is complex (as it is in the Orr-Sommerfeld equation*), it is

*Note that, because of the assumed form of φ in Equation 2-1, φ is now a complex variable. Equation 2-2 may be regarded as two simultaneous equations for the real and imaginary parts of φ.

seen that this is actually equivalent to a system of eight equations. Nevertheless, numerous solutions to these equations have been obtained over the past twenty years (e.g., Reference 20). The majority of these calculations continued on somewhat along the lines originally followed by Tollmien. That is, different approximations were applied in different regions of the boundary layer (thereby solving only partial sets of equations) and the resulting solutions were patched together. The authors of these papers have given some discussion of the approximations involved and, in some cases, the approximations were found to be invalid. See the discussion in Reference 20.

The past 20 years have also seen the growth of a new and powerful tool, the automatic calculator. Development of these machines has made possible the direct integration of the linearized equations by numerical techniques, avoiding the approximate patching techniques by previous authors. A set of such calculations was done by Bryan Brown (Ref. 21) using the equations of Dunn and Lin (Ref. 22) in 1962. Also, Leslie Mack of JPL has made similar studies and published several reports beginning in about 1960 (Refs. 23, 24, and 25).

PRESENT METHOD

In the beginning of the present studies, the authors judged that the capability of the automatic calculator has advanced to the point that one should consider direct integration of the unsteady viscous flow conservation equations. In this approach the unsteady flow equations would be used to calculate the history of an initial disturbance in a laminar flow. It should be clear from the calculated history if the disturbance is growing or decaying. This approach would have several important advantages over the linearized theory. The most important of these, in the view of the authors, is that the method is not a priori limited to small perturbations. Thus, the possibility exists that one could begin to study the actual transition processes to a much greater extent than is possible within the framework of the classical method.

A second important advantage of the present approach is the generality of the method. A single system of equations can be applied to any of the flow cases one wishes to consider. Thus, no specialized techniques are devised for obtaining solutions for certain specific cases. A third advantage of the present approach (important in the minds of the authors at least) is that complex variable mathematics is avoided, and all calculations are carried out in the physical plane. Thus, one need not lose sight of the physical mechanisms; it has been found that the physical ideas have given a great deal of insight into the required mathematical developments.

Since the approximations of the linear theory were all introduced with a view to simplifying the calculations, it is to be expected that the present method would be much more difficult. However, many of the simplifications introduced are not particularly useful in a purely numerical approach, such as that used on a computer. Also, while the linear theory involves fourth derivatives, the present method involves no derivative higher than the second thus simplifying the calculation.

Finally, it may be shown that by restricting the calculation to a discrete wavelength (but still leaving the time variations and disturbance profile arbitrary), it is only necessary to calculate the flow at two x locations, greatly reducing the amount of computation required.

The method was original with the present authors; however, a paper by DeSanto and Keller (Ref. 19) has come to our attention that presents calculations of the behavior of perturbations in an incompressible boundary layer. There are many similarities between the DeSanto-Keller approach and that of the present report. The present calculations are more complex because they consider compressible hypersonic flows in which all fluid properties are variables, whereas DeSanto and Keller's calculations involve an ideal incompressible fluid with constant viscosity. Thus, the present calculations involve the integration of four equations with many terms, while those of Reference 19 involve the integration of only two equations, each with fewer terms. However, DeSanto and Keller were able to treat the actual flow problem with more generality, and treat more elegantly the mathematical problems involved.

In the following sections we describe the development of the new analytic method as it has progressed so far. The authors feel that the feasibility of the method has been demonstrated and a number of calculations are presented. The results are somewhat more explicit than had originally been expected, when it was merely hoped that some qualitative feel for stability would be obtained. The calculations were expected to be more like numerical experiments than specific solutions of stability equations. However, the calculations have also provided wave forms, phase angles, wave speeds, and other details of the disturbances.

The authors have been unable to carry the calculations as far as desired in the time available, and many obvious and important improvements have not been incorporated. For the present application, one of the most important of these improvements would have been the application of a second-order energy method, which would have allowed the determination of the most critical wave length and the minimum critical Reynolds number without the parametric search technique presently necessary. Such a method could be developed along the lines of Stuart's method (Ref. 18), which has already been mentioned.

ANALYTIC FORMULATION

The equations used in the present analysis are obtained from the well-known Navier-Stokes system by decomposing each flow parameter into two terms as follows:

$$\begin{bmatrix}\text{Complete}\\ \text{Flow}\end{bmatrix} = \begin{bmatrix}\text{Steady}\\ \text{State}\\ \text{Flow}\end{bmatrix} + \begin{bmatrix}\text{Time}\\ \text{Dependent}\\ \text{Perturbations}\end{bmatrix} \qquad (2\text{-}4)$$

$$Q = \bar{Q} + Q'$$

where Q represents any flow variable (P, u, etc.).

The steady-state terms are assumed to identically satisfy the steady flow equations, and hence represent the laminar steady flow. The equations so obtained for two-dimensional flow are given in Table I.

It should be noted that decomposing the flow parameters simply leads to an alternate formulation of the complete flow equations, and does not necessarily introduce any approximations. Although the perturbation equations contain many more terms than the original Navier-Stokes system, it is expected that the accuracy of the corresponding numerical system will be improved, particularly in regions where the perturbations are small compared to the steady flow values. In the present report, however, only linearized results are presented; i.e., all products of perturbations have been neglected.

NUMERICAL FORMULATION, STABILITY, AND CONVERGENCE

This section describes the formulation of a set of finite difference equations from the preceding differential equations. Although there are many ways in which this can be done that are equivalent (in the sense that all will reduce to the original differential equations in the limit for very small increments), it was found that some formulations are much better than others. It was found that the "intuitive" numerical equivalent of the differential equations is in fact unconditionally unstable (that is, subject to error that increases without bound for any finite time increment Δt). It was also found that if central differences are used for the spatial derivatives, the numerical form of the differential equations also exhibits a behavior like that of an array of coupled spring-mass systems in addition to the fluid dynamics, and that a means of eliminating this second solution must be employed. For similar reasons, it is common to speak of the "finite difference analog" to a set of differential equations, rather than the "finite difference form" of the equations.

The two major topics discussed in this section are spatial derivatives and time integration. The conclusions are of a general nature and are believed to be applicable in any flow field calculations by the present method. The boundary conditions that characterize the specific problem at hand, laminar flow stability, are discussed in the following section.

SPATIAL DERIVATIVES

The first step in formulating the finite difference analog to the equations of Table I is to replace the spatial derivatives by numerical forms. In the present method the flow field is represented by an x-y plane, with x and y divided into uniform increments Δx and Δy. All calculations are carried out at the mesh points for which

$$x = m\Delta x$$

$$y = n\Delta y$$

with m and n being integers; Δx and Δy are not necessarily equal.

Table I: CONSERVATION EQUATIONS

Mass Conservation:

$$\frac{\partial \rho'}{\partial t} = -\left[\frac{\partial}{\partial x}\left(\rho' \bar{u} + \bar{\rho} u' + \rho' u'\right) + \frac{\partial}{\partial y}\left(\rho' \bar{v} + \bar{\rho} v' + \rho' v'\right)\right] \tag{1}$$

x-Momentum:

$$\begin{aligned}\frac{\partial u'}{\partial t} = -\Bigg[&\bar{u}\frac{\partial u'}{\partial x} + u'\frac{\partial \bar{u}}{\partial x} + u'\frac{\partial u'}{\partial x} + \bar{v}\frac{\partial u'}{\partial y} \\ &+ v'\frac{\partial \bar{u}}{\partial y} + v'\frac{\partial u'}{\partial y} + \frac{\rho'}{\bar{\rho}+\rho'}\left(\bar{u}\frac{\partial \bar{u}}{\partial x} + \bar{v}\frac{\partial \bar{u}}{\partial y}\right)\Bigg] \\ &+ \frac{1}{\bar{\rho}+\rho'}\Bigg\{-\frac{\partial P'}{\partial x} + \frac{\partial}{\partial x}\Bigg[\mu'\left(\frac{4}{3}\frac{\partial \bar{u}}{\partial x} + \frac{4}{3}\frac{\partial u'}{\partial x} - \frac{2}{3}\frac{\partial \bar{v}}{\partial y} - \frac{2}{3}\frac{\partial v'}{\partial y}\right) \\ &+ \bar{\mu}\left(\frac{4}{3}\frac{\partial u'}{\partial x} - \frac{2}{3}\frac{\partial v'}{\partial y}\right)\Bigg] + \frac{\partial}{\partial y}\Bigg[\mu'\left(\frac{\partial \bar{u}}{\partial y} + \frac{\partial u'}{\partial y} + \frac{\partial \bar{v}}{\partial x} + \frac{\partial v'}{\partial x}\right) \\ &+ \bar{\mu}\left(\frac{\partial u'}{\partial y} + \frac{\partial v'}{\partial x}\right)\Bigg]\Bigg\}\end{aligned} \tag{2}$$

y-Momentum:

$$\begin{aligned}\frac{\partial v'}{\partial t} = -\Bigg[&\bar{v}\frac{\partial v'}{\partial y} + v'\frac{\partial \bar{v}}{\partial y} + v'\frac{\partial v'}{\partial y} + \bar{u}\frac{\partial v'}{\partial x} \\ &+ u'\frac{\partial \bar{v}}{\partial x} + u'\frac{\partial v'}{\partial x} + \frac{\rho'}{\bar{\rho}+\rho'}\left(\bar{v}\frac{\partial \bar{v}}{\partial y} + \bar{u}\frac{\partial \bar{v}}{\partial x}\right)\Bigg] \\ &+ \frac{1}{\bar{\rho}+\rho'}\Bigg\{-\frac{\partial P'}{\partial y} + \frac{\partial}{\partial y}\Bigg[\mu'\left(\frac{4}{3}\frac{\partial \bar{v}}{\partial y} + \frac{4}{3}\frac{\partial v'}{\partial y} - \frac{2}{3}\frac{\partial \bar{u}}{\partial x} - \frac{2}{3}\frac{\partial u'}{\partial x}\right) \\ &+ \bar{\mu}\left(\frac{4}{3}\frac{\partial v'}{\partial y} - \frac{2}{3}\frac{\partial u'}{\partial x}\right)\Bigg] + \frac{\partial}{\partial x}\Bigg[\mu'\left(\frac{\partial \bar{v}}{\partial x} + \frac{\partial v'}{\partial x} + \frac{\partial \bar{u}}{\partial y} + \frac{\partial u'}{\partial y}\right) \\ &+ \bar{\mu}\left(\frac{\partial v'}{\partial x} + \frac{\partial u'}{\partial y}\right)\Bigg]\Bigg\}\end{aligned} \tag{3}$$

Energy:

$$\begin{aligned}\frac{\partial H'}{\partial t} = -\Bigg[&\bar{u}\frac{\partial H'}{\partial x} + u'\frac{\partial \bar{H}}{\partial x} + u'\frac{\partial H'}{\partial x} + \bar{v}\frac{\partial H'}{\partial y} \\ &+ v'\frac{\partial \bar{H}}{\partial y} + v'\frac{\partial H'}{\partial y} + \frac{\rho'}{\bar{\rho}+\rho'}\left(\bar{u}\frac{\partial \bar{H}}{\partial x} + \bar{v}\frac{\partial \bar{H}}{\partial y}\right)\Bigg]\end{aligned} \tag{4}$$

Table I (Continued)

$$+\frac{1}{\bar{\rho}+\rho'}\left\{\frac{\partial P'}{\partial t}+\frac{\partial}{\partial x}\left[\frac{\bar{\mu}}{Pr}\frac{\partial H'}{\partial x}+\frac{\mu'}{Pr}\frac{\partial \bar{H}}{\partial x}+\frac{\mu'}{Pr}\frac{\partial H'}{\partial x}\right.\right.$$

$$+(\bar{\mu}+\mu')\left(1-\frac{1}{Pr}\right)\left(\bar{v}\frac{\partial v'}{\partial x}+v'\frac{\partial \bar{v}}{\partial x}+v'\frac{\partial v'}{\partial x}\right)$$

$$+\mu'\left(1-\frac{1}{Pr}\right)\bar{v}\frac{\partial \bar{v}}{\partial x}+(\bar{\mu}+\mu')\left(\frac{4}{3}-\frac{1}{Pr}\right)\left(\bar{u}\frac{\partial u'}{\partial x}\right.$$

$$\left.+u'\frac{\partial \bar{u}}{\partial x}+u'\frac{\partial u'}{\partial x}\right)+\mu'\left(\frac{4}{3}-\frac{1}{Pr}\right)\left(\bar{u}\frac{\partial \bar{u}}{\partial x}\right)\Bigg]$$

$$+\frac{\partial}{\partial y}\left[\frac{\bar{\mu}}{Pr}\frac{\partial H'}{\partial y}+\frac{\mu'}{Pr}\frac{\partial \bar{H}}{\partial y}+\frac{\mu'}{Pr}\frac{\partial H'}{\partial y}\right.$$

$$+(\bar{\mu}+\mu')\left(1-\frac{1}{Pr}\right)\left(\bar{u}\frac{\partial u'}{\partial y}+u'\frac{\partial \bar{u}}{\partial y}+u'\frac{\partial u'}{\partial y}\right)$$

$$+\mu'\left(1-\frac{1}{Pr}\right)\bar{u}\frac{\partial \bar{u}}{\partial y}+(\bar{\mu}+\mu')\left(\frac{4}{3}-\frac{1}{Pr}\right)\left(\bar{v}\frac{\partial v'}{\partial y}\right.$$

$$\left.+v'\frac{\partial \bar{v}}{\partial y}+v'\frac{\partial v'}{\partial y}\right)+\mu'\left(\frac{4}{3}-\frac{1}{Pr}\right)\left(\bar{v}\frac{\partial \bar{v}}{\partial y}\right)\Bigg]$$

$$+(\bar{\mu}+\mu')\left[\frac{1}{3}\left(\bar{u}\frac{\partial^2 v'}{\partial x\,\partial y}+u'\frac{\partial^2 \bar{v}}{\partial x\,\partial y}+u'\frac{\partial^2 v'}{\partial x\,\partial y}\right.\right.$$

$$+\bar{v}\frac{\partial^2 u'}{\partial x\,\partial y}+v'\frac{\partial^2 \bar{u}}{\partial x\,\partial y}+v'\frac{\partial^2 u'}{\partial x\,\partial y}\Bigg)$$

$$+2\left(\frac{\partial \bar{v}}{\partial x}\frac{\partial u'}{\partial y}+\frac{\partial v'}{\partial x}\frac{\partial \bar{u}}{\partial y}+\frac{\partial v'}{\partial x}\frac{\partial u'}{\partial y}\right)$$

$$\left.-\frac{4}{3}\left(\frac{\partial \bar{u}}{\partial x}\frac{\partial v'}{\partial y}+\frac{\partial u'}{\partial x}\frac{\partial \bar{v}}{\partial y}+\frac{\partial u'}{\partial x}\frac{\partial v'}{\partial y}\right)\right]$$

$$+\mu'\left[\frac{1}{3}\left(\bar{u}\frac{\partial^2 \bar{v}}{\partial x\,\partial y}+\bar{v}\frac{\partial^2 \bar{u}}{\partial x\,\partial y}\right)+2\frac{\partial \bar{v}}{\partial x}\frac{\partial \bar{u}}{\partial y}\right.$$

$$\left.-\frac{4}{3}\frac{\partial \bar{u}}{\partial x}\frac{\partial \bar{v}}{\partial y}\right]+\frac{\partial}{\partial x}(\bar{\mu}+\mu')\left[-\frac{2}{3}\left(\bar{u}\frac{\partial v'}{\partial y}\right.\right.$$

$$\left.\left.+u'\frac{\partial \bar{v}}{\partial y}+u'\frac{\partial v'}{\partial y}\right)+\bar{v}\frac{\partial u'}{\partial y}+v'\frac{\partial \bar{u}}{\partial y}+v'\frac{\partial u'}{\partial y}\right]$$

Table I (Concluded)

$$+ \frac{\partial \mu'}{\partial x}\left(-\frac{2}{3}\bar{u}\frac{\partial \bar{v}}{\partial y} + \bar{v}\frac{\partial \bar{u}}{\partial y}\right) + \frac{\partial}{\partial y}(\bar{\mu} + \mu')\left[-\frac{2}{3}\left(\bar{v}\frac{\partial u'}{\partial x} + v'\frac{\partial \bar{u}}{\partial x} + v'\frac{\partial u'}{\partial x}\right) + \bar{u}\frac{\partial v'}{\partial x} + u'\frac{\partial \bar{v}}{\partial x} + u'\frac{\partial v'}{\partial x}\right]$$

$$+ \frac{\partial \mu'}{\partial y}\left(-\frac{2}{3}\bar{v}\frac{\partial \bar{u}}{\partial x} + \bar{u}\frac{\partial \bar{v}}{\partial x}\right)\Bigg\}$$

Equation of State:

$$P' = R(\bar{\rho}\ T' + \rho'\ \bar{T} + \rho'\ T') \tag{5}$$

Viscosity Law:

$$\mu' = (0.2325 \times 10^{-8})\left[\frac{(\bar{T} + T')^{3/2}}{\bar{T} + T' + 216} - \frac{\bar{T}^{3/2}}{\bar{T} + 216}\right] \tag{6}$$

Enthalpy-Temperature Relationships:

$$H' = c_p\ T' + \bar{u}\ u' + \frac{u'^2 + v'^2}{2} \tag{7}$$

Since the flow properties are known only at discrete points, it is necessary to approximate the flow field properties by functions that can be differentiated to obtain the required spatial derivatives. There exist infinitely many approximating functions that could be used that would all yield exact results in the limit as Δx and Δy approach zero. Since Δx and Δy must remain finite in any actual calculation, it is necessary to find that method that yields the best results for finite spatial increments.

The most obvious and most commonly used approximating functions are polynomials, and polynomials were used in all of the present studies. A polynomial of degree n is uniquely determined by n + 1 conditions, which may be conditions on either the values or the derivatives of the polynomials. In numerical flow studies, the commonly applied conditions are that the polynomials agree with the values of the flow field properties at the surrounding mesh points. For example, a second-degree polynomial is uniquely determined by the conditions

$$\begin{aligned} P(x - \Delta x) &= u(x - \Delta x) \\ P(x) &= u(x) \\ P(x + \Delta x) &= u(x + \Delta x) \end{aligned} \tag{2-5}$$

where P is the approximating polynomial. The derivative of P at x is given by

$$\left(\frac{\partial P}{\partial x}\right)_x = \frac{P(x + \Delta x) - P(x - \Delta x)}{2\Delta x} = \frac{\partial u}{\partial x} \tag{2-6}$$

The corresponding second-derivative expression is

$$\frac{\partial^2 P}{\partial x^2} = \frac{P(x + \Delta x) - 2P(x) + P(x - \Delta x)}{(\Delta x)^2} = \frac{\partial^2 u}{\partial x^2} \tag{2-7}$$

Equations 2-6 and 2-7 are known as three-point central-difference forms and were used for all of the results shown in this report.

Several alternative methods were also investigated. Higher-order central differences lead to equations of the form

$$\begin{aligned} \frac{\partial u}{\partial x} = {} & c_1\left[u(x + \Delta x) - u(x - \Delta x)\right] + \\ & c_2\left[u(x + 2\Delta x) - u(x - 2\Delta x)\right] + c_3\left[\ \ \right] + \ldots \end{aligned} \tag{2-8}$$

where c_1, c_2, etc., are constants. The higher-order central-difference formulas were not found to lead to any significant improvements over Equations 2-6 and 2-7 that would compensate for the required additional calculations. Uncentered difference formulas of the form

$$\frac{\partial u}{\partial x} = c_1\left[u(x)\right] + c_2\left[u(x + \Delta x)\right] + c_3\left[u(x + 2\Delta x)\right] + \ldots \qquad (2\text{-}9)$$

were also investigated. It will be noted that, in Equation 2-9 the derivative at a point x_o depends entirely on values for x greater than x_o, and not at all on values for x less than x_o. It was found that use of this equation and similar forms introduced systematic errors that appeared as long-term trends. When the form of Equation 2-9 was reversed,

$$\frac{\partial u}{\partial x} = c_1\left[u(x)\right] + c_2\left[u(x - \Delta x)\right] + c_3\left[u(x - 2\Delta x)\right] + \ldots \qquad (2\text{-}10)$$

an opposite trend was produced. It was therefore clear that uncentered differences were not giving correct results and their use was discontinued.

TIME INTEGRATION

In the present method, four basic perturbation quantities are obtained by integration with respect to time, i.e.:

$$u'(t) = \int_o^t \left(\frac{\partial u'}{\partial t}\right) dt + u'_o \qquad (2\text{-}11)$$

with similar expressions for ρ', v', and H'. As with the approximation of spatial derivations with numerical forms, there are numerous numerical schemes for evaluating the time integrals. The following substitution is exact

$$\int_o^t \left(\frac{\partial u'}{\partial t}\right) dt = \sum_{n=o}^{n=t/\Delta t} \Delta u'_n \, \Delta t \qquad (2\text{-}12)$$

provided the increments $\Delta u'_n$ are evaluated correctly. This can be accomplished by a Taylor expansion:

$$\Delta u'_n = u'(n\Delta t + \Delta t) - u'(n\Delta t) = \Delta t \frac{\partial u'}{\partial t} + \overline{\Delta t}^2 \frac{\partial^2 u'}{\partial t^2} + \ldots$$

Since the flow conservation equations (Table I) provide only the first derivative with respect to time, we first consider the approximation:

$$\Delta u'_n = \Delta t \frac{\partial u'}{\partial t} \qquad (2\text{-}13)$$

Although the error introduced can be made arbitrarily small by reducing Δt, two practical considerations tend to establish a lower limit. First, the number of calculations required for any given problem will be inversely proportional to Δt; second, as Δt becomes very small, $\Delta u'$ does also, and the effect of roundoff errors is relatively greater. It is therefore necessary to examine the errors introduced by Equation 2-13. It is found that if Δt is small, the error introduced by the use of Equation 2-12 is approximately linear in Δt, but that above a certain critical value the error grows exponentially. Before considering accuracy as such, we must first determine conditions for the onset of the exponential behavior, which

is known as numerical instability. Following the discussion of instability, we will return to the subject of accuracy, and present a numerical scheme that yields a great improvement over Equation 2-13 without any additional calculation.

Simple Instability

As noted above, if Δt exceeds a certain critical value, the solution obtained numerically is not even an approximation to the true solution, but rather oscillates in an erratic manner with ever-growing amplitudes. When the latter phenomenon occurs, the solution is said to be numerically unstable. However, this is not the only form of numerical instability that can occur, and so we have adopted the term "simple instability" to refer to the oscillatory exponential growth of small errors.

Because the concept of numerical stability is so basic in the work that follows, we will give a simple example showing a stable and unstable solution of an ordinary differential equation for which an analytic solution is known. Consider the following equation:

$$\dot{y} + y = 0 \tag{2-14}$$

where $\dot{y} = dy/dt$. The solution to Equation 2-14 with $y(0) = 1$ is

$$y = e^{-t} \tag{2-15}$$

For Equation 2-14, the equivalent of Equation 2-13 is:

$$\begin{aligned} \Delta y &= \dot{y}\,\Delta t \\ &= -y\Delta t \end{aligned} \tag{2-16}$$

Using Equations 2-12 and 2-16, we can obtain the following recursive formula* for y:

$$y^{n+1} = y^n (1 - \Delta t) \tag{2-17}$$

It is easily seen that for $y(0) = 1$,

$$\begin{aligned} y^n &= (1 - \Delta t)^n \\ &= e^{n[\ln(1-\Delta t)]} \end{aligned} \tag{2-18}$$

By series expansion

$$\ln(1 - \Delta t) = -\Delta t + \frac{\Delta t^2}{2} - \frac{\Delta t^3}{3} + \cdots \tag{2-19}$$

* We use here the convenient notation commonly used in papers on numerical analysis: $y^n \equiv y(n\Delta t)$. When appearing in a solution to a difference equation n is usually an exponent, however. It should be clear to the reader whether an exponent or a time level is intended.

so that

$$y^n = e^{-n\left(\Delta t - \frac{\Delta t^2}{2} + \frac{\Delta t^3}{3} - \ldots\right)} \tag{2-20}$$

Since $t(n) = n\,\Delta t$, the numerically obtained solution will be

$$y(t) = \left(e^{-t}\right)\left(e^{+t\,\Delta t/2}\right)\left(e^{-t\Delta t^2/3}\right)\ldots \tag{2-21}$$

or, for small values of Δt

$$y \doteq e^{-t}\,(1 + t\,\Delta t/2) \tag{2-22}$$

It is seen that the numerical solution approaches the correct limit for small values at Δt. However, for $\Delta t > 1$, the logarithm of $(1 - \Delta t)$ is complex, and the numerical solution becomes oscillatory. Returning to Equation 2-17, it is seen that y will be negative for all odd values of n, and positive for the even values. For $\Delta t > 2$, the absolute values of y will increase exponentially, as

$$\left|y^n\right| = \left|1 - \Delta t\right|^n \tag{2-23}$$

Thus, the numerical solution will diverge in an oscillatory manner, unlike the true solution, which monotonically decreases with time.

It will of course be much more difficult to determine the stability conditions on Δt for the finite difference analogs to the equations of Table I. An analytical solution to those equations (comparable to Equation 2-18) would be equivalent to a general solution of the differential equations. Since no such general solution has been exhibited, it is unlikely that one will be found in numerical instability studies.

However, it has been possible to establish some of the conditions for numerical stability by considering greatly simplified forms of the perturbation equations. The stability conditions imposed by specific terms in each equation can be discovered in this way, but of course, any conditions arising from interactions of terms will not appear. However, subsequent experience indicates that the limits obtained from the reduced equations are good approximations to the stability limits of the complete equations.

As an example of the manner in which stability limits were determined, a condition imposed by the momentum and continuity equations will be derived.

Examining the x-momentum equation, it will be seen that the acceleration is a function of the velocity components, pressure gradients, and shear forces. By deleting all terms except that for the pressure gradient, the x-momentum equation becomes (with the aid of the equation of state):

$$\frac{\partial u}{\partial t} = -\frac{1}{\rho}\frac{\partial P}{\partial x}$$

$$= -RT\left(\frac{1}{\rho}\frac{\partial \rho}{\partial x} + \frac{1}{T}\frac{\partial T}{\partial x}\right) \qquad (2\text{-}24a)$$

In order to avoid involving the energy equation, the temperature term can be either approximated by isentropic relationships, or neglected entirely. The approximations lead to either

$$\frac{\partial u}{\partial t} = -RT\frac{\partial \rho}{\partial x} \qquad (2\text{-}24b)$$

or

$$\frac{\partial u}{\partial t} = -\gamma RT\frac{\partial \rho}{\partial x} \qquad (2\text{-}24c)$$

Either of the above equations may be used for the numerical stability calculation; the presence of the multiplier γ does not affect the mathematical ideas involved. It will be retained, however, because the final result is more easily related to physical phenomena.

To determine the density, the continuity equation is used, considering only x-direction derivatives:

$$\frac{\partial \rho}{\partial t} = -\rho\frac{\partial u}{\partial x} - u\frac{\partial \rho}{\partial x}$$

$$= -\rho u\left[\frac{1}{u}\frac{\partial u}{\partial x} + \frac{1}{\rho}\frac{\partial \rho}{\partial x}\right] \qquad (2\text{-}25a)$$

In low speed flows the relative change in density is much smaller than that in velocity. For low speeds, therefore, Equation 2-25 can be further reduced:

$$\frac{\partial \rho}{\partial t} = -\rho\frac{\partial u}{\partial x} \qquad (2\text{-}25b)$$

To determine the stability condition imposed by Equations 2-24c and 2-25b, a short calculation is necessary. A flow field is assumed wherein ρ and u are nearly constant. Then a small perturbation is applied to u at a point and the subsequent flow behavior (according to Equations 2-24c and 2-25b) is calculated.

The first few steps of the calculation are reproduced in Table II, where it is seen that after two time steps, the velocity perturbation u reappears, multiplied by the factor, $\left[1 - (\gamma RT\ \Delta t)/2\ \overline{\Delta x^2}\right]$. By comparing this result with Equation 2-17, it will be seen that $\left[(\gamma RT\ \Delta t/(\Delta x)^2\right]$ is the parameter that determines the numerical stability of the system, and must (at least) be held smaller than 2. The specific numerical value of this parameter that will ensure stability is less easily established, however, because the diffusion of the error in the x-direction must be considered as well as that with respect to time. While it is possible to find an analytic solution to the pair (Equations 2-24c and 2-25b), and determine exactly the condition for numerical stability (which turns out to be $\gamma RT\ \Delta t/\overline{\Delta x^2} < 1$),

Table II: SAMPLE CALCULATION

Reduced equations considered:

$$\frac{\partial \rho}{\partial t} = -\rho \frac{\partial u}{\partial x} = -\rho \left(\frac{u(x+\Delta x) - u(x-\Delta x)}{2\Delta x} \right)$$

$$\frac{\partial u}{\partial t} = -\frac{\partial P}{\partial x} = -\gamma RT \frac{\partial \rho}{\partial x} = -\gamma RT \left(\frac{\rho(x+\Delta x) - \rho(x-\Delta x)}{2\Delta x} \right)$$

t	Flow property	x			
		$-\Delta x$	0	Δx	$2\Delta x$
0	u	0	u	0	0
	ρ	ρ	ρ	ρ	ρ
	$\frac{\partial u}{\partial t}$	0	0	0	0
	$\frac{\partial \rho}{\partial t}$	$\frac{-\rho u}{2\Delta x}$	0	$\frac{\rho u}{2\Delta x}$	0
Δt	u	0	u	0	0
	ρ	$\rho - \rho\frac{u\Delta t}{2\Delta x}$	ρ	$\rho + \rho\frac{u\Delta t}{2\Delta x}$	ρ
	$\frac{\partial u}{\partial t}$	0	$-\gamma RT \frac{u\Delta t}{2\overline{\Delta x}^2}$	0	$+\gamma RT \frac{u\Delta t}{4\overline{\Delta x}^2}$
	$\frac{\partial \rho}{\partial t}$	$-\frac{\rho u}{2\Delta x}$	0	$+\frac{\rho u}{2\Delta x}$	
$2\Delta t$	u	0	$u\left(1 - \gamma RT \frac{\overline{\Delta t}^2}{2\overline{\Delta x}^2}\right)$	0	$\frac{u\Delta t^2}{4\overline{\Delta x}^2} \gamma RT$
	ρ	$\rho - \frac{u\Delta t}{\Delta x}$	ρ	$\rho + \frac{u\Delta t}{\Delta x}$	0
	$\frac{\partial u}{\partial t}$	0	$-\gamma RT \frac{u\Delta t}{\overline{\Delta x}^2}$		
			etc.		

the result is not exactly applicable to the complete equations with their many additional terms. Hence, the stability limits for the complete equations were determined by trial and error using the results of the simplified equations as guides. It was found, however, that stability conditions determined from the simplified equations were accurate indicators of the necessary conditions for the complete equations. In the present example the condition

$$\Delta t \leq \frac{\Delta x^2}{\sqrt{\gamma RT}}$$

was obtained. With the complete equations the flow was found to be stable for

$$\Delta t = \overline{\Delta x}^2 / \sqrt{\gamma RT},$$

but unstable for $\Delta t = 2\,\overline{\Delta x}^2 / \sqrt{\gamma RT}$.

With the aid of the simplified equations four separate numerical stability criteria were identified, and subsequently verified with the complete equations. They are:

1) $\Delta t < \dfrac{1.5\,\Delta x}{\sqrt{\gamma RT}}$

2) $\Delta t < \dfrac{\Delta x}{\sqrt{2}\,U}$

} obtained from the continuity equation and the inviscid part of the momentum equations

3) $\Delta t < \dfrac{\overline{\Delta x}^2}{2\nu}$ from the viscous part of the momentum equations

4) $\Delta t < \dfrac{\gamma\,\Delta x}{(\gamma-1)\,U}$ from the energy and continuity equations.

These limits were verified by comparing time histories computed for differing flow conditions with various values of Δt.

Convergence and Resequencing

It was soon found that, even when the stability criteria described above were observed, a long-term divergence occurred. As with simple stability, an analysis of the complete equations of Table I was not practicable, and as before a means of eliminating the long-term divergence was found by considering the reduced system previously introduced:

$$\frac{\partial u}{\partial t} = -\frac{1}{\rho}\frac{\partial P}{\partial x} = -\gamma RT\frac{\partial \rho}{\partial x} = -a^2\frac{\partial \rho}{\partial x} \qquad (2\text{-}26)$$

$$\frac{\partial \rho}{\partial t} = -\rho\frac{\partial u}{\partial x} \qquad (2\text{-}27)$$

Combining derivatives of Equations 2-26 and 2-27 leads to the wave equation:

$$\frac{\partial^2 u}{\partial t^2} - a^2 \frac{\partial^2 u}{\partial x^2} = 0 \tag{2-28}$$

Replacing the spatial derivative with a central difference yields

$$\frac{\partial^2 u}{\partial t^2} - a^2 \frac{u_{i-1} - 2u_i + u_{i+1}}{\overline{\Delta x}^2} = 0 \tag{2-29}$$

Since we are primarily concerned with time integration, we further simplify the problem by imposing boundary conditions as follows:

$$u_{i+1} = u_{i-1} = 0 \tag{2-30}$$

yielding

$$\frac{\partial^2 u_i}{\partial t^2} + \left(\frac{2a^2}{\overline{\Delta x}^2}\right) u_i = 0 \tag{2-31}$$

which has the solution

$$u = A \sin\left(\sqrt{2}\,\frac{a}{\Delta x}\,t\right) + B \cos\left(\sqrt{2}\,\frac{a}{\Delta x}\,t\right) \tag{2-32}$$

Since the acceleration $\partial u/\partial t$ is determined by the density, the forward integration of Equations 2-26 and 2-27 is equivalent to the following numerical scheme for solving Equation 2-31:

$$\begin{aligned} u^{n+1} &= u^n + \Delta t\, \dot{u}^n \\ \dot{u}^{n+1} &= \dot{u}^n + \Delta t\, \ddot{u}^n \\ u^{n+2} &= u^{n+1} + \Delta t\, \dot{u}^{n+1} \end{aligned} \tag{2-33}$$

This equation may be rewritten as the recursive formula

$$u^{n+1} = 2u^n - (1 + \Delta t^2)\, u^{n-1} \tag{2-34}$$

which has the solution*:

$$u^n = \left(\sqrt{1 + \Delta t^2}\right)^{n-1} \left(\frac{\sin n\theta}{\sin \theta}\right); \quad \theta = \sin^{-1}\left(\frac{\Delta t}{\sqrt{1 + \Delta t^2}}\right) \tag{2-35}$$

* The difference equation $U^{n+2} + KU^{n+1} + LU^n = 0$ has the solution $U^n = A\alpha^n + B\beta^n$ where A and B are constants, $(\alpha + \beta) = K$, and $\alpha\beta = L$ (n is an exponent when applied to α and β). In polar form, $\alpha = re^{i\theta}$ with $r = \sqrt{L}$ and $\sin\theta = \sqrt{1 - K^2/4L}$; $\beta = L/\alpha$. Note that both the real and imaginary parts of α and β are solutions.

Thus it is seen that the numerical solution diverges exponentially for any finite value of Δt. The forward integration of the complete equations (Table I) was found to have a similar behavior. Since the purpose of the present study is to determine amplification of disturbance waves the existence of the exponential multiplier would invalidate the results. The integration scheme must (at least) yield exactly constant amplitudes when integrating Equation 2-31.

Such a scheme was soon found. If we replace u^n in Equation 2-33 with u^{n+1} the recursive formula (Equation 2-34) is changed to

$$u^{n+1} = (2 - \Delta t^2)\, u^n - u^{n-1} \tag{2-36}$$

Equation 2-36 has the solution

$$u^n = \sin n\,\theta; \quad \theta = \sin^{-1}\left(\Delta t \sqrt{1 - \Delta t^2/4}\right) \tag{2-37}$$

which is seen to have exactly constant amplitude. It is also seen that Equation 2-37 has a slight error in frequency. While undesirable, this error is not of great importance since we do not require an exact knowledge of the critical frequency A comparison of the two numerical solutions with the exact integral of Equation 2-31 is shown in Figure 2-1. It is seen that the original scheme diverges quickly with the relatively large step size chosen, while the second scheme has the correct amplitude and is only slightly shifted from the exact values.

The change of scheme 2-33 to yield 2-36 involves only interchanging each pair of calculations in Equation 2-33, i.e.,

$$\begin{aligned} \dot{u}^{n+1} &= \dot{u}^n + \Delta t\, u^n \\ u^{n+1} &= u^n + \Delta t\, \dot{u}^{n+1} \\ \dot{u}^{n+2} &= \dot{u}^{n+1} + \Delta t\, u^{n+1} \\ &\text{etc.} \end{aligned} \tag{2-38}$$

Since Equation 2-38 differs from Equation 2-33 only in the sequence of calculations it has come to be known as "resequencing." The analogous change in the integration scheme for the complete equations (Table I) is also effected by merely altering the sequence of the forward integration scheme. The original and resequenced schemes may be summarized as follows:

Step	Original Sequence	Resequenced
1	Calculate $\partial u/\partial t$	Calculate $\partial u/\partial t$
2	Calculate $\partial v/\partial t$	Calculate $\partial v/\partial t$
3	Calculate $\partial \rho/\partial t$	$u(t + \Delta t) = u(t) + (\partial u/\partial t)\,\Delta t$
4	Calculate $\partial H/\partial t$	$v(t + \Delta t) = v(t) + (\partial v/\partial t)\,\Delta t$

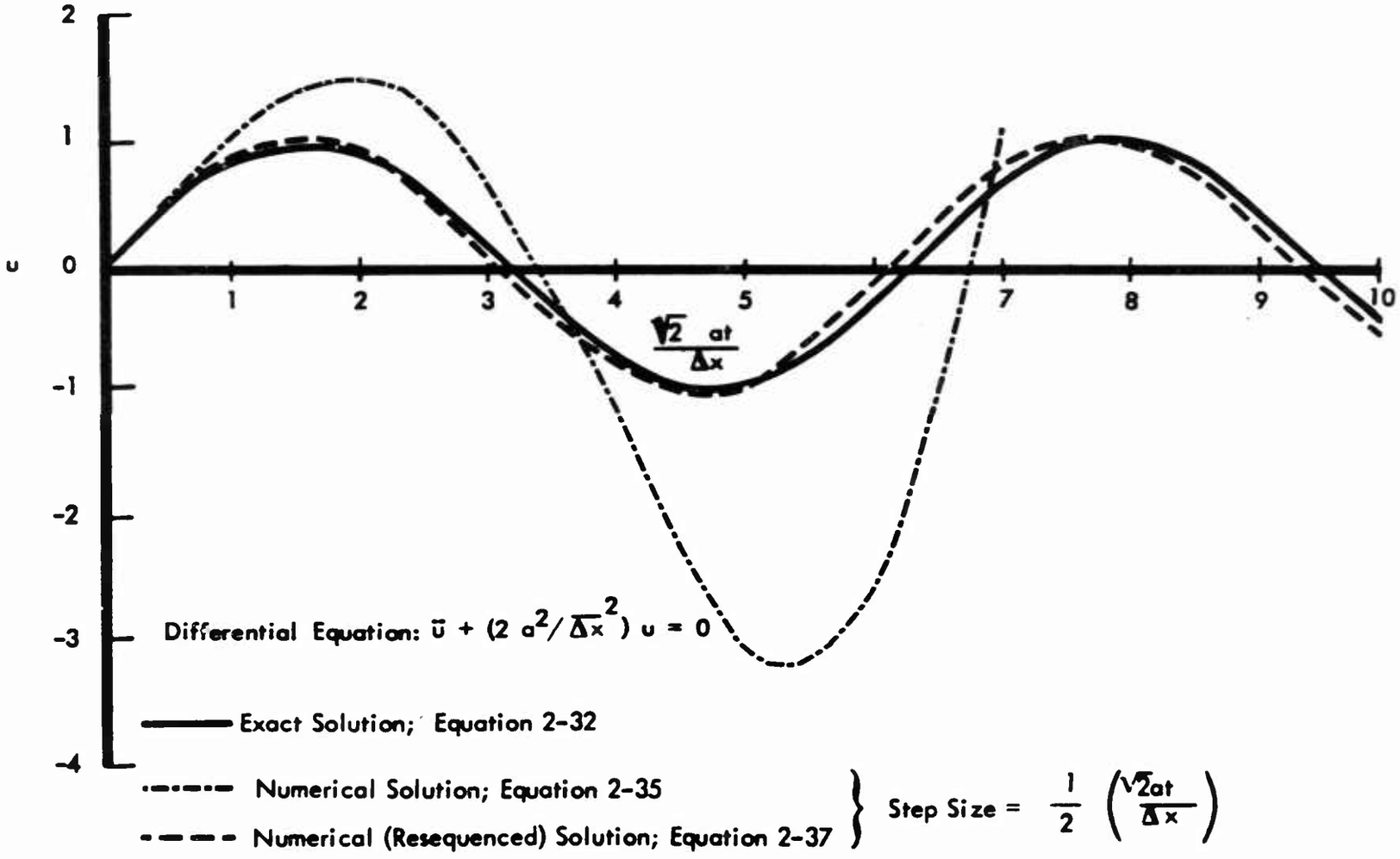

Figure 2-1: EFFECT OF RESEQUENCING ON NUMERICAL STABILITY

5	$u(t + \Delta t) = u(t) + (\partial u/\partial t)\,\Delta t$	Calculate $\partial \rho/\partial t$
6	$v(t + \Delta t) = v(t) + (\partial v/\partial t)\,\Delta t$	Calculate $\partial H/\partial t$
	etc.	etc.

Unfortunately, it is not possible to present an analytic solution (such as Equation 2-35) to determine the stability characteristics of the resequenced scheme. As with all complex numerical schemes, the most complete (and therefore most rigorous) information is obtained by numerical experiments, the results of which show the same trends as do analytic solutions of Equations 2-34 and 2-36, although they are naturally less simple (see Figures 2-2, 2-3, and 2-4).

The effect of resequencing on amplitude is illustrated by a simple flow field calculation in which all velocities were initially zero, and all pressures were set at 100 psf except for one point, at which the pressure was set at 101 psf. In a numerically stable solution, there are irregular velocity and pressure fluctuations that will remain approximately constant in the long run. The amplitudes will increase if the calculation is numerically unstable.

Two calculations are presented in Figure 2-2 showing the behavior of velocity fluctuations as calculated by the original and by the resequenced programs. The resequenced calculation appears to be entirely stable, while that with the original sequence was divergent. The slow nature of the divergence is illustrated by the fact that 200 time steps were made before any obvious increase in amplitude occurred. Later calculations of the same problem with a time increment five times larger than that used in the cases shown in Figure 2-2 also remained stable with the resequenced scheme. It was found that the resequenced calculations remain stable for

$$\Delta t = \frac{1.5\,\Delta x}{\sqrt{\gamma RT}} \tag{2-39}$$

so that the long-term accumulation of errors is apparently entirely eliminated.

The effect of Δt on the frequency of oscillation early in the calculation is shown in Figure 2-3. Again, the effect is similar to that exhibited by Equation 2-37, with the calculations for the larger Δt showing a small phase difference.

It will be recalled that the forward integration is a first-order scheme, neglecting all time derivatives except the first. It is believed that the resequenced scheme is in effect a second-order method, i.e., equivalent to retaining two terms of a Taylor expansion in time. This is difficult to prove for so complex a system, but an indication is provided by the effect of step size on the computation. In a first-order scheme the first neglected term is

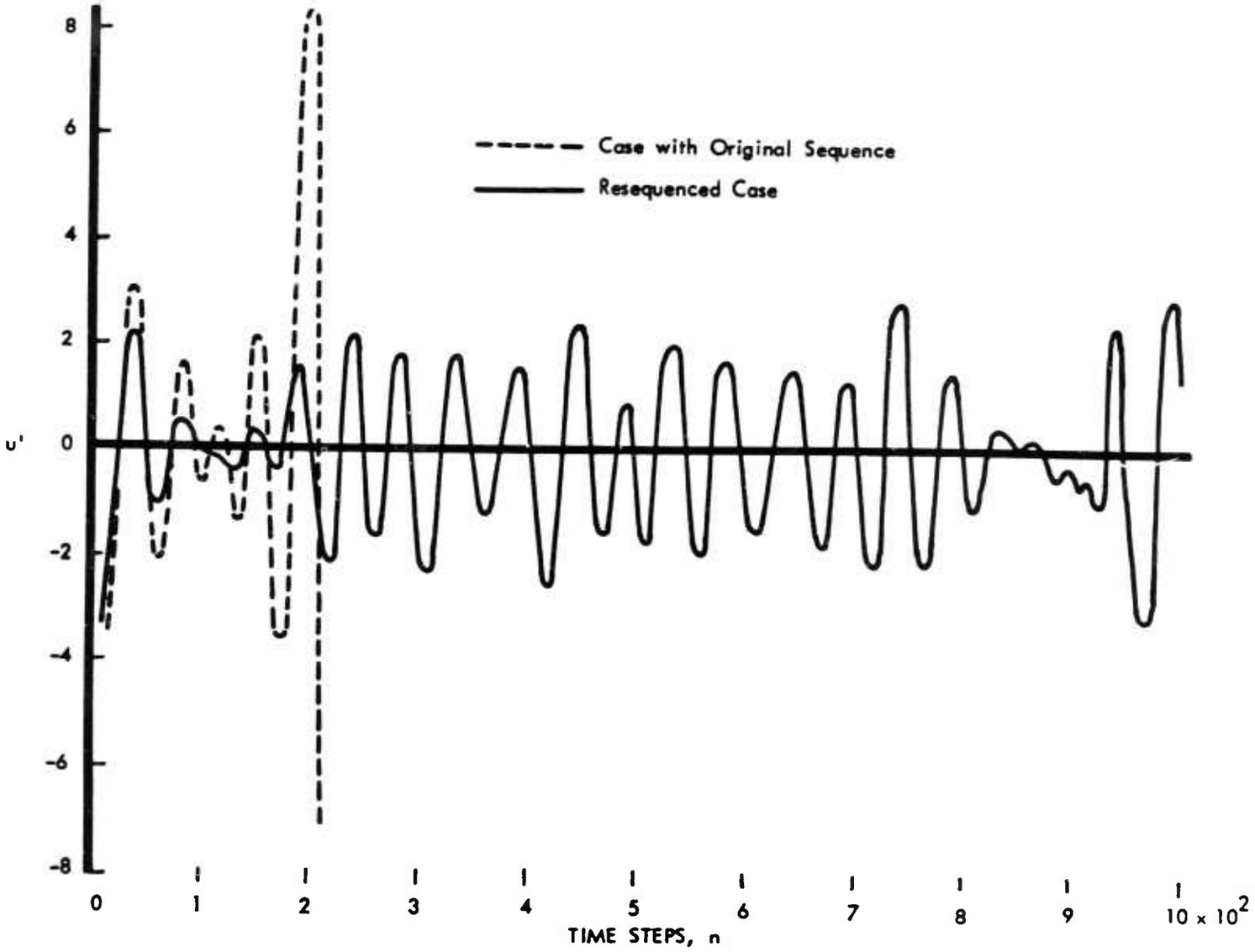

Figure 2-2: EFFECT OF RESEQUENCING ON NUMERICAL STABILITY

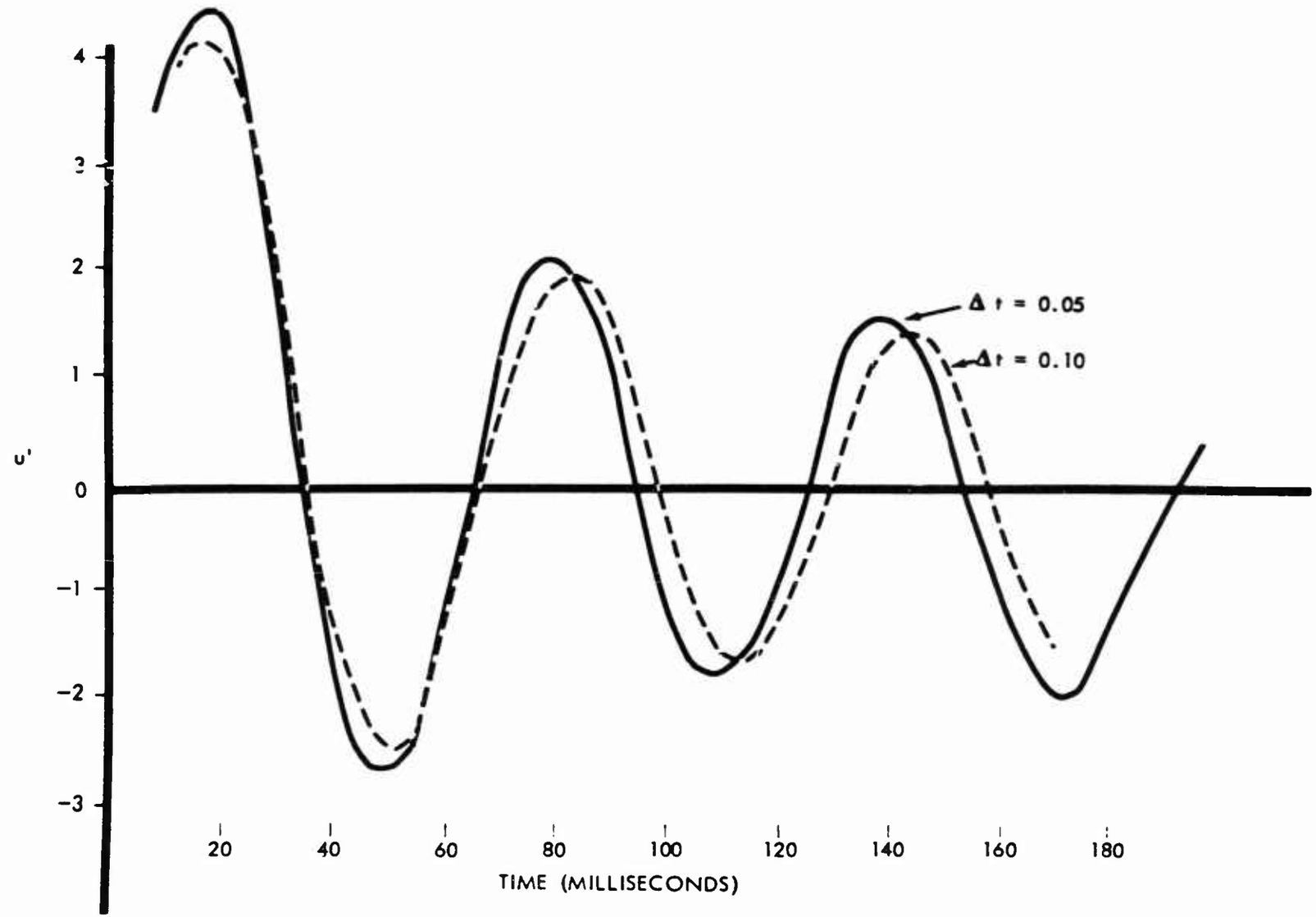

Figure 2-3: EFFECT OF Δt ON PERTURBATION FREQUENCY

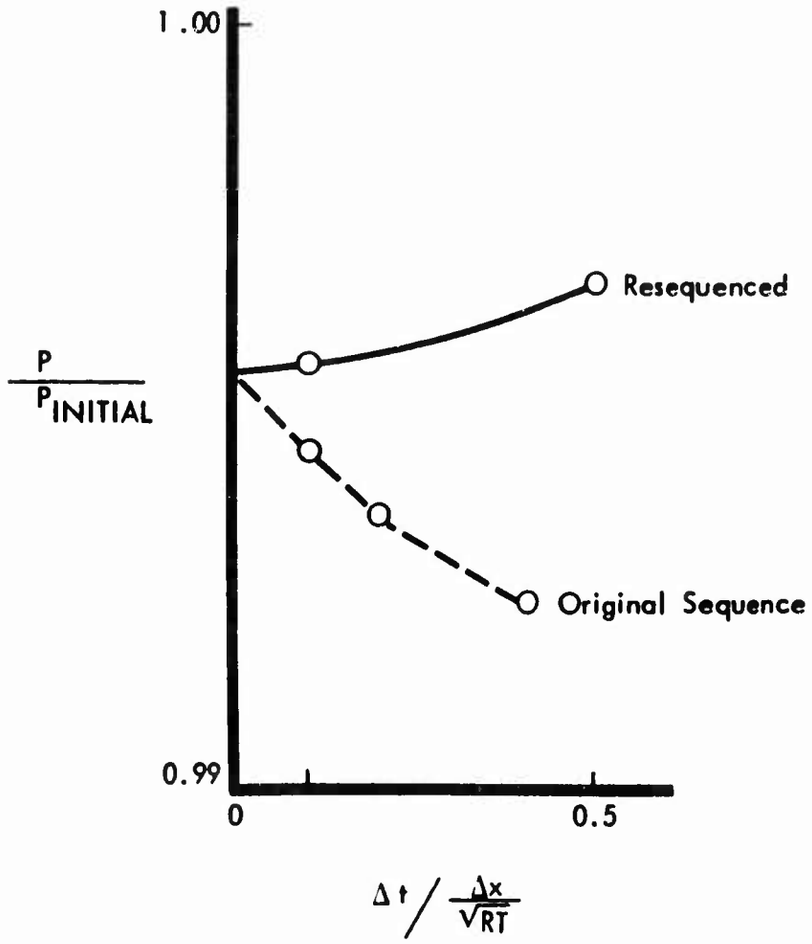

Figure 2-4: EFFECT OF STEP SIZE

$$\left(\frac{\partial^2 u}{\partial t^2}\right)\frac{\Delta t^2}{2} \qquad (2\text{-}40)$$

The error at time t is the sum of the above:

$$\epsilon(t) = \sum_0^t \frac{\partial^2 u}{\partial t^2}\frac{\Delta t^2}{2} = \sum_0^t \left(\frac{\partial^2 u}{\partial t^2}\frac{\Delta t}{2}\right)\Delta t = \left(\overline{\frac{\partial^2 u}{\partial t^2}}\frac{\Delta t}{2}\right) t = \left(\overline{\frac{\partial^2 u}{\partial t^2}}\frac{t}{2}\right)\Delta t \qquad (2\text{-}41)$$

where the bar indicates an average value of the entire time period. The important characteristic of error is the dependence of the final error on Δt. For a first-order system the accumulated error is seen to vary linearly with Δt. By a similar argument it is found that the accumulated error in a second-order scheme varies as the square of the step size.

The effect of step size on calculations with the complete equations is shown in Figure 2-4. It is seen that, with the original sequence, the effect of Δt is in fact approximately linear; for the resequenced calculation the effect is much smaller, and varies as the square of Δt. *

Upon further examination it appears that the resequenced scheme may be thought of as a central difference in time. Consider the following calculations:

Time	Calculation
0	$\left(\frac{\partial \rho}{\partial t}\right)^0 = f(\rho^0, H^0, u^0, v^0)$
	$\left(\frac{\partial H}{\partial t}\right)^0 = f(\rho^0, H^0, u^0, v^0)$
	$\rho^{1/2} = \rho^0 + \left(\frac{\partial \rho}{\partial t}\right)^0 \frac{\Delta t}{2}$
	$H^{1/2} = H^0 + \left(\frac{\partial H}{\partial t}\right)^0 \frac{\Delta t}{2}$
$t = \Delta t/2$:	$\left(\frac{\partial u}{\partial t}\right)^{1/2} = f(\rho^{1/2}, H^{1/2}, u^0, v^0)$
	$\left(\frac{\partial v}{\partial t}\right)^{1/2} = f(\rho^{1/2}, H^{1/2}, u^0, v^0)$
	$u^1 = u^0 + \Delta t\left(\frac{\partial u}{\partial t}\right)^{1/2}$
	$v^1 = v^0 + \Delta t\left(\frac{\partial v}{\partial t}\right)^{1/2}$

* Incidentally, Figure 2-4 illustrates the previous point that there may be many numerical analogs of a differential equation that approach the exact solution in the limit, but are not equivalent for any finite value of Δt.

Time	Calculation
$t = \Delta t$:	$\left(\frac{\partial \rho}{\partial t}\right)^1 = f\ (\rho^{1/2},\ H^{1/2},\ u^1,\ v^1)$
	$\left(\frac{\partial H}{\partial t}\right)^1 = f\ (\rho^{1/2},\ H^{1/2},\ u^1,\ v^1)$
	$\rho^{3/2} = \rho^{1/2} + \Delta t \left(\frac{\partial \rho}{\partial t}\right)^1$
	$H^{3/2} = H^{1/2} + \Delta t \left(\frac{\partial H}{\partial t}\right)^1$
$t = \frac{3}{2}\Delta t$:	$\left(\frac{\partial u}{\partial t}\right)^{3/2} = f\ (\rho^{3/2},\ H^{3/2},\ u^1,\ v^1)$
	$\left(\frac{\partial v}{\partial t}\right)^{3/2} = f\ (\rho^{3/2},\ H^{3/2},\ u^1,\ v^1)$
	$u^2 = u^1 + \Delta t \left(\frac{\partial u}{\partial t}\right)^{3/2}$
	etc.

In this scheme it is seen that each derivative is computed at the midpoint of each integration interval. By comparing the above with the previous listing of the resequenced calculations it is seen that only two differences exist:

1) The very first step is for $(1/2)\Delta t$;

2) The time derivative calculations are mixed, involving two variables at the n^{th} level, the other two at the $(n + 1/2)^{th}$ level.

Calculations were made in which both of these differences were removed. First, a calculation was made using $(1/2)\Delta t$ for the first step. As might be expected, the small change in ρ and H occurring in a half of a time increment had no observable, lasting effects, since typical calculations involved hundreds of iterations.

Other calculations were made in which the mixing of variables was eliminated from the time derivative calculations. This was done by replacing (for example) u^n with $u^{n+1/2}$, using

$$u^{n+1/2} = u^n + \frac{1}{2}\Delta t\ \dot{u}^n$$

These calculations showed only minor (fourth-place) differences after more than 100 iterations.

A time-centered scheme is easily shown to be second order by Taylor expansions about the points $t = t_0$ and $t = t_0 + \Delta t/2$. Expanding about t_0:

$$u(t + \Delta t) - u(t) = \Delta t \left(\frac{\partial u}{\partial t}\right)_0 + \frac{\Delta t^2}{2}\left(\frac{\partial^2 u}{\partial t^2}\right)_0 + \ldots \qquad (2\text{-}42)$$

The expansion about $t_0 + \Delta t/2$ is:

$$u(t + \Delta t) - u(t) = \Delta t \left(\frac{\partial u}{\partial t}\right)_{1/2} + \frac{\Delta t^3}{3!}\left(\frac{\partial^3 u}{\partial t^3}\right)_{1/2} + \ldots \qquad (2\text{-}43)$$

It is seen that the first neglected term in the centered scheme is of the order Δt^3. Thus it is seen that the resequenced scheme used here has the behavior of a second-order scheme, although it is not exactly such. Since the resequenced program involves no more calculations than the original-sequence program, the useful speed of computation has been greatly increased by its use.

NUMERICAL FORMULATION OF BOUNDARY LAYER STABILITY PROBLEM

The solution of any physical problem involves two distinct phases: formulation of the general laws governing the physical processes, and specification of the unique conditions that characterize a particular problem. The discussion so far has been entirely concerned with the numerical formulation of the general laws governing fluid flow. We now describe the conditions that characterize the problem of boundary layer stability. The conditions to be determined are the conditions that apply at the boundaries of the spatial field and the initial values of the perturbation quantities.

Satisfactory specification of the spatial boundary conditions proved to be one of the most difficult parts of the present study. Since the entire study is concerned with the behavior of small disturbances, any disturbance introduced by slightly incorrect specification of boundary conditions could invalidate the results. On the other hand, the boundary conditions in time (initial conditions) are unimportant in stability calculations by the present method as will be shown in the next section. However, with the present method the history of a disturbance can be calculated as well, which is more nearly what is required by a transition method. For such a calculation the initial disturbance is important. A further discussion appears in Section IV.

PHYSICAL DESCRIPTION

In the present analysis, the physical problem to be solved is the stability of a two-dimensional laminar flow boundary layer on a flat plate. Except within the boundary layer, the flow is parallel to the x axis and constant. Within the boundary layer the velocity decreases to zero, and change in other flow properties may occur as well. The flow within the boundary layer can be computed with a reduced set of equations known as the boundary layer equations. The solutions used in this report are obtained by numerical integrations using the computer program described in Reference 26. The program has the capability of calculating real gas

boundary layers for nonsimilar flows, but all cases considered in this report are for the flow of an ideal gas over a flat plate. The Sutherland viscosity law was used with a constant Prandtl number of 0.71, and the specific heat is constant at 0.24 Btu/lb. The plate is impermeable, so that the vertical velocity component is zero at the wall.

BOUNDARY CONDITIONS

It is shown in texts on partial differential equations that the number of boundary conditions required on each dependent variable with respect to a specific independent variable is equal to the order of the highest derivative with respect to that independent variable. Thus, the continuity equation, which contains only first derivatives, requires only one boundary condition on each dependent variable involved (u, v, and ρ) for each independent variable (x and y). The momentum and energy equations contain second derivatives of u and v with respect to x and y, and so require two boundary conditions in each direction.

x-Direction Boundary Conditions

Since the boundary layer Reynolds number decreases with distance upstream, it can be assumed that all perturbations are zero at the plate leading edge. Downstream, however, the flow presumably becomes turbulent and cannot be exactly prescribed, even ideally. In the study of flow stability, however, previous investigations have shown that it can be assumed that the disturbances are traveling waves of the form

$$u'(x) = \|u'\| \sin \alpha(x - x_o) \qquad (2\text{-}44)$$

where α is the wave number and x_o is arbitrary. The double bar $(\| \ \|)$ designates the amplitude of the perturbation. Note that $\|u'\|$ is independent of x, but may vary with time.

It will be seen that, according to Equation 2-44, the disturbance waves extend infinitely far upstream and downstream. While this is clearly incorrect, the use of Equation 2-44 in the present formulation merely implies that the departure of the disturbance wave from a purely sinusoidal wave has no important effect on the local time history of the disturbance. This latter assumption, which is used in all stability calculations, has been exhaustively examined and is believed to be valid, provided that

$$\left(\alpha N_{Re}\right)^{-1/3} \ll 1$$

For smaller values of αN_{Re}, the steady-flow vertical velocity component $\bar{v}$ becomes as important as some of the terms that are retained in the stability theory. For a further discussion of this point see Paragraph 5.1 of Reference 27, Appendix H of Reference 20, and Reference 28. In passing, we should note that the inclusion of the steady-flow $\bar{v}$ terms is apparently easily possible with the present method, but has not yet been done.

With the use of Equation 2-44 the need for further specification of boundary conditions in the x direction is eliminated. The x derivatives can be specified simply and exactly as follows:

$$\left(\frac{\partial u'}{\partial x}\right)_{x=x_o} = \alpha\, u'(x_o + \lambda/4)$$

$$\left(\frac{\partial u'}{\partial x}\right)_{x=x_o+\lambda/4} = -\alpha\, u'(x_o) \qquad (2\text{-}45)$$

$$\left(\frac{\partial^2 u'}{\partial x^2}\right)_{x_o} = -\alpha^2\, u'(x_o)$$

etc.

Thus it is necessary to compute the perturbation quantities at only two x locations separated by a quarter-wavelength, and the amount of work involved in any particular computation is greatly reduced. It has been found that the accuracy of the calculation is also improved by the use of Equation 2-44 and the interpretation of the results greatly simplified as well. Although the use of this equation restricts the results to disturbances of a specific wavelength, the present method is still somewhat more general than previous results, which are all based on the more restrictive assumption

$$u' = \|u'\| \sin\left[\alpha(x-x_o) - \beta t\right] \qquad (2\text{-}46)$$

(See Equation 2-1).

y-Direction Boundary Conditions

The boundary conditions imposed at the surface of the plate (y = 0) are:

$$u' = v' = H' = 0 \qquad (2\text{-}47)$$

$$\partial P'/\partial y = 0 \qquad (2\text{-}48)$$

The conditions on u' and v' are the usual conditions of boundary layer theory. The condition on H' assumes that the response of the body to the temperature fluctuations in the boundary layer is negligible. This condition has been commonly assumed in previous work but is of course realistic only under certain conditions. For a plate surface of poor conductivity, some surface temperature response may occur. As with the vertical velocity effect, the response of the surface to the temperature fluctuations appears to be easily incorporated in the present method, but has not yet been attempted. The boundary condition on pressure is used in conjunction with the H' condition to establish the density perturbation at the plate surface. The condition of Equation 2-48 is derived from the y-momentum equation and is used as a boundary condition on the continuity equation.

The outer boundary conditions are that all perturbations are zero at y = infinity. In a finite difference method it is not possible to calculate over an infinite array, and the boundary condition at infinity must be replaced by some condition at a finite value of y. It was at first assumed that the disturbance could be set equal to zero at some large value of y, but it was found that even when the outer boundary was removed to a distance of 16 boundary layer thicknesses, disturbances occurred that were traced to the outer boundary. The type of behavior observed is shown in Figure 2-5, which shows the history of the vertical velocity component at the point $y = \delta^*$. After the initial disturbance the flow is seen to be well-behaved until approximately t = 100 milliseconds, when both of the two cases shown begin to oscillate. In case I the condition

$$u' = v' = \rho' = H' = 0 \tag{2-49}$$

was applied at $y = 12\ \delta^*$. By applying the same condition at $y = 50\ \delta^*$ it was shown that the observed disturbance did not appear until much later, thus identifying the disturbance as a boundary reflection. In an effort to discover a less reflective boundary, case II was run with the condition

$$\frac{\partial u'}{\partial y} = \frac{\partial v'}{\partial y} = \frac{\partial \rho'}{\partial y} = \frac{\partial H'}{\partial y} = 0 \tag{2-50}$$

at $y = 12\ \delta^*$. As shown, the reflection was somewhat delayed, but the ultimate effect was even more undesirable than in case I.

The presence of the large disturbance shown is not to be expected according to the stability theory, which predicts that the disturbance should have decayed to less than 5 percent of the initial value at $y = 12\ \delta^*$, and the reflection should have been even smaller. This apparent discrepancy between the present result and the classical theory is due to the increased generality of the present method. By allowing arbitrary time-variations, the present method includes acoustic waves as well as the disturbance waves treated by the stability theory. The acoustic waves travel to the outer boundary and return with virtually no loss of energy. The time required for a sound wave to travel from the point of initial disturbance to the outer boundary and back corresponds well to the time of the reappearance of the disturbance in case I.

Boundary reflections were finally eliminated by a numerical "wave trap." Rather than a single outer boundary, two were chosen denoted by y_{match} and y_{max}. In the boundary region between y_{match} and y_{max} all perturbation quantities are periodically replaced by:

$$u(y) = u(y_{match})\, e^{-\alpha(y-y_{match})} \tag{2-51}$$

The condition in Equation 2-51 has the effect of suppressing disturbance waves within the boundary region. The suppression is done with sufficient frequency

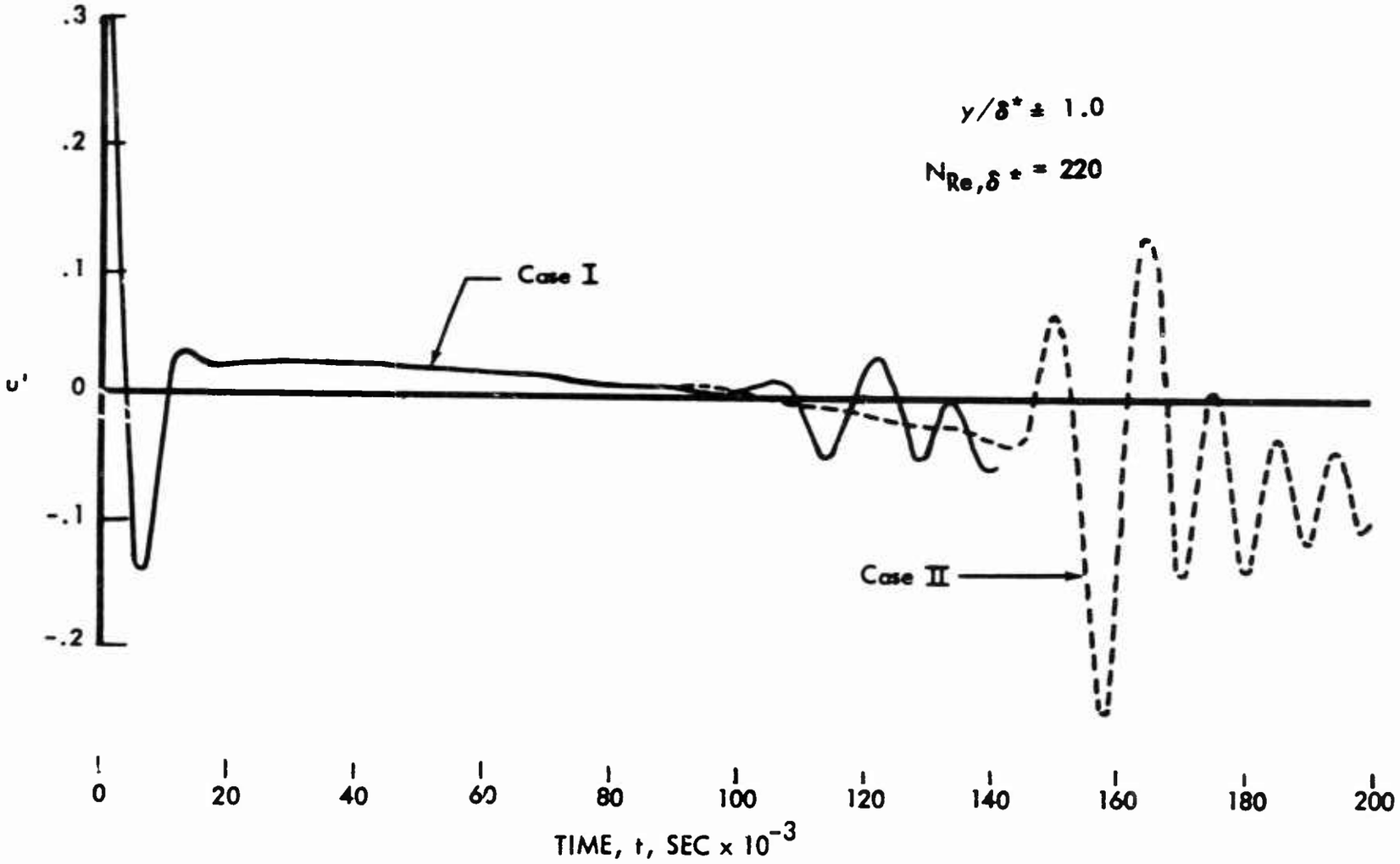

Figure 2-5: EFFECT OF OUTER BOUNDARY CONDITION

so that disturbances reflected from the outer boundary cannot travel inward past y_{match} in the period between suppressions. Thus, y_{match} becomes the equivalent of an open window that absorbs disturbance waves. The actual values of y_{match} and y_{max} were selected by numerical experiment, being moved outward until no effect on the numerical solution was observed. Immediately after applying Equation 2-51, all perturbation quantities are averaged as follows:

$$u'_{ave} = \frac{u'(y+\Delta y) + 2u'(y) + u'(y-\Delta y)}{4} \tag{2-52}$$

This is done to eliminate oscillations of wavelength $4\Delta y$, which are shown in Reference 29 to be spurious. The use of Equation 2-52 also has the effect of minimizing discontinuities in derivatives at y_{match} introduced by the use of Equation 2-51. When Equation 2-51 is applied in the manner described, the boundary conditions at y_{max} were found to have no effect on the solution. The condition used in most of the calculations shown are:

$$u' = \frac{\partial v'}{\partial y} = \rho' = H' = 0 \tag{2-53}$$

The values of y_{match} and y_{max} used herein are approximately two and four boundary layer thicknesses, respectively. It has been found that if y_{match} is less than about one and one-fourth boundary layer thicknesses the results may be adversely affected.

RESULTS OF STABILITY CALCULATIONS

The majority of the stability calculations were made for two cases, one subsonic and one hypersonic. The two cases were selected to avoid the possibility of devising a method that was applicable in only one speed regime. This would easily have been possible since the relative magnitude of the various terms in the equations depends on the Mach number.

The subsonic case was for a Mach number of 0.4 with the wall temperature equal to the free-stream temperature. The Blasius incompressible flow solution was used for the steady-state velocity profile. The temperature and density profiles were obtained by subtraction of the kinetic energy from the total enthalpy, and by the equation of state, respectively.

The subsonic conditions were chosen as a compromise between the limitations of existing knowledge and the limitations of the present method. As stated previously, it is not possible to treat an exactly incompressible flow by the present numerical method since the speed of sound is infinite in that case. At Mach number 0.4, the compressibility effects are still very small, but the flow velocities are such that the stability can be evaluated in a reasonable amount of real time.

The hypersonic calculations were for Mach 7, which was chosen as representative of experimental conditions. Both adiabatic and cooled wall conditions were considered. The steady-state profiles were calculated with the Boeing Nonsimilar Boundary Layer Program (Ref. 26), which uses a finite difference method that includes all fluid property variations. Only ideal gas properties were considered in the present study, however.

After a description of the results that should be anticipated, the subsonic results will be presented. The next section will present a discussion of the Mach 7 results, and also the results that have been obtained at Mach numbers 2 to 10.

EXPECTED BEHAVIOR

As described previously, the classical method obtains the amplification rates only of disturbances that are of a certain characteristic form that is itself part of the solution. There will in general be many of these characteristic forms for any given Reynolds number and wavelength, known as modes, each with a differing amplification rate.

The characteristic disturbance profile will not be observed at any particular instant, however. It is only the values of $\|Q'\|$ that are steady (see Equation 2-43), while the instantaneous perturbations fluctuate rapidly. The usual experimental technique employs electrically heated wires; the rate of cooling can be related to flow velocity. The hot-wire method does not have a sufficiently rapid time response to resolve the individual velocity fluctuations, but rather provides an averaged value, which is proportional to $\| u'\|$.

Some typical experimental subsonic disturbance profiles are presented in Figure 2-6. The profiles shown were obtained by Tani and Komoda and reported in Reference 30. It will be seen that the perturbation amplitude has a minimum at approximately $y/\delta = 0.7$. According to the classical theory, a phase shift of 180 degrees occurs at this point; in many papers the upper branch is plotted as negative values. The experimental phase angles (corresponding to x_0 in Equation 2-44) are also shown in Figure 2-6. It is seen that the expected phase shift was observed. The significance of the theoretical results that follow will be more apparent to the reader if the characteristics shown in Figure 2-6 are kept in mind.

With the classical method only the behavior of a specific disturbance mode can be calculated, while with the present method any initial disturbance can be imposed. However, if the classical theory is correct, an arbitrary initial disturbance should be viewed as a resultant of many modes, most of which will be damped. Thus, it is expected that an arbitrary initial disturbance would at first decay rapidly. After a time, however, the most unstable mode should become dominant, and the vertical distribution of the disturbance amplitudes should be steady, although the disturbances themselves travel in the streamwise direction. Once the steady disturbance profile is established, its amplitude would be expected to increase if the flow is unstable and to decrease if the flow is stable.

It is important to bear in mind that it is only after the characteristic profile has developed that the flow stability can be determined, since a disturbance of any other form will be damped. After the critical profile had been found, the first few calculations were expected to indicate the stability or instability of the flow. It was this expected behavior that led to the use of the conditions specified by Equations 2-50 and 2-51. After applying those conditions the subsequent calculations can be regarded as a stability evaluation of a particular disturbance profile. When the conditions are reapplied after a number of calculations, a new profile is obtained and the results of the next few calculations indicate its stability.

However, the computed profiles are very little changed by the application of Equations 2-50 and 2-51, and the changes that are made are primarily the suppression of spurious boundary reflections and oscillations. Further study of the results obtained has convinced the authors that the conditions of Equations 2-50 and 2-51 need not be regarded as reinitializing the calculation, but that the entire calculated disturbance history is valid.

As shown below, all of the subsonic calculations and many of the supersonic calculations have led to steady profiles as expected. In some of the supersonic cases a cyclic behavior has been observed, the significance of which is still not clear.

SUBSONIC RESULTS

Development of Disturbance Profiles

The calculated development of subsonic perturbation profiles from initial disturbances is shown in Figure 2-7. To demonstrate that the final profile is independent of the type of initial disturbance, two calculations are shown in this figure. As shown, the initial disturbance is quite different in the two cases. However, after a dimensionless time $\tau = 56$ the two profiles have become essentially identical. Note that since $\tau = \bar{u}_e t/\delta^*$, the results shown in Figure 2-7 also indicate that the disturbance would be transported about 50 boundary layer displacement thicknesses downstream before assuming the characteristic shape. It is now considered that this fact is of more significance than is the determination of the critical Reynolds number. This will be discussed more fully in Section IV.

The values shown in Figure 2-7 are amplitudes, $\|u'\|$, such as would be observed by hot wire techniques. The instantaneous profiles at two specific points in the flow field are shown in Figure 2-8. The three profiles presented illustrate the behavior of the majority of the subsonic cases calculated. The left-hand plot presenting the disturbance profiles at two locations within the field at $\tau = 60$ shows that the profile at $x = x_R$ has developed into the expected characteristic form with a reversal in the sign of the perturbation at about 3/4 of the boundary layer thickness. However, at $x = x_L$ the profile does not have the expected shape. Since it appeared that the characteristic profile had not yet fully developed, further calculations were made. As shown in the center plot by the time $\tau = 72$, the

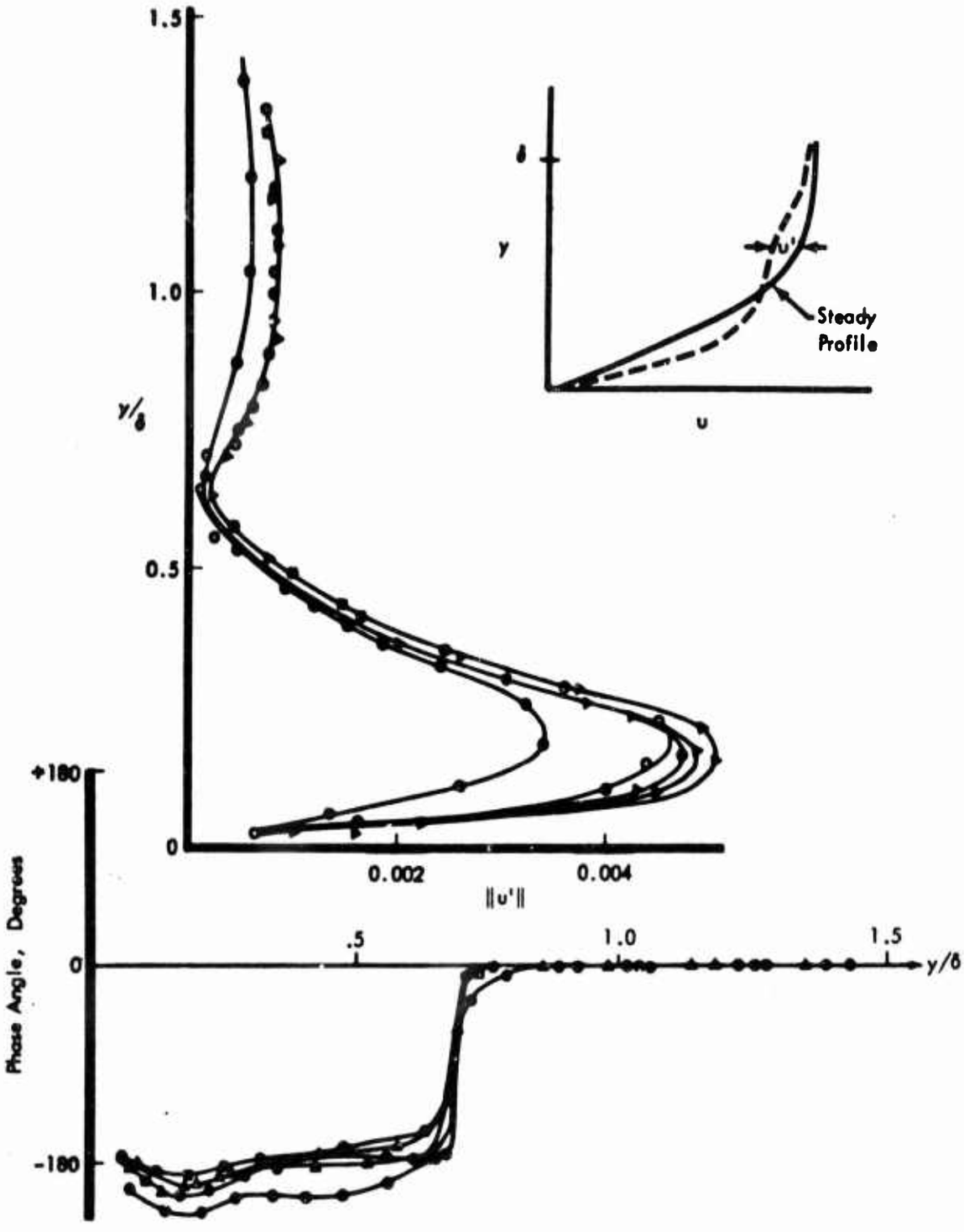

Figure 2-6: EXPERIMENTAL DISTURBANCE PROFILES FROM REFERENCE 30

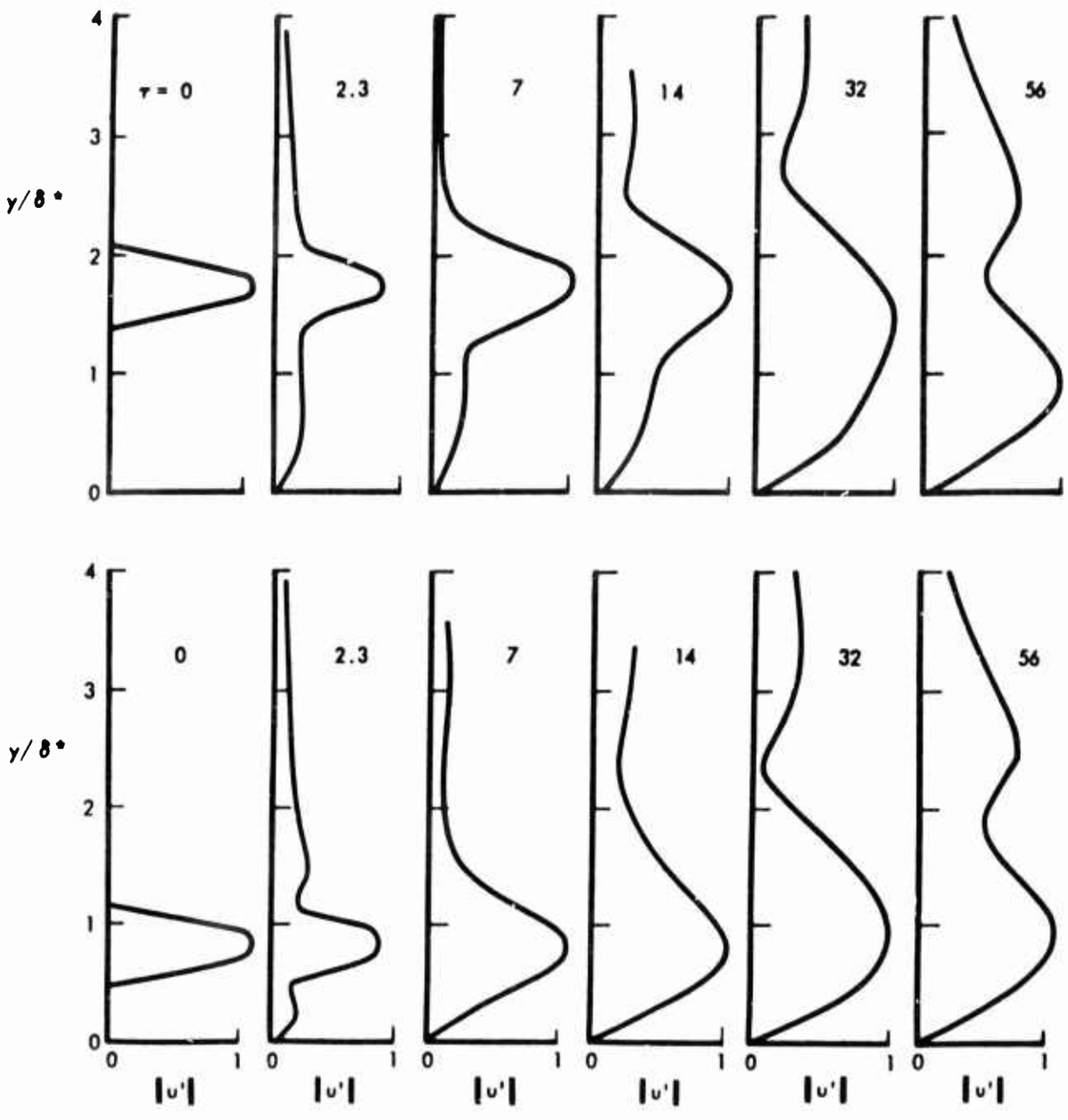

Figure 2-7: DEVELOPMENT OF DISTURBANCE PROFILES — $M_e = 0.4$, $N_{Re,\delta^*} = 4000$

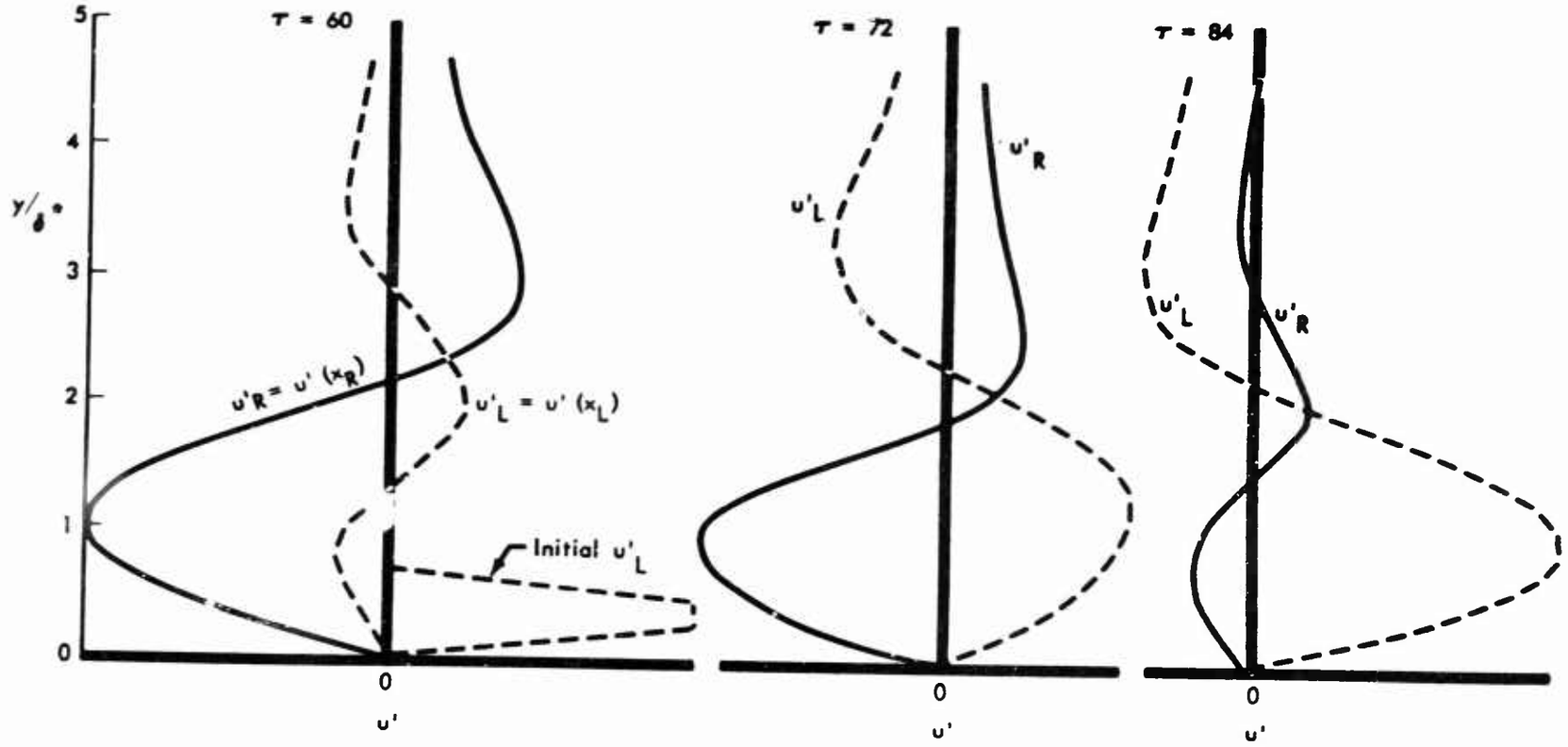

Figure 2-8: VELOCITY DISTURBANCE PROFILES—M_e = 0.4, N_{Re,δ^*} = 200

profile at $x = x_L$ had much improved, but the profile at $x = x_R$ is beginning to depart from the expected behavior. Further calculations showed that at $\tau = 84$ the profile at $x = x_L$ is well developed and of the expected form, but the profile at $x = x_R$ has degenerated and now closely resembles the original profile at $x = x_L$. When still further calculations showed no improvement, the profiles were replotted in polar form with the radius equal to the amplitude of the disturbance velocity, and the angle equal to the phase angle of the disturbance wave. When plotted in polar form all three profiles of Figure 2-8 were found to be nearly identical, as shown in Figure 2-9. Note that the profile shape, and not orientation, determines the $\|u'\|$ profile. From this result it was found that the phase velocities, amplification rates, and other quantities of interest could be determined easily from the polar plots.

The phase loops, as the diagrams such as Figure 2-9 are called, are not precisely of the expected form. According to the classical theory, it is expected that the phase angle is constant through the boundary layer except at the critical layer. At the critical layer a phase shift of 180 degrees is predicted. In the form of Figure 2-9 such a phase plot would be reduced to a straight line through the origin. Considering the approximations in the linear theory, it is to be expected that the 180-degree wave shift may be somewhat smeared out, and so does not occur exactly at the critical line. Comparisons of phase loops from different Reynolds numbers to some extent supports this assumption. It is seen in Figure 2-10 that the phase loop at a Reynolds number of 2000 is considerably thinner than that for a Reynolds number for 500. However, it is still not linear, nor is it closed. Some calculations were also made at a Mach number of 0.1 to determine if the form of the phase loop was a compressibility effect. The Mach number 0.1 result was essentially identical with those for Mach 0.4, however.

Recalling Figure 2-6, it was seen that the experimental phase angles were qualitatively similar to those predicted by the classical theory. On closer inspection, however, it will be seen that there is an appreciable variation in phase angle in the lower part of the boundary layer. When plotted in phase loop form, as has been done in Figure 2-11, the experimental data exhibit significant similarities to the present theoretical results. In neither case is the phase loop closed or straight; the phase angle variation in the lower part of the boundary layer is approximately 45 degrees in both cases. This phase angle relationship is one of the most novel results from the present method. Originally the phase angle variations were highly disconcerting; however, in view of the experimental results, the phase angle variations are taken as evidence of the correctness of the present calculations. The accuracy Tani and Komoda ascribe to their phase angle data is not known, but the measurement of phase angles in the outer branch where $\|u'\|$ is small (and where the greatest departure from the present calculations occurs) must be very difficult.

The very short wavelength calculations by the present method exhibit characteristics that have not yet been fully investigated. A typical profile, shown in Figure 2-12, shows the second maximum in u' that normally occurs at the boundary layer

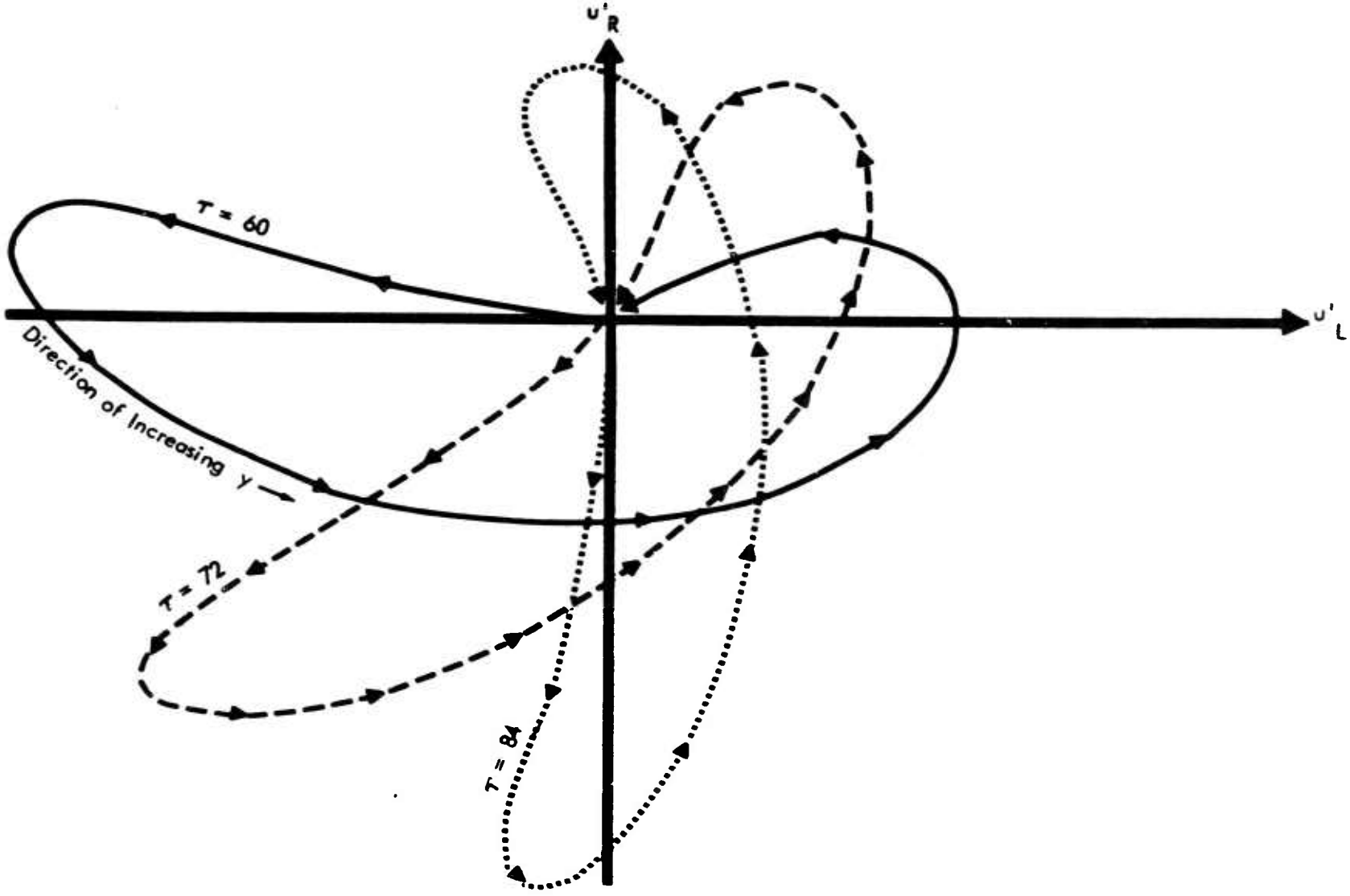

Figure 2-9: PHASE LOOPS — $M_e = 0.4$, $N_{Re,\delta^*} = 200$

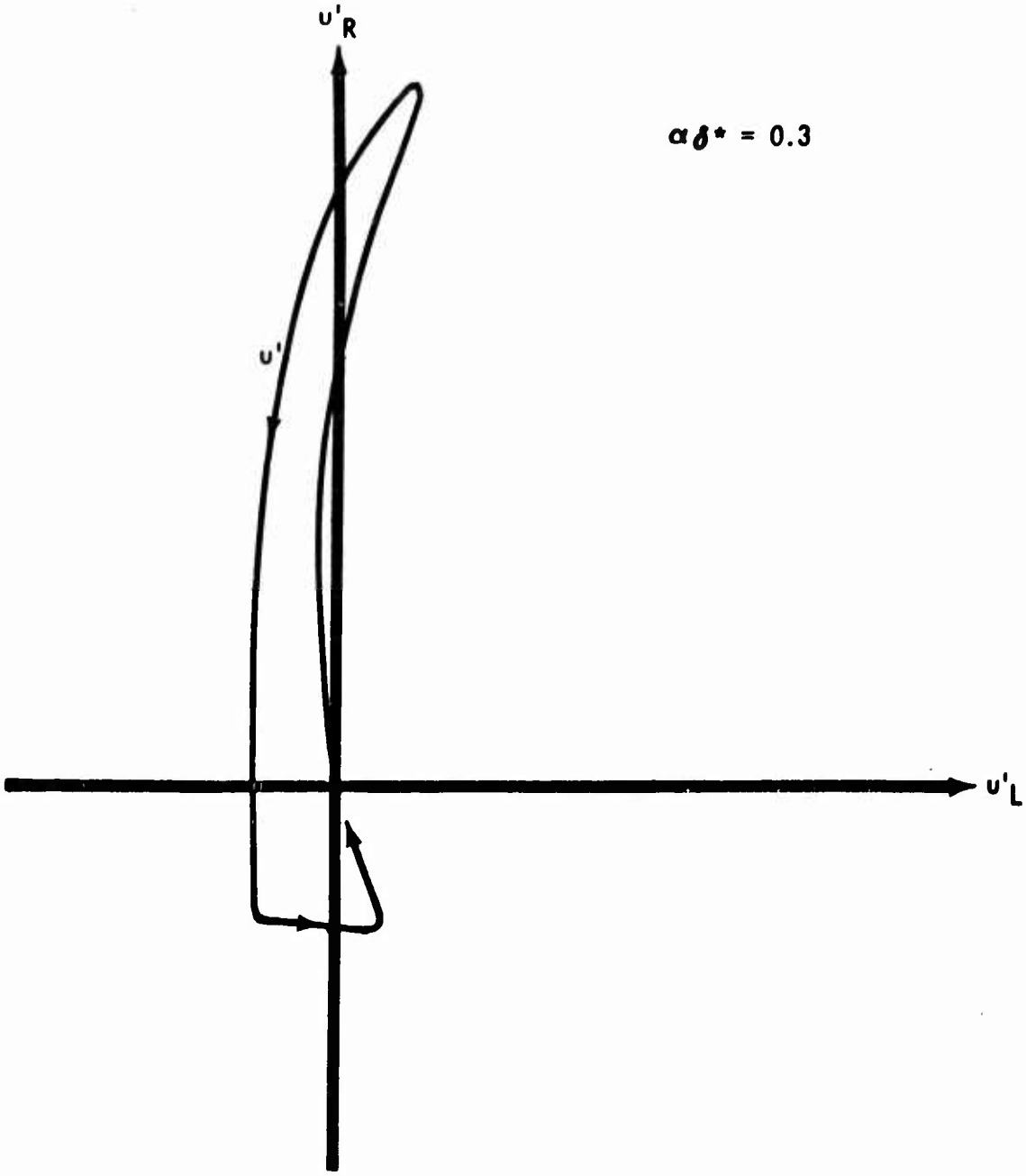

Figure 2-10a: TYPICAL PHASE LOOP — $M_e = 0.4, N_{Re,\delta^*} = 500$

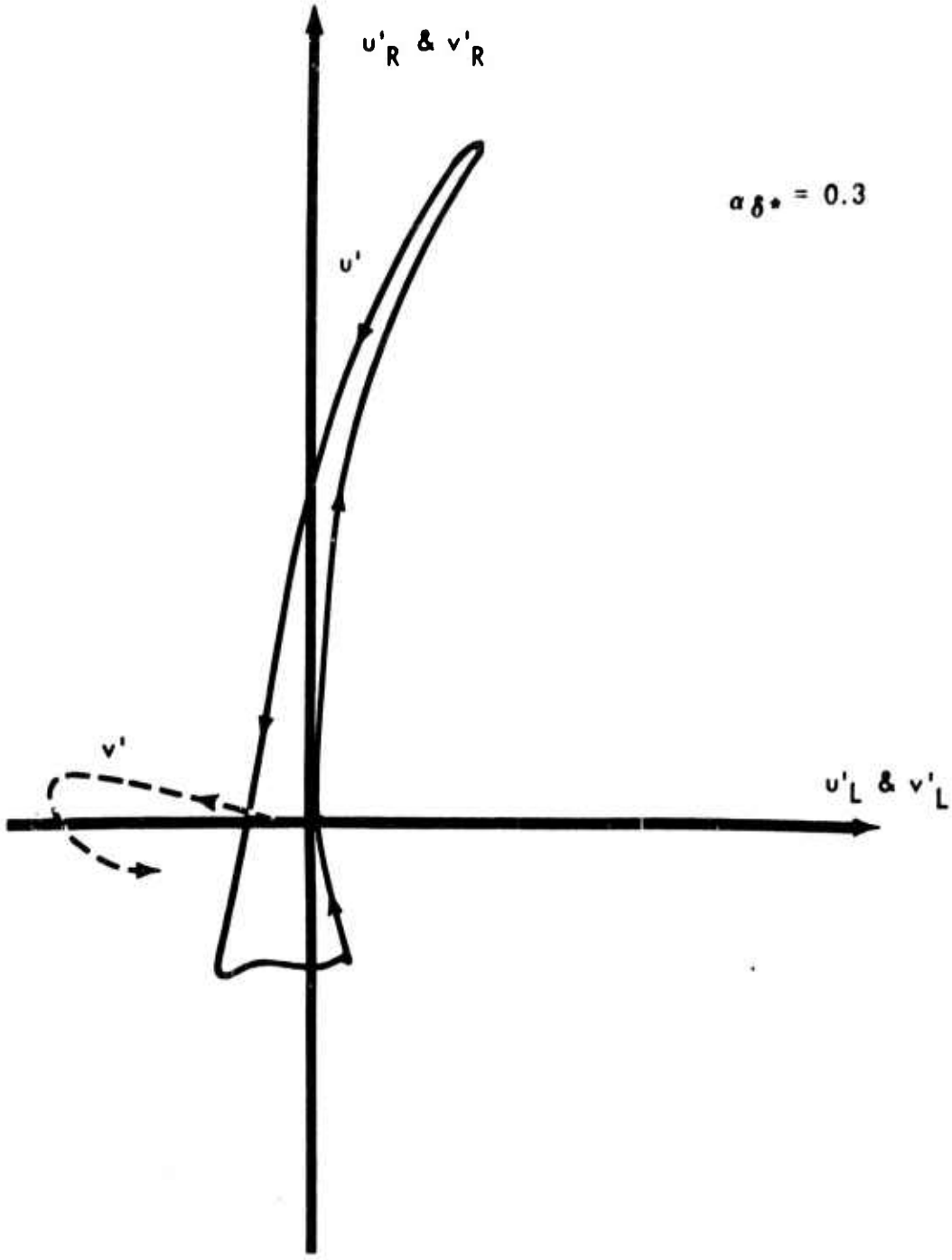

Figure 2-10b: TYPICAL PHASE LOOP — $M_e = 0.4$, $N_{Re,\delta^*} = 2000$

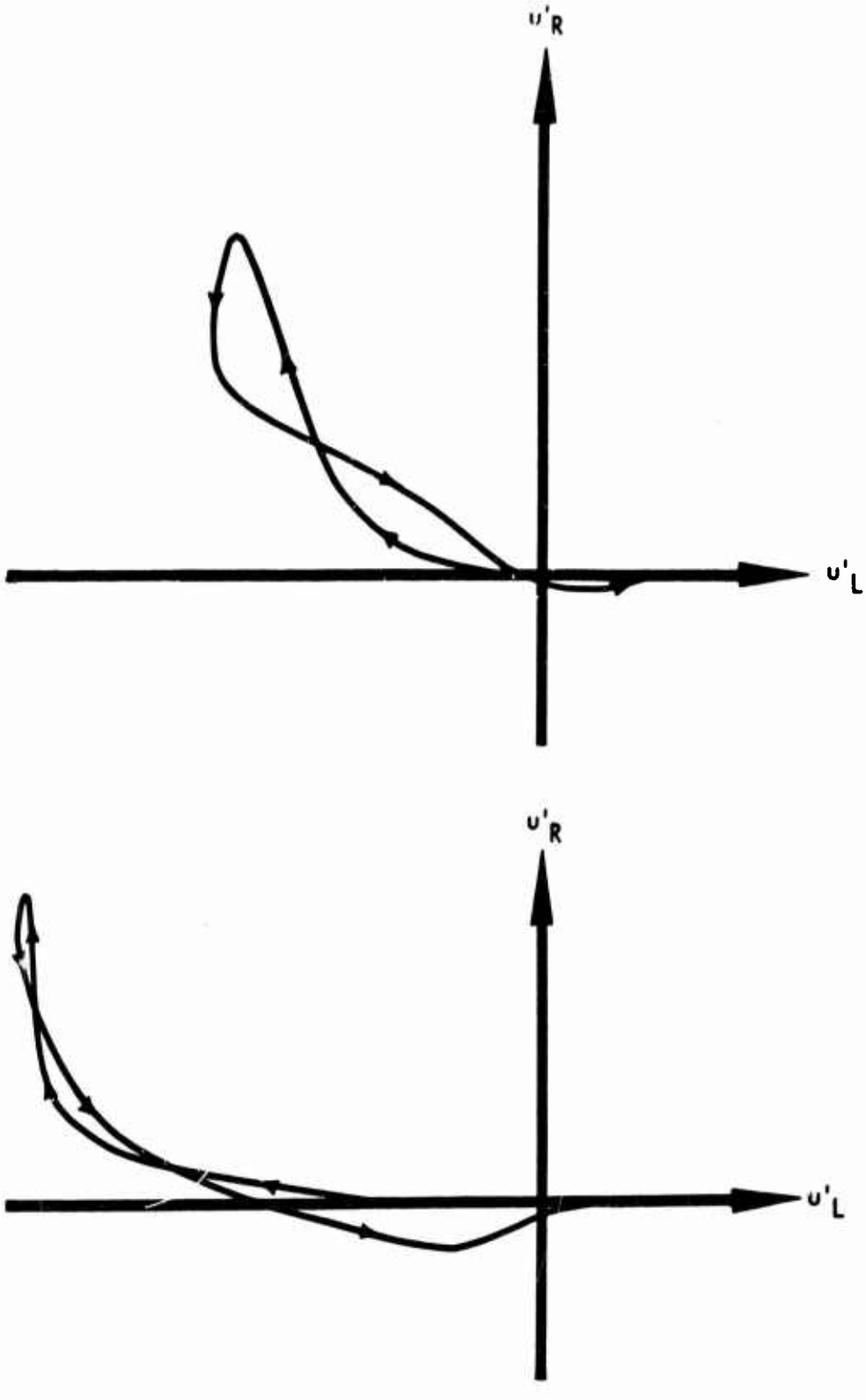

Figure 2-11: EXPERIMENTAL PHASE LOOPS Tani and Komoda (Ref. 30)

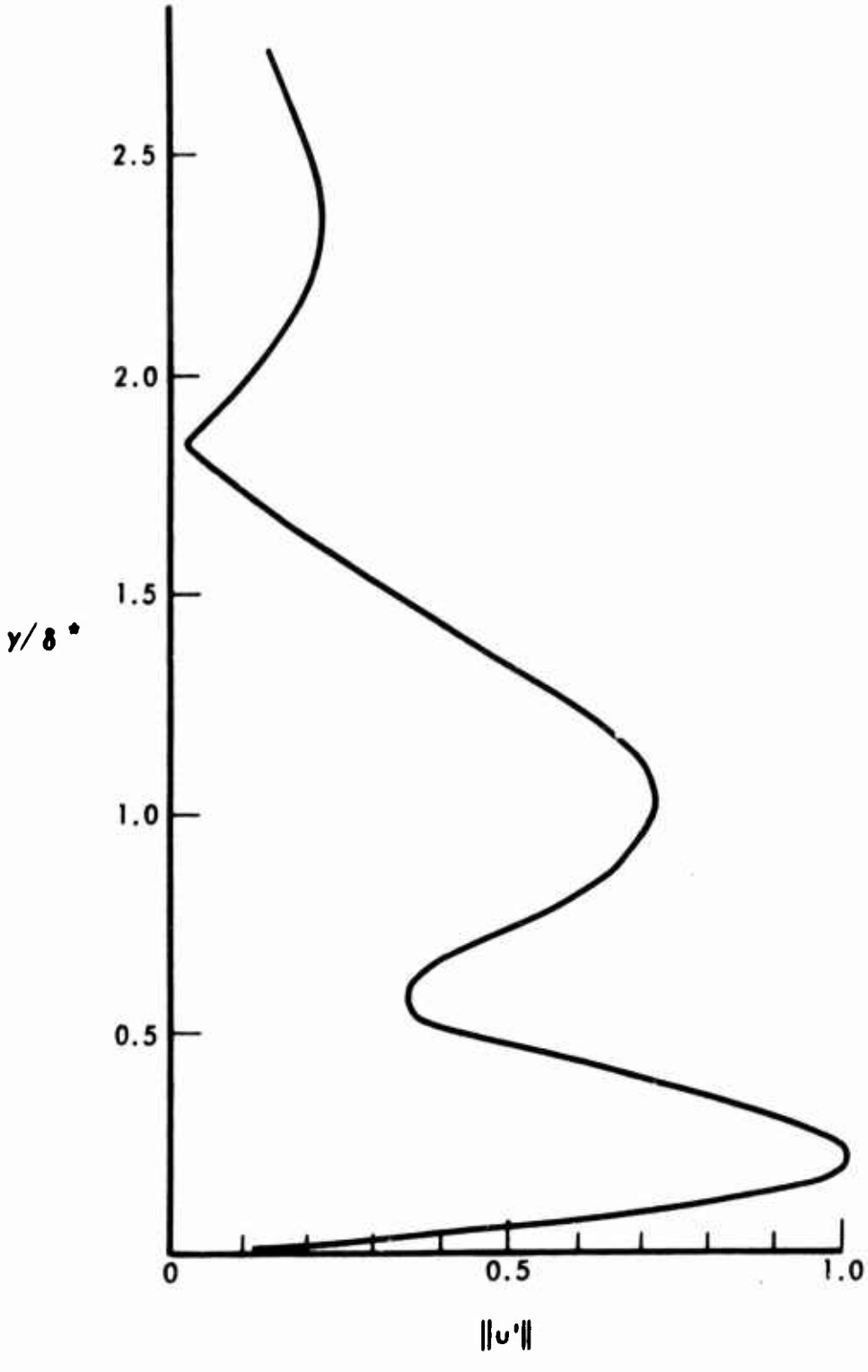

Figure 2-12: TYPICAL SHORT-WAVELENGTH DISTURBANCE PROFILE—
$M_e = 0.4$, $N_{Re,\delta^*} = 4000$, $\alpha\delta^* = 0.6$

outer edge to be almost as large as the principal lobe within the boundary layer. It has been found that the amplitude of the short-wavelength cases is also much less well-behaved than the longer wavelength cases, as is shown in a later figure.

It is not known at this time whether the calculated short-wavelength characteristics are physically correct or not. The results were obtained with the same equations and boundary conditions as were all other results presented and do not exhibit any of the previously observed numerical inaccuracies. However, additional work is required before their validity can be determined.

Subsonic Stability

After the initial disturbance has developed into a characteristic profile such as that shown in Figure 2-6, the flow stability can be determined from the behavior of any of the perturbation quantities. At the present time, calculations must be carried out for a constant Reynolds number and a constant wavelength. Thus, there are two parameters to be varied in searching for the minimum critical Reynolds number. Some typical subsonic results are presented in Figure 2-13 that show the effect of both parameters on the streamwise velocity perturbation, u'.

The longer wavelength cases shown in Figure 2-13 are apparently all stable, and show very little Reynolds number effect. With a shorter wavelength ($\alpha\ \delta^* = 0.30$) the effect of Reynolds number is more pronounced, and the critical Reynolds number is seen to be a little less than 500. For the shortest wavelength ($\alpha\ \delta^* = 0.6$), the previously discussed unsteady behavior is apparent. As already noted, the results for the several Reynolds numbers are consistent, but it is not clear that any of the cases are stable.

Figure 2-13 illustrates the major difficulty that remains in the use of the present method for calculating stability limits: interpretation of the results. According to previous theory, the curve of u' versus time for any combination of $\alpha\delta^*$ and Reynolds number should be a smooth monotonic curve. It is seen that all of the present results exhibit some oscillatory behavior. The oscillations shown are of course variations with respect to time at a point; however, in the stability theory time and distance are interchangeable within the assumed formulation (Equation 2-1). In view of the success of the stability theory, it seems that the present results could also be viewed as streamwise oscillations. Inasmuch as the oscillations persist for the equivalent of many boundary layer thicknesses, which would often be equivalent to an appreciable change in Reynolds number, it seems questionable that an exactly steady disturbance profile would ever be developed at any given point in a boundary layer. As a result of these oscillations, the stability of some of the cases is very difficult to determine.

It is traditional in the study of flow stability to present the results in the form of wave number as a function of Reynolds number with the region of neutral stability

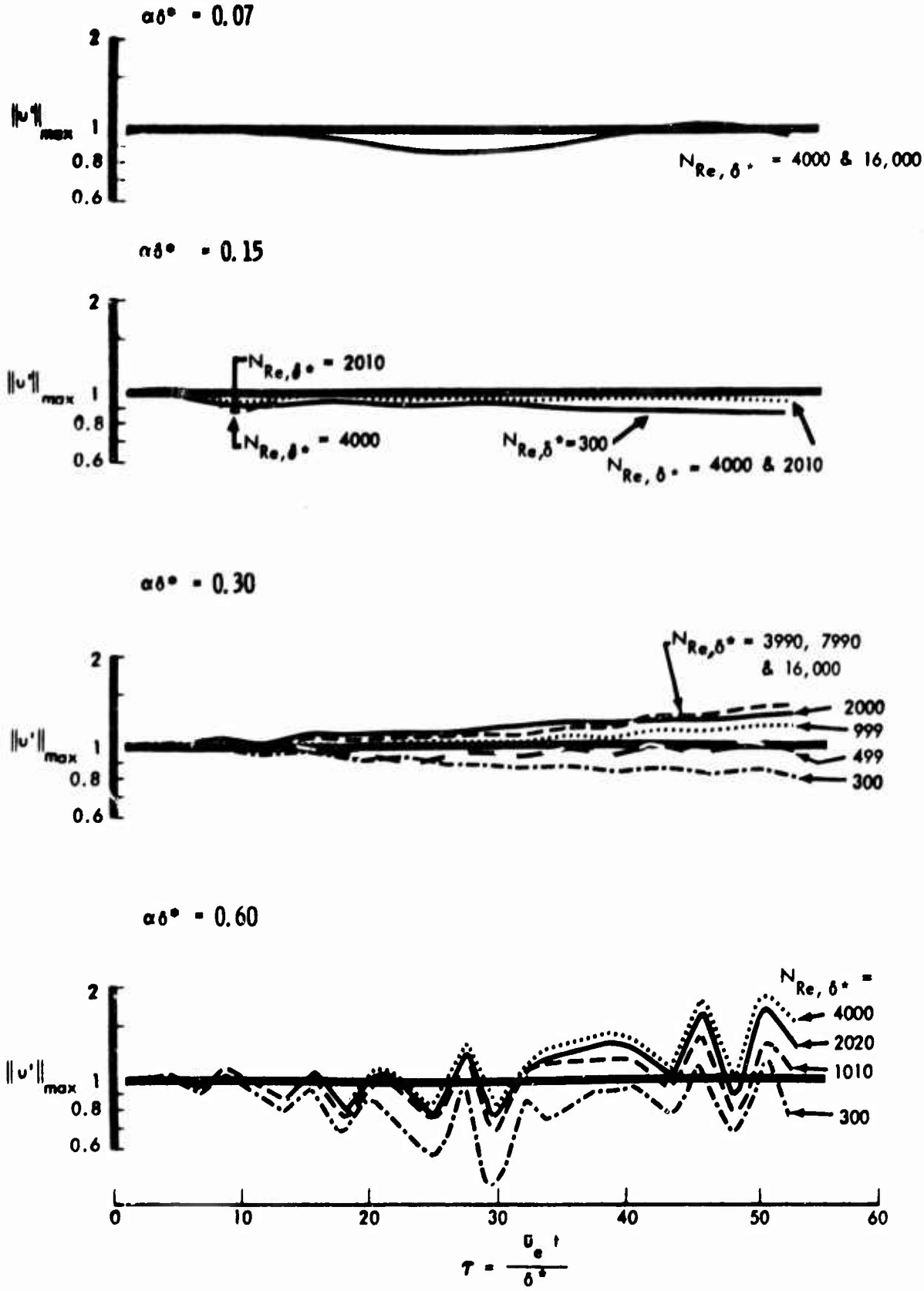

Figure 2-13: VARIATION OF DISTURBANCE AMPLITUDES WITH TIME — M_e = 0.4

indicated by curve. The calculations of Figure 2-13 are replotted in the traditional form in Figure 2-14, which also shows the neutral stability loop calculated by Lees (Ref. 33). The curve shown is interpolated from Lees' curves for $M_e = 0$ and $M_e = 0.5$. It is seen that the present method yields a good minimum critical Reynolds number. The higher Reynolds number points do not agree with the previous calculations, however, either as to the effect of Reynolds number or that of λ. These results must be taken with some reserve; however, current knowledge of the behavior of long-term numerical integration of partial differential equations is far from complete.

SUPERSONIC AND HYPERSONIC RESULTS

As in the subsonic case, it is believed that an initial disturbance to a hypersonic boundary layer must take on a certain characteristic form before any amplification can occur. This belief is not so well established as with the subsonic flow, for which there is a considerable amount of definitive experimental data. As noted in the description of previous analytic results, all of the existing theory is based on solutions to differential equations that are themselves derived by assuming the existence of perturbations of the form of Equation 2-1. The resulting equations can, of course, only lead to solutions for characteristic steady disturbance profiles.

Many of the results calculated by the present method do converge to steady profiles, although the initial development is often much more violent than for subsonic flows. In some cases, however, the behavior is much more complex, with the phase loops and profiles undergoing cyclic variations. The cyclic solutions have been obtained with the same equations and same numerical techniques as those used for all other cases. None of the previously encountered types of numerical instability appear to be responsible for the cyclic behavior. However, there has not yet been sufficient study to rule out the possibility of numerical effects.

Development of Steady Disturbance Profiles

A typical example of the development of a disturbance profile in a hypersonic flow is presented in Figures 2-15 and 2-16. In Figure 2-15 the steady-flow velocity profile is shown and (to a much larger scale) the initial disturbance. As shown, the disturbance decreases rapidly in amplitude and spreads through the boundary layer in much the same manner as the previously presented subsonic

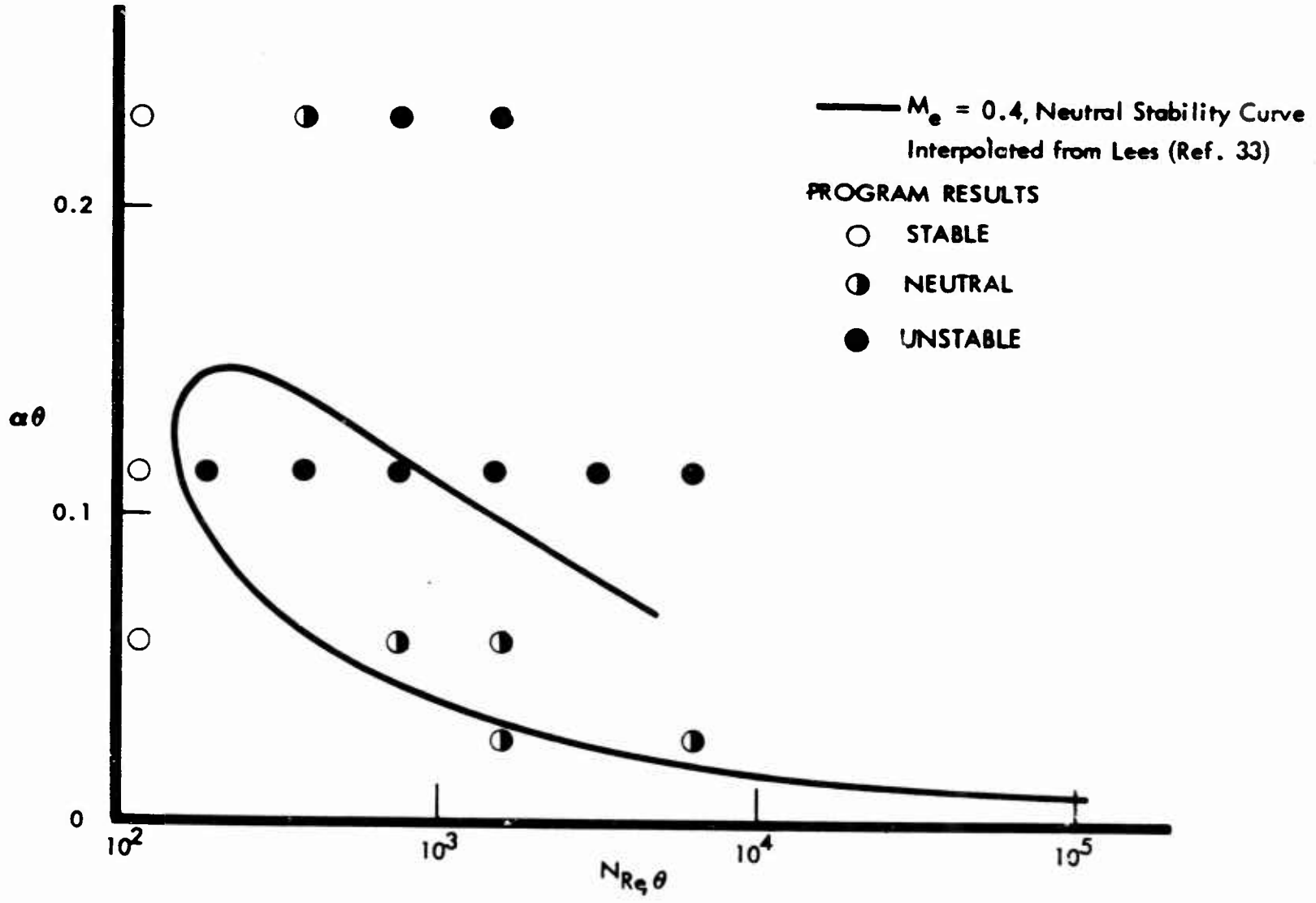

Figure 2-14: STABILITY LOOP — M_e = 0.4

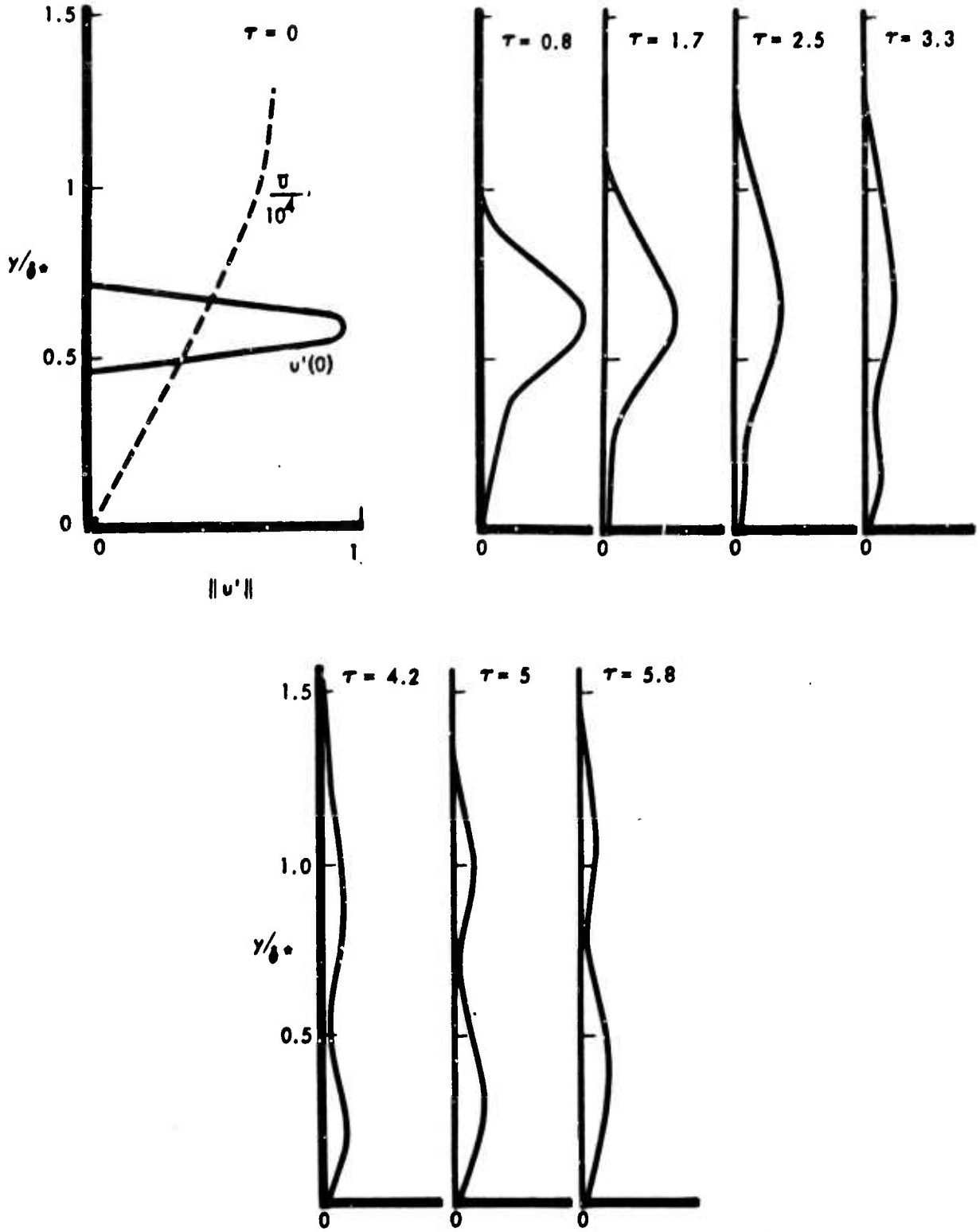

Figure 2-15: DISTURBANCE PROFILE DEVELOPMENT — $M_e = 7$, $N_{Re,\delta^*} = 2000$

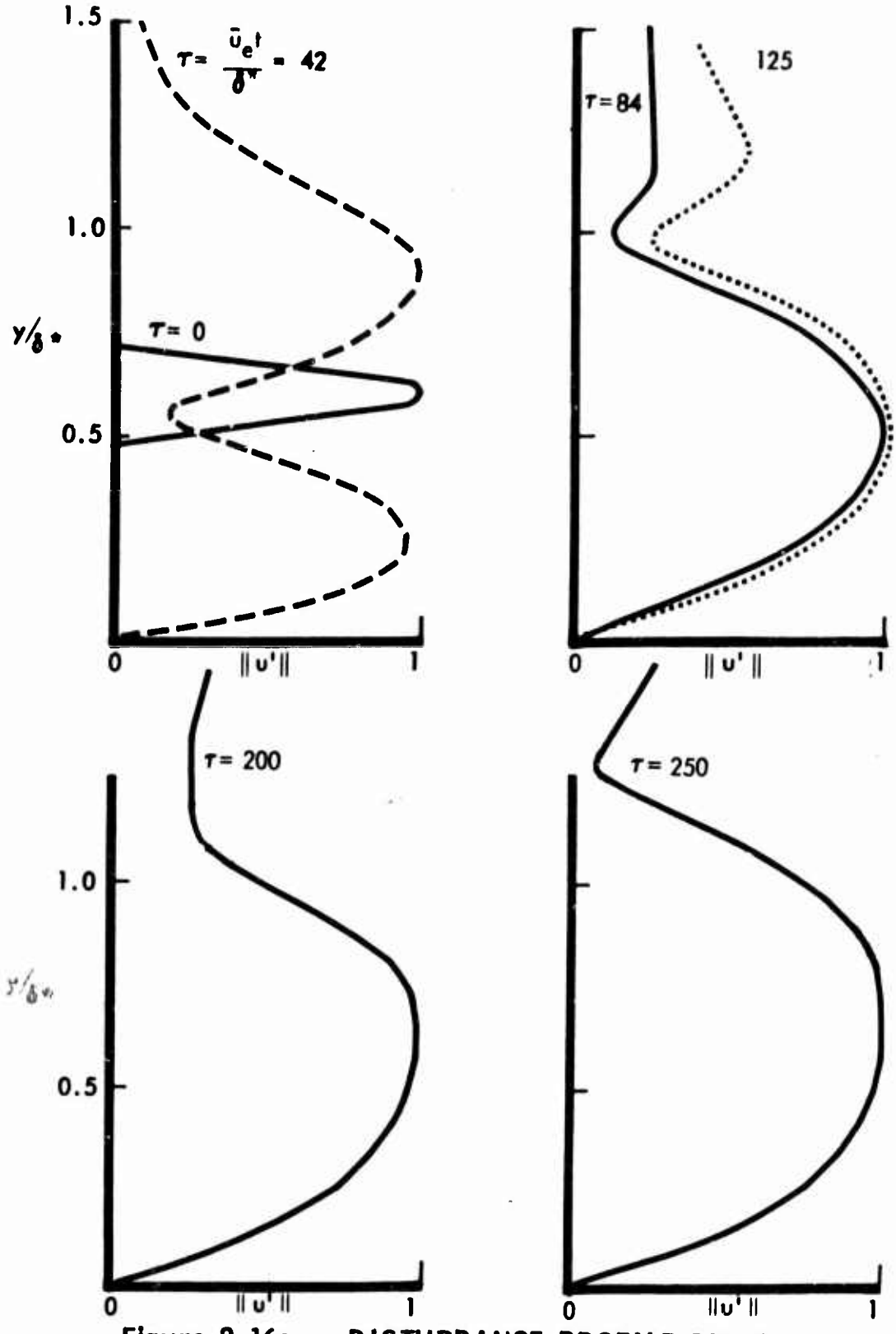

Figure 2-16a: DISTURBANCE PROFILE DEVELOPMENT — $M_e = 7, N_{Re,\delta^*} = 2000$

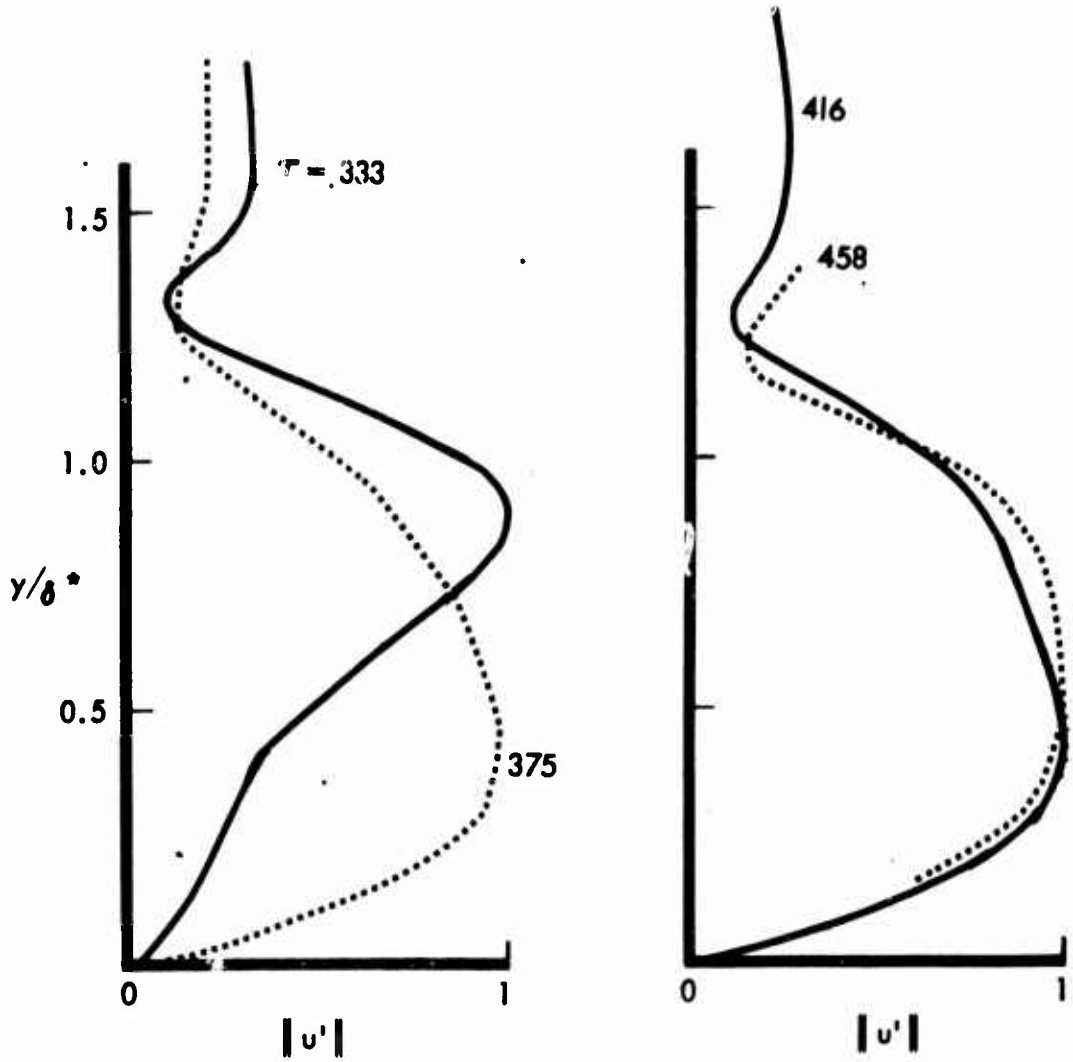

Figure 2-16b: DISTURBANCE PROFILE DEVELOPMENT — $M_e = 7$, $N_{Re,\delta^*} = 2000$

case. It is seen that at a τ of approximately 5.8 the disturbance profile has readjusted such that the point of maximum perturbation is at approximately $y/\delta^* = 0.4$ rather than at $y/\delta^* = 0.6$ where the initial disturbance was introduced.

The continued development of the profile through a much longer time period is shown in Figure 2-16, where all profiles have been renormalized so that the maximum value of the perturbation is unity. It is seen that at $\tau = 42$ the disturbance profile has developed to two equally prominent lobes. With further time the upper lobe decreases in amplitude while the lower one becomes much more prominent. By $\tau = 250$ the well-behaved profile of the type obtained in subsonic flow has developed. However, as shown in Figure 2-16c, the profile does not remain steady, but goes through a violent readjustment in the period from $\tau = 333$ to 375. The details of this readjustment are presented in more detail in Figure 2-17. It is seen that the profile begins to develop a second major lobe at $y \doteq \delta^*$. The upper lobe soon becomes larger than the previously mentioned one, which was that $y/\delta^* \doteq 0.4$. Beginning at about $\tau = 325$ the profile changes rapidly and soon develops several points of inflection. The maximum at $y \doteq \delta^*$ then becomes very pronounced, after which the velocity in the lower part of the boundary layer rapidly increases and a profile returns to much the same shape as had been seen at $\tau = 250$. After this period of unsteadiness and readjustment, the profile settled down to a steady characteristic form which was then repeated steadily until at least $\tau = 1200$.

The history of the velocity at a point within the boundary layer such as that shown in Figure 2-18 illustrates the entire cycle. In Figure 2-18 the amplitude of the disturbance at a point $y = \Delta y$ is presented throughout the entire calculation. Each 50 iterations the entire velocity profile was renormalized, which accounts for the periodic discontinuities in the velocity. Presented in this manner, a steady profile that is either amplified or damped will have a sawtooth appearance. It is seen that the plotted velocity behaves in an erratic manner until τ is approximately 700, after which the sawtooth behavior occurs. The previously noted readjustment that occurs at approximately $\tau = 300$ is plainly evident in Figure 2-18. The final study sawtooth behavior indicates an unstable boundary layer with the perturbation velocity increasing.

Some final steady disturbance profiles as obtained from the calculations are presented in Figure 2-19. It is seen that these profiles have a superficial resemblance to the subsonic disturbance profiles. A corresponding phase loop is presented in Figure 2-20. As shown, this phase loop also resembles the previously shown subsonic phase loop.

Supersonic Stability

The results of Mach 7 stability calculations for the boundary layer flow over an adiabatic plate are presented in Figure 2-21. For this case three wavelengths were examined, of which the value $\alpha\delta^* = 1.224$ appears to be the most critical.

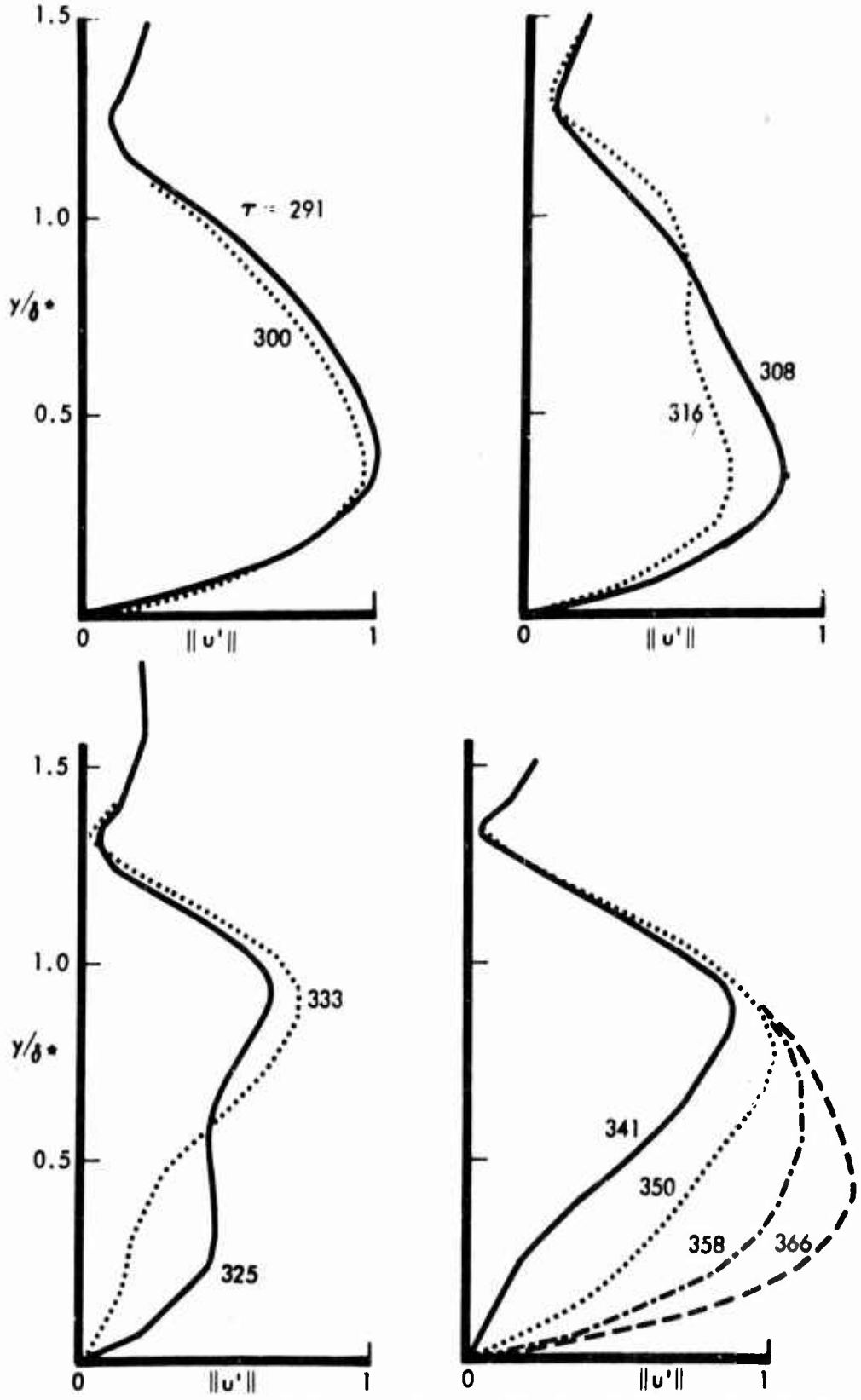

Figure 2-17: DISTURBANCE PROFILE VARIATIONS WITH TIME — $M_e = 7$, $N_{Re,\delta^*} = 2000$

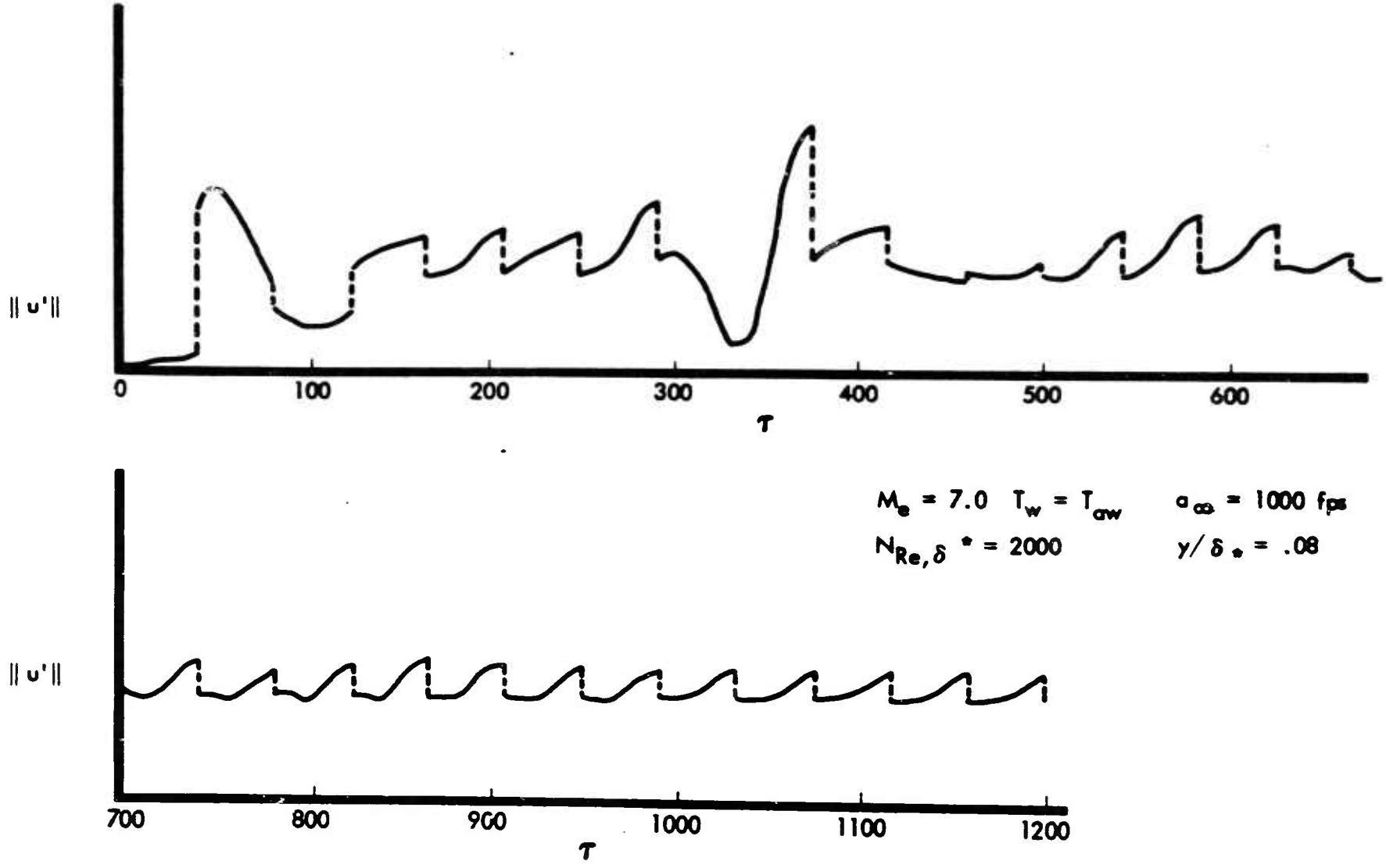

Figure 2-18: VELOCITY PERTURBATION HISTORY

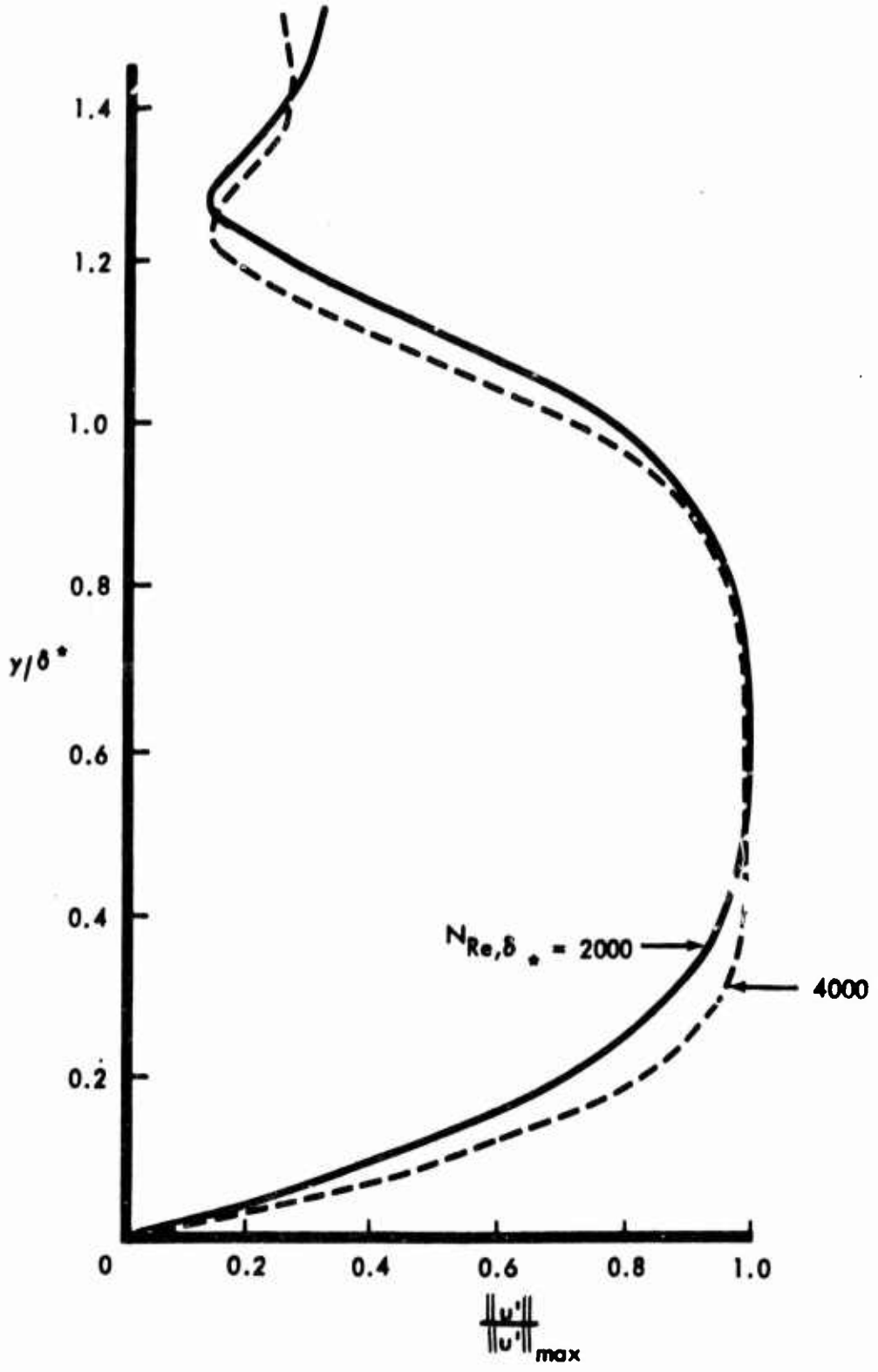

Figure 2-19: REYNOLDS NUMBER EFFECT ON $\|u'\|$ PROFILES — $M_e = 7$

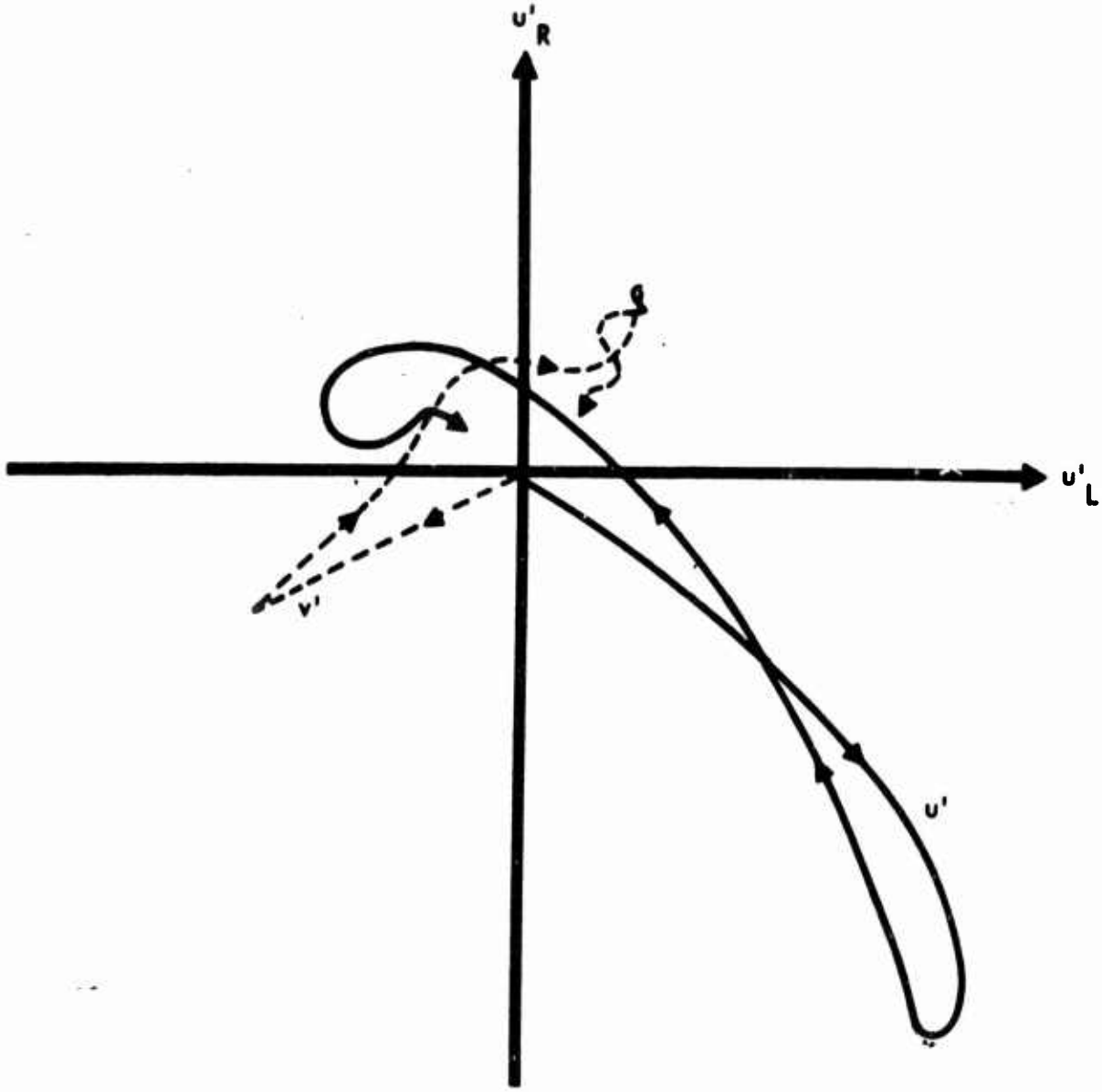

Figure 2-20: TYPICAL PHASE LOOP — $M_e = 7$, $N_{Re,\delta^*} = 2000$

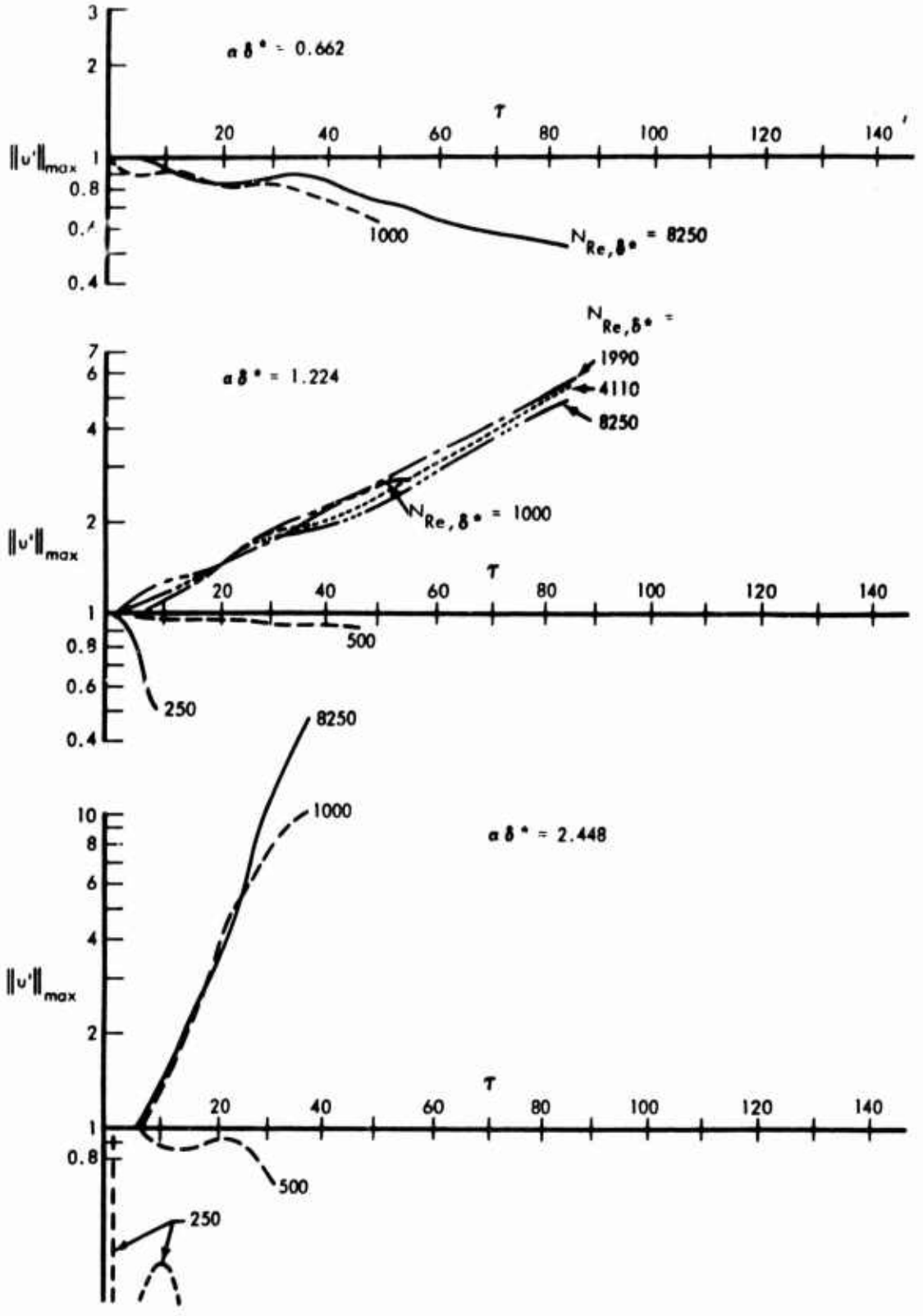

Figure 2-21: VARIATION OF DISTURBANCE AMPLITUDES WITH TIME — $M_e = 7$, $T_w = T_{aw}$

Although increasing $\alpha\delta^*$ generally increases amplification rates at the higher Reynolds numbers, it appears that decay rates are also increased at subcritical Reynolds numbers, so that the minimum critical Reynolds number occurs at the intermediate value. It is seen that, with a Reynolds number of 500, the flow is only slightly stable, and amplifies rapidly at a Reynolds number of 1000, so that the critical value is only slightly above 500.

The calculations presented in Figure 2-22 are much less thoroughly examined than those so far presented, and present some surprising results. The calculations of Figure 2-22 are also for a Mach number of 7, but with the wall temperature reduced to approximately 0.6 of the recovery temperature. It had been expected that wall cooling would somewhat increase the critical Reynolds number. However, as shown, the calculations indicated unstable flow at Reynolds numbers as low as 250.

Stability calculations for Mach numbers of 2, 4, and 10 are shown in Figure 2-23. For these cases no systematic search for the critical wavelength has been made. Critical values were estimated based on previous calculations and on an asymptotic rule given by Lees and Reshotko (Ref. 34).

These results all have an oscillatory character that is not at present explainable by the authors. From past experience it had been expected that by extending the calculations in real time an asymptotic steady growth rate would be achieved. However, the calculations shown are already extended well beyond the time normally required for the steady growth to be observed with no real indication that a steady flow will ever occur.

The results shown in Figures 2-22 and 2-23 are certainly to be viewed with caution. Current knowledge of the characteristics of numerical solutions to partial differential equations is such that the possibility of numerical instability cannot be ruled out. It is known, however, that none of the forms of numerical instability previously encountered in this study are responsible. All calculations were made with the same computer program that has provided all of the previously presented data, and further, there is great consistency between the many different cases shown in those two figures.

With regard to the oscillatory behavior shown in Figure 2-23, it should be noted that the linear theory cannot be expected to find such solutions, since it is a priori assumed that the disturbance is of the form given by Equation 2-1. The existence of such steady solutions does not appear to preclude the existence of oscillatory solutions as well.

The authors know of nothing really comparable in the literature that can be used to check either Figure 2-22 or Figure 2-23, and as already stated, know of no explanation, either physical or numerical, for the behavior shown. However, with a system of equations as complicated as those being used in the present study it is easily possible for errors to creep into the program. Judgment of the results shown in Figures 2-22 and 2-23 must be reserved until further investigations can be made.

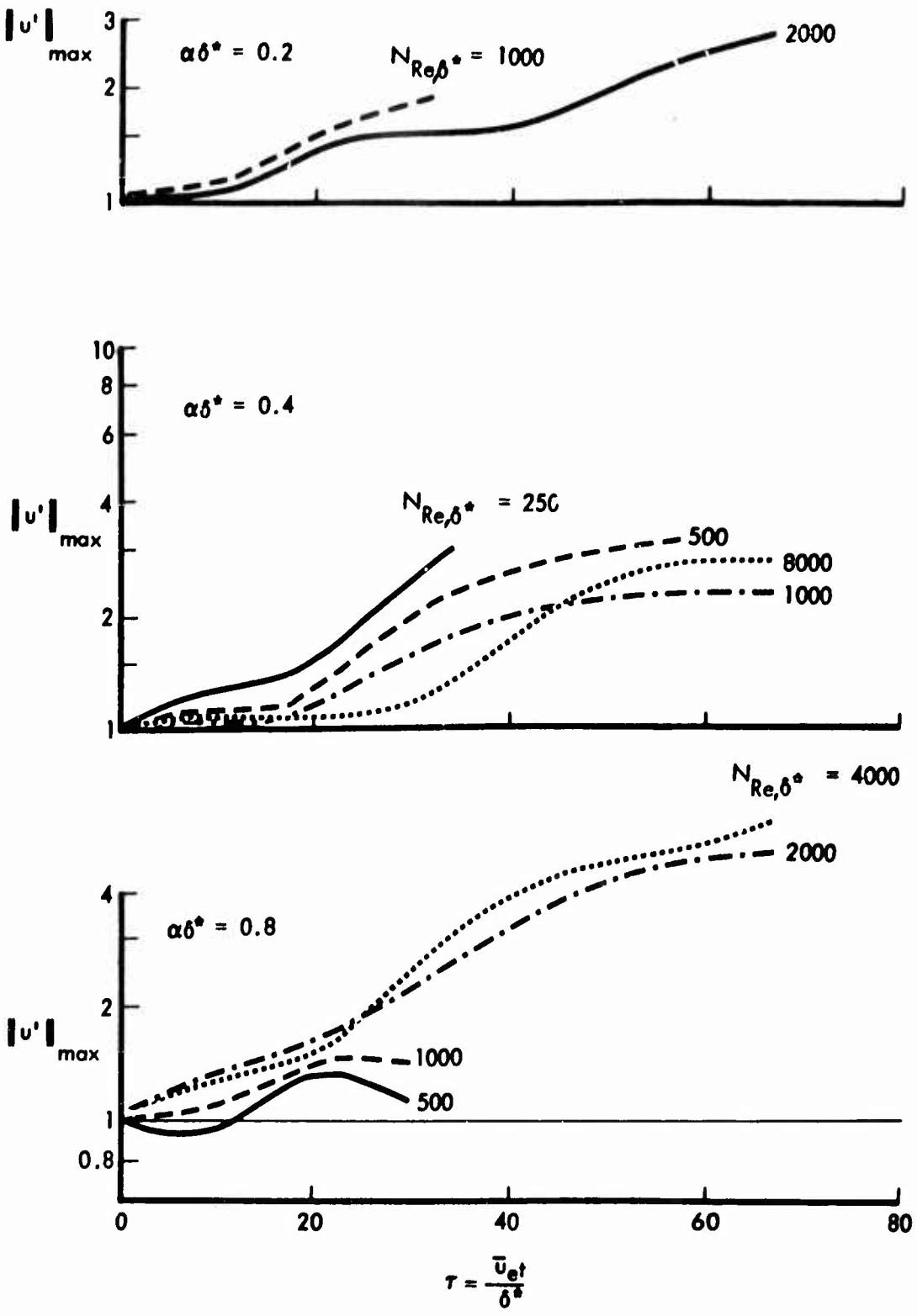

Figure 2-22: VARIATION OF DISTURBANCE AMPLITUDES WITH TIME — $M_e = 7$, $T_w/T_{aw} = 0.6$

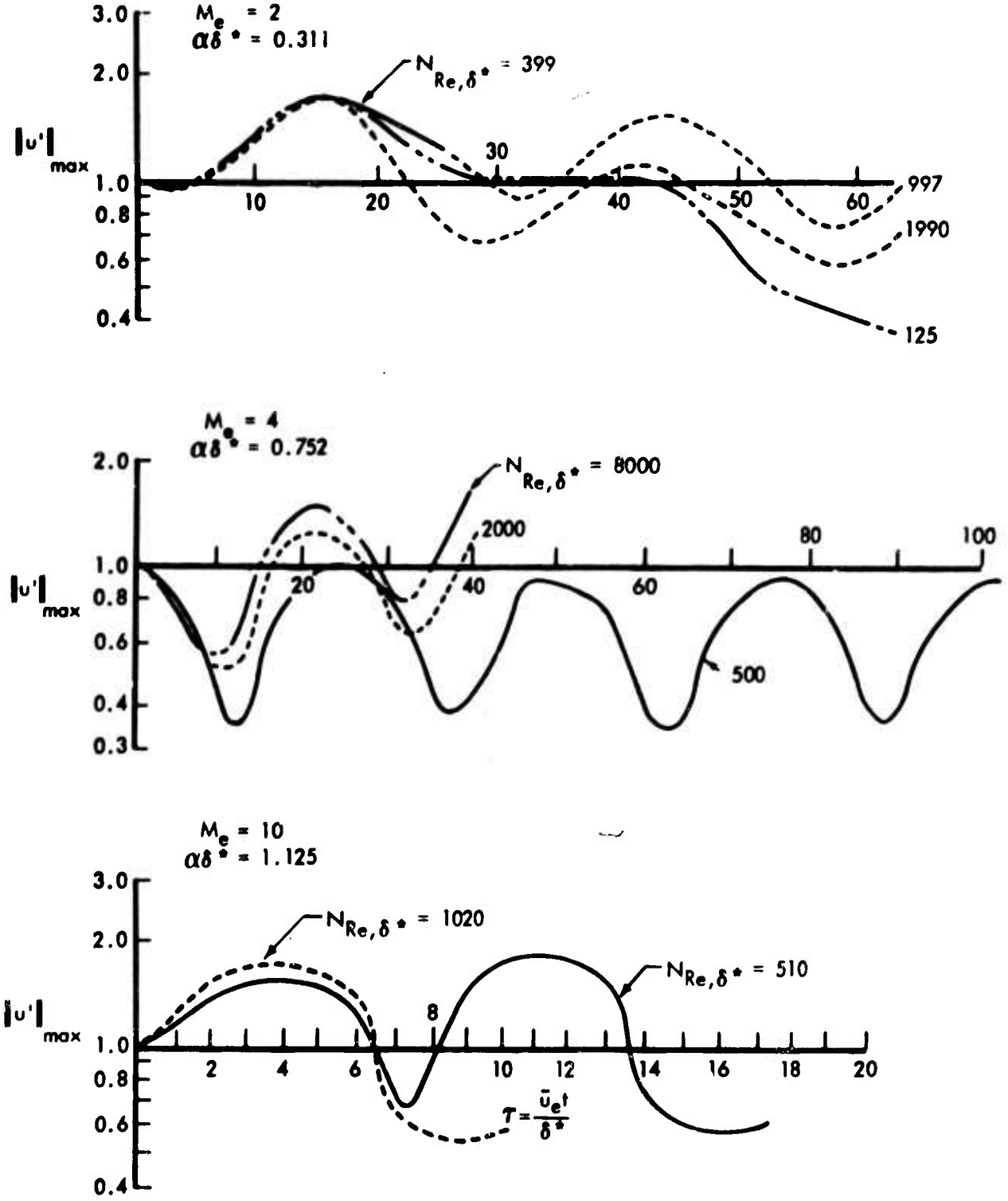

Figure 2-23: VARIATION OF DISTURBANCE AMPLITUDE WITH TIME — $T_w = T_{aw}$

Wave Speed

According to the classical method, the perturbation waves are assumed to have not only a definite profile but also a definite wave speed. While no such restriction is imposed in the present method, it is possible to determine from the calculated results the speed with which the disturbances are traveling. Since each rotation of a phase loop corresponds to a movement of one wavelength it is only necessary to find the rotation rate, which is easily done. The disturbance (or phase) velocities that have been found with the present method are shown in Figure 2-24. It is seen that the perturbation velocity increases with Mach number, not only in absolute value, but also in relation to the free-stream velocity. This result is in accordance with previous results, both analytic and experimental.

The dashed curve, $1 - 1/M_e$, is the boundary between subsonic and supersonic wave speeds. Above the curve the perturbation velocity will be subsonic with respect to the free stream; below the curve the waves would be supersonic. The linear theory solutions for supersonic flows are all restricted to subsonic perturbations, and it is believed that these would be the most critical. It is argued that, if a supersonic perturbation wave were to exist, it would create shock waves that would be accompanied by large energy losses. The energy losses would be stabilizing; therefore, the supersonic waves would not be the most critical.

Vertically traveling pressure waves are clearly observed in the early stages of many of the solutions by the present method (see Figure 2-5), but none of the final solutions exhibit them, and as shown, the final wave speed corresponds to a subsonic perturbation wave. Thus it is seen that the present calculations support the arguments against supersonic perturbations. Conversely, the results shown tend to confirm the validity of the present calculations.

SUMMARY OF STABILITY RESULTS

Accepting, for the moment, the calculations shown in Figure 2-23 , it is possible to sketch the curve of critical Reynolds number against Mach number for the range from Mach number 0.4 to 10. The results already presented are summarized in Figure 2-25, with filled symbols denoting unstable points, open symbols stable points, and half-filled points denoting neutral or indeterminate values. It is seen that a smooth curve can be drawn for all of the results presented. Of course, it is only the points at Mach 0.4 and Mach 7 that are at all well established. The Mach 4 point at a Reynolds number of 500 seems to be almost exactly neutral. The Mach 10 points are less clear, but it appears that the calculation for Reynolds number of 500 is stable; that for 1000 should be extended but is apparently not strongly divergent.

It should be noted here that the steady-flow boundary layer profiles were all for a sharp flat plate without pressure gradient. At the critical Reynolds numbers shown, the boundary layer displacement effect will cause an increase in the local pressure and a favorable pressure gradient, particularly at the higher Mach numbers. This effect will alter the steady-flow profile somewhat, and would probably lead to a higher critical Reynolds number.

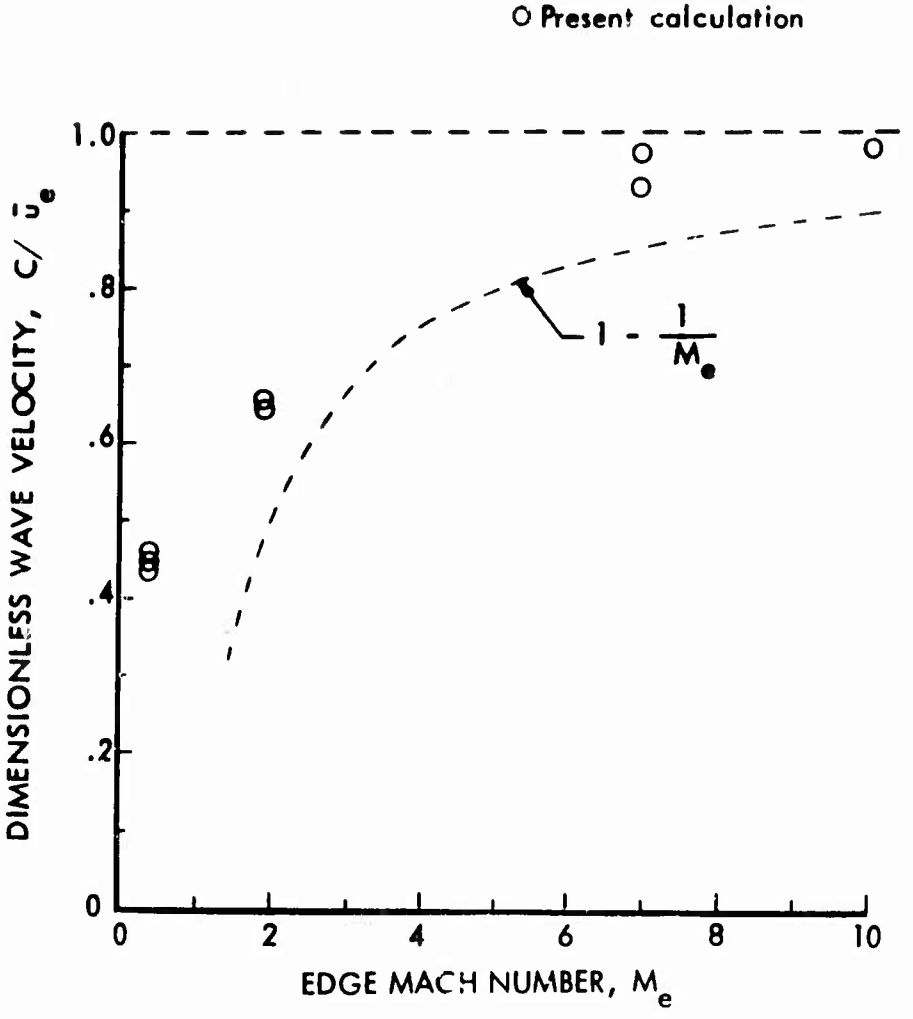

Figure 2-24: EFFECT OF MACH NUMBER ON PERTURBATION WAVE VELOCITY— $T_w = T_{aw}$

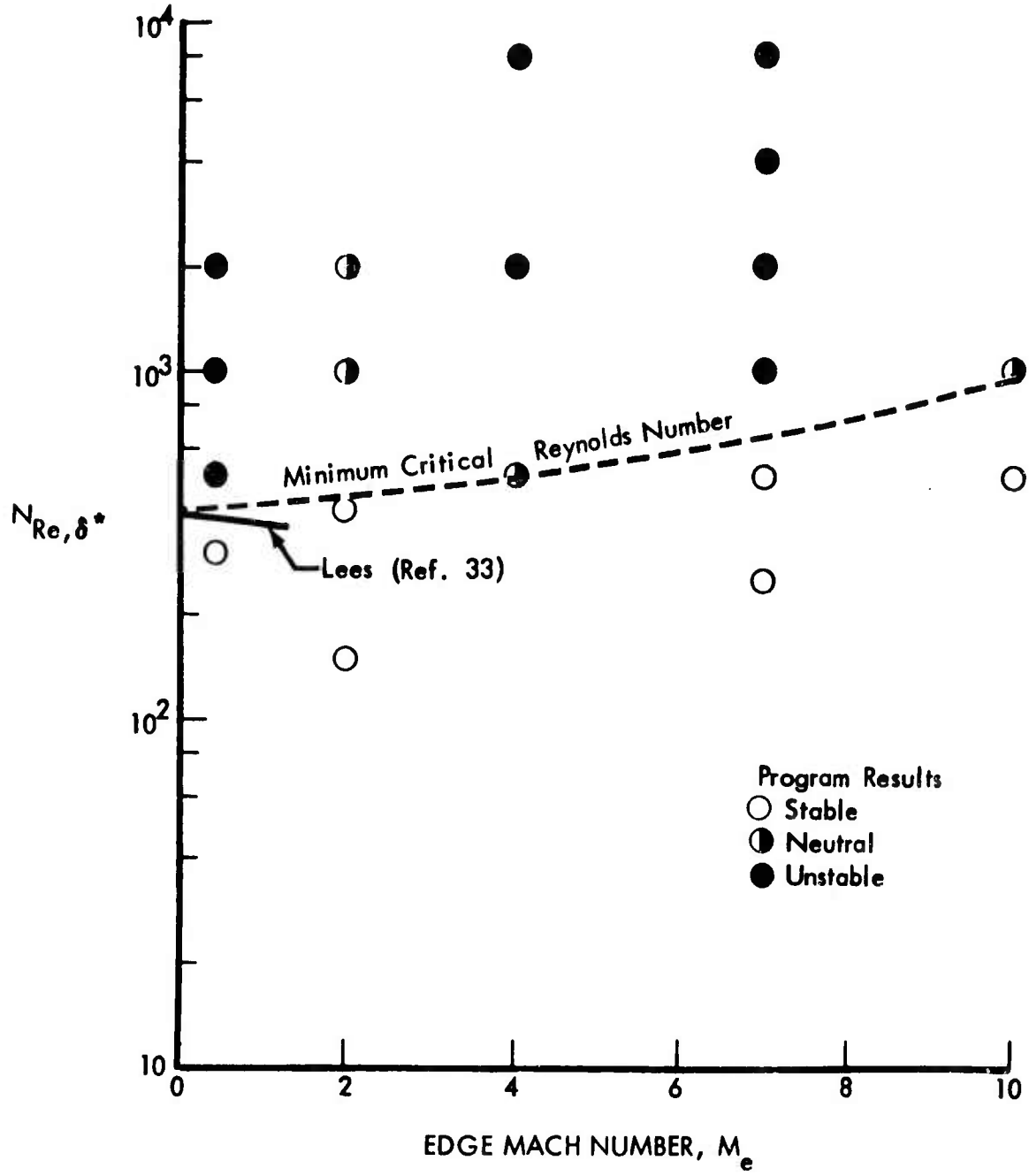

Figure 2-25: EFFECT OF MACH NUMBER ON CRITICAL REYNOLDS NUMBER — $T_w = T_{aw}$

III

EXPERIMENTAL PROGRAM

The discussion of Section II has several important implications concerning experimental investigations into boundary layer transition:

1) Although the analysis indicates that laminar flow is always possible at any Reynolds number in the total absence of disturbances, it is also shown that any disturbance, however small, will be amplified if the Reynolds number exceeds a certain minimum critical value. Thus, it is not possible to entirely eliminate small unintentional disturbances as a transition-producing mechanism.

2) In view of the impossibility of entirely eliminating spurious disturbances, it is probable that the "natural transition" observed in wind-tunnel tests results from such unintentional disturbances. Some such sources are very difficult to eliminate, such as sound radiation from the turbulent boundary layer on the tunnel walls, model and model support system vibrations, model surface roughness, weak shocks emanating from imperfections on the tunnel walls, etc., as well as the effects of probes, sublimation, or other transition detection equipment. It is emphasized that it is not sufficient to make the disturbance very small; it must be eliminated entirely. It is, however, to be expected that reducing the initial disturbance will increase the length of laminar flow that would occur.

3) Since transition may begin with infinitesimal disturbances, the experimental equipment should be of the highest possible sensitivity.

Considering the above, the authors concluded that attempts to trip the boundary layer should be made, thus relating transition to known disturbances. Data obtained in this manner should verify the predictions described in Section II — that there exists a lower limit on the Reynolds number below which the boundary layer could not be tripped. Of course, such verification would be valid only for very small disturbances. The tripped data would then also provide some information about the relation of initial disturbance and the actual transition Reynolds number. Thus, in addition to verifying the stability calculations, the trip data should also provide an empirical lower limit on transition Reynolds number. Of course, in any particular test, tripping would be attempted only after verifying that natural transition would not occur.

Accordingly, a review was made of the various methods that might be used to trip the boundary layer and it was decided to use mass injection. This method had the advantages of being controllable from outside of the wind tunnel without interrupting

the test and allowing controlled variations in the strength of the disturbance. It was also believed that mass injection would prove to be one of the most effective means of tripping. Korkegi (Ref. 16) had found that mass injection was successful when several other techniques had failed. Several investigators have found that roughness had not been effective in producing transition at hypersonic speeds. In particular, the data of James (Ref. 12) showed that small amounts of roughness consistently increased the transition Reynolds number rather than reduced it.

Many practical difficulties were encountered in the present test program, including probe leakages, probe interference, lengthy delays for model temperature stabilization, etc. It was concluded that, in view of the traditional requirement for excellence in transition experiments, the data were sufficiently questionable that a lengthy detailed data reduction was not justified. An examination of the pitot probe data was made, however, and a summary of the results obtained is presented in this section. In spite of the aforementioned difficulties, the data present a coherent and consistent picture. The trends exhibited by the presented data have been used to analyze previous data from several sources, and it was found that comparable data exhibit similar trends, lending further credence to their validity. Thus, the experimental investigation met its primary objectives of determining the effects of angle-of-attack and free-stream conditions on the transition Reynolds number for the models tested, although a small number of verifying reruns would be very desirable.

TEST EQUIPMENT AND FACILITIES

WIND TUNNELS

These tests were conducted at AEDC in Tunnels B and C of the Hypersonic Branch of the Von Karman Facility. Both tunnels have a 50-inch-diameter test sections and provide continuous flow. Tunnel B operates at nominal Mach numbers of 6 and 8; Tunnel C operates at Mach 10. The general arrangement of the Tunnel C test region is shown in Figure 3-1; further details are given in Reference 35. The operating conditions used in this program are shown in Figure 3-2; details are given in Reference 36.

MODELS

Three configurations were tested (Figures 3-3 and 3-4): unswept leading-edge models with 0.0005- and 0.125-inch-radii interchangeable leading edges; and a 75-degree swept delta wing with a 0.0005-inch-radius leading edge.

The sting adapter was common to both models and provided a 6- by 16-inch platform to support the model frames. One bolt at the center of the adapter ties the frame to the adapter. Six 2-inch-long rails on the surface of the adapter mate with the model frames to prevent vertical motion but permit relative fore and aft horizontal motion due to differing thermal expansions.

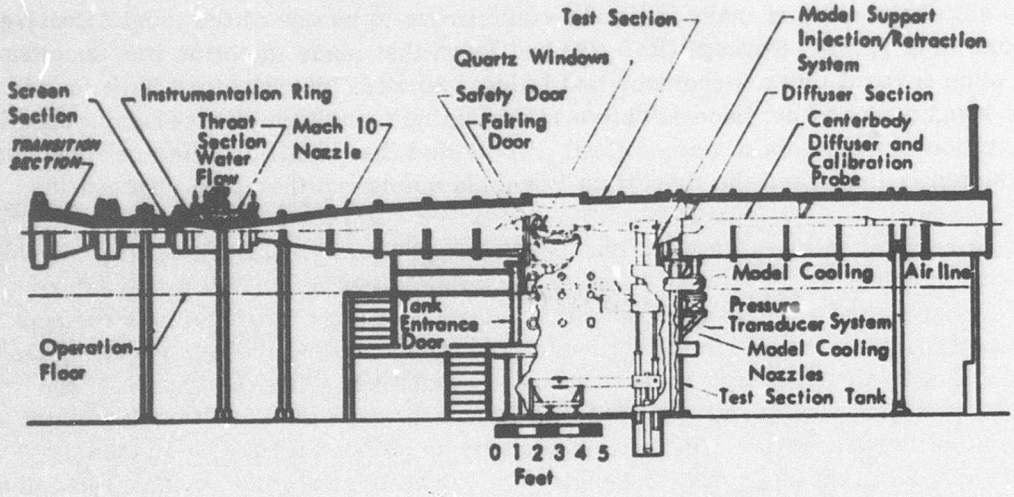

TUNNEL ASSEMBLY

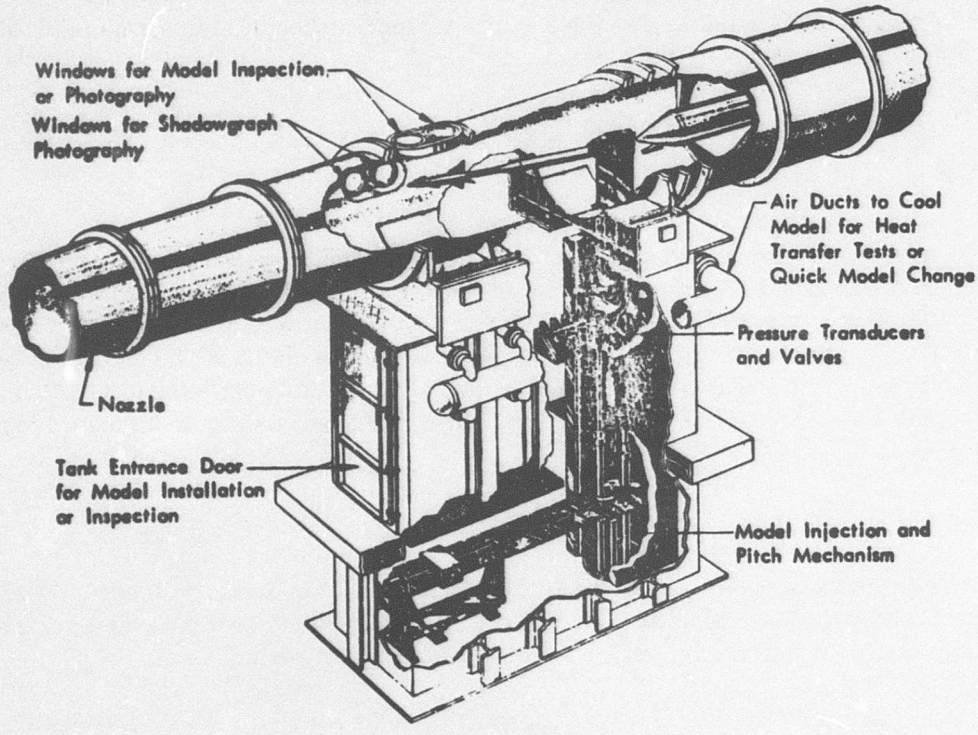

TEST SECTION

Figure 3-1: TUNNEL C, VON KARMAN FACILITY

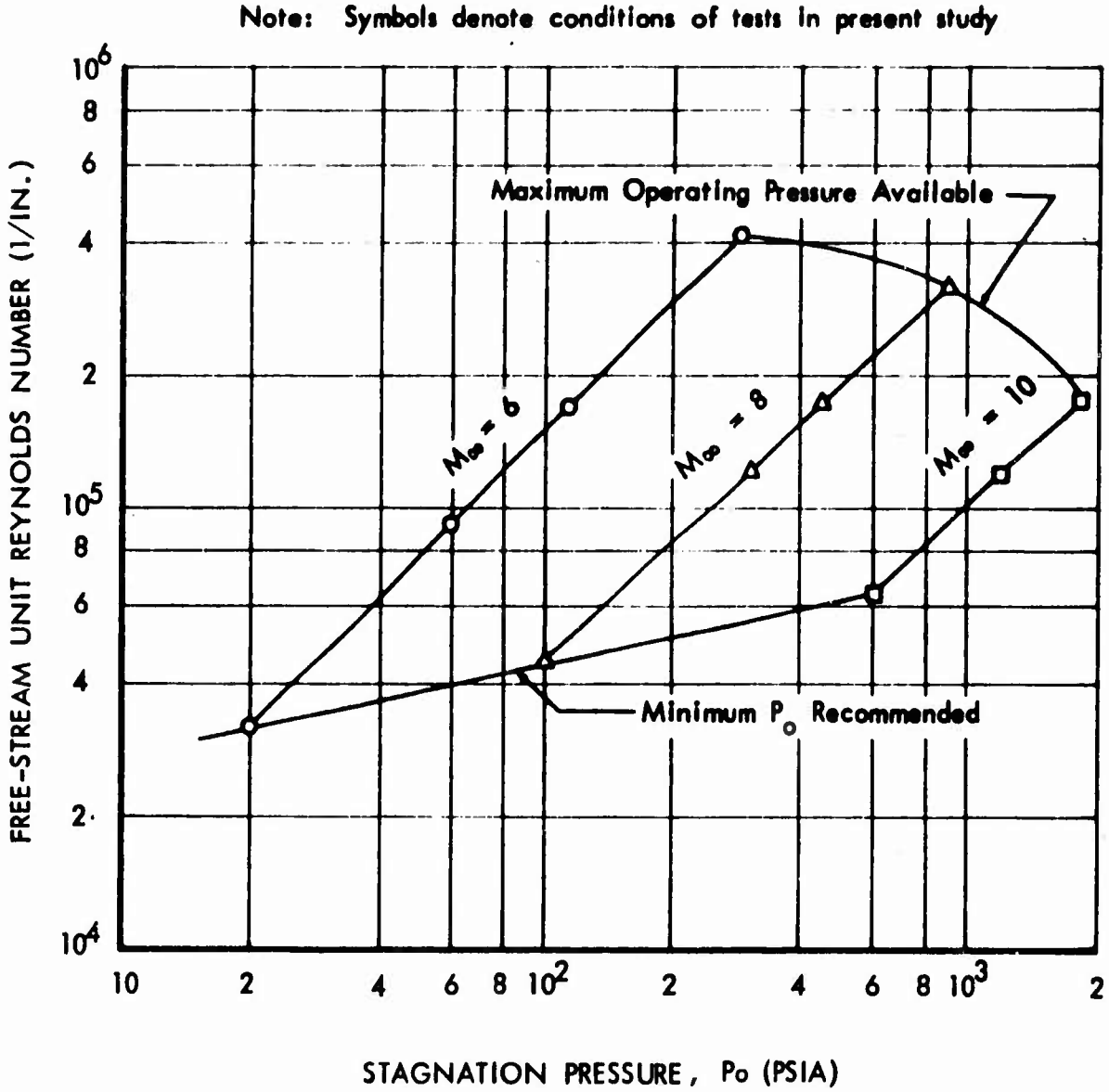

Figure 3-2: TUNNEL OPERATING CONDITIONS

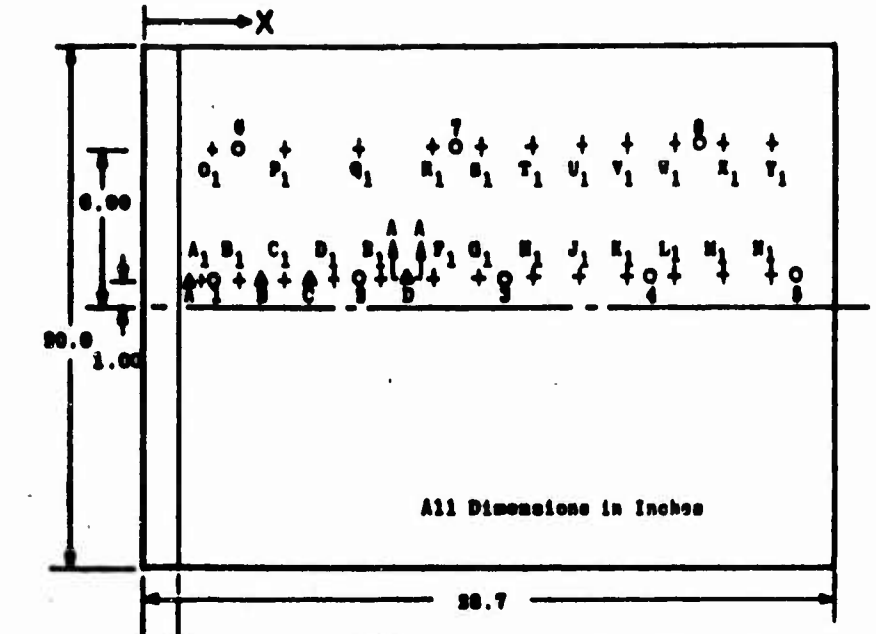

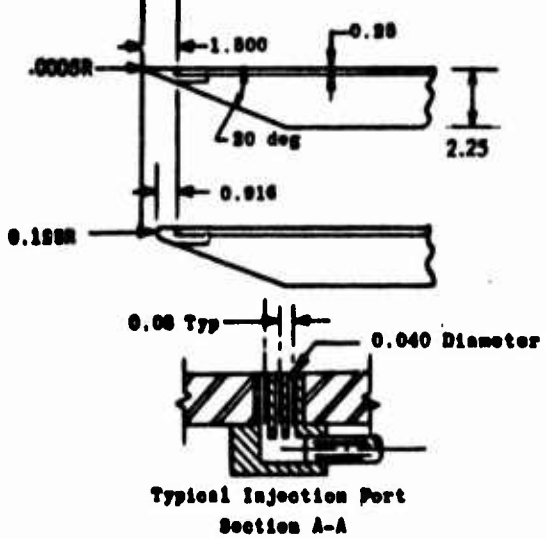

O Pressure Tap
△ Mass Injection Port
+ Thermocouple

Instrument Number	x, in.	Type Instrument
1	3.0	Pressure
2	9.0	
3	16.0	
4	21.0	
5	27.0	
6	4.0	
7	13.0	
8	23.0	
A	2.0	Injection Port
B	5.0	
C	7.0	
D	11.0	
A_1	2.5	Thermocouple
B_1	4.0	
C_1	6.0	
D_1	8.0	
E_1	10.0	
F_1	12.0	
G_1	14.0	
H_1	16.0	
J_1	18.0	
K_1	20.0	
L_1	22.0	
M_1	24.0	
N_1	26.0	
O_1	3.0	
P_1	6.0	
Q_1	9.0	
R_1	12.0	
S_1	14.0	
T_1	16.0	
U_1	18.0	
V_1	20.0	
W_1	22.0	
X_1	24.0	
Y_1	26.0	

Figure 3-3: UNSWEPT LEADING-EDGE FLAT PLATE MODEL

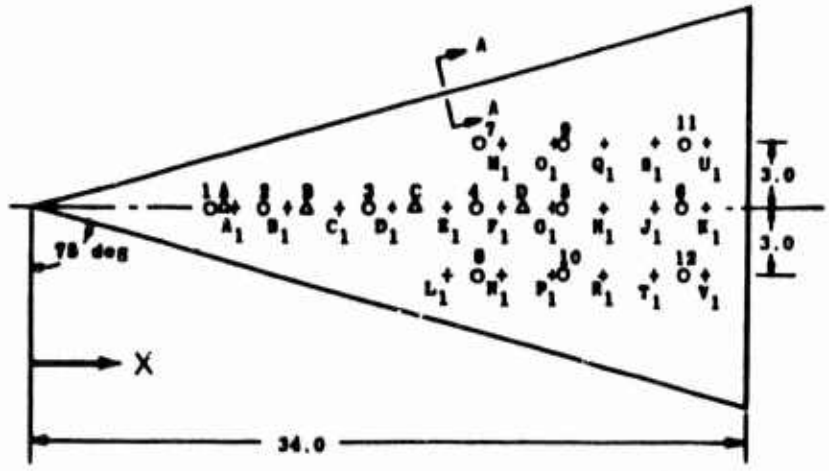

All Dimensions in Inches

O Pressure Tap
Δ Mass Injection Port
+ Thermocouple

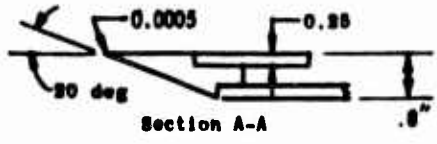

Instrument Number	x, in.	Type Instrument
1	8.5	Pressure
2	11.0	
3	16.0	
4	21.0	
5	25.0	
6	31.0	
7	21.0	
8	21.0	
9	25.0	
10	25.0	
11	31.0	
12	31.0	
A	9.0	Injection Port
B	13.0	
C	18.0	
D	23.0	
A_1	9.5	Thermocouple
B_1	12.0	
C_1	14.5	
D_1	17.0	
E_1	19.5	
F_1	22.0	
G_1	24.5	
H_1	27.0	
J_1	29.5	
K_1	32.0	
L_1	19.5	
M_1	22.0	
N_1	22.0	
O_1	24.5	
P_1	24.5	
Q_1	27.0	
R_1	27.0	
S_1	29.5	
T_1	29.5	
U_1	32.0	
V_1	32.0	

Figure 3-4: 75-DEGREE SWEPT DELTA WING MODEL

Unswept Model

The unswept leading-edge model parts are made of 321 stainless steel. The leading edges, illustrated in Figure 3-3 , are rigidly attached to a supporting frame. The 0.25-inch-thick surface has 24 I-sections attached to the underside at approximately equal spacing. The lower ends of these fit into tracks in the frame and maintain the vertical location of the 0.25-inch plate but permit horizontal motion due to differing thermal expansions.

Measurements indicating the flatness of the surface and sharpness of the leading edge are given in Figure 3-5 .

75-Degree Delta Model

The swept leading-edge model parts are made of 17-4 PH stainless steel. The number 32 finish test surface consists of a detachable leading edge followed by a 1/4-inch-thick plate that makes up the remainder of the surface. The detachable leading edge is sandwiched between the 1/4-inch plate and the frame. Bolts fastened to the 1/4-inch plate pass through elongated holes in the leading edge and frame. This construction maintains a smooth surface joint between the leading edge and the 1/4-inch plate and allows for movement along the joint due to differing thermal expansions The other leading edge is integral with the lower surface. A spacer is used between the plate and frame in place of the tongue.

Figure 3-6 gives measurements indicating surface flatness and leading-edge sharpness. These data were obtained with the model mounted on the "small" sting adapter. This adapter was replaced with a larger adapter, but no measurements were obtained.

Trip Ports

Each model has a set of boundary layer trip ports located in the test surface as shown in Figures 3-3 and 3-4 . These ports permit air from an external source to be injected to trip the laminar boundary layer.

MODEL INSTRUMENTATION

The locations of thermocouples on the plates are shown in Figures 3-3 and 3-4 . A special high-temperature thermocouple wire (trade name MEG-O-PAC) was used. This consists of number 30 gage chromel and alumel wires encased with insulation in a 1/16-inch-diameter stainless-steel tube. The ends are spotwelded to the back of the test surface. The special leads are held in place by steel clips spotwelded to the surface and extend approximately 3 feet in back of the model

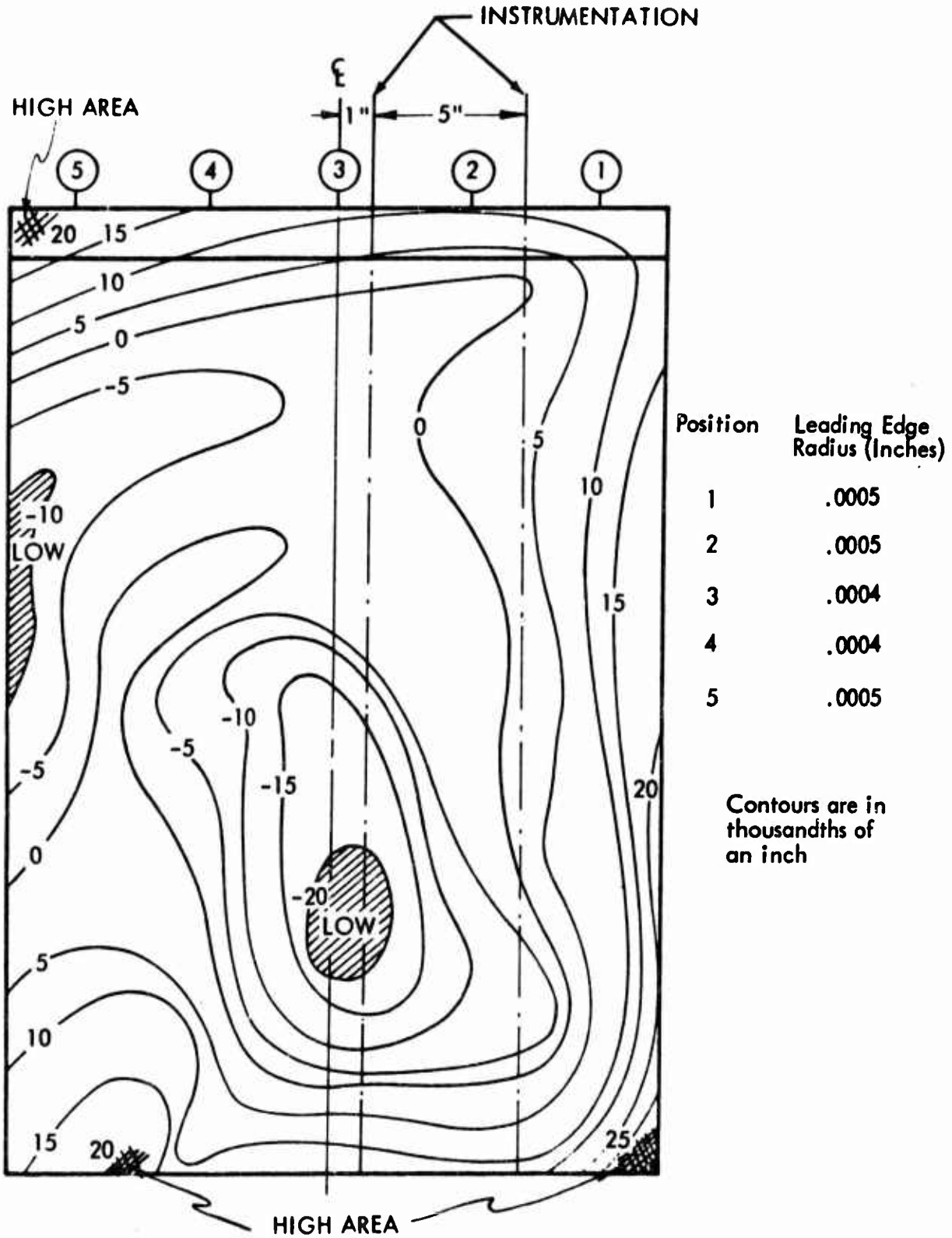

Figure 3-5: SURFACE CONTOURS AND LEADING-EDGE RADIUS— Unswept Plate

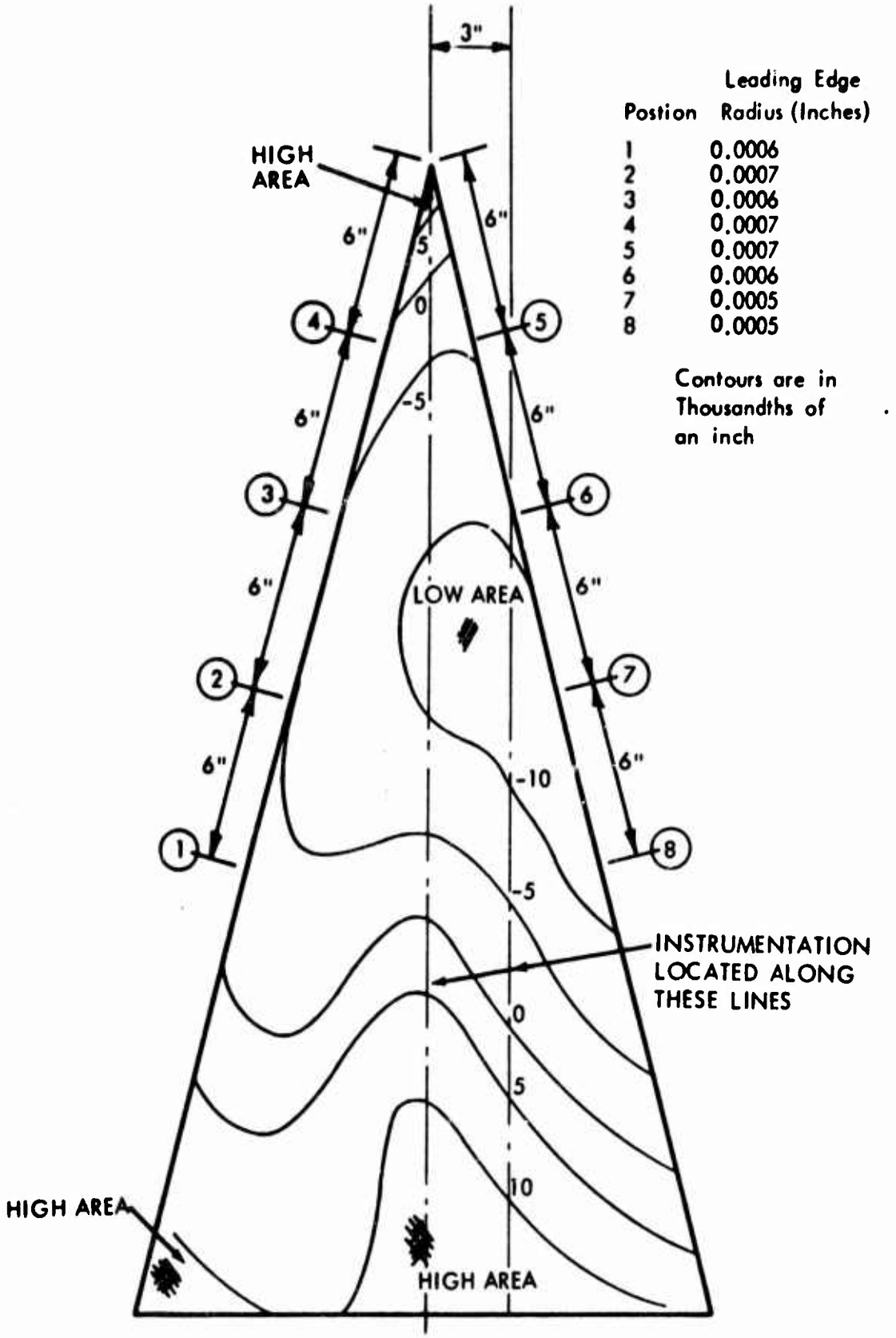

Figure 3-6: SURFACE CONTOURS AND LEADING-EDGE RADIUS — 75-Degree Swept Delta Wing

into the water-cooled section of the sting. Here, they are welded to standard number 30 gage chromel alumel thermocouple leads. The joint in each lead is encased in tubing and potted with Eccobond 104.

The reference junction of the thermocouples was maintained at 132°F. The temperature measurements are estimated to be accurate within ±2 degrees. The locations of surface static pressure ports are shown in Figures 3-3 and 3-4 . The ports are 0.073 inch in diameter. Pressures are communicated to instrumentation outside of the test section through 0.094-inch-diameter tubing.

Pressures were measured in tunnel B with 15-psia transducers, whereas in tunnel C, 1- and 15-psia transducers were switched in and out of the system automatically to allow measuring to better precision. The precision of the tunnel B measurements is estimated to be ±0.003 psia or 1 percent, and of tunnel C to be ±0.001 psia or 1 percent, whichever is larger.

A pressure port and thermocouple are located in the small plenum of the injection port at location "A" on both models to provide information for calculation of gas velocity.

INSTALLATION

Representative installation photographs are shown in Figure 3-7 . The upper view shows the original unswept leading-edge model and support in the test section. The lower view shows the delta-wing model and revised support retracted into the installation tank.

The upper view shows the traversable pitot probe. The probe is attached to the large housing by a double-wedge-section strut and a 1/2-inch-diameter shaft. The probe is moved by remote drive 4 inches along the axis of the 1/2-inch-diameter support shaft and rotated through the angle-of-attack range of these tests about a point in the housing. In addition to these motions, the probe housing is power driven approximately 37-1/2 inches parallel to the tunnel axis and manually moved 7 inches vertically and 7 inches laterally. The model support system provides the required angle of attack and a vertical motion that is related to the location of the center of rotation. The location of the unswept leading edge model and probe support in tunnel C is shown in Figure 3-8. The delta-wing model is mounted with the trailing edge and lower surface in the same locations as the unswept model. The location of the models in tunnel B is understood to be the same as shown for tunnel C.

The pitot pressure and total temperature probe designs used during the test program are shown in Figure 3-9 . Note that the probe attaches to the support identified in Figure 3-8 by "probe mount limits." A light in the control room indicates when contact is made between the probe tip and the surface of the model. The probe pressure was measured with a 5-psia transducer using a variable reference pressure, which allowed measurements within a precision of +0.002 psia or 1 percent, whichever is larger.

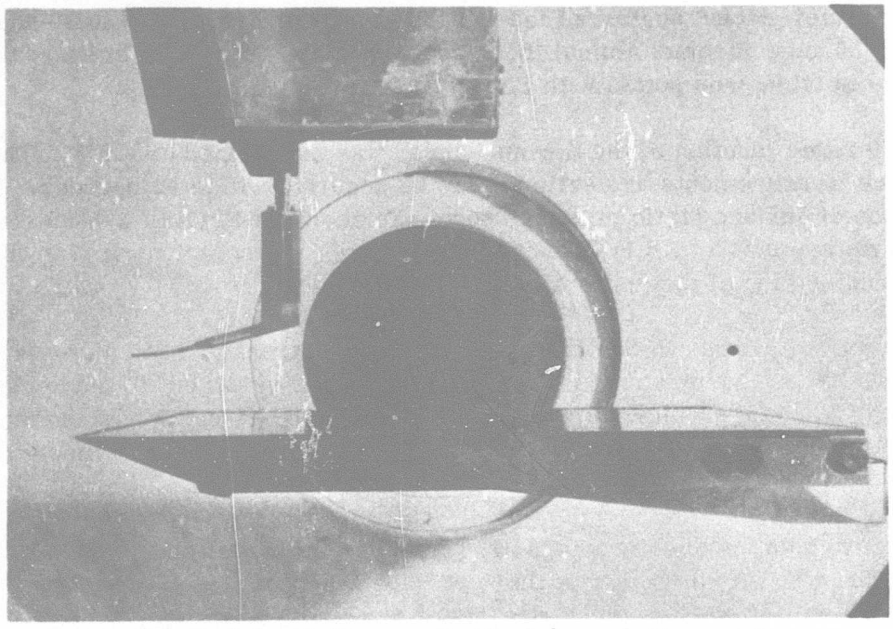

(a) Original Unswept Model and Support
VIEW THROUGH SIDE WINDOW OF TUNNEL

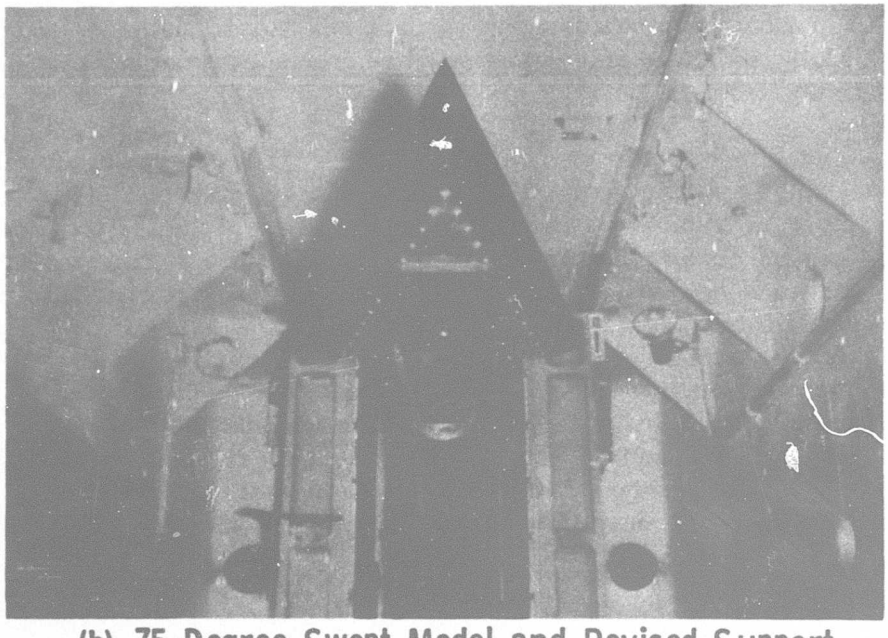

(b) 75-Degree Swept Model and Revised Support
VIEW INTO TANK WITH TEST SECTION ABOVE

Figure 3-7: MODEL INSTALLATION

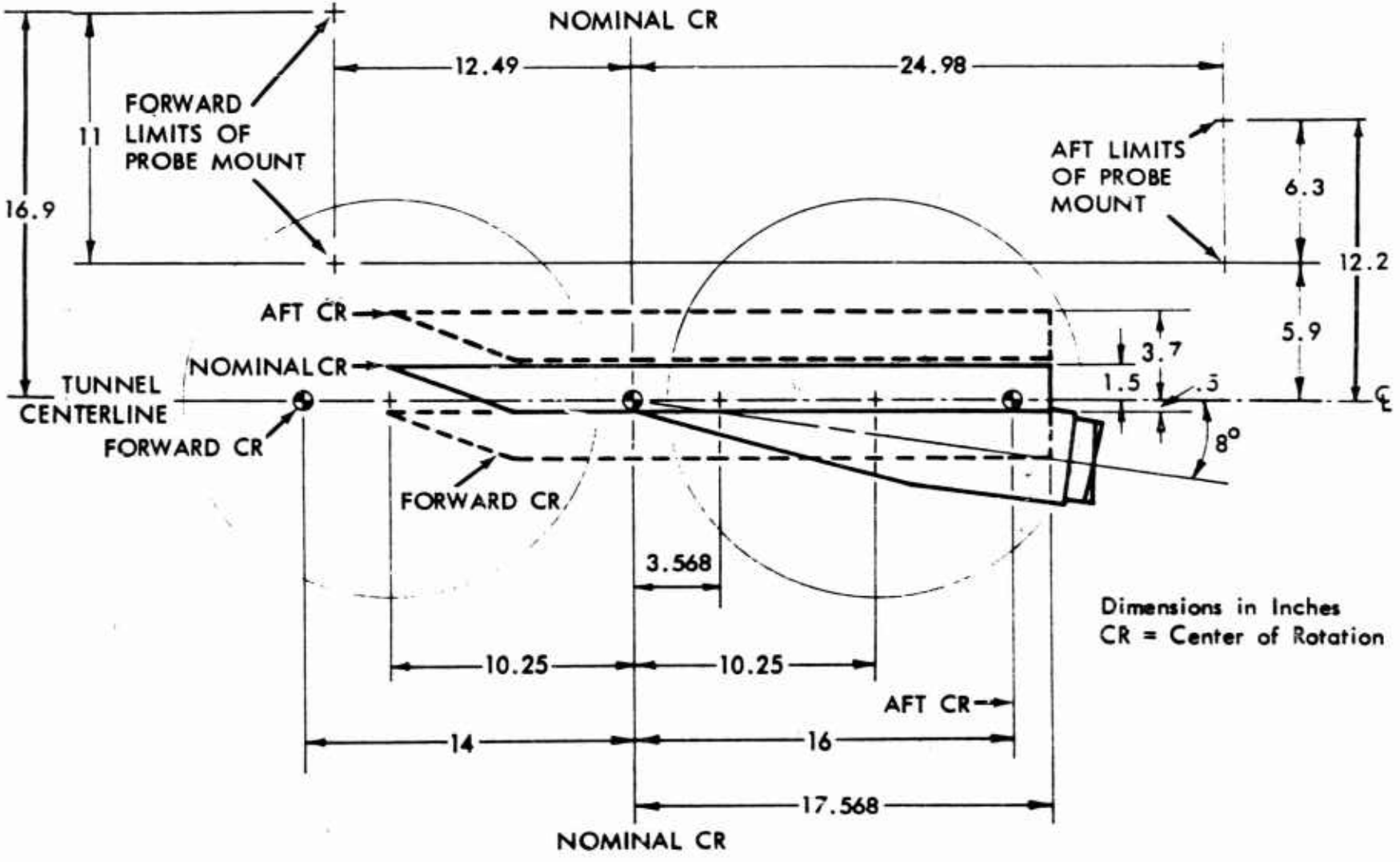

Figure 3-8 UNSWEPT MODEL AND PROBE-SUPPORT GEOMETRY — Tunnel C

DIMENSION NO.	PROBE 1	PROBE 2 *	PROBE 3
1	5.70	5	5.2
2	5.4	3.25	3.0
3	1.0	1.8	1.5
4	5.10	5.4	6.0
5	0.5	0.5	0.5
6	2.55	—	—
7	0.35	0.55	0.715
8	1.10	0.9	1.0
9	1.5	—	—
10	0.75	0.75	0.75
11	0.9	0.9	0.965
12	0.041	?	?
13	0.030	0.032	0.032
14	0.007	0.007	0.007

* This pitot probe was destroyed, so that no dimensions are available. The dimensions shown are scaled from the Schlieren photographs of the test, except 13 and 14 which were recorded during the test.

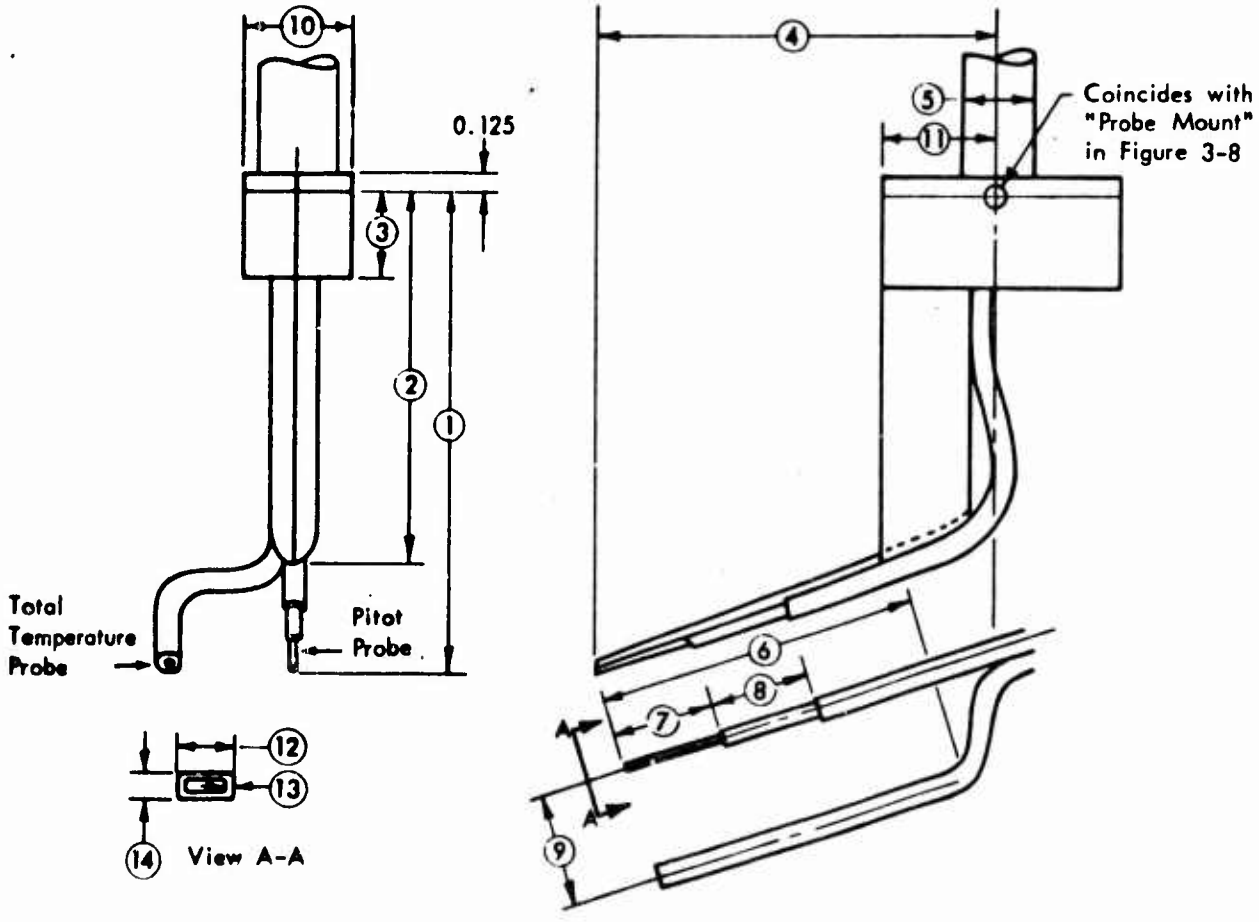

Figure 3-9: PITOT AND TOTAL TEMPERATURE PROBE CONFIGURATIONS

Figure 3-10 shows the trip flow control system and calibration. The mass flow for the injection ports was measured using calibrated orifices in a flowmeter. The pressure upstream of the orifice and the differential pressure across the orifice were measured with a 100- and a 15-psia FM transducer, respectively. The supply air to the flowmeter was maintained at room temperature. Based upon calibrations of the flowmeter and upstream-pressure transducer, the precision of the mass flow measurement is estimated to be ±5 percent.

EXPERIMENTAL TECHNIQUES

The majority of the data taken in the present investigation and all data analyzed in the remainder of this section were obtained with the pitot probe. However, several different techniques were used to acquire the probe data. A description of the techniques used and some examples of the results are given in this section. The transition data so obtained are discussed in the following section.

AXIAL SURVEY METHOD

The axial survey method consists of measuring the streamwise variation of pitot pressure in the lower part of the boundary layer. Near the surface the turbulent boundary layer velocity is greater than the laminar value. Hence, transition is accompanied by an increase in pitot pressure. The anticipated and actual axial survey results are shown in Figure 3-11. The expected behavior is sketched in Figure 3-11a. As indicated in the laminar part of the boundary layer the pitot pressure is expected to decrease with distance from the leading edge due to the growth of the laminar boundary layer. In the transition region the pitot pressure is expected to increase as turbulent mixing during transition increases the boundary layer velocity near the wall. Finally, when fully turbulent flow has developed, a decreasing trend in pitot pressure is again expected as the turbulent boundary layer grows with distance. Thus, the complete pitot pressure trace should have minimum and maximum points, which are here defined as the beginning and end of transition. Differences in level are unimportant; only the location of the minimum and maximum points is of interest.

Figure 3-11b presents some actual experimental results. The upper curve shows a pitot pressure trace obtained with a continually moving probe, and the lower shows the measurements made with the probe system brought to rest for a sufficient time to stabilize the pressure. It is seen that both the minimum and maximum points appear further forward with the stationary technique than with the moving probe technique. Because of the difference shown, all of the axial survey data that are used in this report were obtained by the stationary probe technique.

Figure 3-11c presents some additional comparisons showing the effect of mass injection. It is seen that, with mass injection, the location of the maximum point is moved far forward and no well-defined minimum is apparent. There is an erratic behavior both upstream and downstream of the maximum point, but little doubt, however, that the mass injection did cause transition at a lower Reynolds

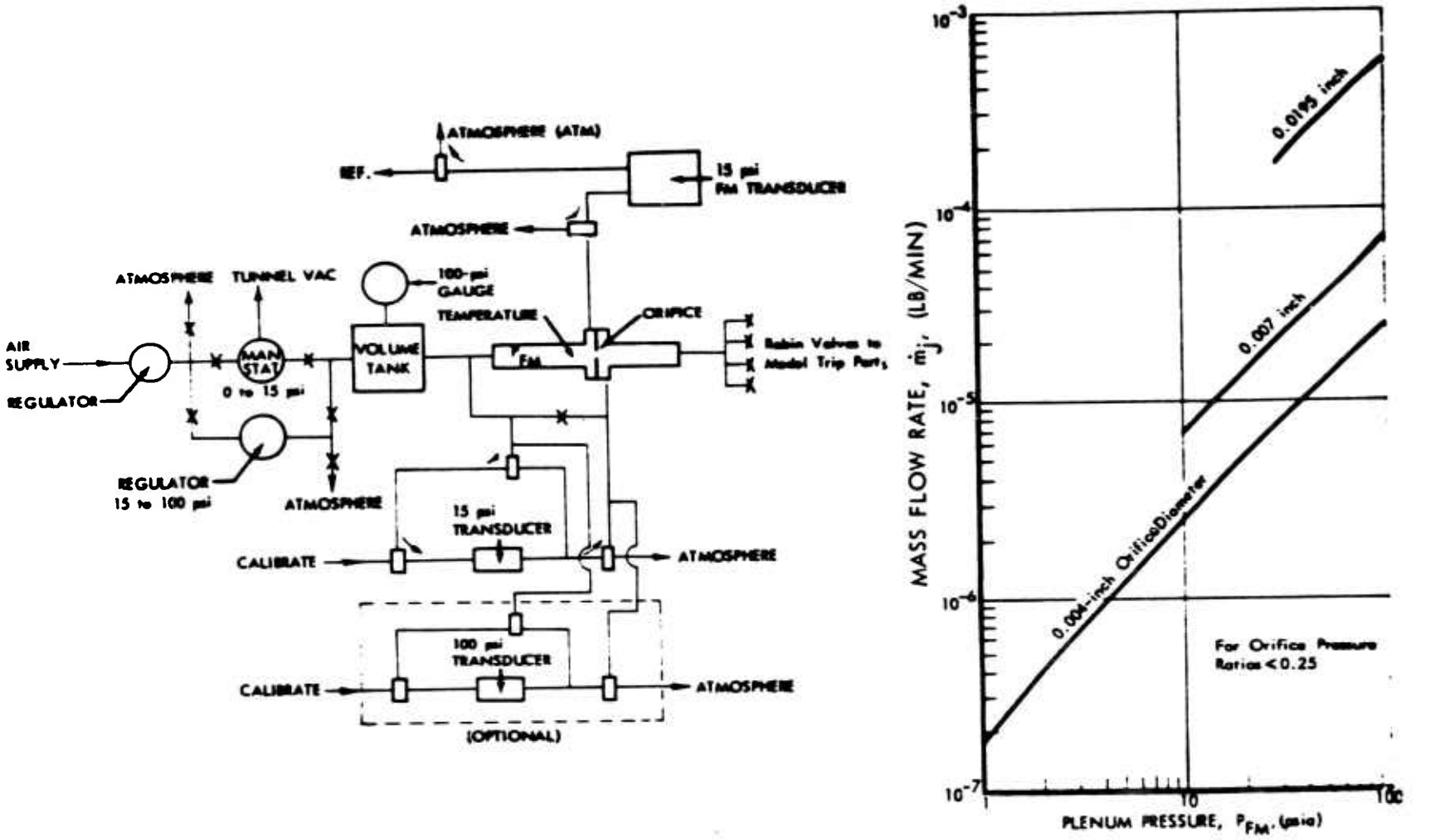

(a) Trip System Schematic

(b) Calibration Curve For Mass Flow Rates of Injection System

Figure 3-10: TRIP SYSTEM AND MASS FLOW CALIBRATION

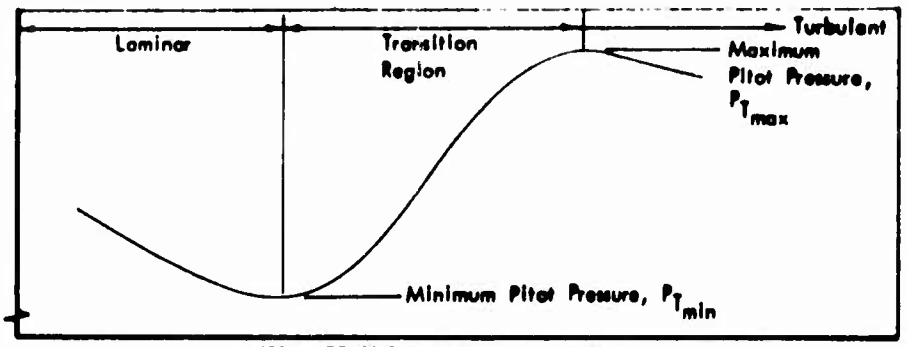

(a) Definition of Flow Regimes

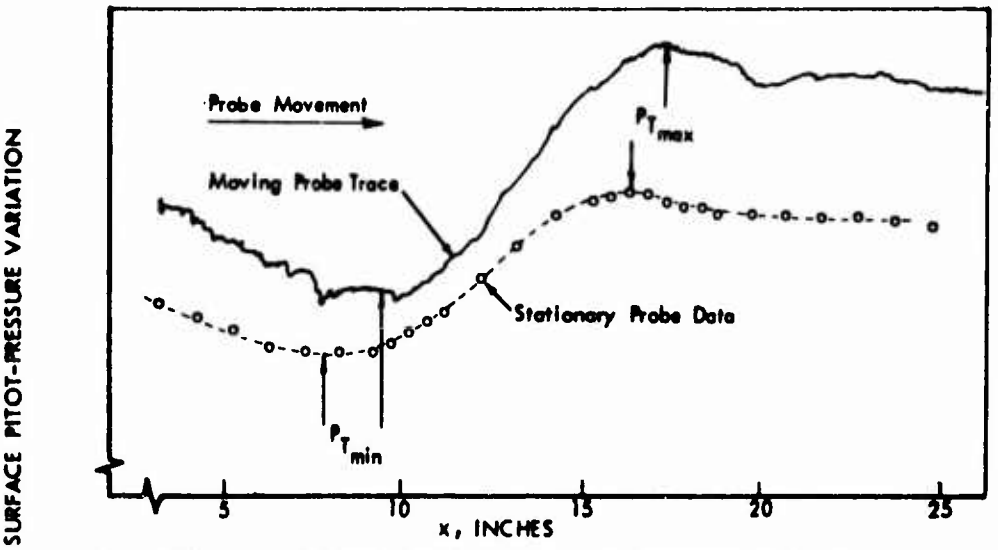

(b) Effects of Pitot System Lag in Untripped Flow

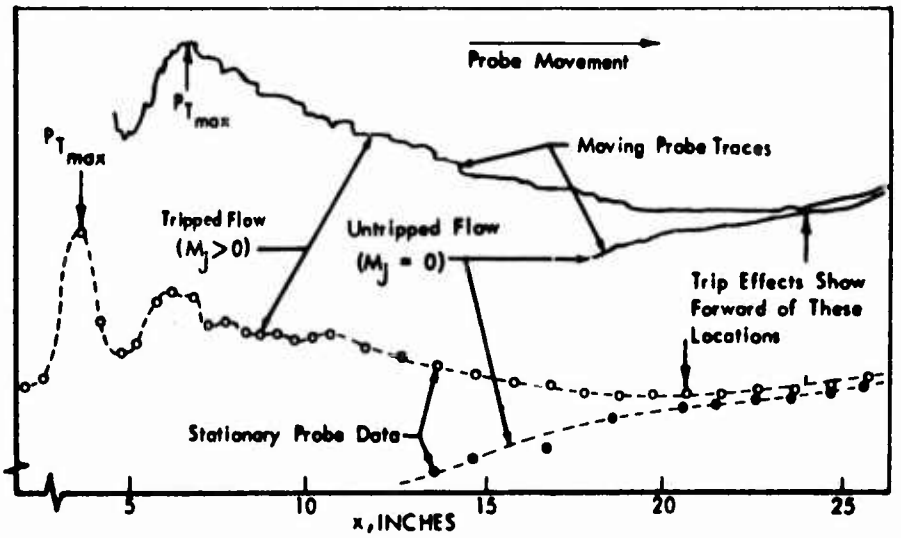

(c) Effects of Pitot System Lag in Tripped Flow

Figure 3-11: SURFACE PITOT PRESSURE AXIAL SURVEY TECHNIQUE FOR TRANSITION LOCATION

number in this case. The two critical points in Figure 3-11c, denoted by arrows are (1) the location $P_{T_{max}}$, which again seems to be much further forward with the use of the stationary probe system, and (2) the point at which the data with mass-injection begins to depart from the data for zero mass injection. It is seen that this location is also moved forward.

Transition occurs between approximately 8 and 20 inches without mass injection at the flow conditions used for Figure 3-11. An important objective of the tests was to determine whether mass injection would cause transition. It was therefore necessary to start with a laminar boundary layer over the length of the plate for untripped flow. This required a low unit Reynolds number, especially for the sharp plates. In fact, the minimum operating pressure shown in Figure 3-2 limited the useful investigation of tripped flow to angles of attack below about 5 degrees for the sharp plates.

Figure 3-12 shows typical data obtained at the low unit Reynolds numbers required for laminar flow. Figure 3-12a, the pitot survey data, shows the existence of a minimum which is poorly defined, but appears to be at about x = 13 inches. However, it is seen in Figure 3-12b that the wall pressure data from the model surface also show a minimum in the same vicinity. The curve presented in Figure 3-12c, which is the difference between the pitot and wall pressure, shows that the apparent minimum point has moved to about x = 11 inches. It will be seen later that the difference between the minimum point as deduced from Figures 3-12a and 3-12c corresponds approximately to the scatter that exists in the final data.

Figure 3-12 also shows some anomalies in the pressure measurements. Large differences in surface static pressure are shown in Figure 3-12b; the lowest values are larger than the surface pitot pressure in the vicinity of transition. These cast doubt on the transition locations.

The use of the pitot probe system leads to an angle-of-attack limitation caused by impingement of the shock system from the support fairing on the plate. Figure 3-13 shows shock locations at 10 degrees angle of attack. With the plate at 15 degrees angle of attack and the probe at forward locations, the shock system from the support housing intersects the plate toward the rear. Owing perhaps to the intersection with the cylindrical probe support this shock system is unsteady and causes a noticeable vibration in the 75-degree delta wing. Although it had not been observed with the unswept plate, the 15-degree angle of attack was avoided with both configurations during the subsequent testing.

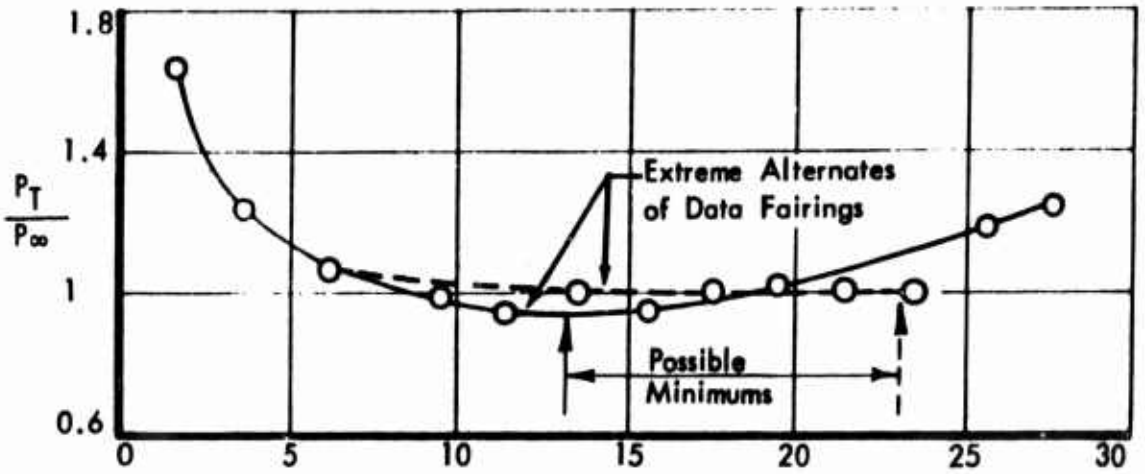

DISTANCE FROM APEX, x, (INCHES)

(a) Surface Pitot Pressure Survey Data

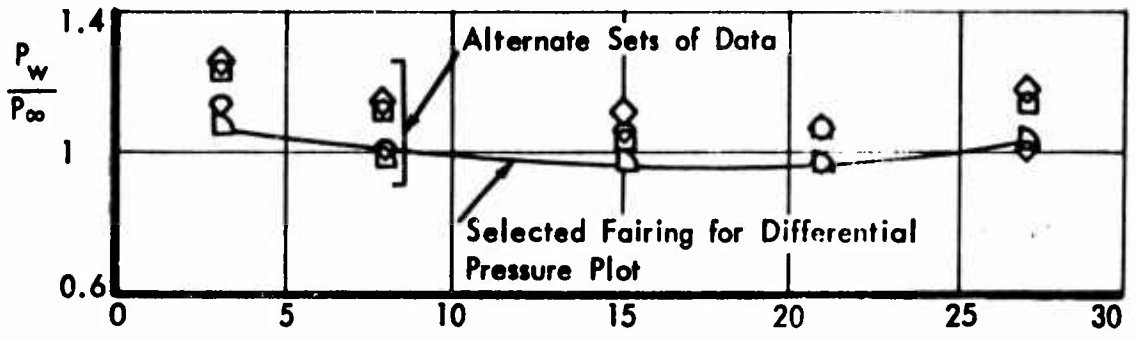

(b) Wall-Pressure Data

x, (INCHES)

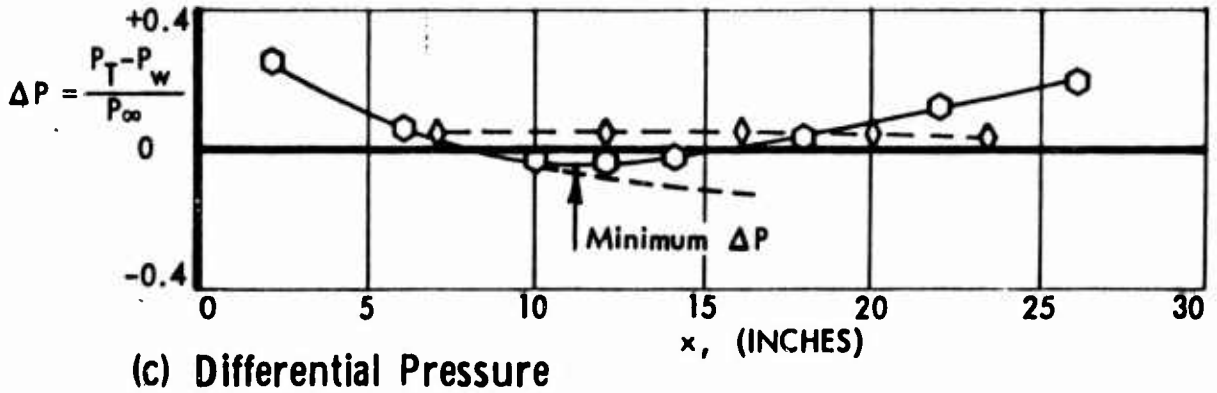

x, (INCHES)

(c) Differential Pressure

Figure 3-12: PROBLEMS ENCOUNTERED IN SURFACE PITOT PRESSURE SURVEYS

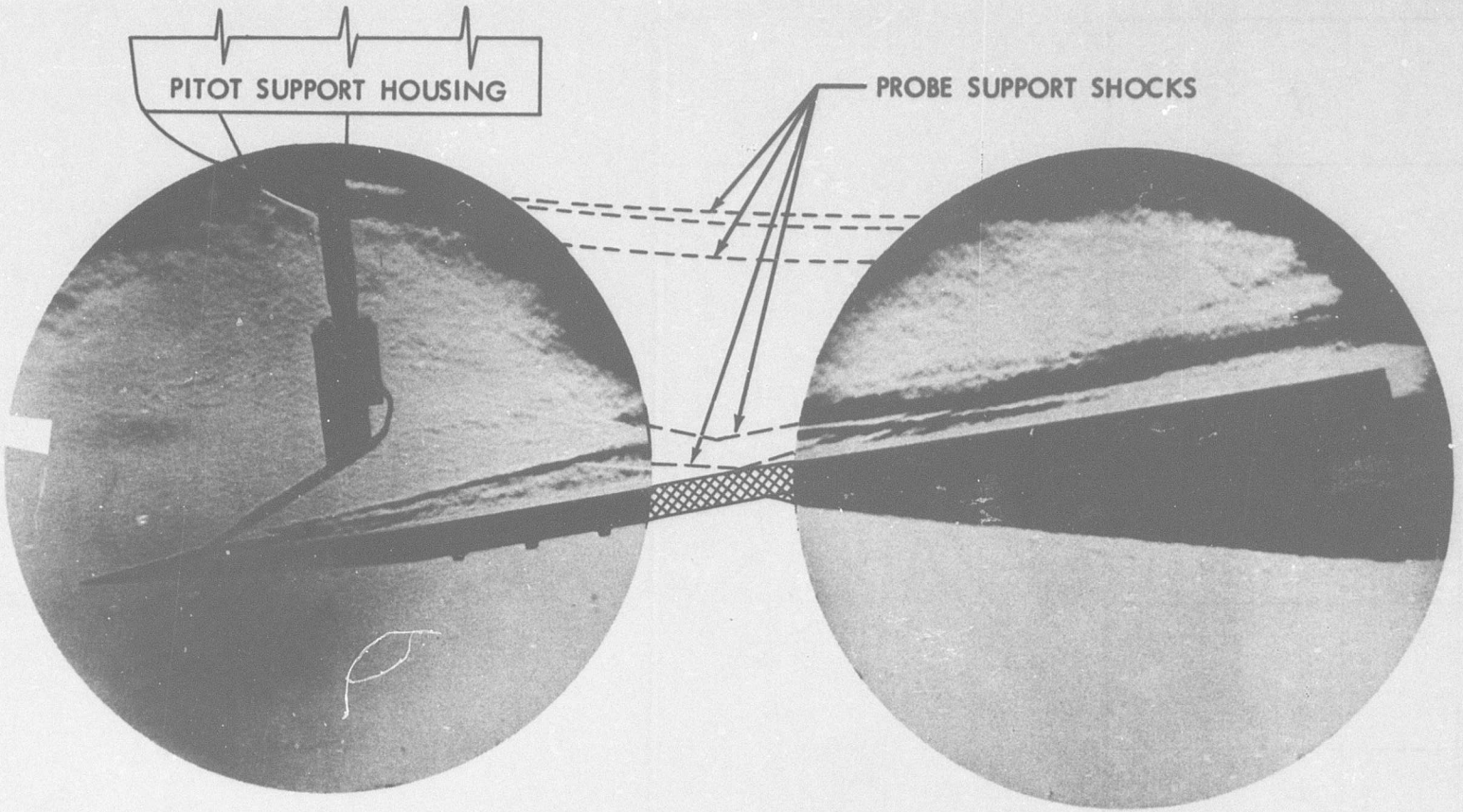

Figure 3-13: SHOCK SYSTEM CAUSED BY PROBE AND SUPPORT

RECOVERY TEMPERATURE METHOD

According to the terms of the contract under which the present investigation was conducted, the principal secondary technique for detecting transition was to be the use of model equilibrium temperatures. The expected behavior of the model equilibrium temperature is presented in Figure 3-14a. Ideally, the model equilibrium temperature should be equal to the adiabatic wall temperature, which is constant for either laminar or turbulent flow. Thus in the laminar region the model equilibrium temperature should be uniform, and in the turbulent region the model equilibrium temperature should also be uniform at a somewhat higher value. In the transition region previous experiments have shown that the adiabatic wall temperature increases to a maximum that is greater than the final turbulent value. If the heat losses from the model are small, the behavior of the model equilibrium temperatures should be similar to that of the recovery temperature. This ideal behavior is sketched in Figure 3-14a;some typical experimental results are presented in Figure 3-14b. As shown, the actual temperatures shov little resemblance to the ideal sketch in Figure 3-14a. Even with aid of the locations for the beginning and end of transition as given by the pitot survey data, it is still very difficult to recognize any of the expected characteristics. It is also seen that there is an appreciable difference between the temperatures obtained in the centerline region of the model and those obtained away from centerline.

After reviewing these data, it was determined that small heat losses could lead to relatively large perturbations in the model temperatures. Some typical heating rates for an element of model skin are presented in Figure 3-15 as a function of model surface temperature. Examining first the convective heating rate curves it is seen, that with no heat losses from the model, there would exist a difference of approximately 50°R in model temperature between the laminar and turbulent regions, as indicated by the intersections of the convective curves with the abscissa. The intersections of the convective curves with the radiation curves indicate equilibrium temperatures, i.e., temperatures at which the net heat transfer to the plate surface is zero. It is seen from the intersections of the curves that equilibrium temperatures will be 30 to 40°R below the recovery temperature due to external radiation alone. External radiation should not cause any large difficulty in locating transition, however; it is seen that the difference between laminar and turbulent flow equilibrium temperatures will be larger than the difference in recovery temperatures.

The temperature reduction caused by internal radiation is somewhat smaller than that due to external radiation, but, due to a complicated internal geometry in the model and the internal supports for the model surface, the effect of the internal radiation could range from 0 to 20°R, and could thus account for many of the small differences that were shown in Figure 3-14b.

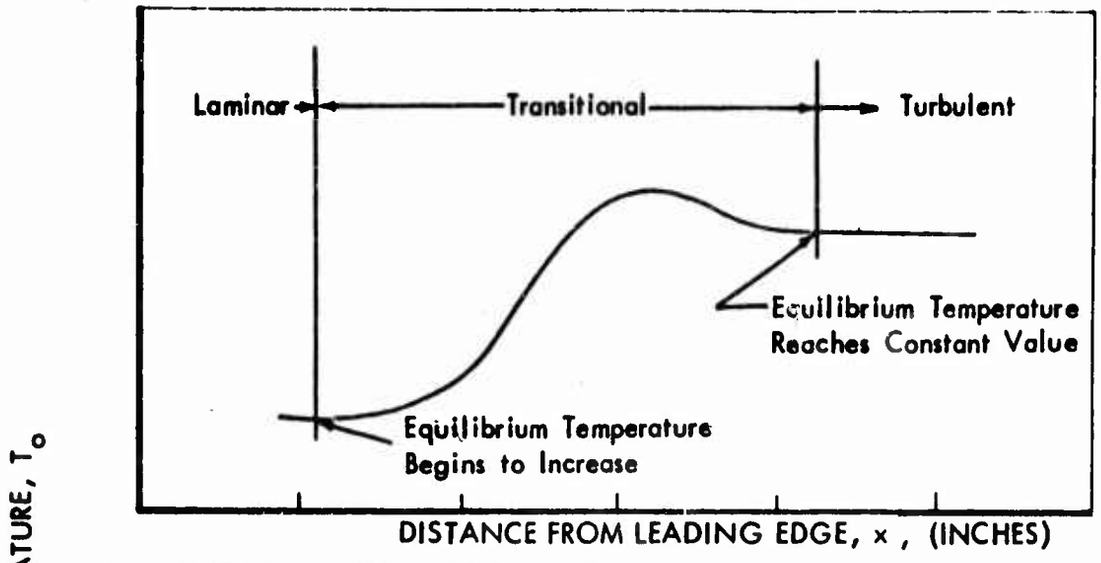

a) Ideal Temperature Distribution

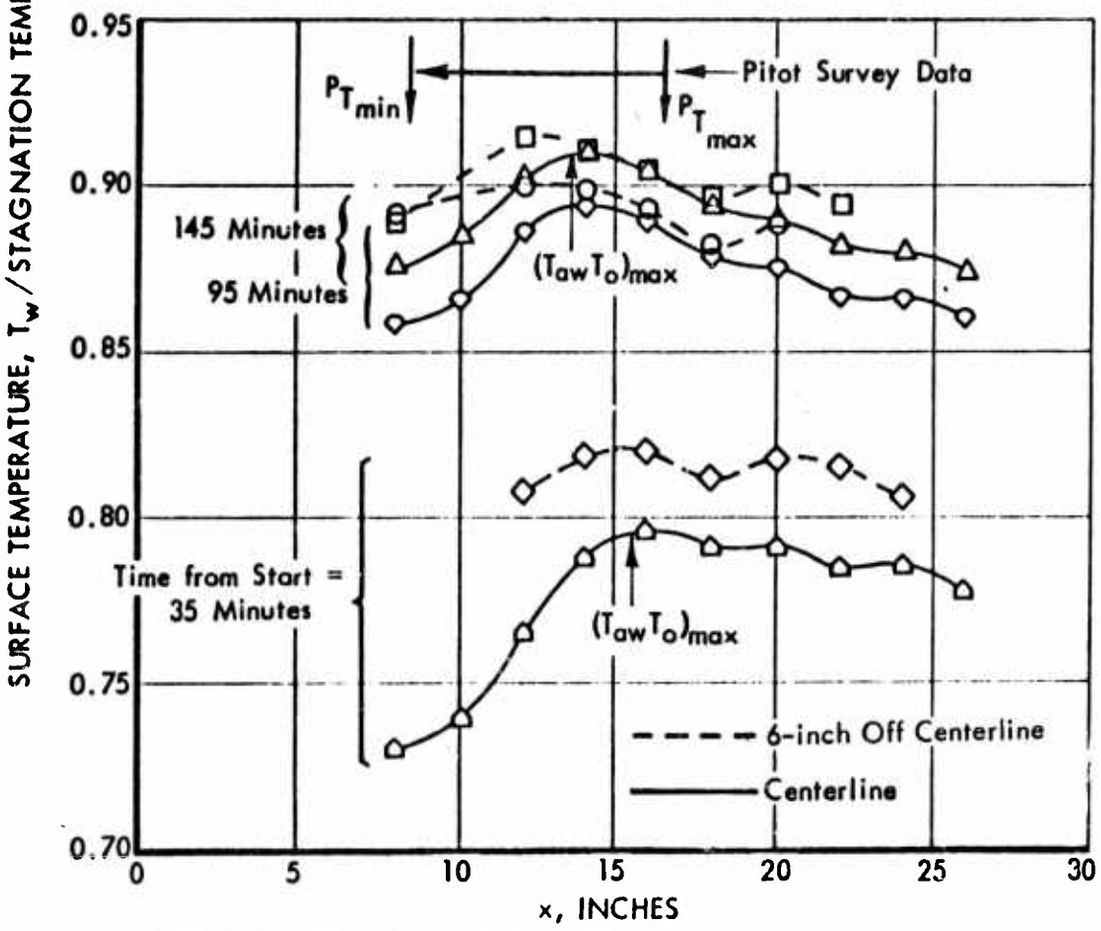

b) Actual Temperature Distribution

Figure 3-14: SURFACE TEMPERATURE DISTRIBUTION TECHNIQUE FOR TRANSITION LOCATION

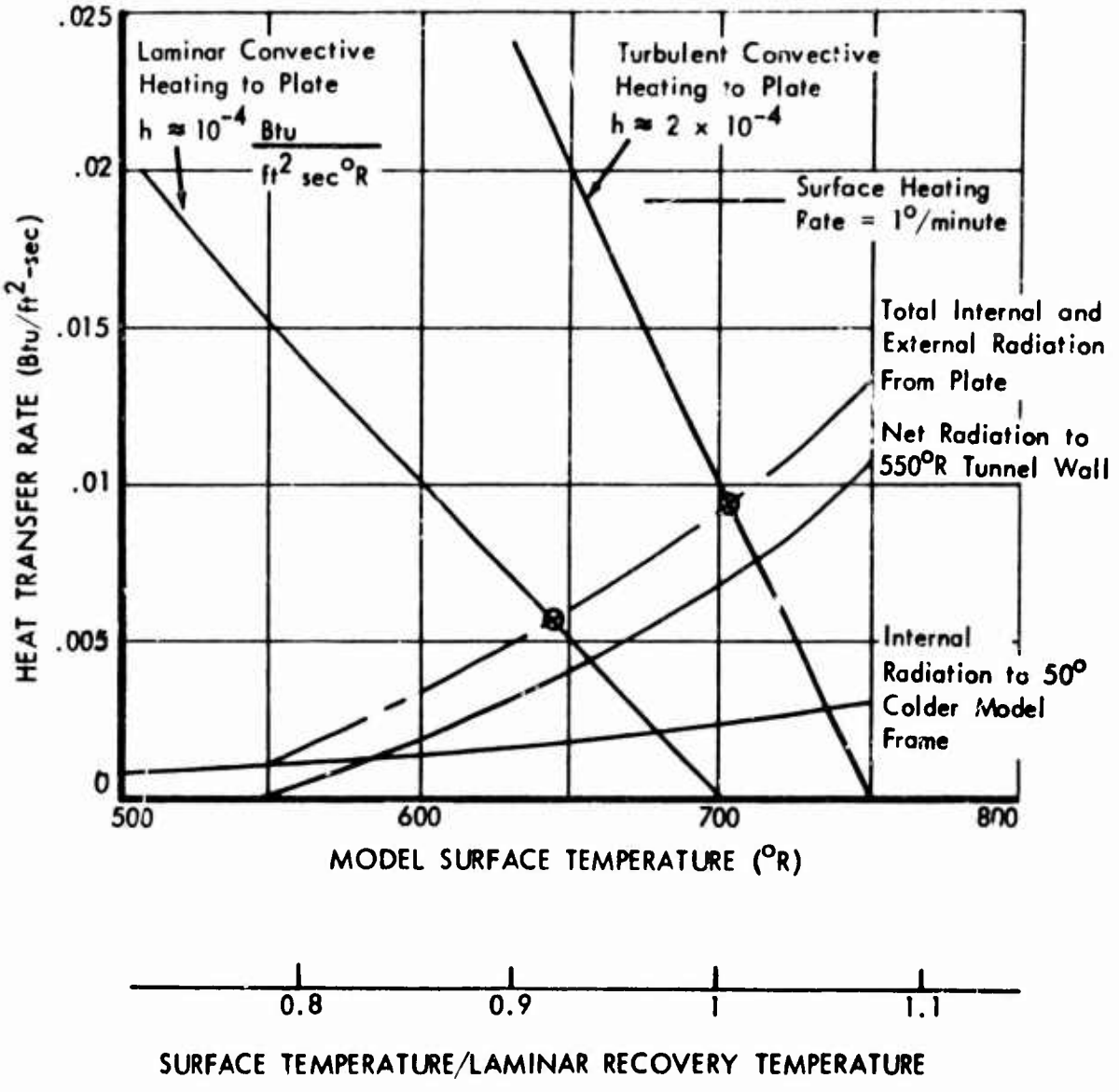

Figure 3-15: PROBLEMS ENCOUNTERED IN SURFACE TEMPERATURE DISTRIBUTION TECHNIQUE

The calculated internal radiation is a nominal value based on a 50°F internal temperature differential near the base of the model. It is known that heat was lost to the water-cooled sting, which may explain the trend toward lower temperatures far aft that appears in Figure 3-14b.

Also shown in Figure 3-15 is the equivalent heat storage rate corresponding to a model surface temperature rate of change of 1°R per minute. It is seen that, with a laminar boundary layer, this storage rate corresponds to a reduction in equilibrium temperatures of almost 200°R. From this comparison, it is clear that equilibrium temperatures will not be approached until long after the test has begun, which was in fact experienced all through the present test program. For example, in one test period of 24 hours, the tunnel was operated for a total of 14 hours; at no time during this period was model surface temperature at equilibrium. Conditions of near equilibrium were achieved for only about 4 hours.

As a result of the effects illustrated in Figure 3-15, no useful transition data were obtained by the recovery temperature method.

VERTICAL SURVEY METHOD

Many of the data presented in this report were obtained from vertical pitot pressure surveys. The typical expected behavior is presented in Figure 3-16a. The laminar profile characteristically shows very little increase in pitot pressure with distance from the surface near y = 0. The pitot pressure then increases rapidly to the boundary layer edge value. The turbulent profile as sketched is characteristically much more linear. It is seen that the turbulent values near the wall are higher than in the laminar case, a result that is consistent with the previously noted behavior of the axial survey. The turbulent boundary layer is considerably thicker than the laminar so that some distance out from the wall the pitot pressures are lower than the laminar values. The pitot pressure of the outer edge of the boundary layer remains constant along the length of the plate.

Figure 3-16b presents some of the pitot pressure profiles that were actually obtained. The profiles obtained with the double probe (number 1 in Figure 3-9) show an anomolous overpressure at the outer edge of the boundary layer. The effect is more pronounced at x = 6 than x = 24; however, when the profile at x = 24 is taken with the single probe (number 2 in Figure 3-9), the overpressure is absent and it is apparent that the pitot pressure in the outer half of the boundary layer was also affected by the double probe. A similar effect was also observed with the single probe when the boundary layer was thin, or very near the leading edge.

This overpressure was present in a considerable amount of the present data and was also observed in a previous investigation (Ref. 15). The reason for this overpressure was not shown by any of the shadowgraphs that were taken during the test.

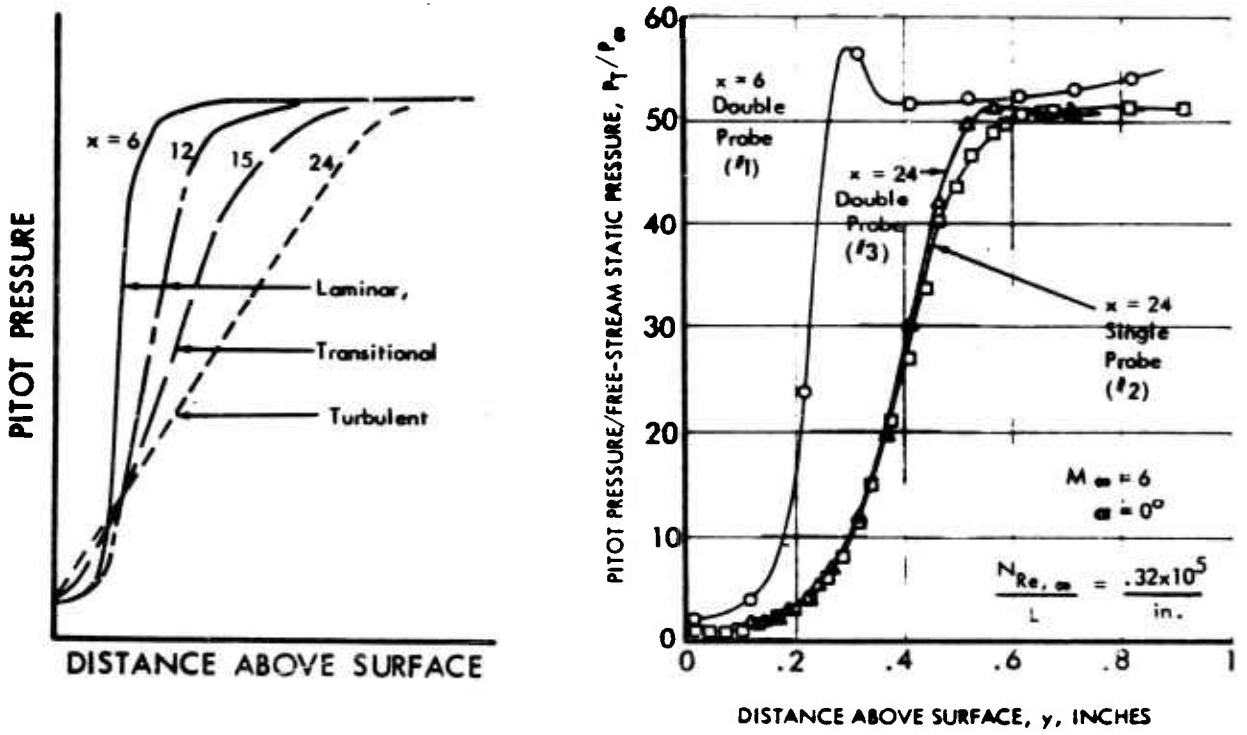

a) Idealized Pitot Surveys

b) Representative Pitot Data

Figure 3-16: BOUNDARY LAYER PROFILE ANALYSIS TECHNIQUE FOR TRANSITION LOCATION — Unswept Sharp Plate, Untripped Flow

However, it is believed that when the probe is near the outer edge of the boundary layer its shock system can cause slight separation of the laminar boundary layer. Such a separation would produce a slight compression, increasing both the static and pitot pressures. In the external flow the pitot shock would be highly swept so that, as the pitot moves away from the boundary layer, the point of shock-boundary-layer interaction is moved downstream, and although it may still exist it no longer affects the pitot reading.

Many of the probe data showed evidence of interference at the wall as well. A typical result is shown in Figure 3-17a. The extrapolation of the pitot pressures to y = 0 should agree with the measured wall pressure. It is seen that the pitot data of Figure 3-17a clearly indicate a higher value than the model surface data.

The effects of the anomalies shown in Figure 3-17a on velocity distribution are shown in Figure 3-17b. Two facts are noted:

1) The peak in pitot pressure shown in the profiles obtained with the double probe in Figure 3-16b is not apparent. However, tabulated data show free-stream velocities of 3012 and 2993 feet per second for x = 6 and 24 inches, whereas the maximum velocity at the edge of the boundary layer is 3023 and 3029 feet per second. Edge velocities would be expected to be slightly less than the free-stream values.

2) Velocity at the wall is 945, 1003, 636, and 911 feet/second for x = 3, 6, 15, and 24 inches, respectively, a result which is physically impossible. This characteristic was observed to a greater or lesser extent in all of the data when reduced to the form of velocity distributions and is believed to be indicative of some type of probe interference. Because of this incorrect character, none of the velocity distribution data have been analyzed or are presented in this report.

Leakage of the probe pressure reference system was also encountered in many of the test runs which resulted in the behavior shown typically in Figure 3-17c. These data were considered unsuited for analysis.

In the absence of any known spurious effects, the vertical survey data may still appear somewhat different than the ideal profiles shown in Figure 3-16a. Some profile survey results from the unswept sharp plate are presented in Figure 3-18 for several different Reynolds numbers. The free-stream Mach number is 8 and the angle of attack is -5 degrees. The data are plotted against η, a nondimensional boundary-layer thickness parameter, which should reduce all the profiles from the various locations on the plate to a single curve. However, it is seen that at this lowest Reynolds number, the boundary layer is relatively thinner and the external pitot pressure is much higher than at higher Reynolds numbers. This behavior is attributed to viscous interaction near the leading edge of the plate. Near the leading edge the boundary layer alters the effective shape of the plate, causing higher static pressure. As shown in several papers (Ref. 38 contains

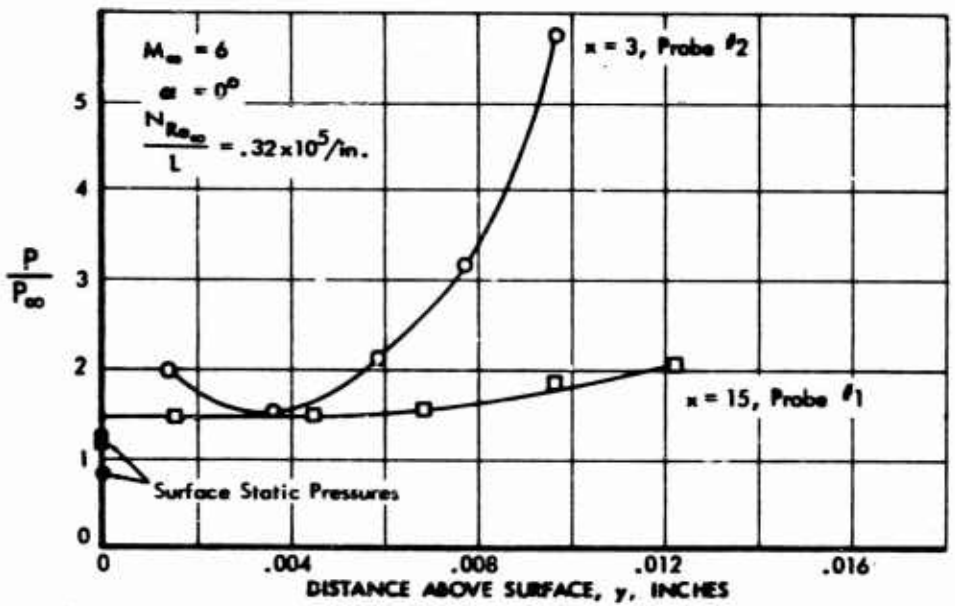

(a) Probe Interaction at the Wall

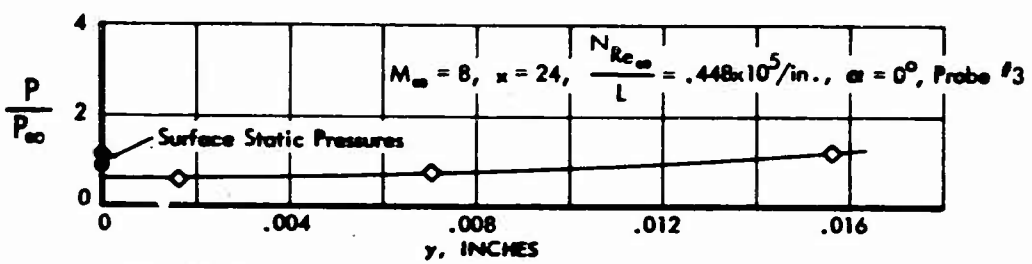

(c) Leaking Probe Reference Pressure

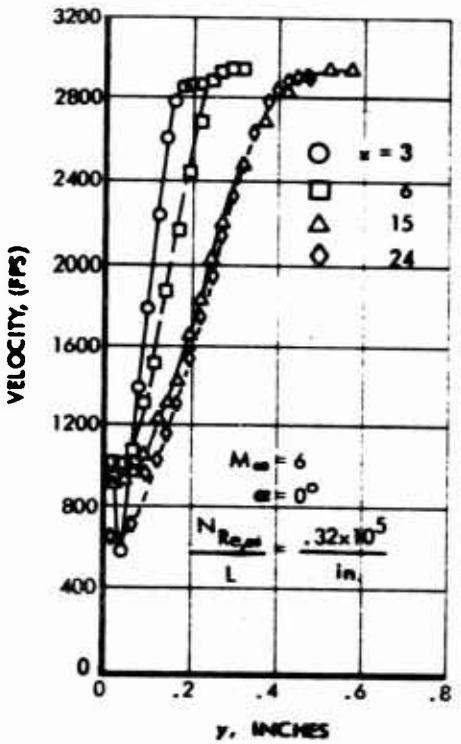

(b) Representative Velocity Data

Figure 3-17: PROBLEMS ENCOUNTERED IN BOUNDARY LAYER PROFILE ANALYSIS — Unswept Sharp Plate, Untripped Flow

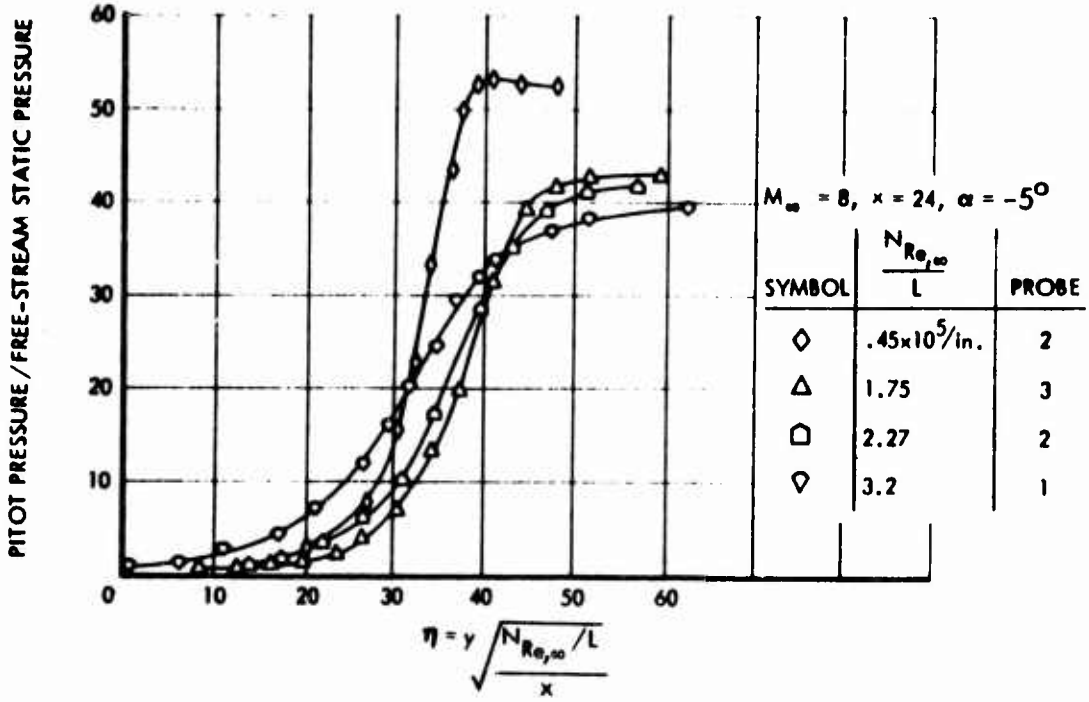

Figure 3-18: BOUNDARY LAYER PROFILES — Unswept Sharp Plate, Untripped Flow

a description of the theory), the pressure increase is approximately proportional to the parameter $\bar{x}$ defined by

$$\bar{x} = \frac{M^3}{\sqrt{N_{Re,e}}} \tag{3-1}$$

It is seen that the effect will be most pronounced at low Reynolds numbers, and is therefore largest at the lowest tunnel total pressure and nearest the leading edge. The increase in static pressure will be accompanied by an increase in dynamic pressure, as may be easily verified by oblique shock calculations. It is seen that the data presented in Figure 3-18 are consistent with this explanation (except for the most downstream profile, which exhibits the previously described transitional behavior).

Some typical pitot pressure profiles from the blunt-leading-edge flat plate are presented in Figure 3-19. As may be seen in Figure 3-19a, the outer edge of the boundary layer is not so well defined as in the previous sharp-leading-edge flat-plate data. The entire flow has a gradient of pitot pressure with distance that extends well out into the flow field. This behavior is attributed to leading-edge bluntness, which causes the shock wave to be curved at the leading edge. The larger entropy gain associated with the more nearly normal curved shock leads to lower local dynamic pressures and lower local Reynolds numbers. This effect is related entirely to the leading-edge bluntness and so should be independent of the tunnel total pressure, unlike the displacement effect of the laminar boundary layer, which is Reynolds number dependent. Thus two distinct regions should be observable in the data, a region wherein the pitot pressure distribution varies with tunnel pressure and a second wherein no change occurs. Replotting the data as shown in Figure 3-19b shows that the two regions do in fact exist. In Figure 3-19b the vertical coordinate y is adjusted by adding an arbitrary constant that has been selected to make the data in the outer region most nearly coincident. When this is done it is seen that the data from several different Reynolds numbers agree very well in the region away from the wall and that the boundary layer itself is easily recognized.

The effect of unit Reynolds number on the pitot pressure profile is shown in Figure 3-20, again using the nondimensional coordinate η. As before, the two profiles should be identical when plotted against η if the flow is laminar in both cases. As shown the profile obtained at the highest Reynolds number is transitional and begins to exhibit turbulent flow characteristics. It is also seen that the pitot pressure at the outer edge of the boundary layer is slightly higher at the lowest Reynolds number, as expected on the basis of the previous discussion.

Some typical pitot pressure profiles obtained from the sharp delta wing model are given in Figure 3-21. The most forward profile is clearly laminar; the other two profiles are transitional. It is expected that for fully turbulent flow, the profile would not exhibit the increase in pressure that is seen at y = 0.2 inch.

$M_\infty = 6$, $\alpha = 0$, $X = 24$ in.

Symbol	□	○	△	☆	▱	◇
$N_{Re,\infty}/L\left(\frac{10^5}{\text{in.}}\right)$	.32	.92	1.39	1.83	2.28	4.13

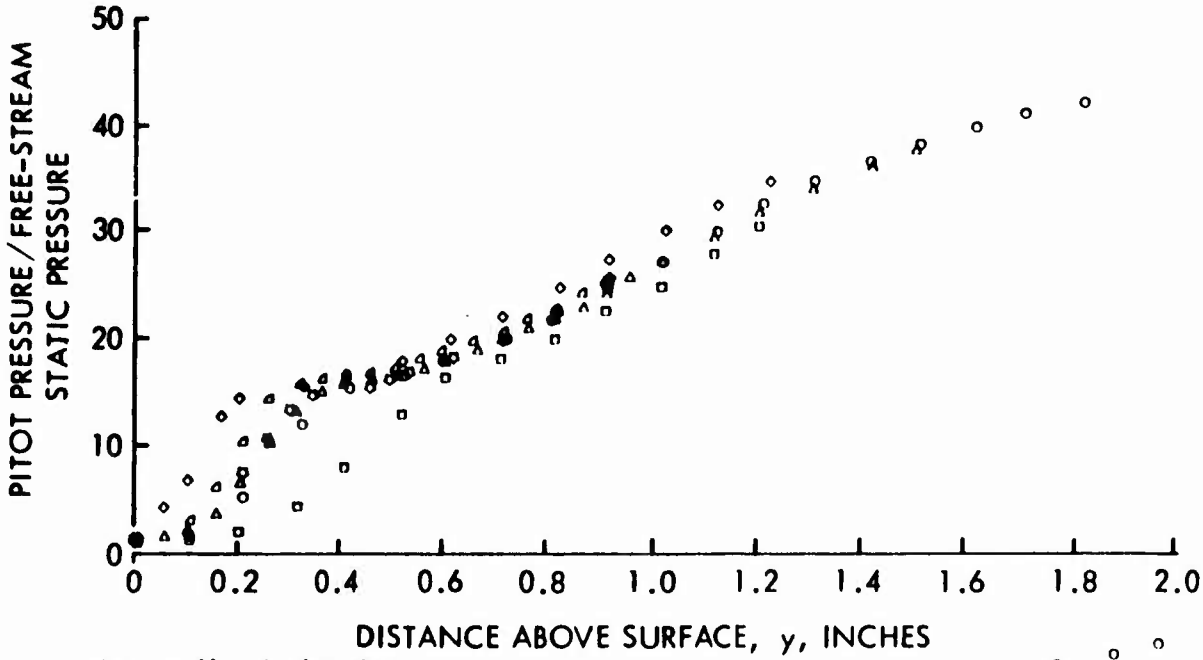

a) Unadjusted Data

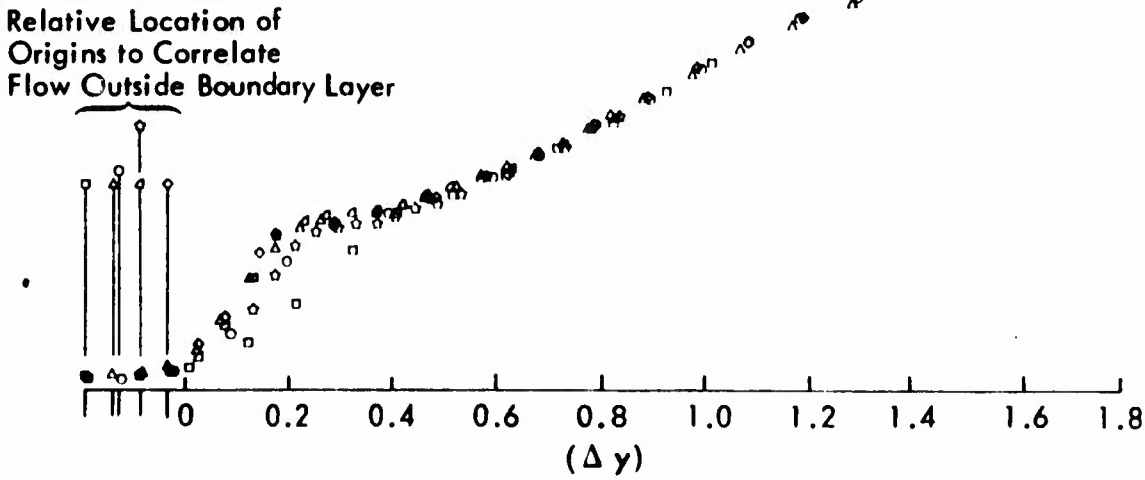

b) Abscissas Shifted to Correlate Flow in the Shear Layer

Figure 3-19: BOUNDARY LAYER PROFILES — Unswept Blunt Plate, Untripped Flow

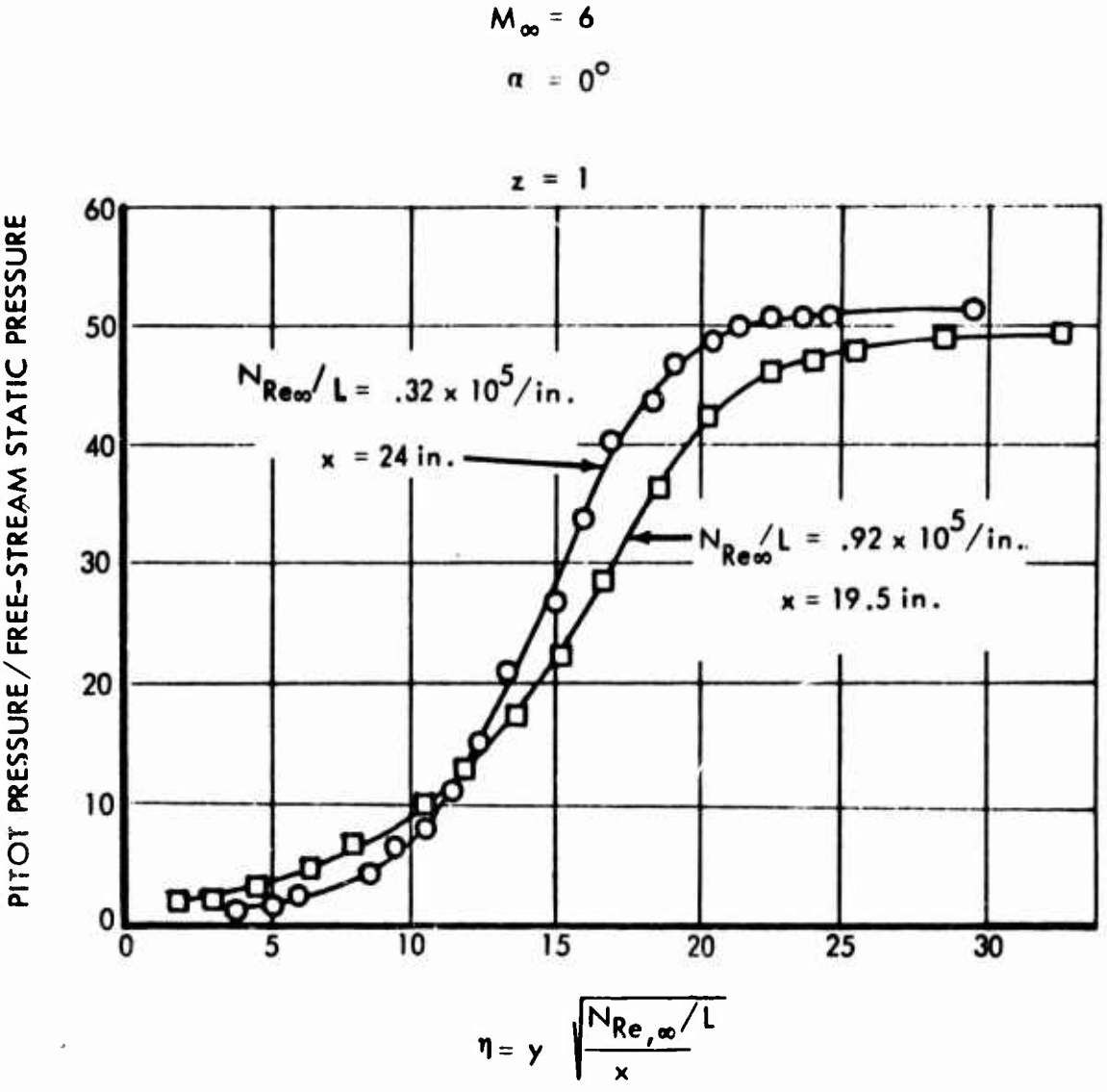

Figure 3-20: BOUNDARY LAYER PROFILES — Unswept Sharp Plate, Untripped Flow

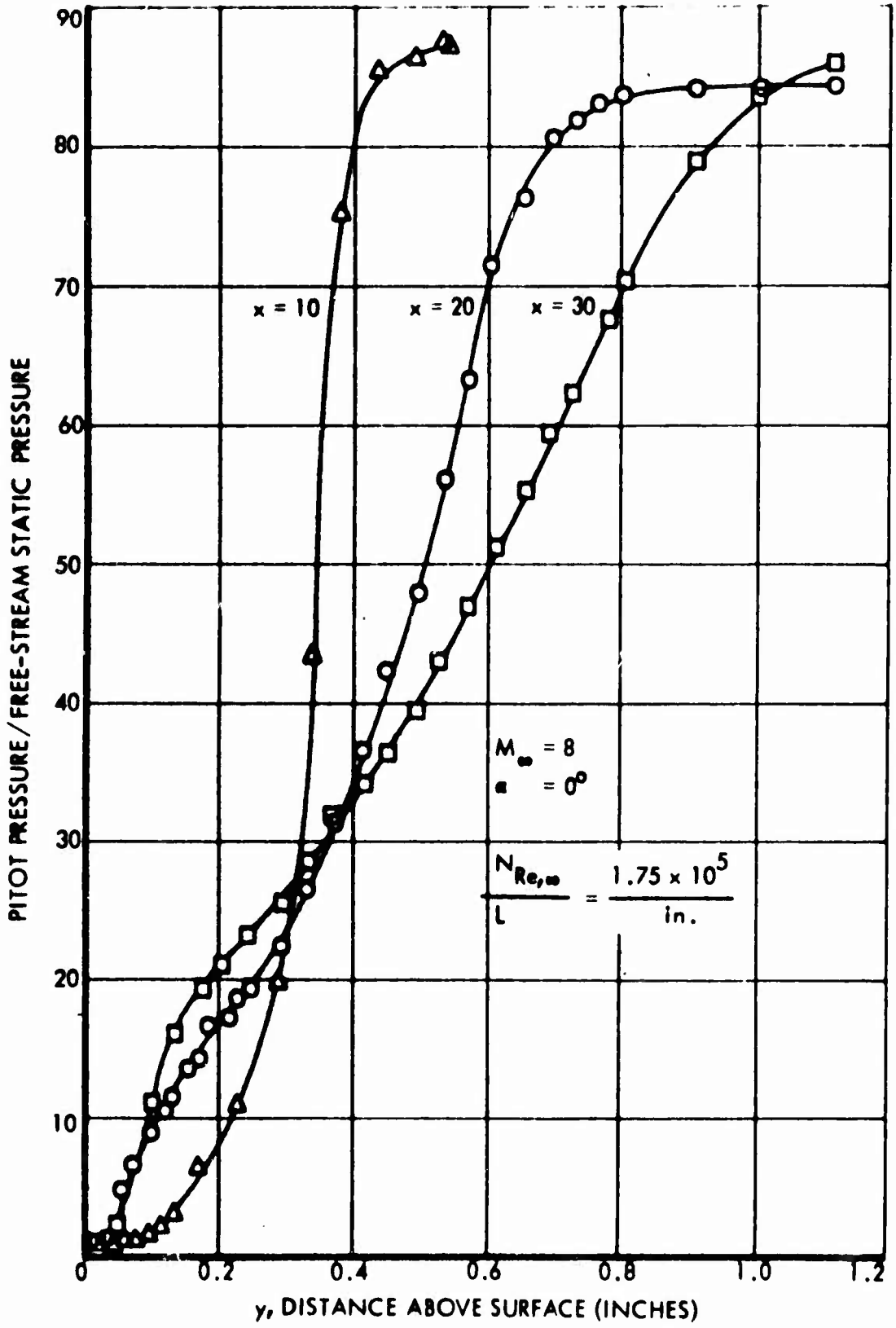

Figure 3-21: CENTERLINE BOUNDARY LAYER PROFILES — 75-Degree Swept Delta Wing, Untripped Flow

Effect of Mass Injection on Vertical Survey Results

In many of the tests mass injection was used in an attempt to cause transition. The typical effects of mass injection on the vertical survey results are shown in Figure 3-22. With very small injection rates, $M_j \leq 0.5$, the only apparent effect is a reduction in external pitot pressure. This latter trend is not interpreted as transition, however, in view of the results shown in Figure 3-23. In that figure data are compared for two rates of mass injection to the profile obtained without mass injection. It is seen that, in both cases the pitot pressure near the outer edge of the boundary layer is reduced, and that the reduction is approximately proportional to the mass injected. It is further shown that the effect is independent of the mass injection trip locations. These results indicate the observed trend is not associated with boundary layer instability at the trip location, but is merely the effect of adding mass to the boundary layer. It is seen that, with increasing mass injection rate, profiles of the turbulent type were achieved. The effect of mass injection for large injection rates is not desireable, as indicated by the typical data presented in Figure 3-24. It is seen that near the leading edge large disturbances were produced both within and outside of the boundary layer. Further downstream these effects had largely disappeared and the profile resembles the expected turbulent profile, but in view of the effects shown near the leading edge, it is clear that the data with large mass injection rates cannot be used for verifying the present analytic method, which analyzes the stability of the undisturbed profile. Obviously, this pattern of interference outside of the boundary layer will also occur at some smaller injection rates than shown in Figure 3-24.

The development of a turbulent profile from a laminar flow tripped by mass injection is shown in more detail in Figure 3-25. Again all data are plotted against the nondimensional coordinate η. A laminar profile without mass injection is also shown. It is seen that far forward on the plate mass injection had the effect of lifting the entire boundary layer away from the plate and that further downstream the boundary layer develops the expected turbulent profile. Again it is clear that the initial disturbance necessary to produce transition was not small. It was found generally throughout the entire test program that small amounts of mass injection were not effective in causing transition.

OTHER PITOT PROBE TECHNIQUES

Critical Injection Rate Method

Three other techniques for detecting transition by the pitot probe system were also investigated. In the first technique the model was held at a constant angle of attack, the pitot instrument location was fixed and the mass injection rate varied. It was expected that, with increasing mass injection rate, two opposing trends could be observed. First, the mass injection should cause a decrease in the observed pitot pressure if transition were not being produced, due to the momentum loss of the boundary layer in accelerating the injected mass. However, if transition were caused, then an increase in the measured pitot pressure should occur due

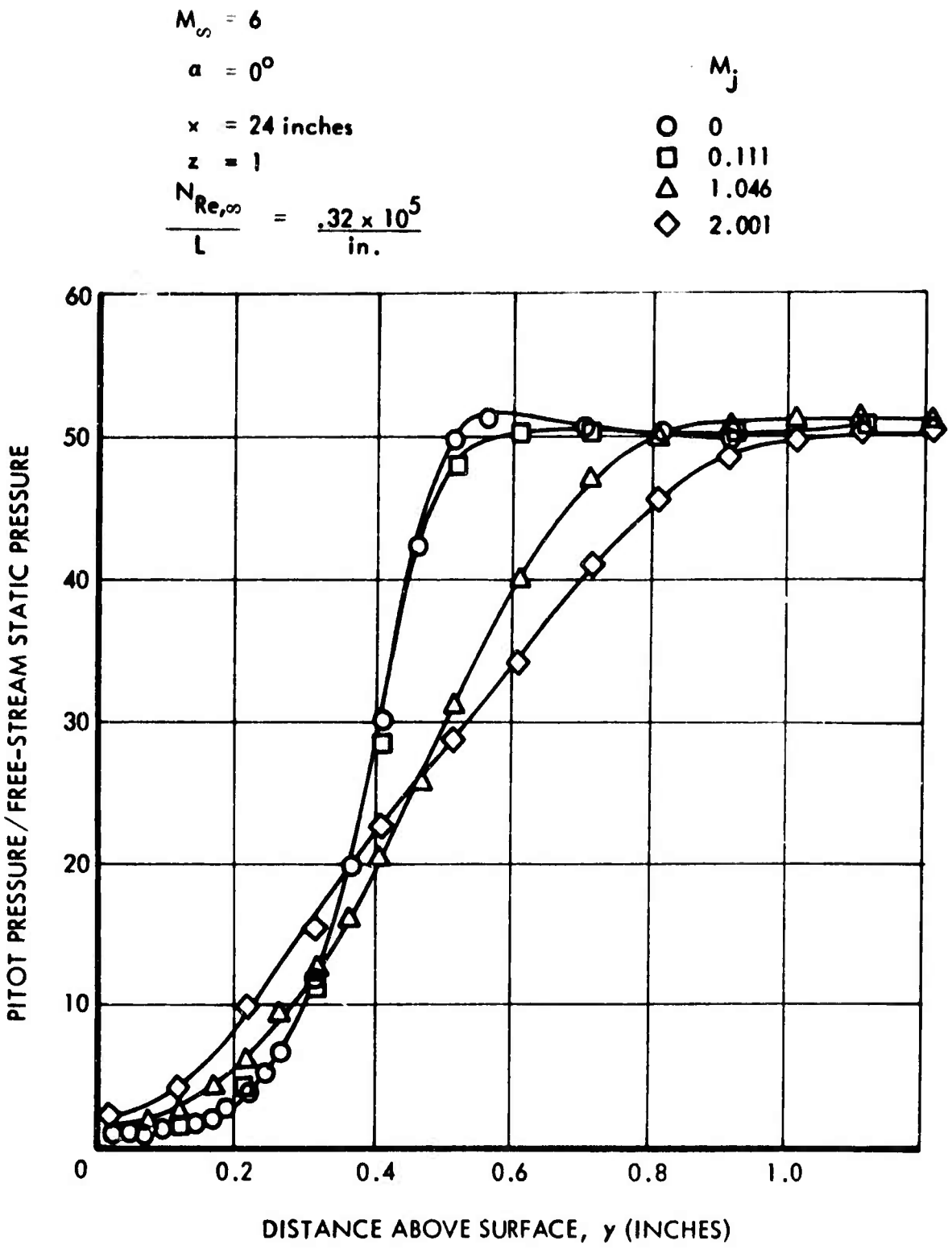

Figure 3-22: EFFECT OF BOUNDARY LAYER TRIP FLOW RATE ON PROFILES — Unswept Sharp Plate

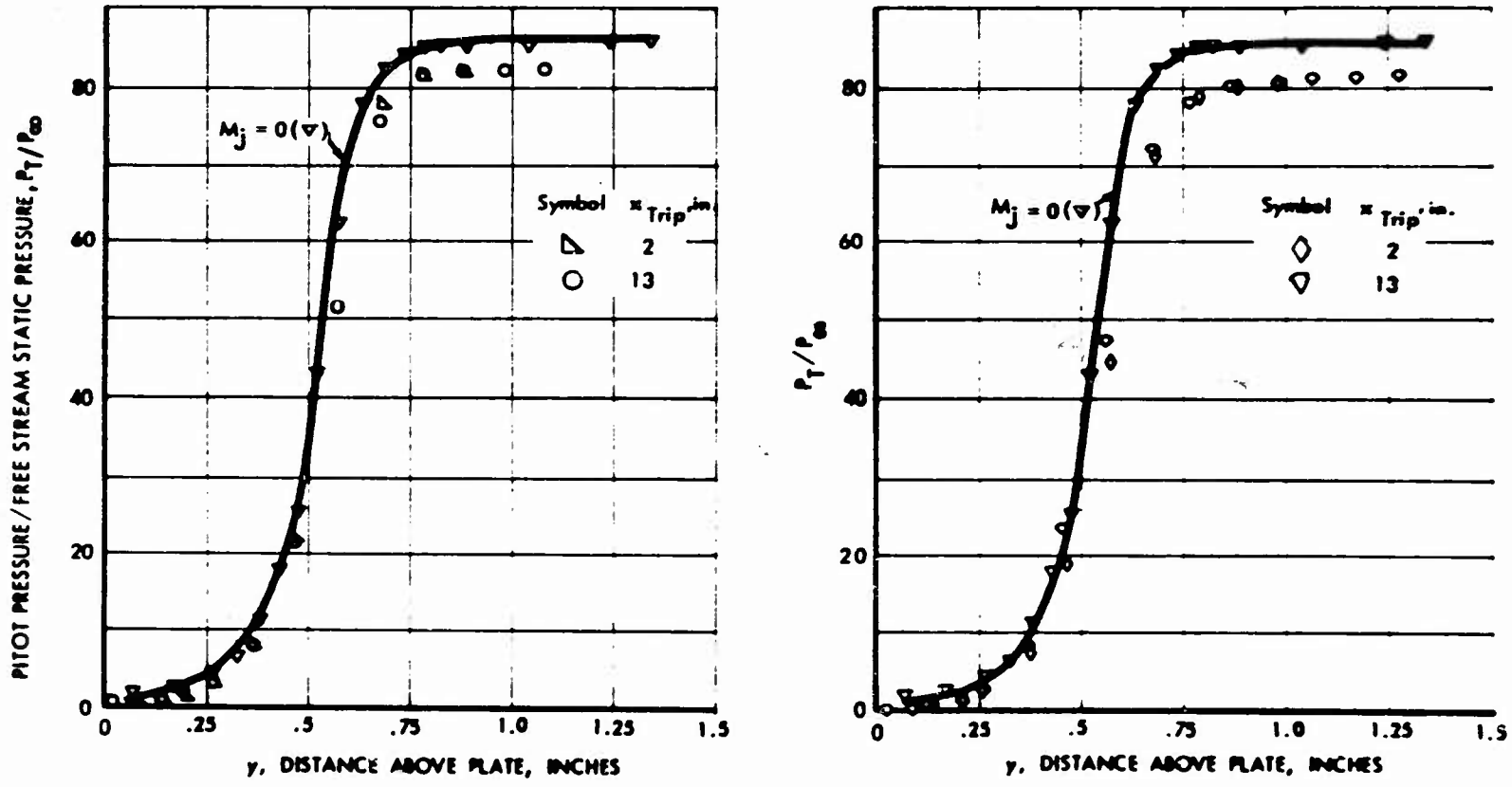

(a) $M_j = 0.2$

(b) $M_j = 0.43$

$M_\infty = 8$, $\alpha = 0°$, $\frac{N_{Re_\infty}}{L} = \frac{0.45 \times 10^5}{\text{in.}}$, $x = 24$ in. $Z = 1$ in.

Figure 3-23: EFFECT OF SMALL TRIP MASS FLOW RATE ON BOUNDARY LAYER PROFILES — Unswept Sharp Plate

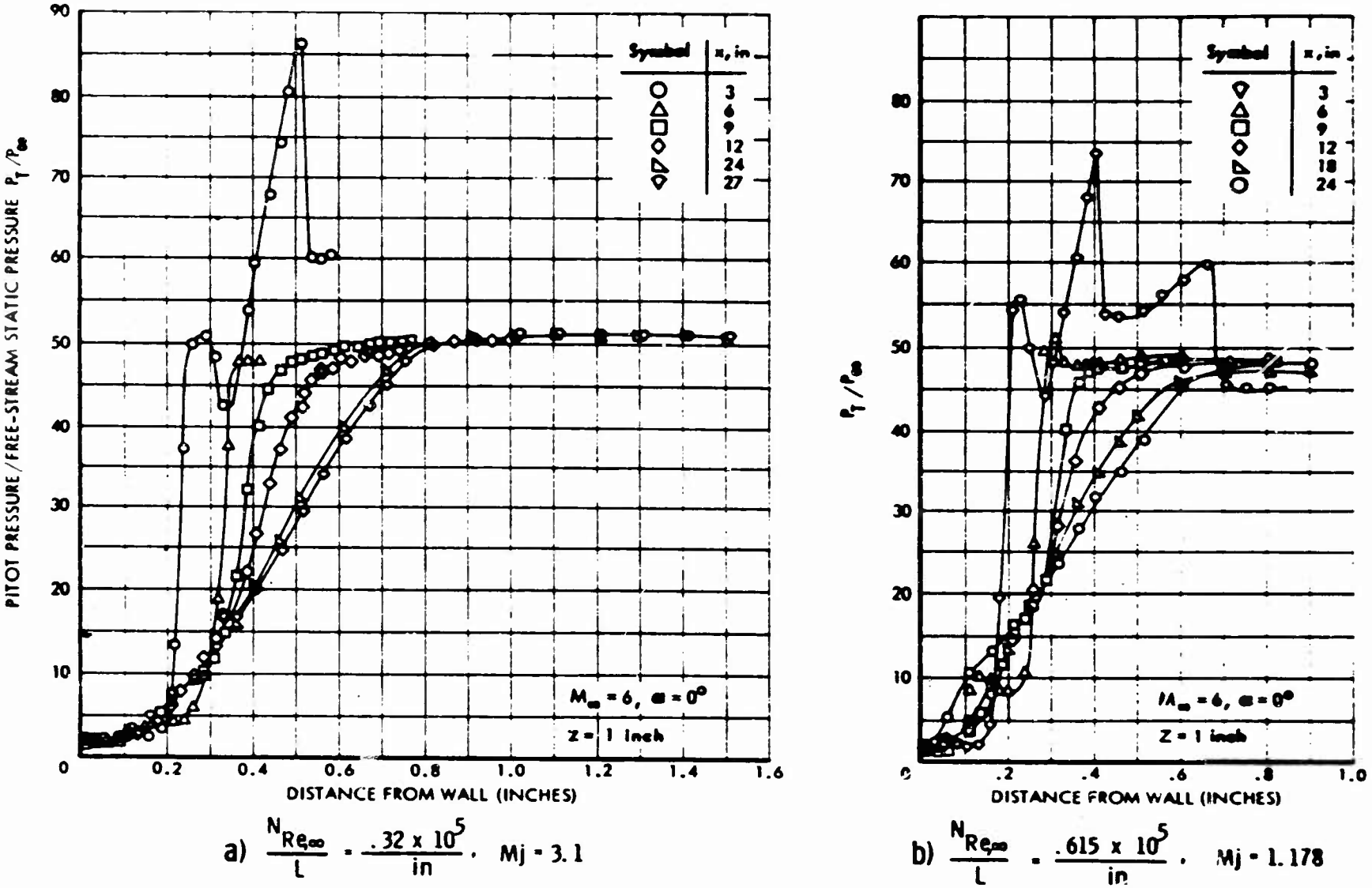

Figure 3-24: BOUNDARY LAYER PROFILES — Unswept Sharp Plate, Tripped Flow

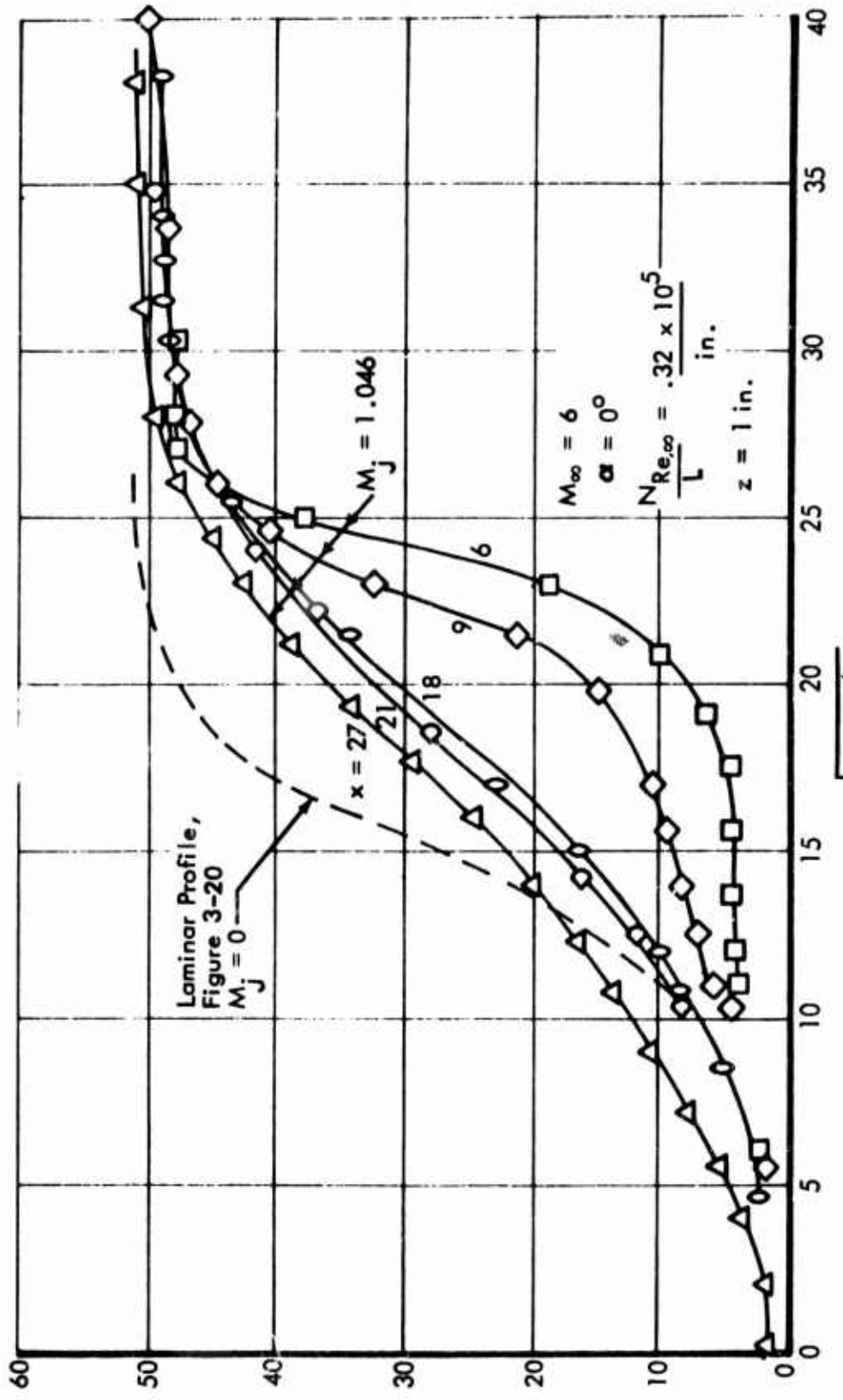

Figure 3-25: BOUNDARY LAYER PROFILE CORRELATION SHOWING TRIP EFFECTS — Unswept Sharp Plate

to the aforementioned increase in velocity near the wall. Some typical results of this technique are shown in Figure 3-26. It is seen that, at zero angle of attack and at the lowest Reynolds number, the anticipated behavior was approximately realized. For small injection rates the pitot pressure is reduced by mass injection, but begins to increase with larger rates. At the higher Reynolds number the pitot pressure began to increase with even the smallest amount of mass injection. This suggests that transition was in process or incipient without mass injection. Smaller effects were shown at -5 degrees angle of attack. At the time of testing, this technique did not appear to be particularly successful since all of the data were difficult to interpret. Only a few data points were obtained by this method.

Boundary Layer Thickness Method

A second technique that was used was based on the boundary layer thickness. With the sharp leading edge, the outer edge of the boundary layer could, in most cases, be determined reasonably well from the vertical pitot survey results. It is, of course, well known that the boundary layer thickness varies as the square root of the distance with a laminar boundary layer, but approximately as the 0.8 power of the distance in turbulent flow.

The observed effect of mass injection on the boundary layer thickness is shown in Figure 3-27. There appears to be some evidence of the expected trend of transition in the case for the lowest mass injection rate, but this contradicts the conclusion drawn from about the same condition in Figure 3-22. At the highest mass injection rate a very definite effect was observed. It does not however correspond to the anticipated turbulent boundary layer growth rate. Because of these results, the method was not used.

Critical-Angle-of-Attack Method

Attempts were also made to determine transition by varying the angle of attack with the pitot probe held at a particular location on the model. The vertical distance above the plate was held constant, as well as the chordwise location. The pitot-wall pressure ratio was expected to remain small while the flow was laminar and to increase rapidly during transition. If a particular mass injection rate caused transition, the pitot pressure was expected to be higher for the same attitude.

Typical data are shown in Figure 3-28 with the predicted variation for laminar flow shown for comparison. The rapid increase in pressure ratio at small positive angles of attack is generally consistent with the results by other techniques. However, the data approaches the predicted laminar variation very gradually and intersects it at a relatively large negative angle. If transition is considered to begin at the point where the data depart from the predicted laminar variation, the results are in poor agreement with data obtained by all other techniques. In view of the pitot and wall pressure measurement problems discussed in connection with Figure 3-12 (unknown at the time), a successful result could not very well be expected.

z = 1 in.

$M_\infty = 6$

Symbol	α	x, in.	$N_{Re,\infty}$ /L	Probe
○	0°	19.5	$.92 \times 10^5$/in.	1
□	0°	25.5	.32	1
△	-5°	24	.32	1
◺	-5°	18.2	.92	1

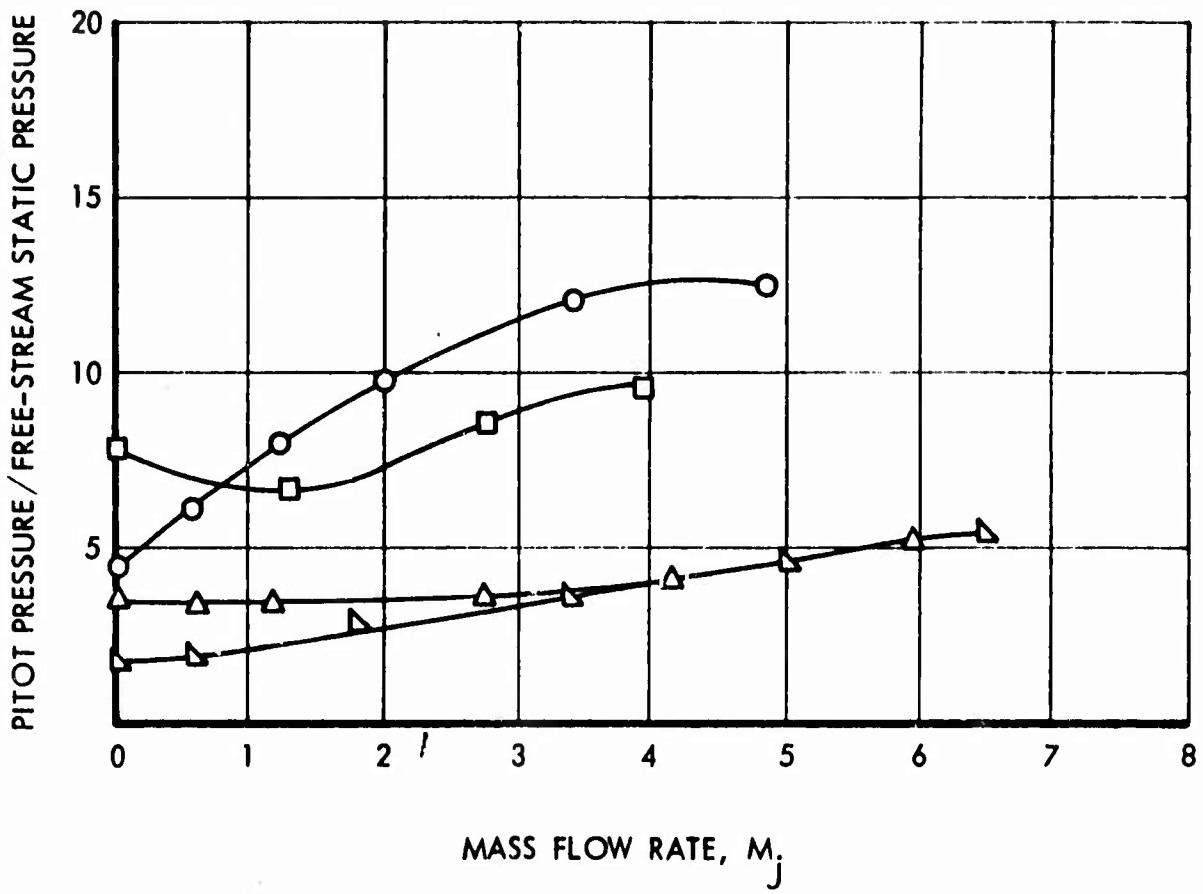

Figure 3-26: EFFECT OF MASS INJECTION RATE ON PITOT PRESSURE — Unswept Sharp Plate

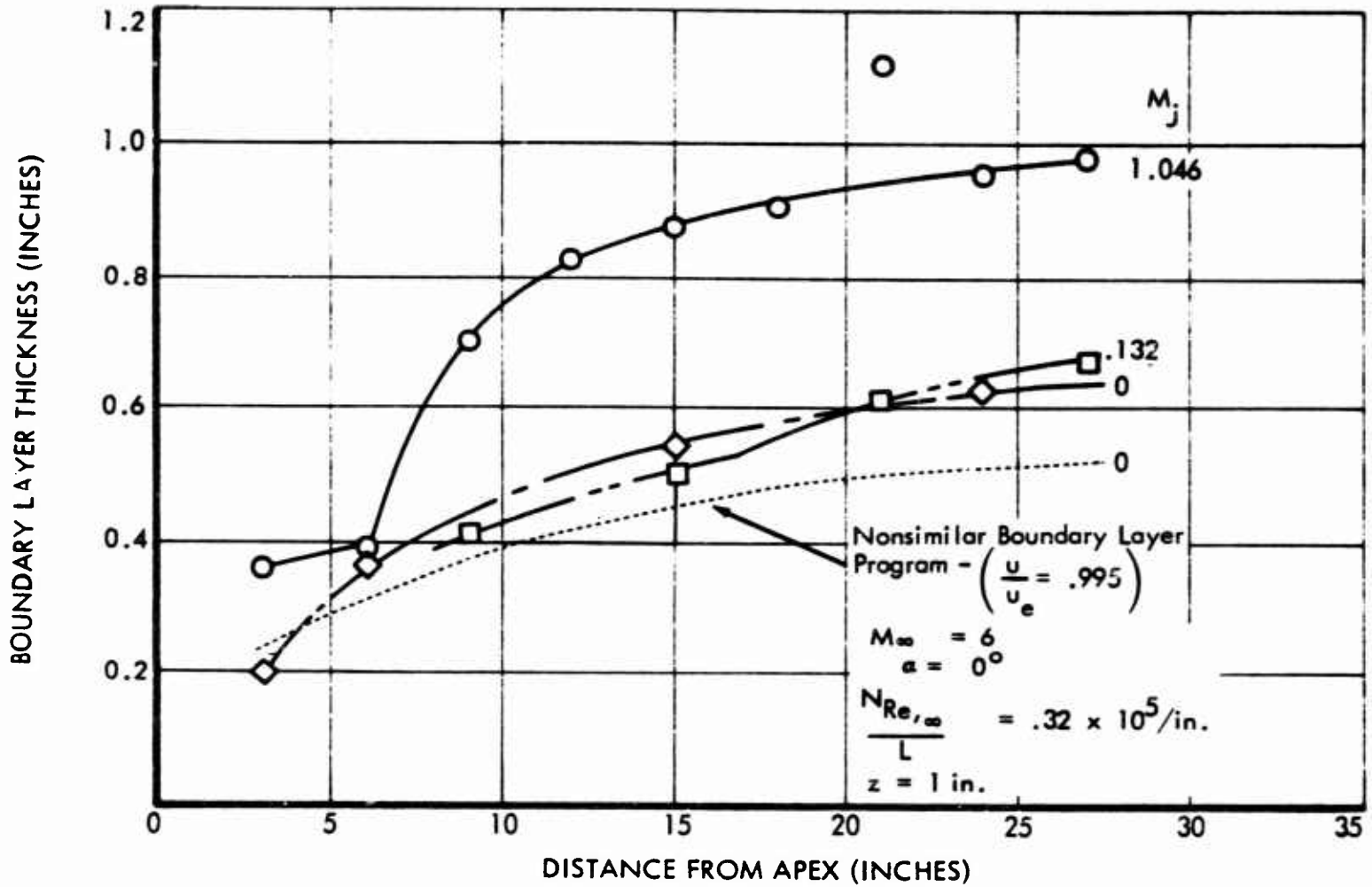

Figure 3-27: EFFECT OF TRIP FLOW RATE ON BOUNDARY LAYER THICKNESS DISTRIBUTION—Unswept Sharp Plate

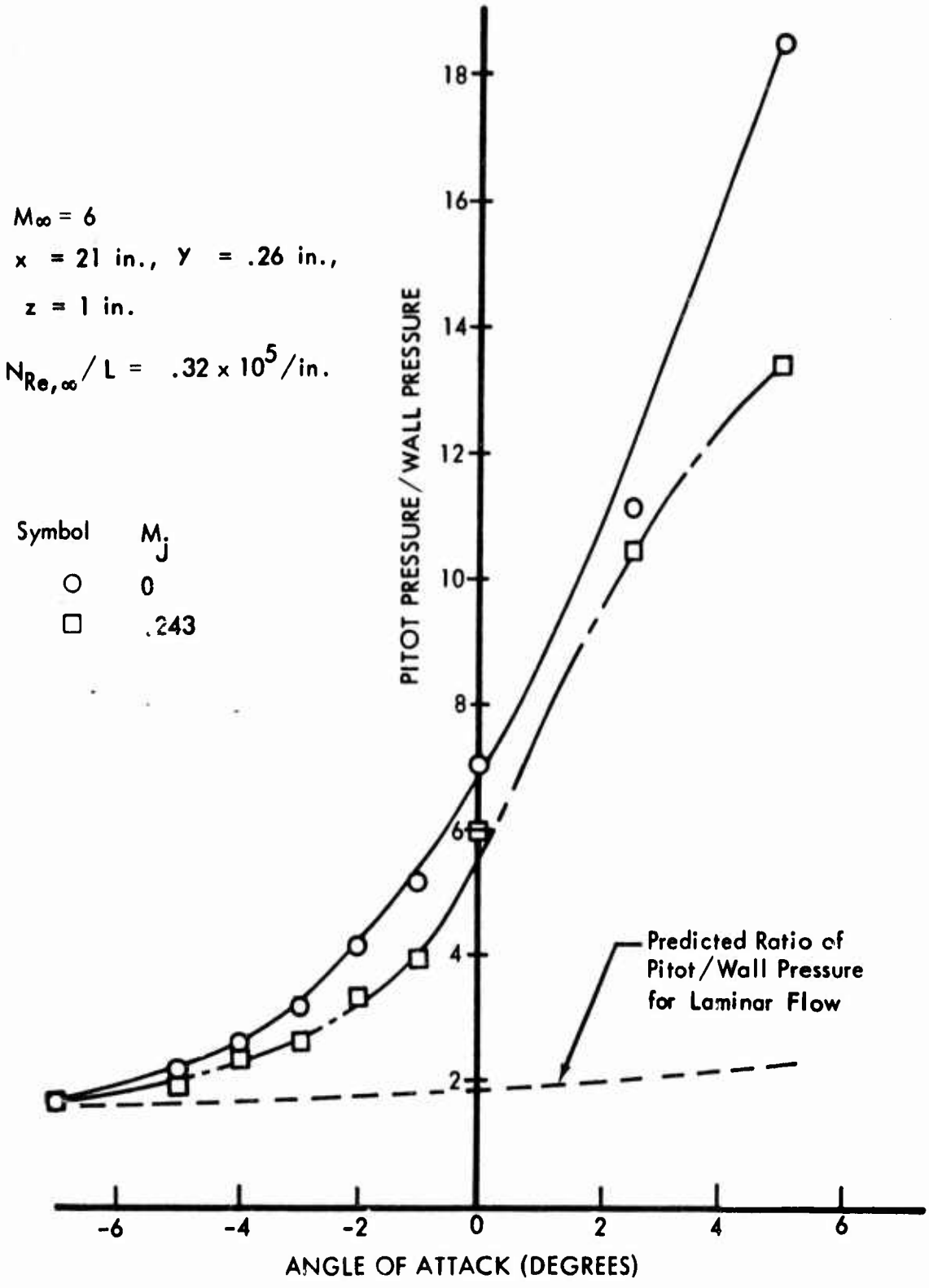

Figure 3-28: EFFECT OF ANGLE OF ATTACK ON BOUNDARY LAYER PITOT PRESSURE — Unswept Sharp Plate

The data with mass injection suggest that the injection rate was too small to advance transition.

DISCUSSION OF EXPERIMENTAL RESULTS

NATURAL TRANSITION

Although not the primary purpose of the present test program, a considerable amount of natural transition data was acquired. As stated previously, it was necessary to determine if natural transition had occurred before any tripping was attempted. In those cases for which transition had already occurred, there was, of course, no purpose in tripping. As a result, more data were obtained on natural transition than on tripped transition.

However, since the objective of the tripped flow program required operation at low unit Reynolds numbers and the axial survey and other attempted techniques produced such uncertain assessments of the transition location at these conditions, it was considered necessary to use the more-time-consuming boundary layer pitot profile technique much of the time. Consequently, the number of conditions that could be tested in the matrix of three configurations and three Mach numbers, and the ranges of unit Reynolds number, angle of attack, trip location, and blowing rate were less than desired.

Nevertheless, the present series of tests extends the previous untripped information by determining the effect of angle of attack at Mach numbers from 6 to 10 and the effect of bluntness in the same range, and provides measurements of natural transition on a highly swept, sharp leading-edge delta wing in hypersonic flow. The data obtained are tabulated in the following pages (Table III).

All local flow properties used in Table III are based on theoretical calculations. Wedge theory was used for all properties of the flow over the sharp-leading-edge flat plate. For the blunt plate, only the static pressure was calculated from wedge theory; all other properties were calculated by isentropic expansion from stagnation conditions downstream of the bow shock. For the delta wing, the surface pressure and shock-wave angles were calculated by equations given in Reference 39. All other delta-wing flow properties were calculated by isentropic compression from conditions downstream of the wing shock to the surface pressure. The resulting values are slightly higher than those given by wedge theory.

Unswept Sharp Plate

Natural transition data for the sharp unswept plate as obtained by the axial survey technique are presented in Figure 3-29 and tabulated in Table III. In this figure (and in all axial survey data to be presented in this report) the open symbols indicate the beginning of transition as determined from the minimum in the surface pitot pressure distribution. Filled symbols denote the end of transition as determined from the maximum in the surface pitot pressure distribution.

Table III: UNTRIPPED TRANSITION REYNOLDS NUMBER — AXIAL SURVEY TECHNIQUE

Configuration	M_∞	α deg.	M_e	Unit Reynolds No. (10^5 per inch)		Begin Transition (Minimum Surface Pitot Pressure) (10^6)				End Transition (Maximum Surface Pitot Pressure) (10^6)			
				$N_{Re,\infty}/L$	$N_{Re,e}/L$	x in.	$N_{Re,\infty}$	$N_{Re,e}$	$(N_{Re,e})_{adj}$	x in.	$N_{Re,\infty}$	$N_{Re,e}$	$(N_{Re,e})_{adj}$
Unswept Sharp Flat Plate	6	$-4\frac{1}{2}$	6.73	2.45	1.837	8	1.96	1.47	1.512	25	6.03	4.59	4.73
		0	6	3.07	3.07	5.5	1.69	1.69	1.432	10	3.07	3.07	2.6
				2.725	2.725	6.5	1.77	1.77	1.553	15	4.09	4.09	3.59
				1.62	1.62	7.5	1.215	1.22	1.313	23.5	3.81	3.81	4.13
				1.389	1.389	9.5	1.32	1.32	1.956	24.5	3.4	3.4	3.92
				0.917	0.917	17	1.51	1.51	2.05	--	--	--	--
		$1\frac{1}{2}$	5.77	1.68	1.85	9.5	1.6	1.75	1.797	22	3.7	4.06	4.17
		$7\frac{1}{2}$	4.95	1.369	1.918	6.3	0.86	1.21	1.218	15.5	2.12	2.97	3.06
		15	3.97	1.371	2.03	4.2	0.58	0.85	0.842	12.3	1.69	2.50	2.48
				0.907	1.34	6	0.54	0.80	0.94	15.7	1.42	2.11	2.41
	8	-5	9.41	3.2	1.7	9.3	2.98	1.58	1.673	--	--	--	--
		0	8	1.74	1.74	10	1.75	1.75	1.845	26.5	4.64	4.64	4.89
				1.22	1.22	13	1.588	1.59	1.92	--	--	--	--
		5	6.92	0.45	0.63	19.5	0.88	1.23	1.94	--	--	--	--
		10	5.82	1.685	2.53	6	1.01	1.52	1.38	17	2.87	4.30	3.90
				1.217	1.82	6.5	0.79	1.18	1.228	18.75	2.28	3.42	3.54
		15	4.72	1.74	2.47	5	0.875	1.24	1.14	11.8	2.06	2.92	2.69
				0.45	0.639	11.4	0.513	0.73	1.14	26.3	1.18	1.68	2.62
	10	-5	12.2	1.74	0.87	15.5	2.7	1.35	1.87	--	--	--	--
		10	6.63	1.2	1.8	8	0.96	1.44	1.49	22.7	2.7	4.08	4.22
Unswept Blunt Flat Plate	6	0	3.2	2.26	0.248	17.7	4.0	0.44	1.004	--	--	--	--
		15	2.02	2.30	0.39	13.5	3.11	0.53	1.0	25	5.75	0.975	1.85

Table III: UNTRIPPED TRANSITION REYNOLDS NUMBER — AXIAL SURVEY TECHNIQUE (Cont)

Configuration	M_∞	α, deg.	M_e	Unit Reynolds No. (10^5 per inch) $N_{Re,\infty}/L$	$N_{Re,e}/L$	Begin Transition (Minimum Surface Pitot Pressure) (10^6) x in.	$N_{Re,\infty}$	$N_{Re,e}$	$(N_{Re,e})_{adj}$	End Transition (Maximum Surface Pitot Pressure) (10^6) x in.	$N_{Re,\infty}$	$N_{Re,e}$	$(N_{Re,e})_{adj}$
Unswept Blunt Plate	8	-5	--	3.25	--	--	--	--	--	--	--	--	--
		0	--	1.73	--	--	--	--	--	--	--	--	--
		15	2.12	3.22	0.436	--	--	--	--	27.3	8.8	1.19	2.175
				1.75	0.189	16	2.8	0.302	0.77	--	--	--	--
	10	10	2.52	1.76	0.104	17.5	3.08	0.182	0.589	--	--	--	--
				1.2	0.0695	23.5	2.82	0.163	0.617	--	--	--	--
75° Swept Delta Wing (z=0)	6	-5	6.82	4.19	2.86	10	4.19	2.86	2.71	15.6	6.54	4.46	4.20
				1.75	1.20	21	3.68	2.52	2.69	32.5	5.69	3.90	4.19
		0	6	4.20	4.20	3.8	1.60	1.60	1.44	8.2	3.44	3.44	3.10
				1.76	1.76	8.8	1.55	1.55	1.58	17	2.99	2.99	3.05
		$7\frac{1}{2}$	5.21	1.78	2.50	--	--	--	--	8.5	1.51	2.12	2.06
		15	4.30	1.75	2.82	2.8	0.49	0.79	0.74	6	1.05	1.69	1.60
				0.617	0.994	6.6	0.407	0.656	0.722	14.8	0.913	1.47	1.62
	8	-5	9.41	2.93	1.58	6	1.76	0.947	0.98	16	4.68	2.53	2.62
				1.78	0.96	9.7	1.72	0.93	1.03	--	--	--	--
		0	8	1.78	1.78	11	1.96	1.96	1.98	25.7	4.58	4.58	4.66
				0.925	0.925	16.7	1.54	1.54	1.72	--	--	--	--
		10	6.05	1.78	2.92	3.4	0.605	0.99	0.94	9	1.6	2.63	2.50
	10	-5	12.2	1.77	0.89	11	1.95	0.98	1.10	--	--	--	--
				1.19	--	--	--	--	--	--	--	--	--
		0	10	1.75	1.75	18	3.15	3.15	3.20	--	--	--	--

Table III: UNTRIPPED TRANSITION REYNOLDS NUMBER — AXIAL SURVEY TECHNIQUE (Cont)

Configuration	M_∞	α deg.	M_e	Unit Reynolds No. (10^5 per inch) $N_{Re,\infty}/L$	$N_{Re,e}/L$	Begin Transition (Minimum Surface Pitot Pressure) (10^6) x in.	$N_{Re,\infty}$	$N_{Re,e}$	$(N_{Re,e})_{adj}$	End Transition (Maximum Surface Pitot Pressure) (10^6) x in.	$N_{Re,\infty}$	$N_{Re,e}$	$(N_{Re,e})_{adj}$
75° Swept Delta Wing (z=0)	10	10	6.63	1.73	2.89	3.5	0.605	1.01	0.96	12	2.07	3.47	3.29
				0.64	1.06	9	0.577	0.95	1.61	25	1.6	2.65	2.90
75° Swept Delta Wing (z=3)	6	-5	6.82	4.19	2.86	4.8*	2.01	1.37	1.30	13.8	5.77	3.95	3.76
				1.72	1.17	10.8	1.86	1.27	1.39	--	--	--	--
		0	6.0	1.73	1.73	5.8	1.00	1.00	1.022	14.2	2.46	2.46	2.52
	8	-5	9.41	2.93	1.56	9.8	2.87	1.53	1.58	--	--	--	--
				1.77	0.94	9.3	1.65	0.87	0.97	--	--	--	--
		0	8	1.81	1.81	7.2	1.30	1.30	1.32	19.3	3.50	3.5	3.55
		10	6.05	1.77	2.90	1.8	0.32	0.52	0.49	5.2	0.92	1.51	1.43

* Distances shown for z =3 data (and used in analysis) are distance from leading edge measured parallel to centerline.

NOTE:

$$\left(N_{Re,e}\right)_{adj} = \left(N_{Re,e}\right)\left\{\frac{2 \times 10^5}{\left(N_{Re,e/L}\right)}\right\}^n$$

where

n = 0.4 for unswept plate, and n = 0.14 for delta wing.

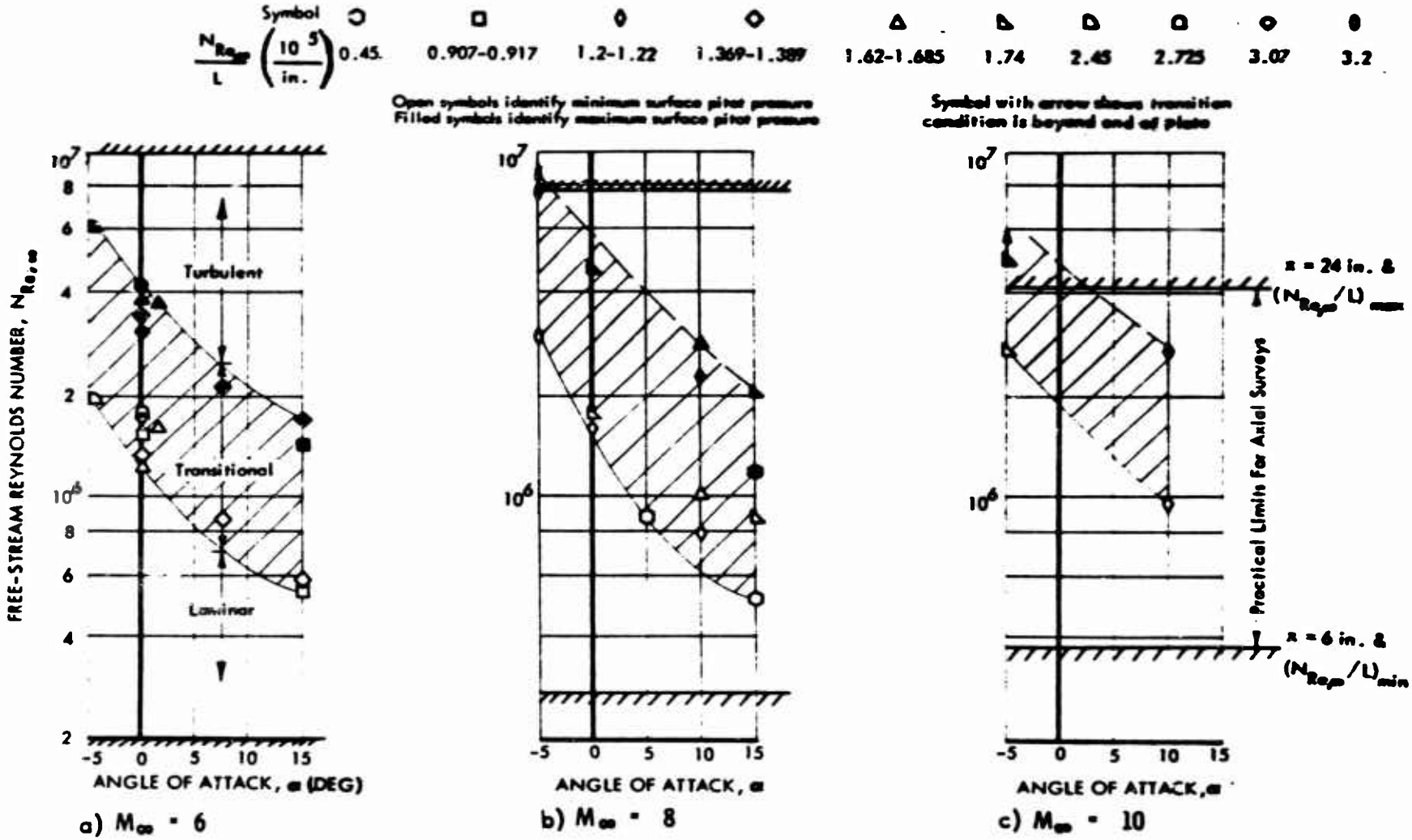

Figure 3-29: TRANSITION REYNOLDS NUMBERS ACCORDING TO AXIAL SURVEY METHOD— Unswept Sharp Plate, Untripped Flow

It is seen in Figure 3-29 that the free-stream Reynolds number based on distance to the transition point is greatly decreased by increasing angle of attack. It is also seen that the effect of free-stream Mach number is rather small. There is a variation with the free-stream unit Reynolds number, which will be examined more closely in later plots.

The vertical survey results are presented in Figure 3-30. Also shown is the shaded band from Figure 3-29 to allow comparison with the axial survey data. In Figure 3-30 the open symbols denote laminar profiles, the half-filled symbols denote transitional flow, and the filled symbols denote turbulent flow. It is seen that there is good agreement between the two methods for the Mach 6 and Mach 8 data. At Mach 10 there seems to be some disagreement, with the profile data indicating laminar flow in the region thought to be transitional from the previous figure.

The only effect of angle of attack on transition that can be calculated with certainty is the effect on the local flow properties and, of course, this effect should be accounted for before any attempt is made to analyze the data. Accordingly, the data of Figure 3-29 are replotted against the unit Reynolds number at the edge of the boundary layer, $N_{Re,e}$ in Figure 3-31. It is seen that there is a consistent trend toward higher transition Reynolds numbers at higher unit edge Reynolds numbers. Dashed curves have been drawn to indicate a 4/10-power variation of the transition Reynolds number with the unit edge Reynolds number, which was used by James (Ref. 12) and adopted in Reference 15. As shown, the present data are in reasonable agreement with the predicted variation, except for the Mach 6 data, which are badly scattered. There is also a trend toward higher transition Reynolds numbers at the lower angles of attack, which is attributed to higher edge Mach numbers.

To isolate the Mach-number trend, the axial survey data are again replotted in Figure 3-32, this time against the Mach number at the edge of the boundary layer, M_e. All data have been adjusted to a unit edge Reynolds number of 2×10^5 per inch using the aforementioned 4/10-power relationship. With the exception of a single point at Mach 6, the adjusted data for the end of transition (maximum pitot pressure) are seen to fall within a narrow band, essentially independent of the angle of attack. The scatter of the data about a mean line shown in the figure is only 17% (again excepting the very low point at Mach 6). Examined statistically, the distribution of the data about a mean line is approximately normal, and if normality is assumed, only 1% of the data would fall more than 22% distant from the mean line. Thus, the scatter in the natural transition data is little more than that encountered in heat transfer data. *

As will be shown later, data from other sources agree with the present data when adjusted in the same manner, so that it appears that angle of attack, as such, does not have a large effect on natural transition. This result will be discussed more fully under "Comparisons with Other Data" and "Concluding Remarks."

* For example, the Rose and Stark stagration point data (Journal of the Aeronautical Sciences, Feb. 1958) show 35% scatter at the 99th percentile.

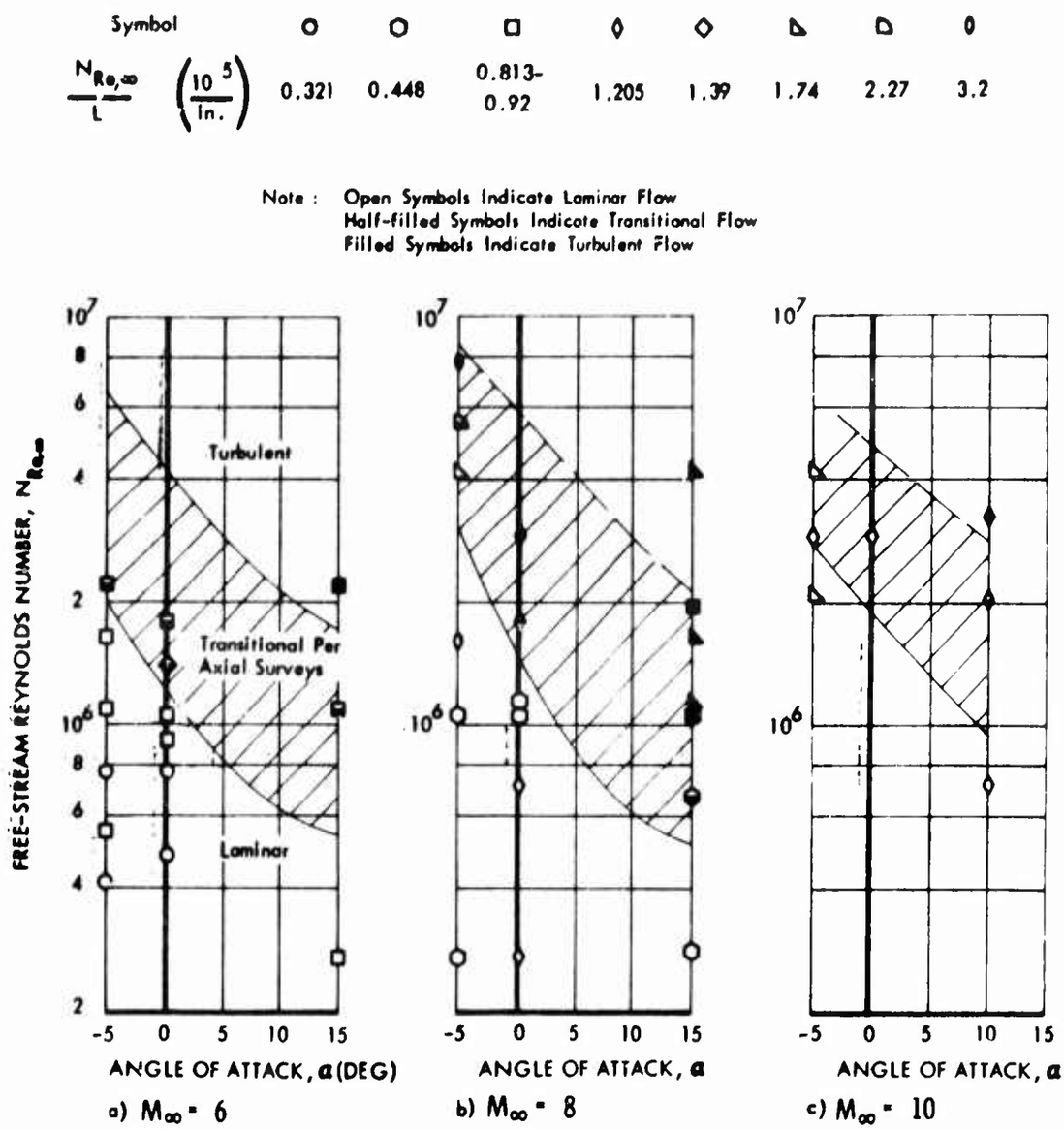

Figure 3-30: COMPARISON OF VERTICAL SURVEY AND SURVEY RESULTS — Unswept Sharp Plate, Untripped Flow

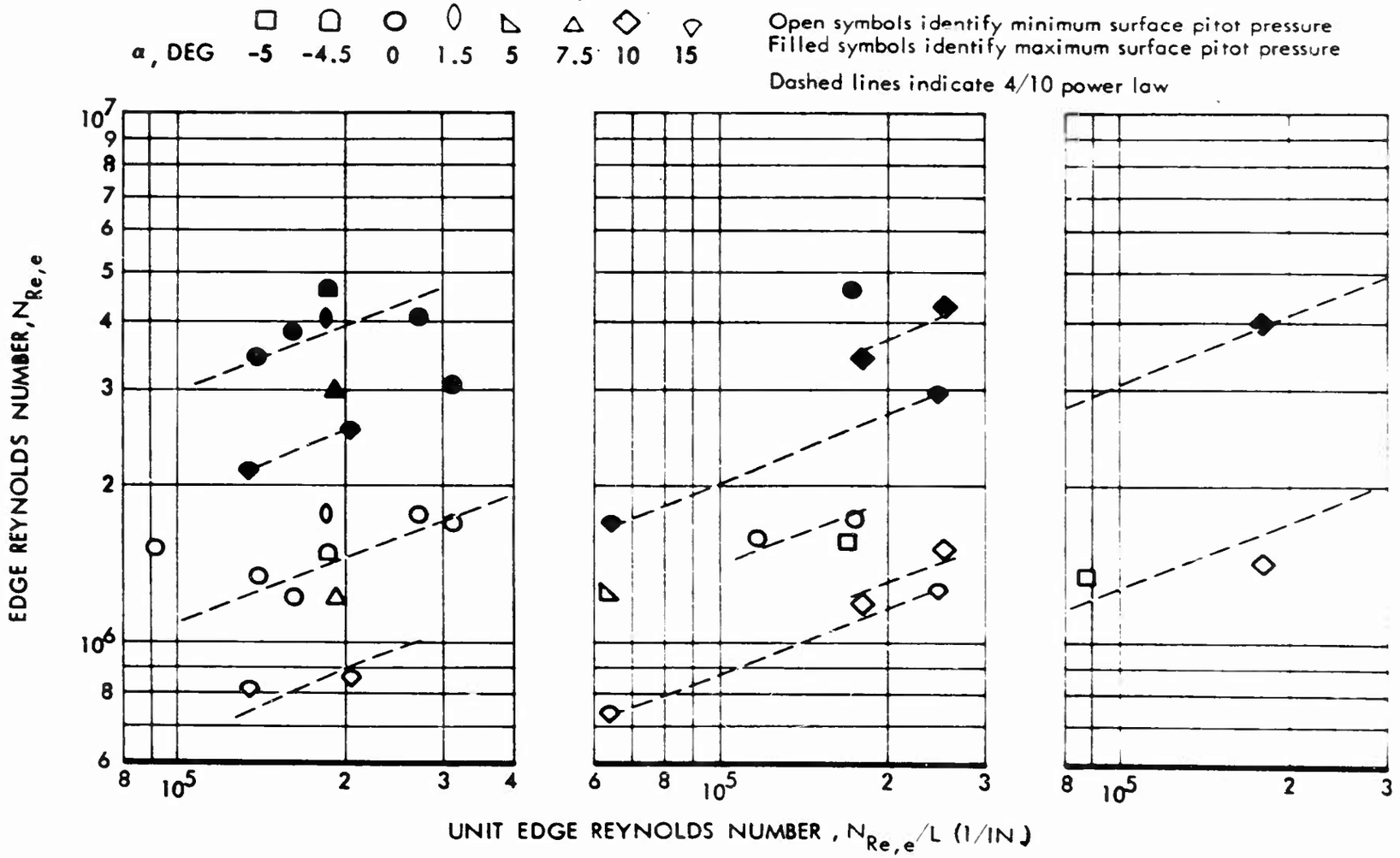

Figure 3-31: LOCAL TRANSITION REYNOLDS NUMBER ACCORDING TO AXIAL SURVEY METHOD — Unswept Sharp Plate, Untripped Flow

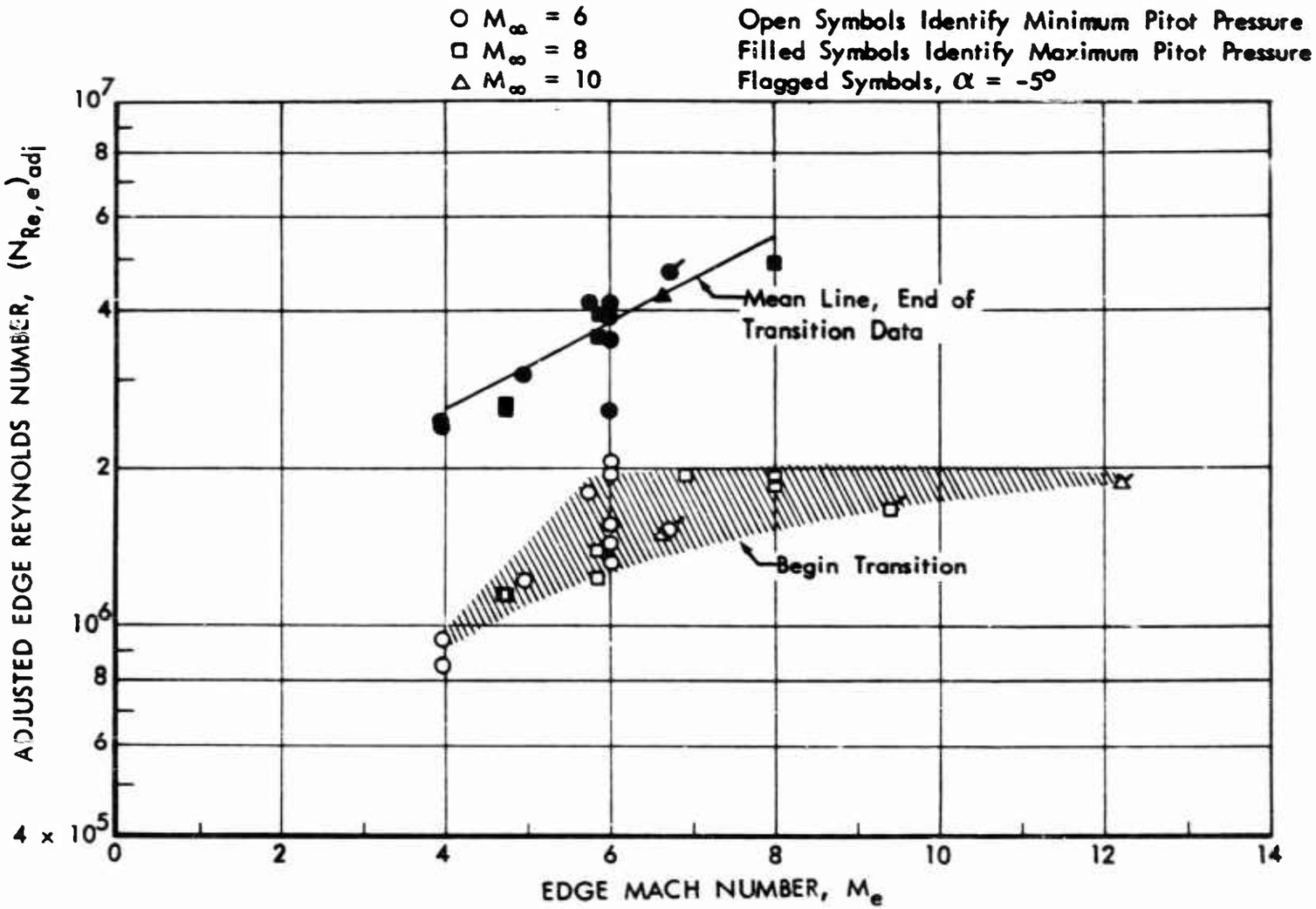

Figure 3-32: ADJUSTED TRANSITION REYNOLDS NUMBER ACCORDING TO AXIAL SURVEY METHOD — Unswept Sharp Plate, Untripped Flow

Data for the beginning of transition are somewhat more scattered. There are several possible explanations for the increased scatter. The 4/10-power adjustment may not be applicable to the beginning of transition; the experimental error may be larger due to the lower pitot pressures being measured; or the increasing surface pressure noted near the trailing edge may have more effect on the location of $P_{T_{min}}$ than on $P_{T_{max}}$. Also, in some test runs a minimum pressure was observed but no maximum point was found on the model, so that there are fewer data for end-of-transition than beginning of transition. With more data points a wider scatter band is to be expected.

Vertical profile results, similarly adjusted to a common Reynolds number of 2×10^5, are presented in Figure 3-33. The end-of-transition data agreee well with the axial distribution data of Figure 3-32, which are indicated by the curve of Figure 3-32. However, the profile data indicate laminar flow at somewhat higher Reynolds numbers than appeared in the axial survey data. Comparing the data of Figures 3-32 and 3-33, it is seen that the disagreement occurs for edge Mach numbers greater than 7. In Figure 3-32, it is seen that the beginning of transition at $M_e > 7$ is based primarily on data obtained at -5 degree angle of attack. It is considered possible that the previously noted tendency for the static pressure on the plate to increase near the trailing edge of the model may have significantly affected the apparent location of the beginning of transition. It is also considered that the profile data give a more reliable indication of the beginning of transition than the slight variation in the axial pressure traces. For this reason it is believed that the beginning of transition generally occurs at higher Reynolds numbers than appears from Figure 3-32. A line has been drawn in Figure 3-33 to indicate the beginning of transition based on the profile data.

Unswept Blunt Plate

Natural transition data for the unswept blunt model are presented in Figures 3-34 and 3-35 and tabulated in Table III. The data are coded as in Figures 3-29 and 30, with open symbols indicating the beginning of transition in the axial data of Figure 3-34 and indicating laminar profiles in Figure 3-35, etc. Relatively few data were obtained on the blunt configuration, since transition occurred only at the highest angles of attack and highest unit Reynolds numbers. It was very difficult to interpret the axial traces for this model, which are particularly subject to spurious effects. At hypersonic speeds bluntness produces a relatively thick layer of low-energy air near the surface of the plate, thus rendering all pitot pressures low and tending to allow base pressures to bleed forward, an effect that would [illegible]e transitional in the axial survey technique.

[illegible]hat all of the blunt plate data indicate higher free-stream transition [illegible]umbers than those for the sharp plate, but that there are some inconsistencies between the axial survey data and the profile data. The greatest inconsistency occurs in the Mach 6 zero-angle-of-attack data, with the profile data indicating laminar flow under the condition for which the axial survey indicated transitional flow.

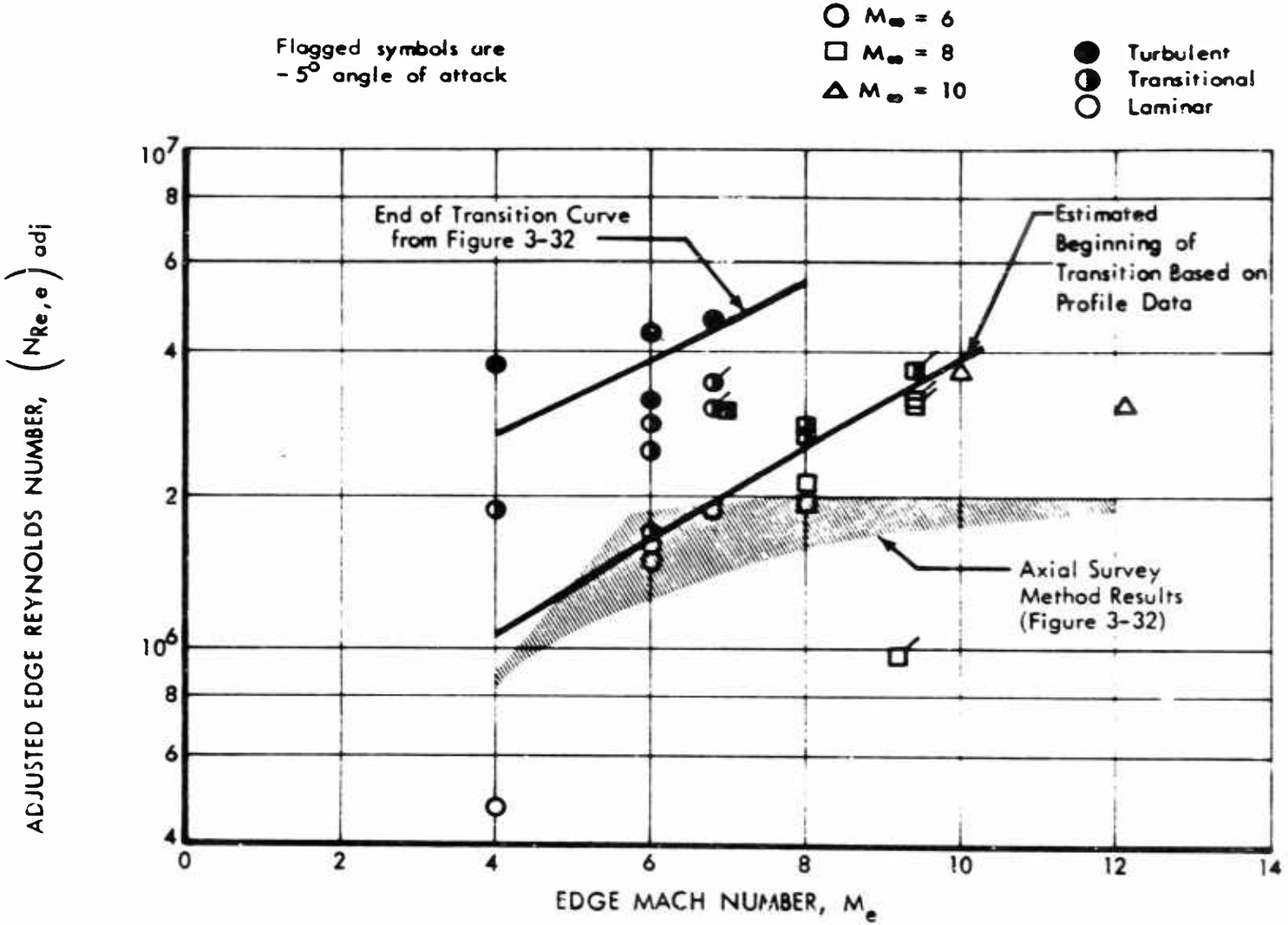

Figure 3-33: COMPARISON OF VERTICAL SURVEY AND AXIAL SURVEY TRANSITION REYNOLDS NUMBERS — Unswept Sharp Plate, Untripped Flow

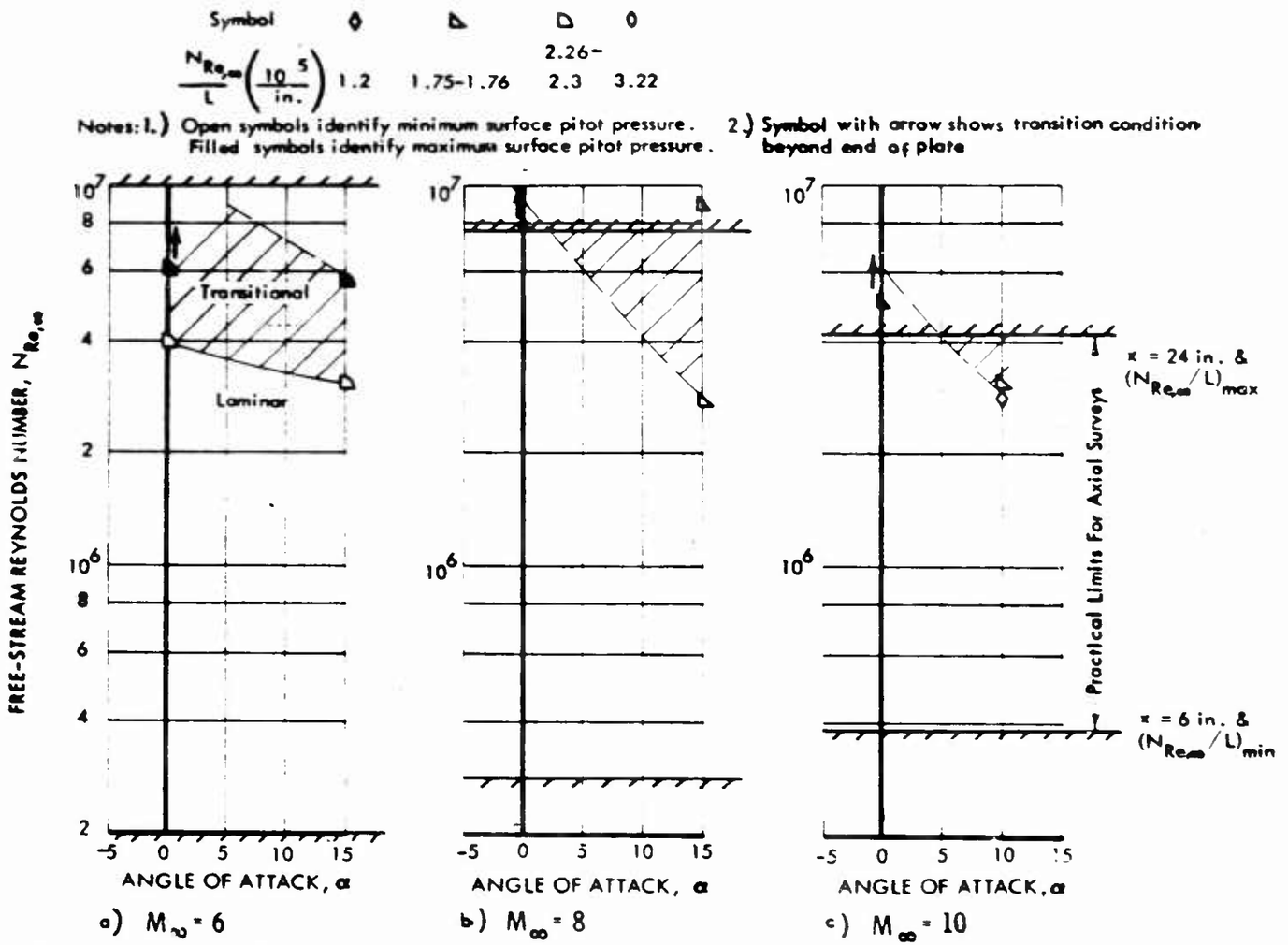

Figure 3-34: TRANSITION REYNOLDS NUMBER ACCORDING TO AXIAL SURVEY METHOD — Unswept Blunt Plate, Untripped Flow

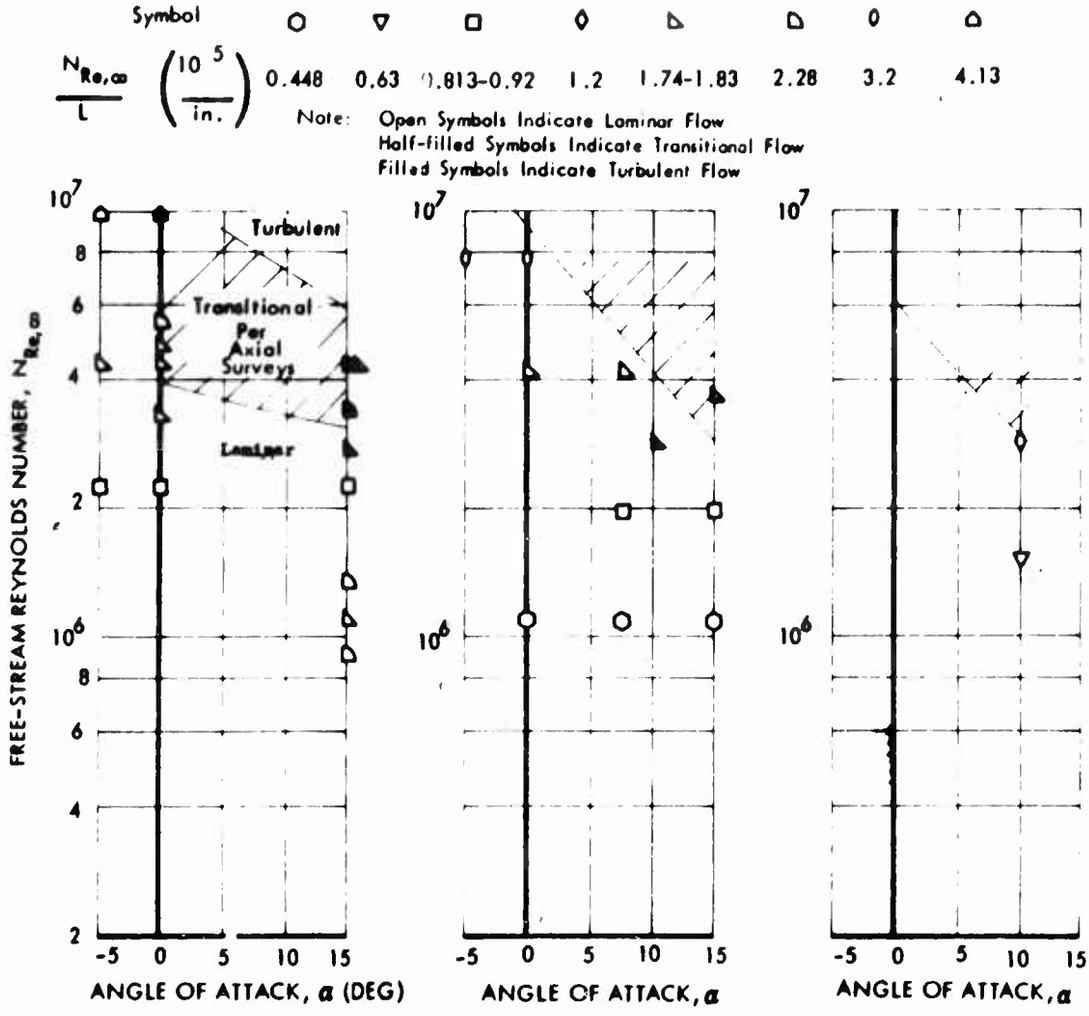

a) $M_\infty = 6$ b) $M_\infty = 8$ c) $M_\infty = 10$

Figure 3-35: COMPARISON OF PROFILE DATA WITH AXIAL SURVEY RESULTS — Unswept Blunt Plate, Untripped Flow

The blunt plate axial survey data are plotted against unit edge Reynolds number in Figure 3-36. These data appear to show much less unit Reynolds number effect than the previously noted 4/10-power law. There are few directly comparable data, however, so that the adoption of a different power law is not justified. For this reason, the 4/10-power law was used to adjust the data to a unit edge Reynolds number of 2×10^5 per inch for comparison with the sharp plate data. As shown in Figure 3-37, the data so adjusted are not inconsistent with the previous data, but exhibit a strong effect of free-stream Mach number. The Mach number trend could be reduced by assuming a different unit Reynolds number variation, since the unit Reynolds number was varied with the free-stream Mach number. However, it should also be noted that the higher the free-stream Mach number the more pronounced will be the external flow gradients discussed in connection with Figure 3-19. It is believed, but not proven, that these external gradients are a destabilizing effect. Also, since the Reynolds numbers are lowest for the highest Mach numbers, the boundary layers are also thickest in the high Mach number cases. With thicker boundary layers the vorticity within the boundary layer is decreased, which would make the external vorticity more important. For these reasons it is believed that the observed variation should not be attributed to a unit Reynolds number effect.

75-Degree Swept Delta Wing

The natural transition data for the 75-degree swept delta wing obtained from axial surveys are presented in Figure 3-38 and tabulated in Table III. By comparing these data with those of Figures 3-29 and 3-30, it will be seen that the transition Reynolds numbers based on free-stream properties are less than those for the unswept sharp plate, particularly at the highest angle of attack. The corresponding vertical survey results are presented in Figure 3-39. It is seen that in several instances the profile data indicate laminar flow in the region found to be transitional by the axial survey method. As with the previous data, the vertical survey data are considered to be the more reliable. Some axial and profile data were also taken along a line parallel to the centerline, but offset 3 inches. These data are presented in Figures 3-40 and 3-41.

The axial survey results are replotted in Figure 3-42 and 3-43 as a function of unit edge Reynolds number. The local flow properties were calculated with the aid of Reference 39 formulae for pressure and shock wave angle. The results of these calculations were compared with the evidence of the pitot surveys, and only minor differences were found.

The sharp delta wing data also exhibit a consistent trend with unit edge Reynolds number, but the effect appears to be smaller than that shown in Figure 3-31 for the unswept plate. As will be discussed more fully in the final section, this difference from the unswept plate result is considered to be important, and for that reason the apparent discrepancies between Figures 3-38 and 3-39 should be reexamined for their effect on Figure 3-42. Unfortunately, it is not practical to attempt to determine the unit-Reynolds-number trend from the vertical survey profile results alone since they do not provide a means of determining the transition location, but serve to establish the state of the boundary layer at a particular point.

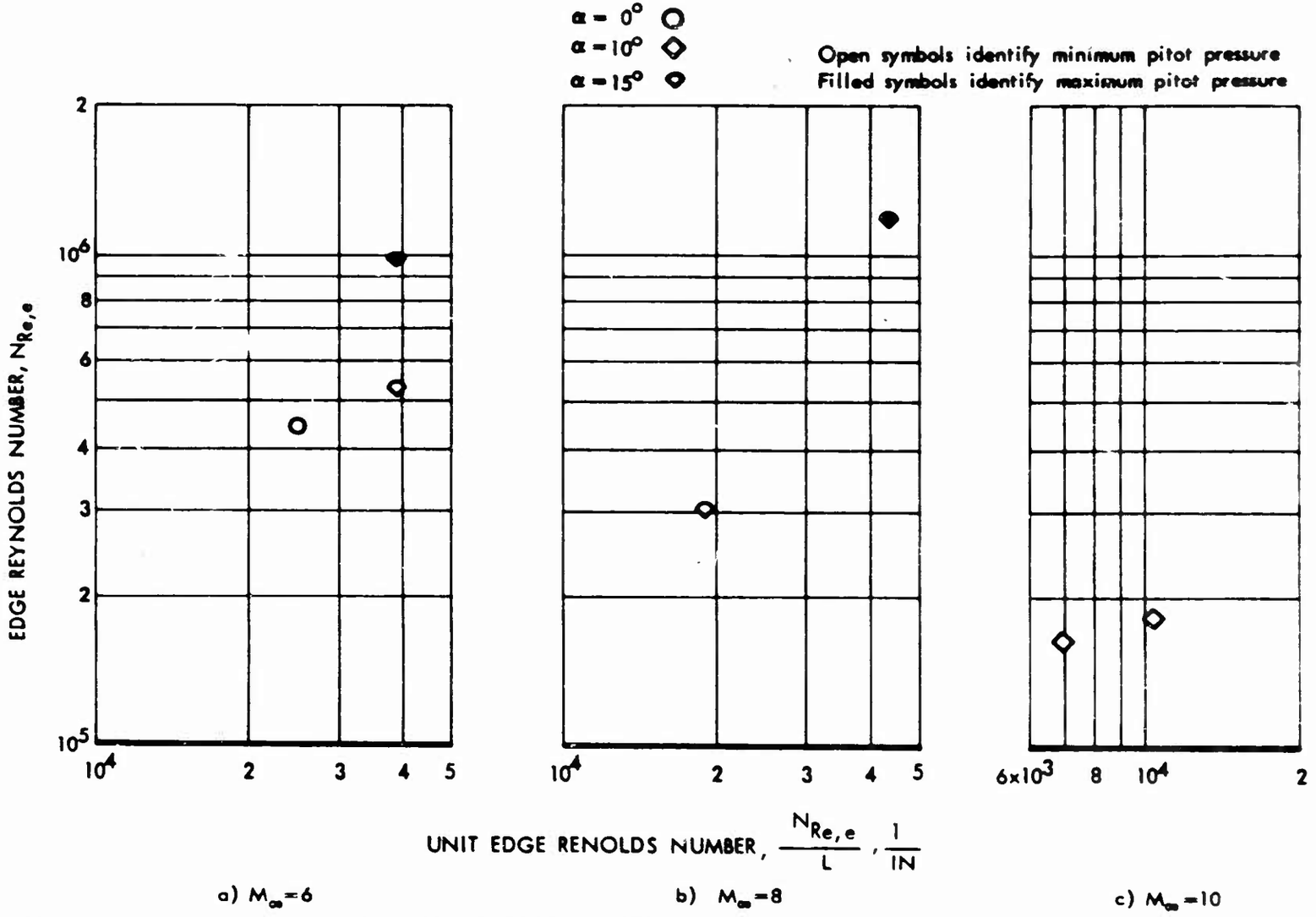

Figure 3-36: LOCAL TRANSITION REYNOLDS NUMBERS ACCORDING TO AXIAL SURVEY METHOD — Unswept Blunt Plate, Untripped Flow

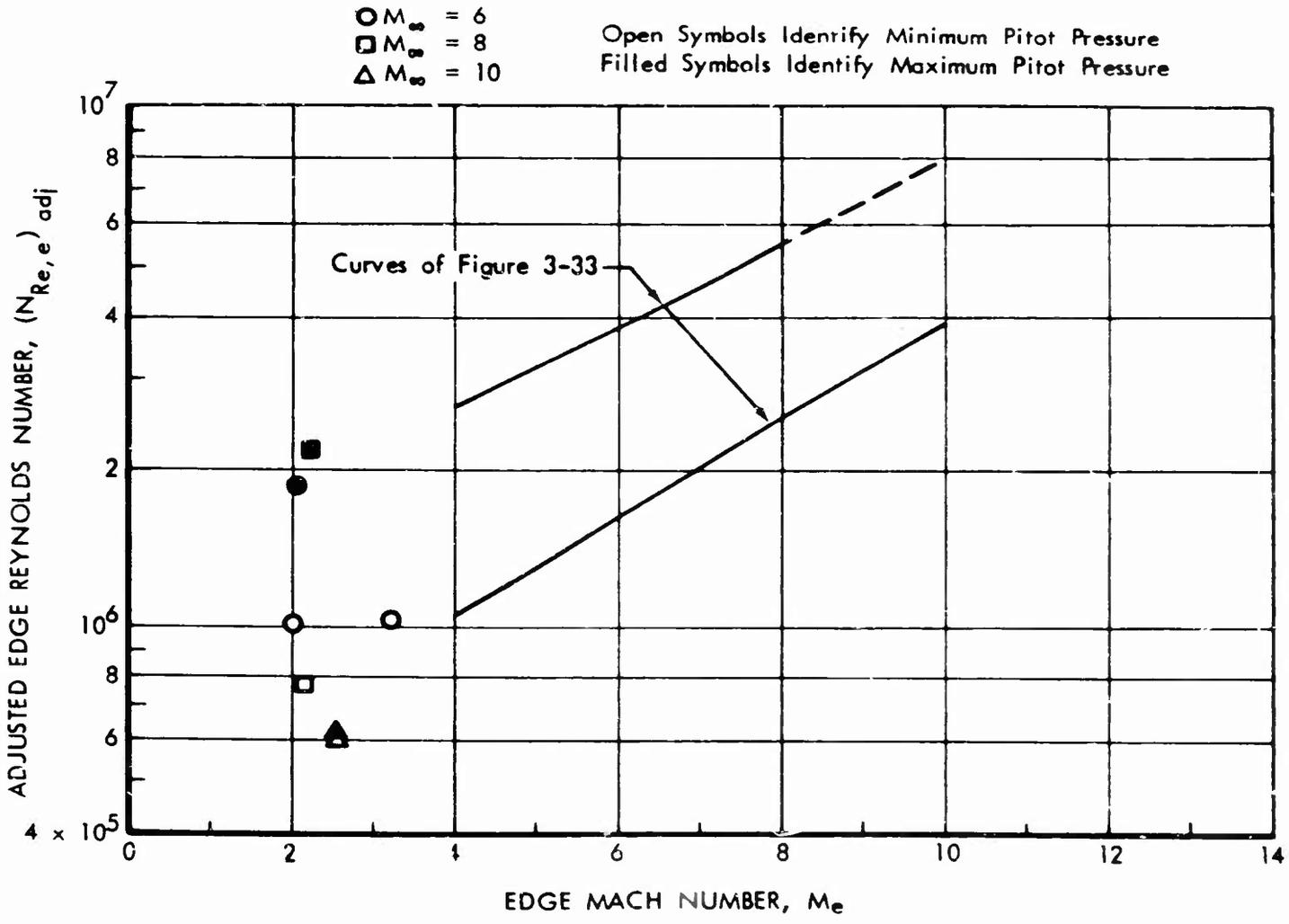

Figure 3-37: COMPARISON OF SHARP AND BLUNT LEADING EDGE AXIAL SURVEY TRANSITION RESULTS — Unswept Flat Plate, Untripped Flow

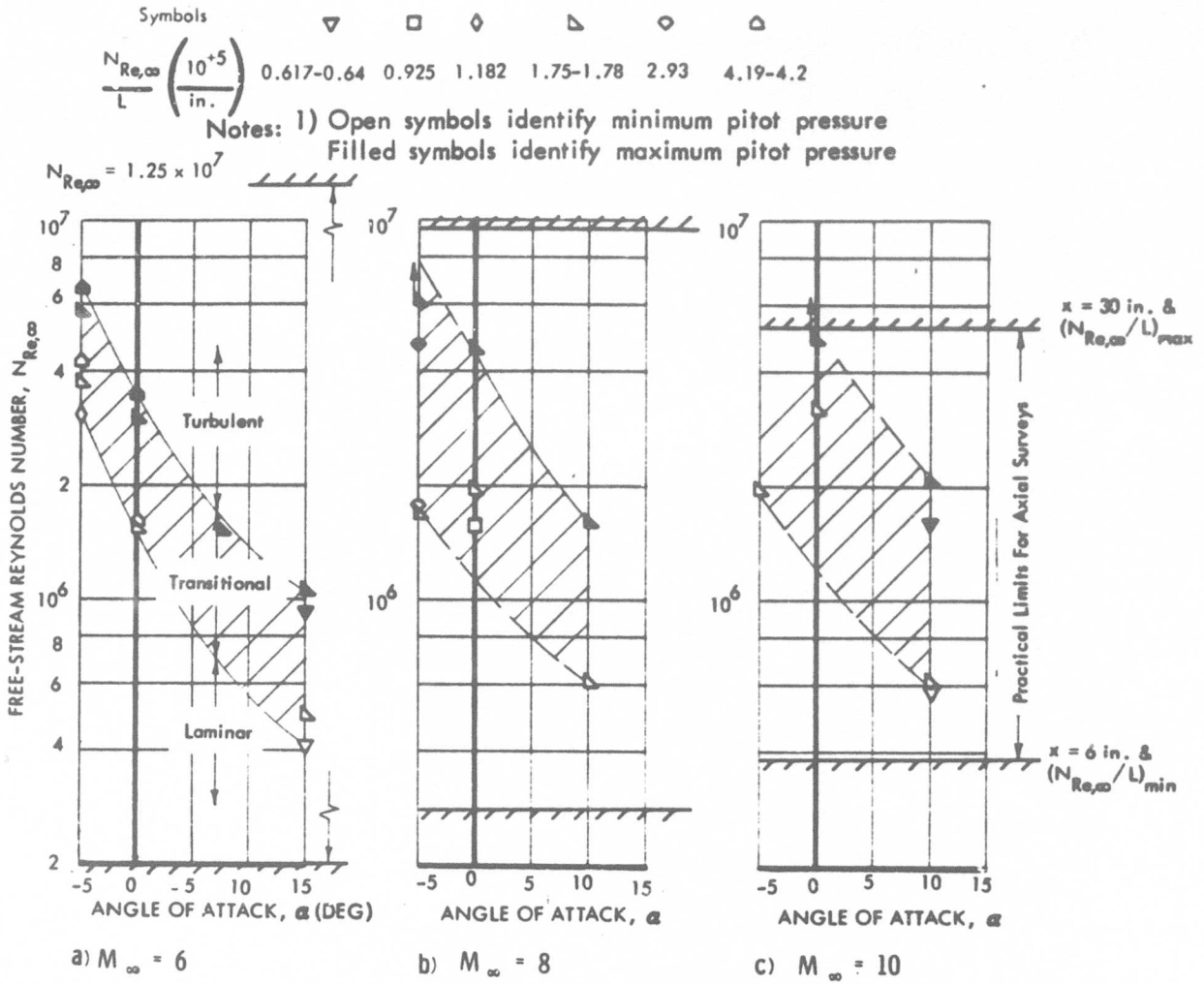

Figure 3-38: LOCAL TRANSITION REYNOLDS NUMBERS ACCORDING TO AXIAL SURVEY METHOD — Unswept Blunt Plate, Untripped Flow

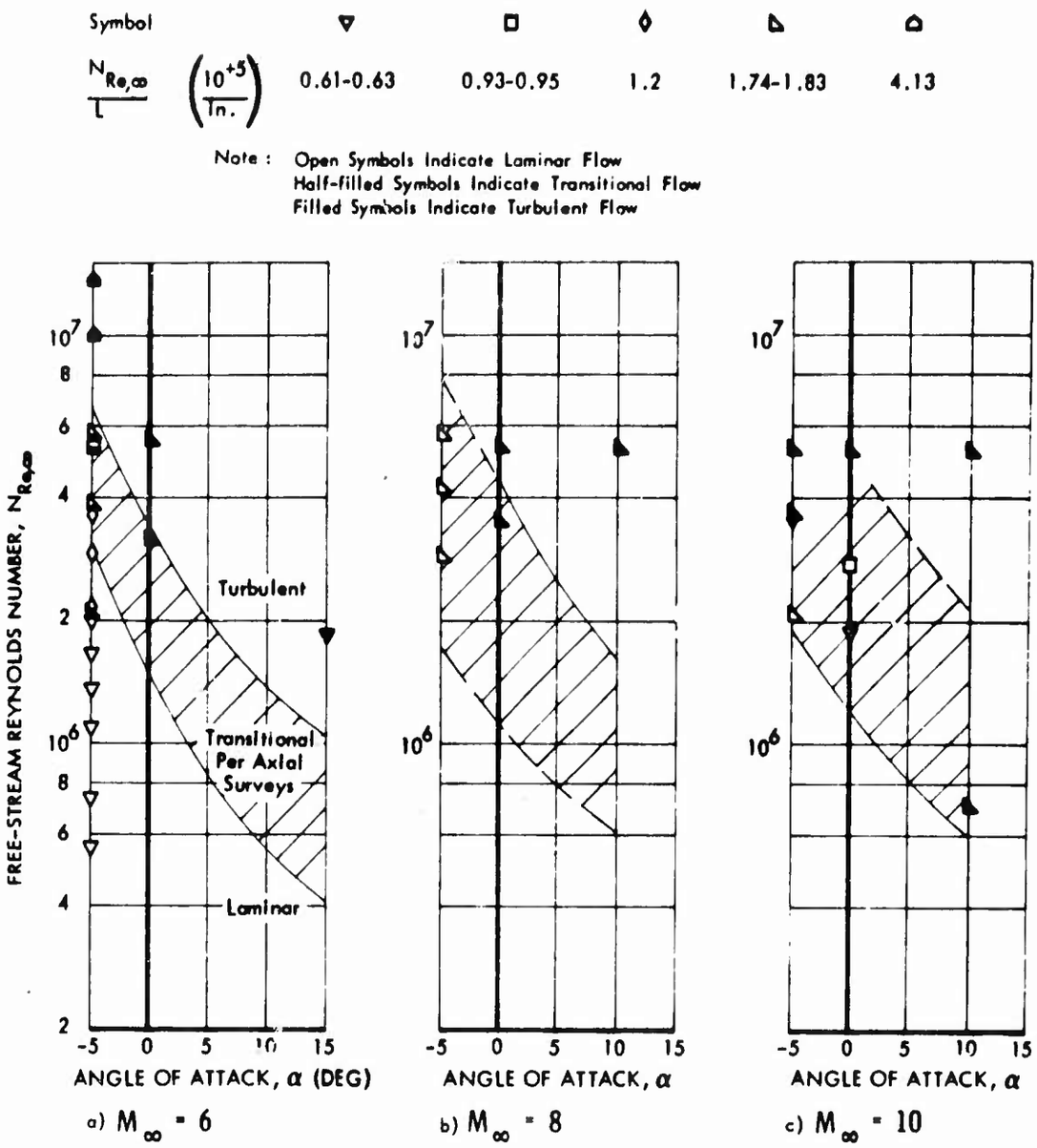

Figure 3-39: COMPARISON OF VERTICAL SURVEY AND AXIAL SURVEY RESULTS — 75° Swept Delta Wing Centerline, Untripped Flow

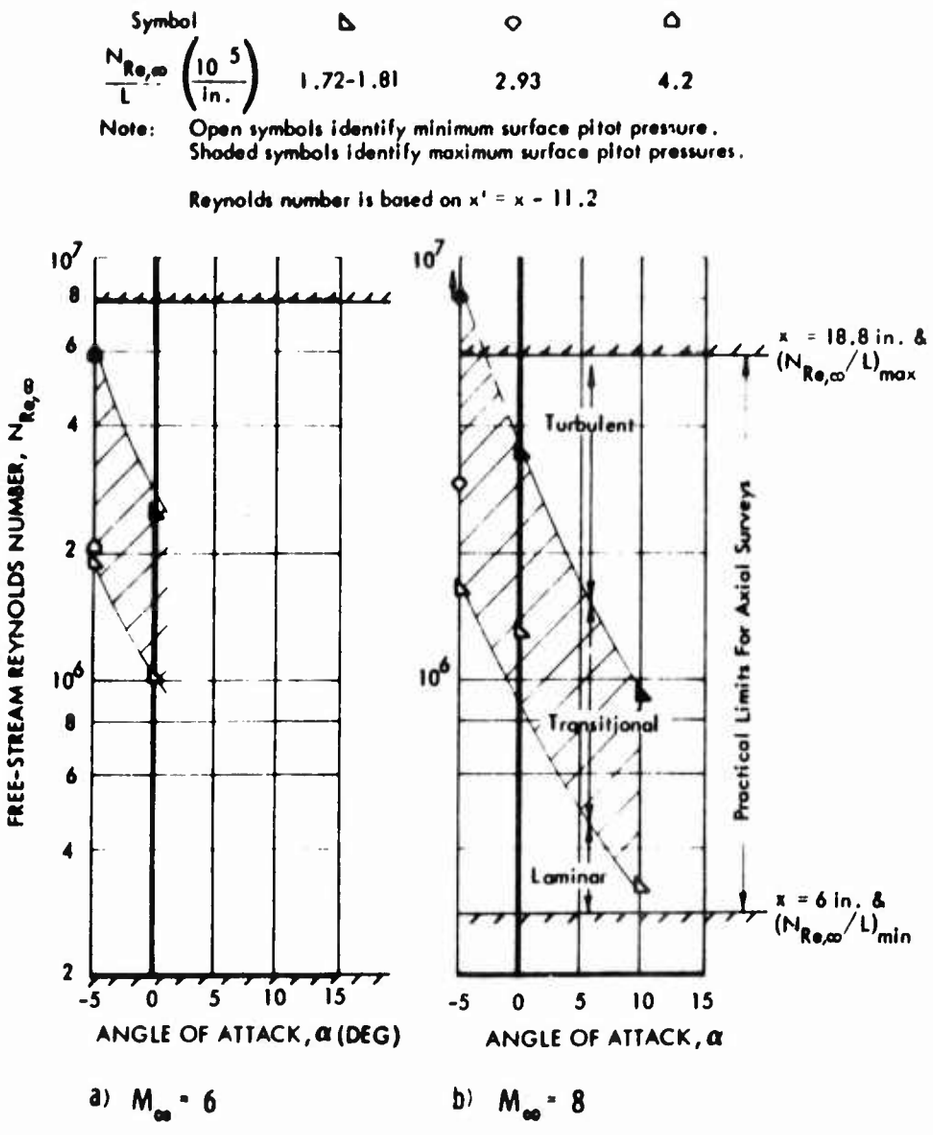

Figure 3-40: TRANSITION REYNOLDS NUMBERS ACCORDING TO AXIAL SURVEY METHOD — 75° Swept Delta Wing 3 Inches Off Centerline, Untripped Flow

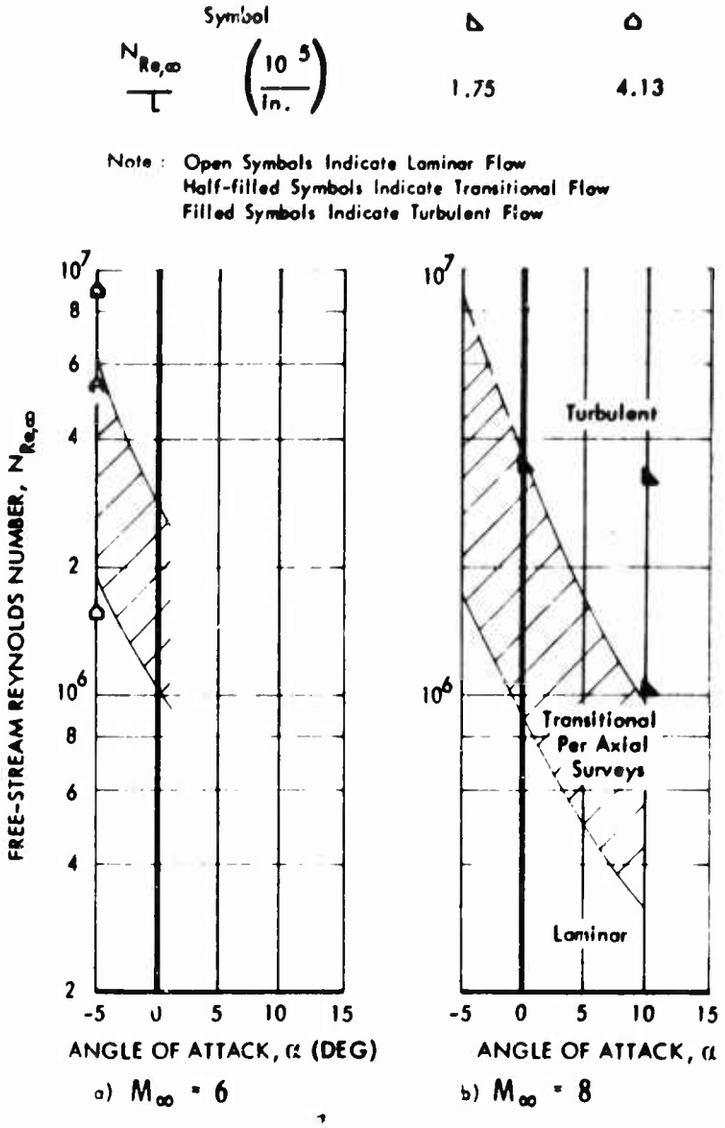

Figure 3-41: COMPARISON OF VERTICAL SURVEY AND AXIAL SURVEY RESULTS — 75° Swept Delta Wing 3 Inches Off Centerline, Untripped Flow

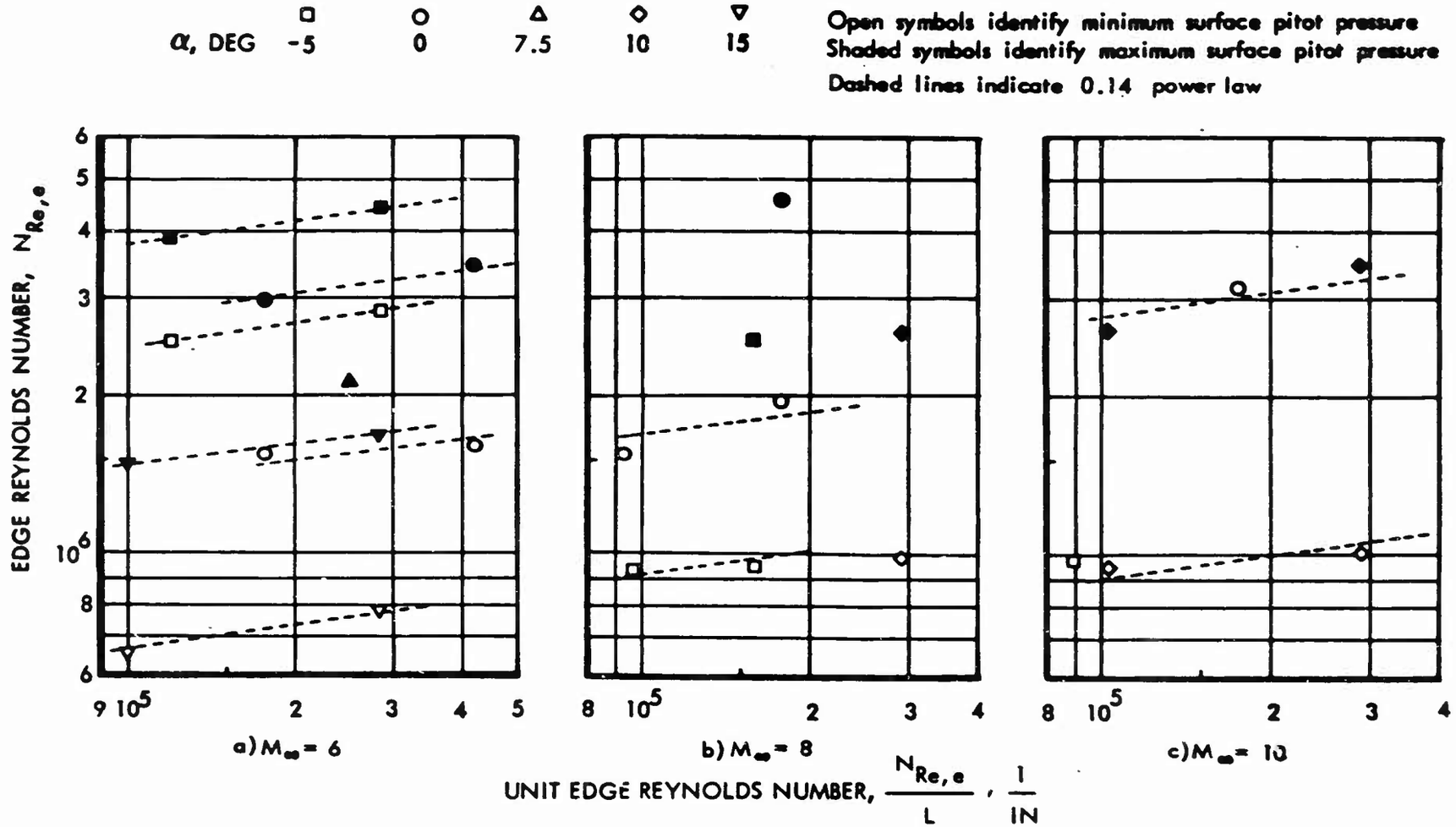

Figure 3-42: LOCAL TRANSITION REYNOLDS NUMBERS ACCORDING TO AXIAL SURVEY METHOD — 75° Swept Sharp Delta Wing Centerline, Untripped Flow

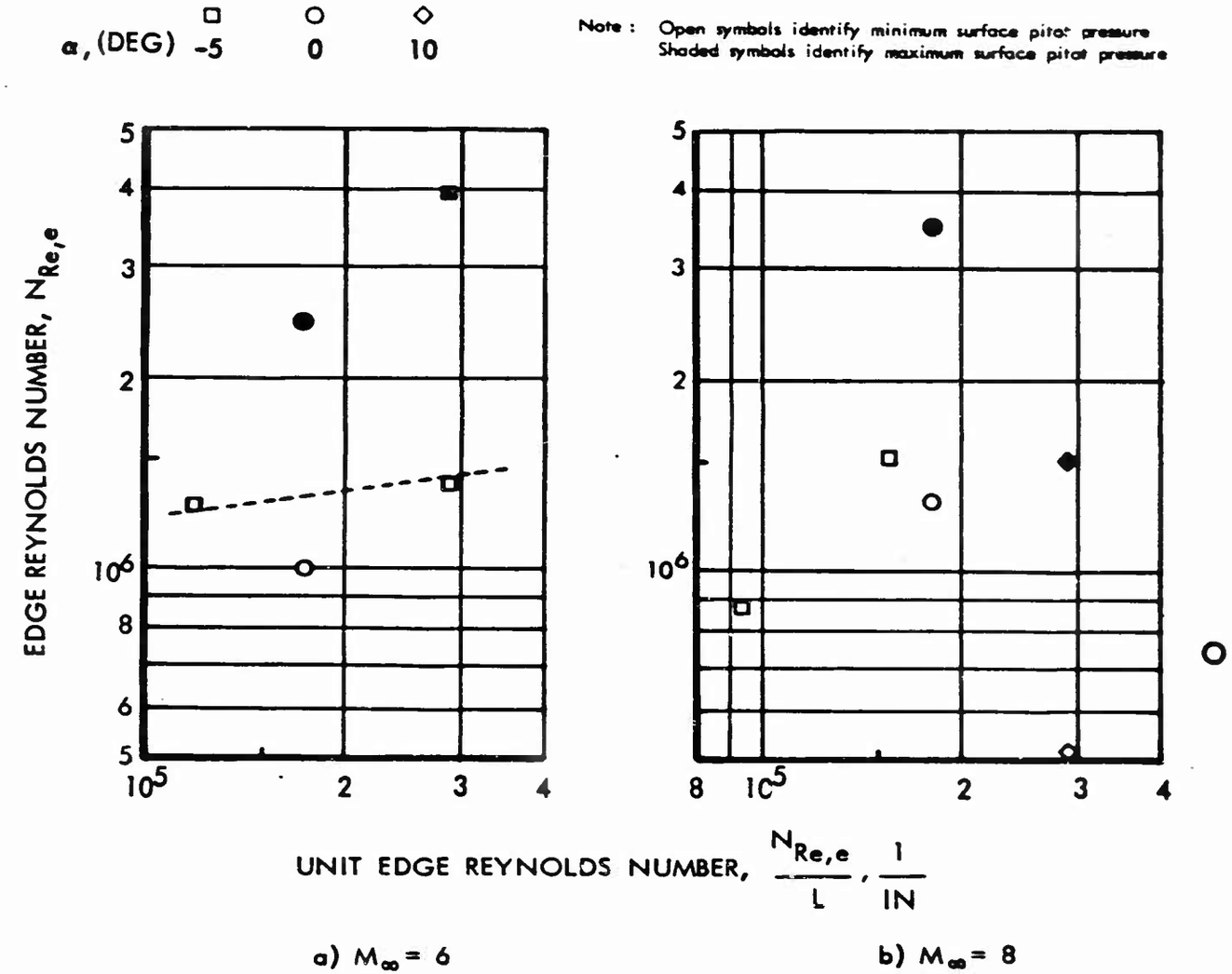

Figure 3-43: LOCAL TRANSITION REYNOLDS NUMBERS ACCORDING TO AXIAL SURVEY METHOD — 75° Swept Delta Wing 3 Inches Off-Centerline, Untripped Flow

In Figure 3-42, it will be noted that by directly comparable data the unit Reynolds number trend can be established for 11 specific cases. Checking each of these cases against Figure 3-39 it is found that in five of the cases the profile data conflict with the transition conditions determined by axial survey and five agree, with one case being indeterminate:

Case	M	α	Point in Transition	Unit Reynolds Number (N_{Re}) Exponent According to Fig. 3-42	Evidence of Fig. 3-39
1	6	-5	Beginning	0.14	Conflicts
2	6	0	Beginning	0.05	Agrees
3	6	15	Beginning	0.17	Agrees
4	6	-5	End	0.16	Conflicts
5	6	0	End	0.15	Indeterminate
6	6	15	End	0.13	Agrees
7	8	-5	Beginning	Negative	Conflicts
8	8	-0	Beginning	0.04	Conflicts
9	8	-5	End	Negative	Conflicts
10	10	10	Beginning	0.05	Agrees (no upper bound)
11	10	10	End	0.27	Agrees

Excluding the conflicting data, which are seen to be primarily the negative angle-of-attack data, it is seen that the exponent varies from 0.05 to 0.27. The mean value of the exponent for nonconflicting data is 0.14. This value has been used to allow comparison of the data as a function of the edge Mach number.

The adjusted sharp delta wing natural transition data are plotted against Mach number in Figure 3-44. It is seen that the delta wing centerline data (Figure 3-44a) fall somewhat below the flat plate curves of Figure 3-33. The difference in level is, however, related to the common unit Reynolds number that has been selected for Figures 3-33 and 3-44 (2×10^5 per inch). Since the effect of unit Reynolds number is greater for the unswept flat plate than for the delta wing, the apparent agreement could be improved by selecting a lower common unit Reynolds number for the data comparisons.

More important is the variation of the delta wing data with Mach number, which is seen to be greater than that shown by the flat plate data. This trend is shown most clearly by the end of transition data for a free-stream Mach number of 6. There are fewer points at the other free-stream Mach numbers, but similar trends can be discerned. As before, some of the negative angle-of-attack data show evidence of spurious effects.

While it is not necessarily to be expected that the Mach number effect would be the same for the two configurations, it will be noted that the zero angle-of-attack data ($M_e = M_\infty$) follow the flat plate trend closely. Dashed lines have been added to Figure 3-44a to facilitate comparison. These lines are 20% below the flat plate curves, and so have exactly the same variation with Mach number. It is seen that

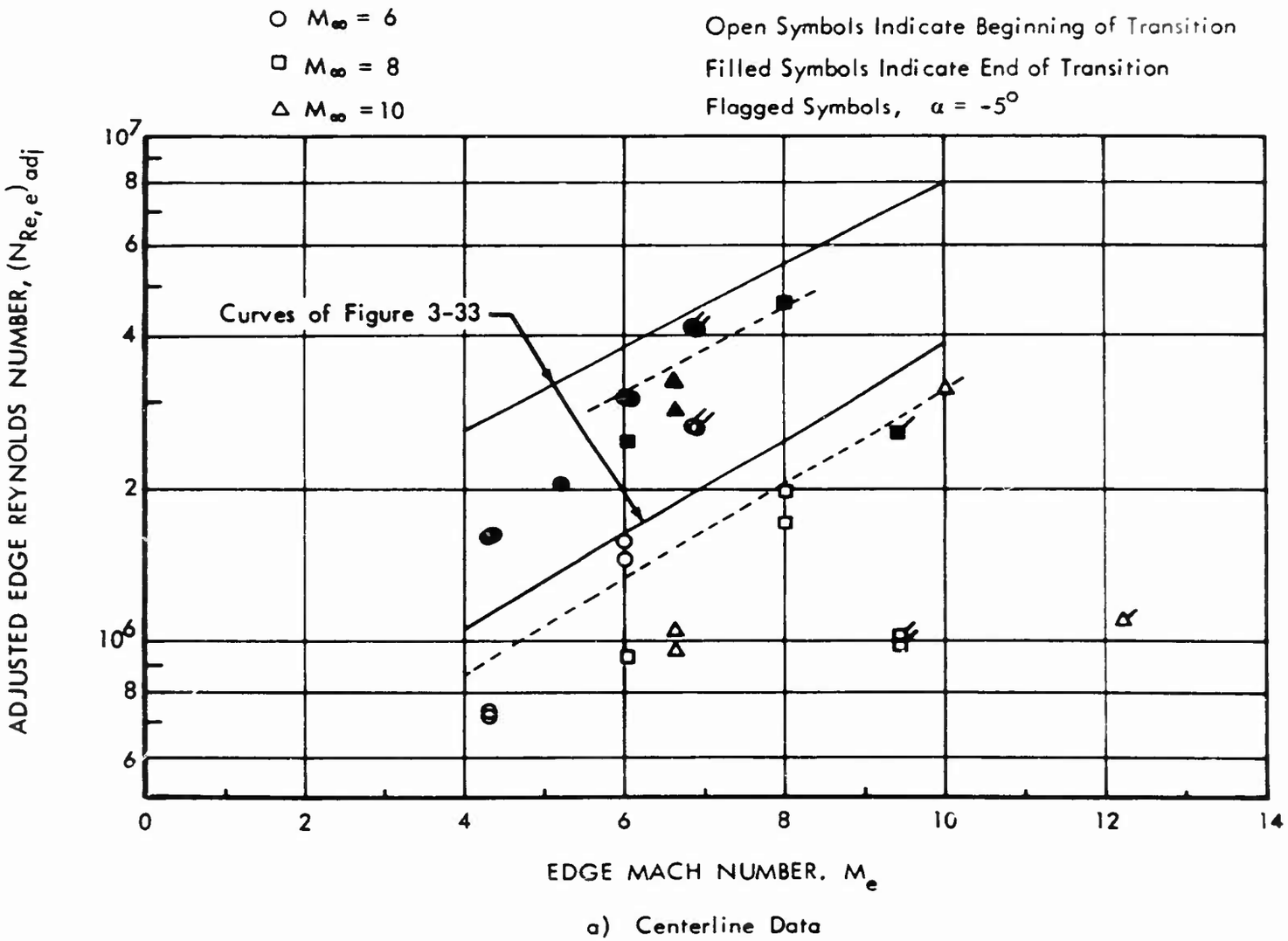

a) Centerline Data

Figure 3-44: ADJUSTED TRANSITION REYNOLDS NUMBERS ACCORDING TO AXIAL SURVEY METHOD — 75° Swept Delta Wing, Untripped Flow

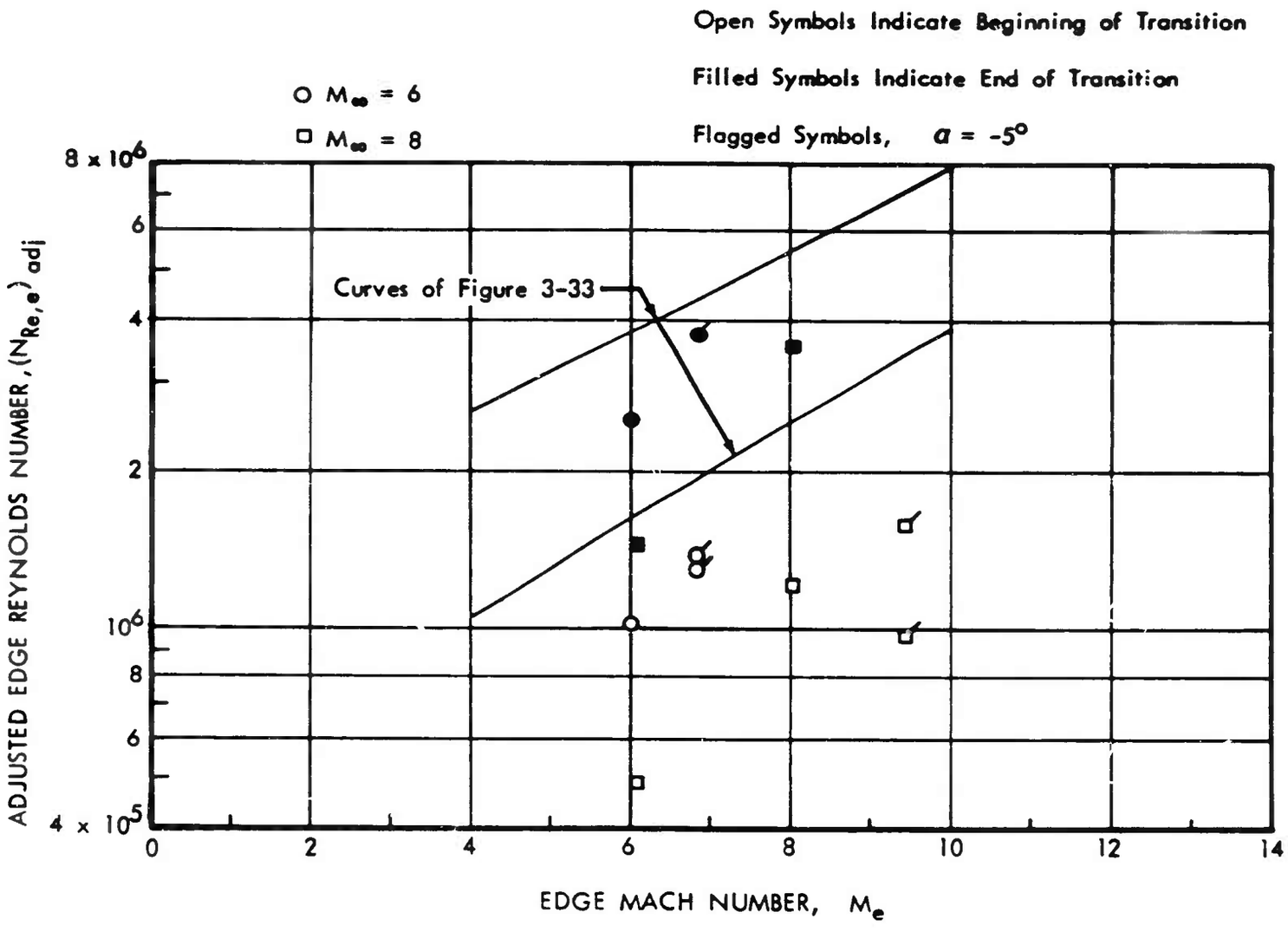

b) 3" Off-Centerline Data

Figure 3-44: Concluded

the data scatter about the dashed curves, and that the end of transition data are in essentially exact agreement with the curves.

It therefore appears that the apparent variation with local Mach number for the other data should be attributed to the effect of angle of attack rather than to the Mach number, per se. This is supported by data from other sources, and discussed in a following section. The effect of angle of attack could be due to spanwise pressure gradients that occur on delta wings at angle of attack.

The off-centerline data, shown in Figure 3-44b, indicate somewhat lower transition Reynolds number than do the centerline data. This difference could well be due to a transverse spread of turbulence. It will be noted that the two end-of-transition data show the expected effect of Mach number.

SUMMARY OF NATURAL TRANSITION RESULTS

With due allowance for the experimental errors and uncertainty of interpretation that were discussed earlier, the present experimental program nonetheless leads to certain general conclusions that are probably correct:

1) The sharp unswept plate data exhibit a consistent effect of unit edge Reynolds number that is approximately 4/10-power relationship. This effect appears to be independent of free-stream Mach number, free-stream unit Reynolds number, and angle of attack in the range tested.

2) When adjusted to a common unit Reynolds number using the 4/10-power-law rule, data from the unswept sharp plate show an increase in transition Reynolds number with local Mach number. The Mach number effect is independent of free-stream Mach number and angle of attack.

3) The 75-degree swept delta wing centerline data show less effect of edge unit Reynolds number than do the unswept plate data. When adjusted to a common unit Reynolds number using a 0.14-power-law adjustment, the data show the same effect of Mach number as the unswept plate data. There is, however, an additional effect of angle of attack.

TRIPPED TRANSITION

For conditions wherein natural transition did not occur, tripping was often attempted. Mass injection was selected as the tripping technique, largely on the basis of results reported in References 12 and 16.

Testing for tripped transition was found to be very time-consuming. Attempts to use the axial survey method were not successful, so that it was necessary to use the much slower vertical survey method. However, sufficient data were obtained to show that the boundary layer is very difficult to trip for the present test conditions.

The vertical survey results for the three configurations tested are presented in Figures 3-45, 3-46, and 3-47. The data is superimposed on the corresponding untripped results taken from Figures 3-29, 3-34, and 3-38. It is seen that for the sharp leading-edge configurations it is only at Mach 6, zero angle of attack that any reduction in transition Reynolds number was achieved by mass injection, and that even for that case the data failed to repeat well. For the blunt leading-edge unswept plate, for which the local Mach number is always less than 4, reductions of about 50% were obtained.

It is seen that, in this form, the coverage is inadequate to define a lower bound of tripped transition. However, when adjusted to a common unit Reynolds number by the previously described methods, it was found that transitional profiles were being observed at lower Reynolds numbers than previously. The adjusted data are presented in Figure 3-48, together with the beginning transition curve of Figure 3-33. It is seen that several of the data fall well below the flat plate beginning transition curve. A dashed curve has been added to Figure 3-48 to indicate the lowest Reynolds numbers at which transitional profiles were observed. It is believed that this curve is a conservative lower bound on the present data. The high Mach number portion of the curve is based entirely on a negative angle of attack datum at a free-stream Mach number of 10. It has previously been noted that much of the negative angle of attack data does not agree well with other measurements. In this case it will be noted from Figure 3-33 that the corresponding natural transition point is well below the curve shown in that figure, and that the actual reduction in transition Reynolds number will be seen to be less than 30%. It will be noted that in only one case (M_e = 6) was a reduction of more than 30% observed.

COMPARISON WITH PREVIOUS DATA

It has been shown that the present natural transition data exhibit little scatter when adjusted to a common unit Reynolds number on the basis of a 4/10-power-law variation. This consistency led to a review of other data available in the literature to determine how universal this agreement would be.

Generally, it was found that direct, meaningful comparisons could be made in only a few cases, because most authors have used different techniques to determine transition, and in many cases, do not give a precise definition of the quantity that they measured. It has been shown that the length of the transition region (by the present definition) is usually greater than the length of laminar flow ahead of the transition region. Therefore, unless the data are taken in a manner that allows the beginning and end of transition to be clearly determined, quantitative comparisons with the present results are not possible. This was usually not done, and it has been possible to make only a few comparisons.

Reference 15 reports on a previous investigation in the same wind tunnels used in the present tests, plus some additional data from AEDC Tunnel A. The Reference 15 investigation was confined to zero angle of attack so that the sharp leading-edge

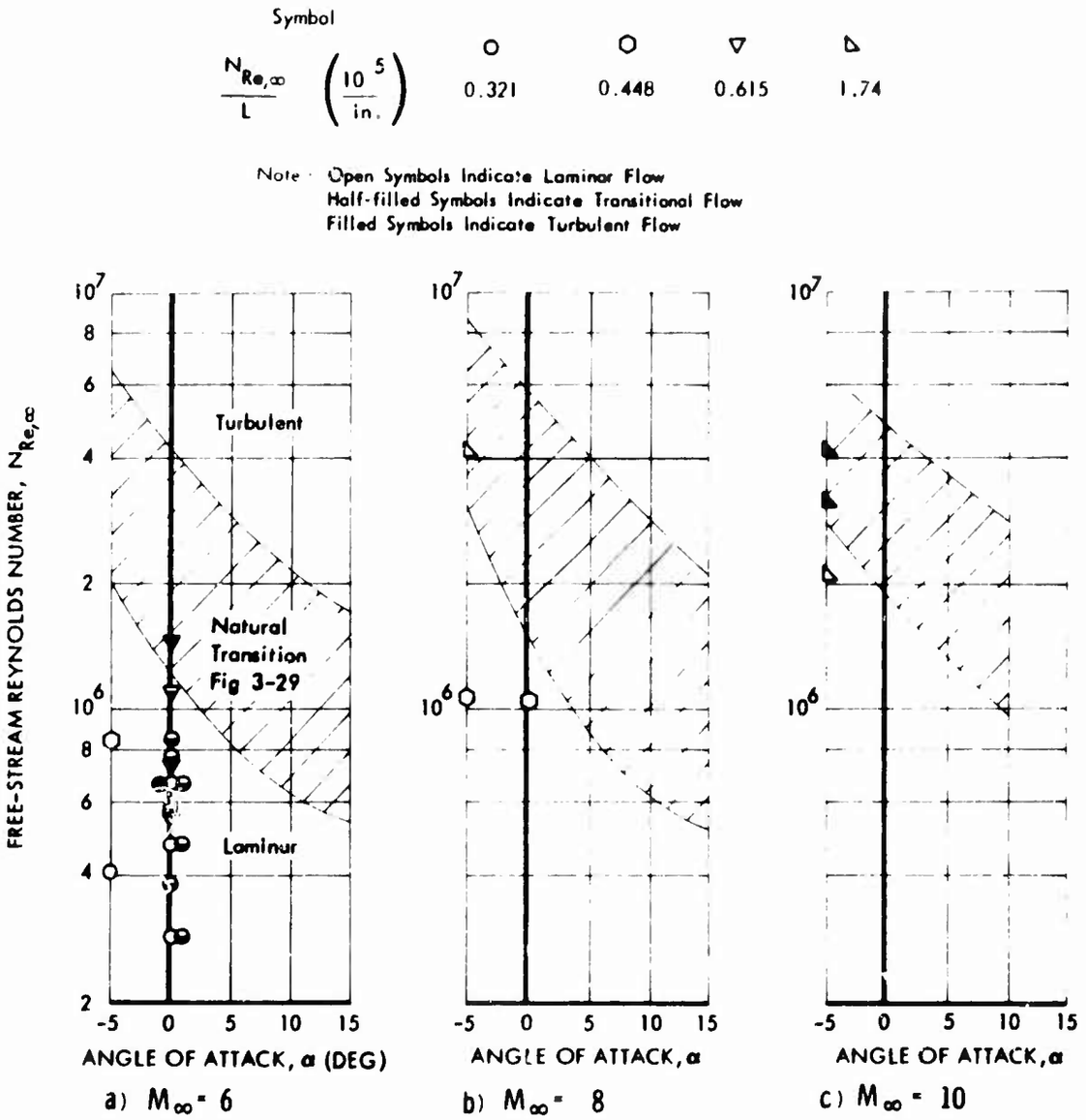

Figure 3-45: EFFECT OF BOUNDARY LAYER TRIP ON TRANSITION— Unswept Sharp Plate

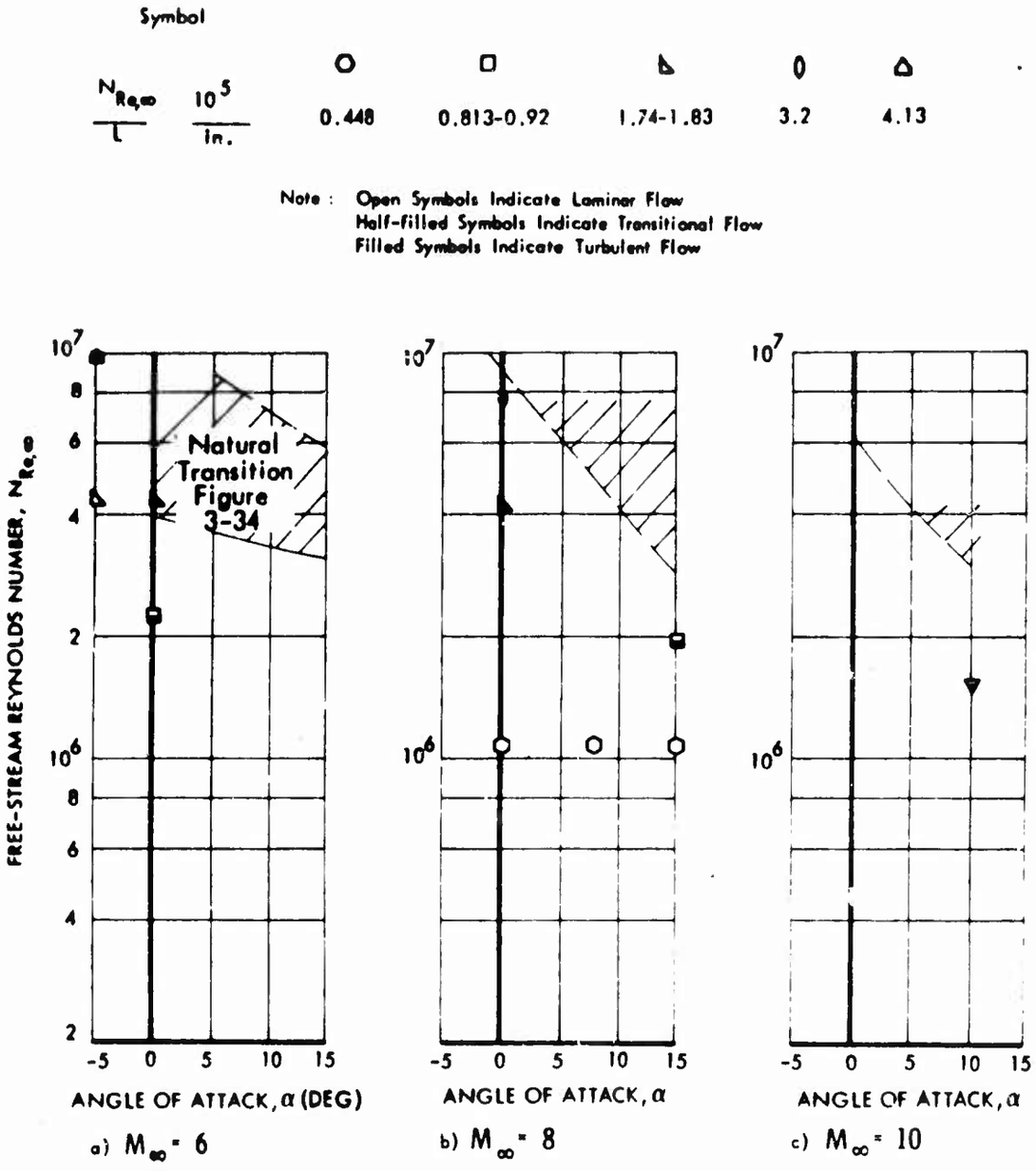

Figure 3-46: EFFECT OF BOUNDARY LAYER TRIP ON TRANSITION — Unswept Blunt Plate

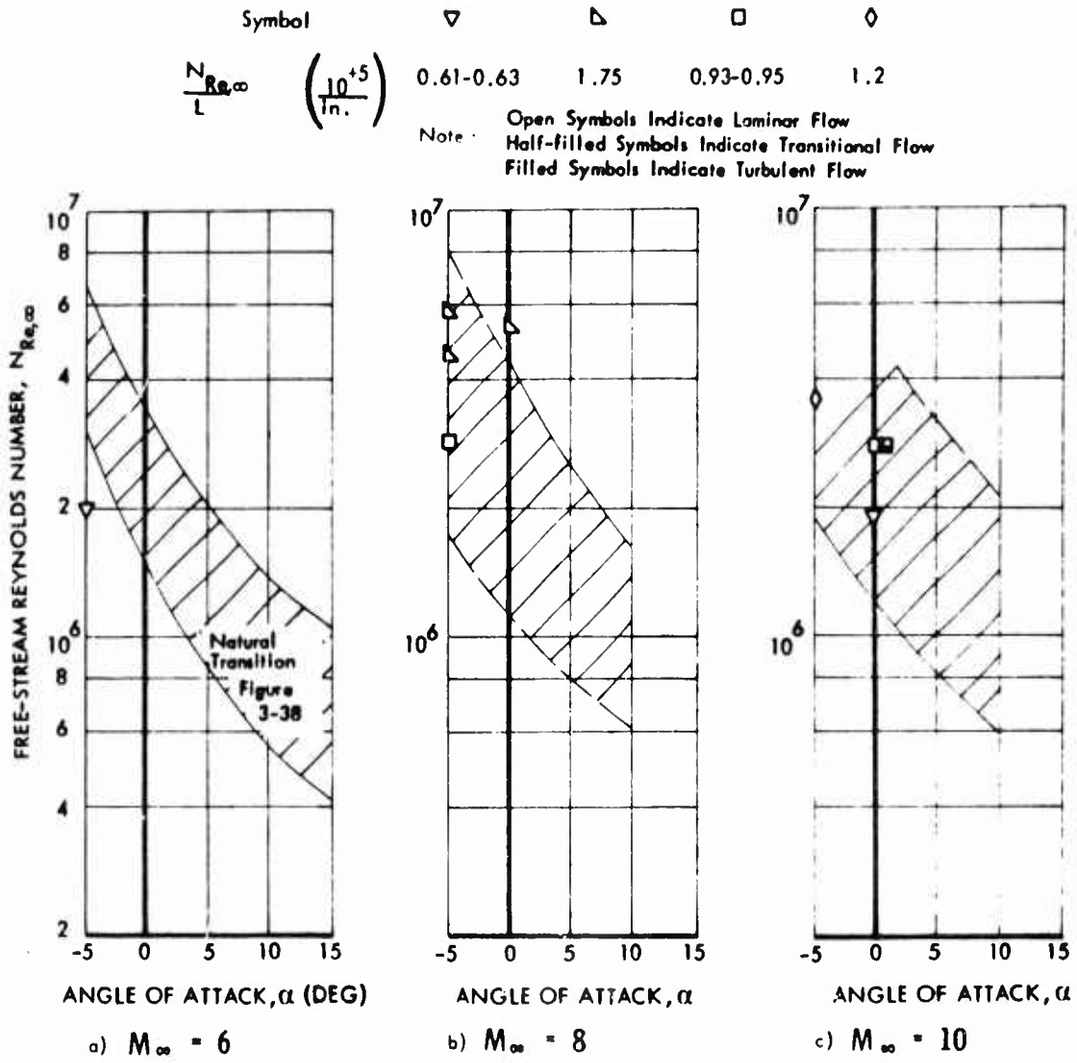

Figure 3-47: EFFECT OF BOUNDARY LAYER TRIP ON TRANSITION — 75° Swept Delta Wing at Centerline

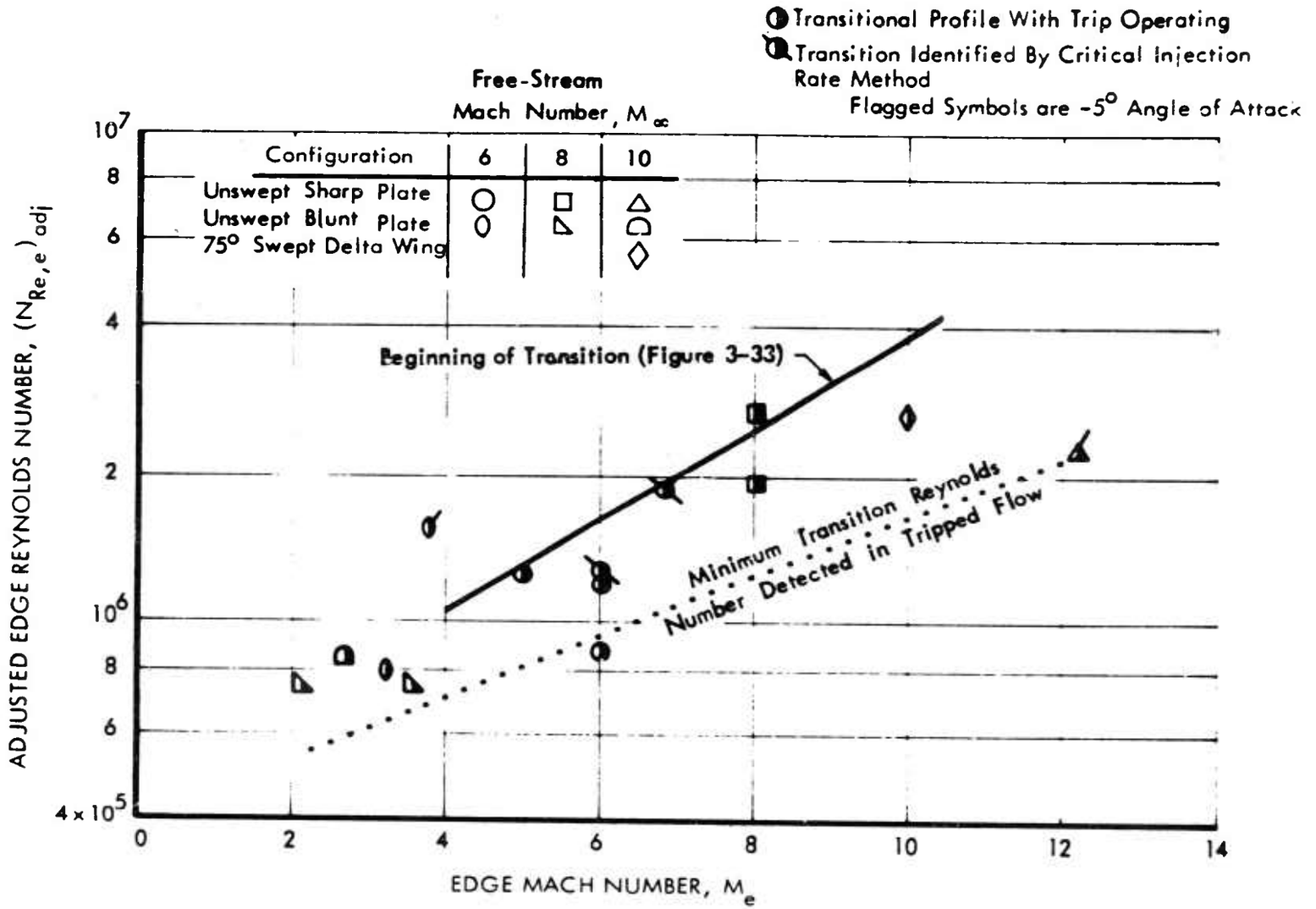

Figure 3-48: EFFECT OF BOUNDARY LAYER TRIP ON TRANSITION REYNOLDS NUMBERS

data presented are all for three discrete Mach numbers (5, 8, and 10). As shown in Figure 3-49, the Reference 15 data are in excellent agreement with the present results, represented by the faired curves of Figure 3-33. The model used in the Reference 15 investigation was somewhat longer than that of the present program so that the end of transition was also observed at Mach 10. The Mach 10 datum is seen to agree well with an extension of the Figure 3-33 curve.

Data from two different wind tunnels are given by References 16 and 40. The datum of Korkegi (Reference 16) is taken from Figure 8 of his paper and adjusted to a unit Reynolds number of 2×10^5 in the same manner as all previous data. The beginning of transition point is much above the present data, as shown in Figure 3-49; no end of transition data was obtained (without tripping). The large disagreement between the Reference 16 data and the present data is rather surprising in view of the comparisons presented below, and it is not now known if the apparent difference will be verified by further examination. Korkegi remarks that waves emanating from the tunnel throat had the effect of thickening the laminar boundary layer in his tes but it is not clear that any increase in transition Reynolds number should follow. It is not likely that the discrepancy is a unit Reynolds number effect; the adjustment for unit Reynolds number was less than 10%, and downward.

The data of Morkovin (Reference 40) are at a much lower Mach number than any of the present data, so that direct comparisons cannot be made. It will be noted that his data are well above extensions of the Figure 3-33 curves. However, previous data from many sources have shown a different Mach number trend at supersonic speeds than that shown by the present hypersonic data. Morkovin notes in his paper that his results actually appear to be somewhat low when compared with other data.

Also shown in Figure 3-49 are some data obtained by Coles (Reference 41). Coles' data were taken in the JPL 20-inch hypersonic wind tunnel by two techniques. One method involved the direct measurement of skin friction force by measuring the force on a free element of the model surface. Ideally, the minimum and maximum points in the curve of skin friction against distance would correspond to the minimum and maximum pitot pressures in the present investigation. In actual practice some differences are to be expected; the friction balance technique is susceptible to pressure gradient and roughness effects, while the pitot system may be affected by lags and interferences, as already noted.

Coles' second technique is based on the static pressure measured at the model surface. A small ($\approx 5\%$) but definite change in static pressure occurred in the transition region that was used by Coles as a measure of transition. Both sets of data are shown in Figure 3-49. The original data cover a range of unit Reynolds numbers; the values shown here are read from the author's faired curves at a unit Reynolds number of 2×10^5.

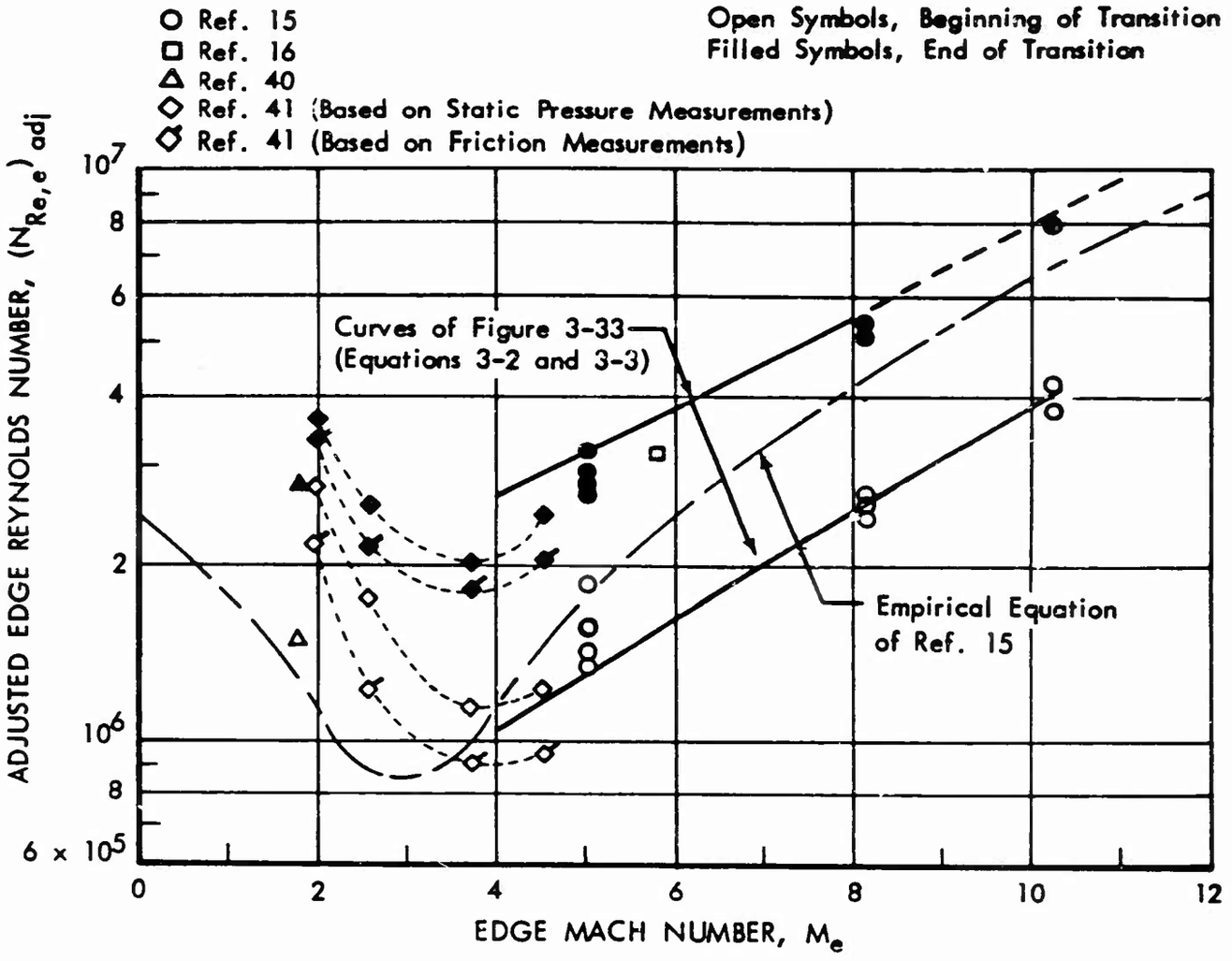

Figure 3-49: COMPARISONS OF SHARP FLAT PLATE TRANSITION DATA

The data obtained by Coles are generally at lower Mach number than are the present results. The data at about Mach 4 are directly comparable, however, and it is seen that the friction balance data are 30 to 40% below the faired curve of Figure 3-33. The greatest discrepancy occurs at the end of transition where it will be recalled that the Figure 3-33 curve coincides very closely with the actual data. The present data for beginning transition at Mach 4 are somewhat below the Figure 3-33 curve, and very close to Coles' friction balance measurements.

Coles' static pressure method data indicate somewhat higher transition Reynolds numbers than do the friction balance data. As shown in Figure 3-49, Coles' static pressure data are closer to the present data, but the relation of static pressure to pitot pressure in the transition region is not well established (to the author's knowledge) so that the significance of the comparison is somewhat obscure. The friction data would seem to provide the more meaningful comparison. It does appear, however, that Coles' data are in as close agreement as could be expected (even if the transition Reynolds numbers were truly identical) considering the different instrumentation involved.

The authors of Reference 15 devised an empirical formula for predicting transition based on their review of the data then available. Their formula, which is not specifically identified with either the beginning or end of transition, is seen to follow the trend of the data reasonably well, particularly at the higher Mach numbers. It is stated in Reference 15 that the standard deviation for the 291 data points considered in that report is 33%, corresponding to a probable error of 21%.*

A similar calculation for the present end of transition data shows a probable error of 11%; if the single very low point at Mach 6 (Figure 3-32) is deleted the remaining data are represented with a probable error of only 6.5%. This latter figure is probably more comparable with the 21%, since it is common experimental practice to throw out widely divergent data. Thus, it would seem that empirical formulas could be developed specifically for the beginning and end of transition that would represent the data much more accurately than the Reference 15 equation, and perhaps allow some geometry effects to be determined. The curves of Figure 3-33, which seem adequate for hypersonic speeds, are equivalent to:

$$\log_{10}\left[N_{Re,Tr,begin}\right] = 3.53 + 0.094\, M_e + 0.4 \log_{10}\left(\frac{N_{Re,e}}{L}\right) \qquad (3\text{-}2)$$

and

$$\log_{10}\left[N_{Re,Tr,end}\right] = 3.99 + 0.0793\, M_e + 0.4 \log_{10}\left(\frac{N_{Re,e}}{L}\right) \qquad (3\text{-}3)$$

We will now examine some cone and cylinder data in view of Equations 3-2 and 3-3.

---

* The probable error is defined to be that error which is exceeded by 50% of the data.

Two sets of sharp cone data for the end of transition are presented in Reference 14, each covering a range of unit Reynolds numbers. The range of unit Reynolds numbers involved is not large, so that the trend is not well defined by the data themselves, but the effect shown is not inconsistent with the 4/10-power law that has so far been assumed. The adjusted data are shown in Figure 3-50, where it is seen that the cone data are somewhat above the flat plate curve.

Cone data from lower Mach numbers are reported in References 10 and 42. Those data also show a unit Reynolds number effect that is approximately a 4/10-power law.* The data at a unit Reynolds number of 2×10^5 are presented in Figure 3-50, and are also seen to fall somewhat above the flat plate data of Figure 3-49.

Finally, some higher Mach number, sharp cone data are given in Reference 43 by Sanator, et al. When adjusted for the unit Reynolds number effect the Reference 43 data for both the beginning and end of transition are about 25% above the flat plate curves of Figure 3-33. Unfortunately, there are important differences between the test conditions and test techniques that preclude firm conclusions. The Reference 40 data are for highly cooled wall conditions, with T_w/T_o ranging from 0.075 to 0.365, while the present data are for T_w/T_o ratios of 0.7 to 1.0. However, the Reference 40 data show no large effect of wall temperature ratio in the range tested, nor does the flat plate data in Figure 46 of Reference 15. It is tempting to conclude that the wall temperature effect is negligible, and that, in view of the consistency of the data from these four references, there exists a body geometry effect leading to higher transition Reynolds numbers on cones than on flat plates.

It should be noted that the experimental results are not in agreement with expectations based on the stability calculations of the previous section. According to that theory, it is the Reynolds number based on the boundary layer thickness that determines stability, not the length Reynolds number. It is well known from boundary layer theory that the boundary layer is much thinner on a cone than on a flat plate, so that for equal boundary layer thickness Reynolds numbers, the distance Reynolds number on a cone must be three times higher than on a flat plate. If the transition Reynolds number could be simply related to the critical Reynolds number, one would expect the transition Reynolds number to be three times higher as well. Even considering the deficiencies in the present data and the small number of data available, it hardly seems likely that a factor of three does actually exist.

There is, however, a calculation by Emmons and Bryson (Reference 44) that agrees with the data trends. Assuming that turbulent bursts are generated in the transition region in a random manner, not dependent on body shape and assuming that the turbulent spots spread downstream at an angle of 9.8 degrees, Emmons and Bryson calculated that the transition on a cone (assumed to occur when the turbulent bursts had spread to cover the entire body) would occur at a Reynolds number 1.34 times higher than on a flat plate. As shown in Figure 3-50, applying

* Best fit to the data is obtained with an exponent of 0.355.

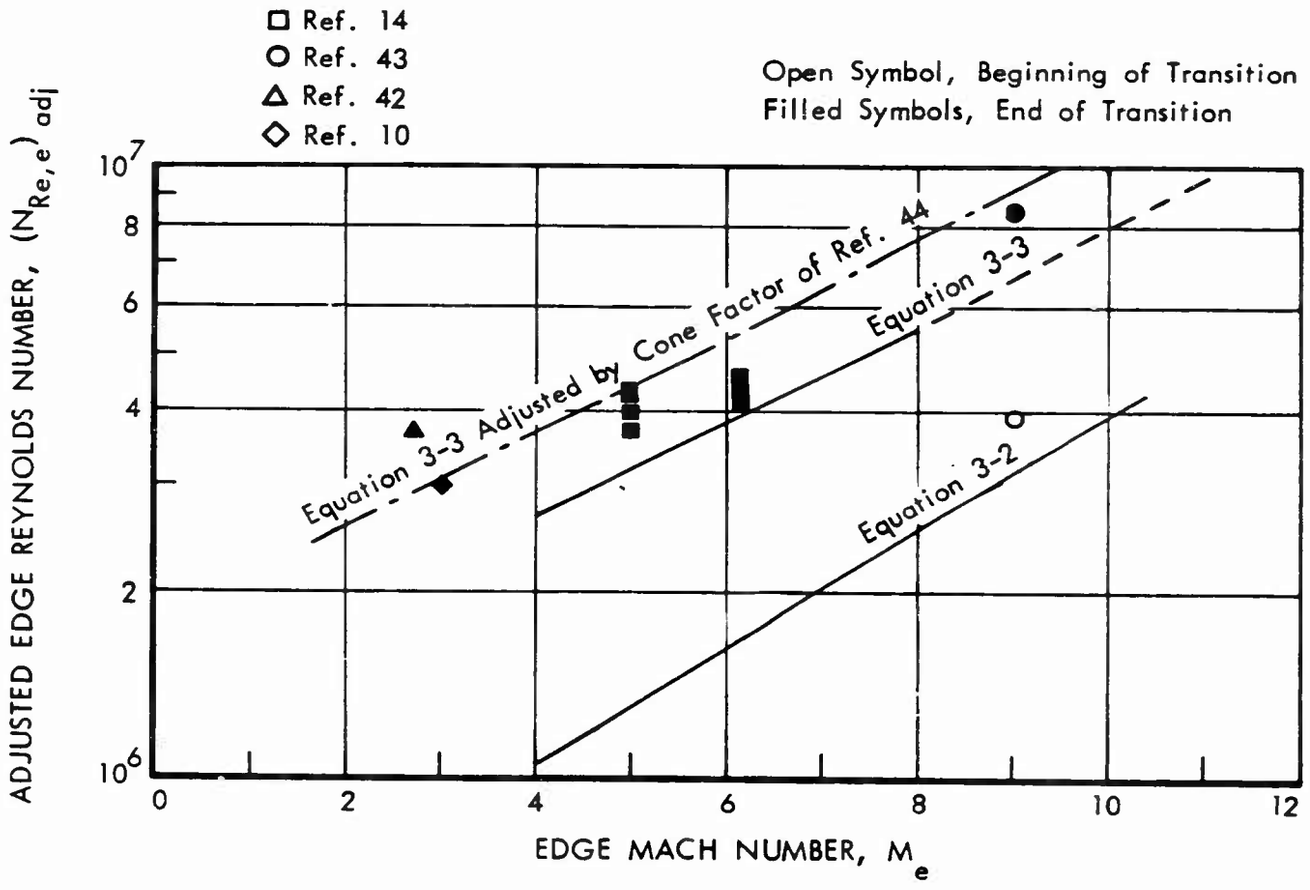

Figure 3-50: COMPARISON OF CONE AND FLAT PLATE NATURAL TRANSITION DATA

their factor to Equation 3-3 leads to fairly good agreement with the experimental data.

Some data are presented in Reference 14 that may be used to further investigate the effect of body shape. Hollow cylinder data at a Mach number of 8 are presented in Figure 5 of that report, covering a range of unit Reynolds numbers from 6.3×10^4 to 2.7×10^5. The hollow cylinder data appear to correlate very well with the 4/10-power-law correction for unit Reynolds number. The only pitot survey data presented are for the end of transition, which are shown in Figure 3-51 to fall about 20% above the present flat plate curve.

Perhaps this small difference should not be considered to be meaningful; however, referring to Figures 3-32 and 3-49 it will be seen that the actual data obtained at Mach 8 are slightly below the faired curve. Thus the actual difference shown by the data is closer to 30%. Considering that both the cylinder and the flat plate data were obtained in the same facility, at the same Mach number, in the same range of unit Reynolds numbers, and by the same experimental technique, the comparisons strongly suggest that some small model geometry effect is actually involved.

One of the most systematic and carefully done experimental investigations of transition is that reported by C. S. James in Reference 12. James' data was taken on free-flying models, using schlieren photography to locate transition points. Many repeat tests were made so that a statistical evaluation of the percentage of turbulent flow at any particular model location could be made. In this way the beginning and end of transition could be defined based on 0 and 100% probability of turbulent flow.

As presented in Figure 3-51, James' results are based on his estimated end-of-transition values, adjusted to a unit Reynolds number of 2×10^5 per inch. James' data are shown in Figure 3-51 to fall above the flat plate curve by an amount that is consistent with the hollow cylinder data of Reference 14. The data cannot be said to support a general conclusion, however, due to the differences in both the experimental techniques and test facilities. The James' data are also taken at a much higher unit Reynolds number than the other data presented ($\approx 3 \times 10^6$ per inch); altering the 4/10-power law to a 0.45-power law would bring James' data into almost exact agreement with the present flat plate curve.

Before leaving the cylinder data, it should be noted that the stability theory calculation for the cylinder has not been made. According to boundary layer theory, there should be no effect of transverse curvature as long as the boundary layer is thin. However, an examination of the profiles shown in Section II shows that the perturbation profiles do not decay nearly as rapidly as does the boundary layer velocity defect, and the effect of curvature may be more important. The effect of curvature, if any, would appear to be stabilizing. The aforementioned paper by Emmons and Bryson does not include a calculation for cylinder flow, but based on the assumptions involved it would appear that a shorter transition region would be predicted, depending on the ratio of the length of the transition region to the

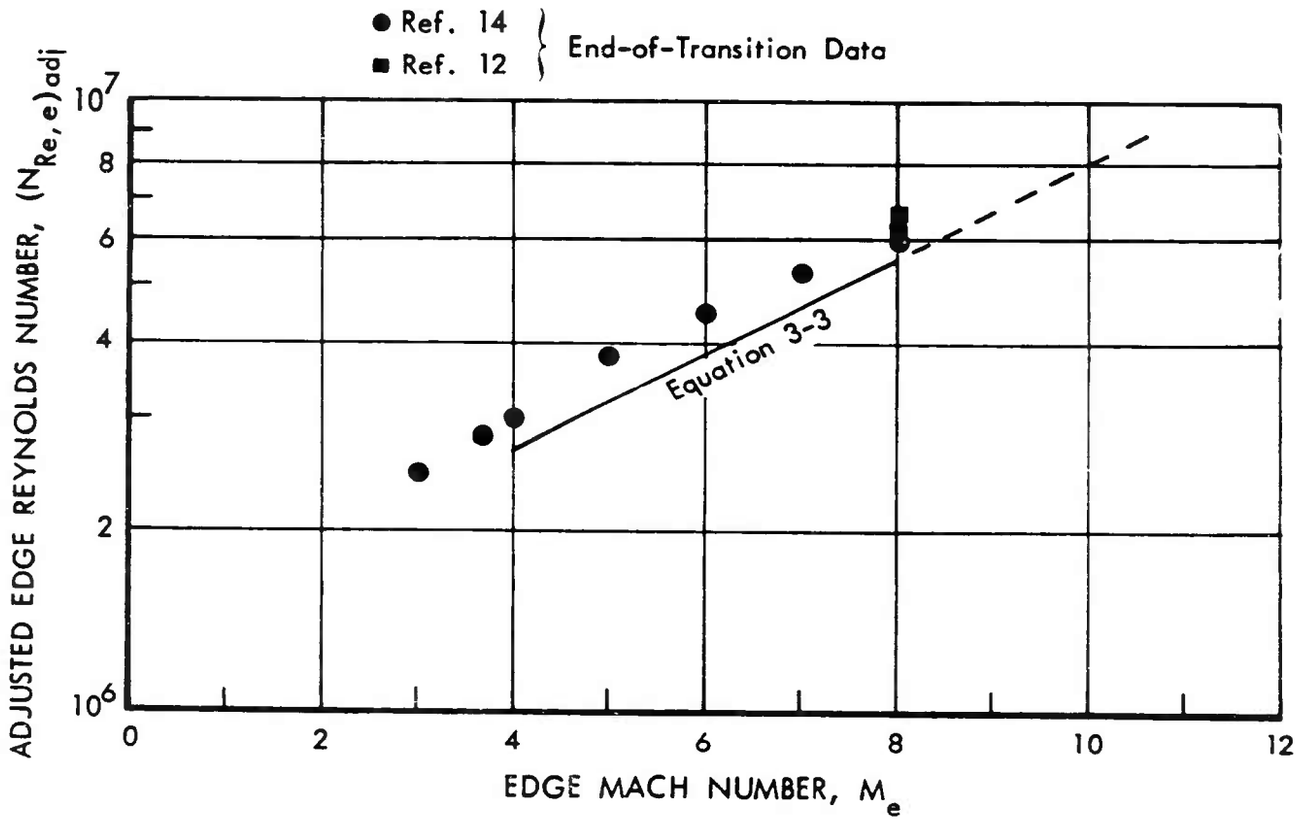

Figure 3-51: COMPARISON OF HOLLOW CYLINDER AND FLAT PLATE NATURAL TRANSITION DATA

cylinder diameter. This expectation is based on the fact that for slender cylinders, turbulence could spread transversely entirely around the cylinder, but this is not possible on a plate.

Some comparisons with previous tripped transition data are presented in Figure 3-52. The present tripped transition data are represented by faired curve taken from Figure 3-48.

Data by Korkegi (Reference 16) for both the beginning and end of transition are shown at a Mach number of 5.8. His data were obtained by the axial survey method. It is seen that the Reference 16 data for both the beginning and the end of transition are well above the Figure 3-48 curve. The latter curve is an estimated lower bound on tripped transition based on vertical survey data, and is believed to correspond more closely to the beginning of transition than to the end. Comparing the Reference 16 data to the Figure 3-48 curve, it will be seen that the ratio of the two sets of data is approximately the same as that shown in the natural transition data. Again, the significance of this discrepancy is not clear.

As a part of his experiments, James had some of his models constructed with screw-thread roughnesses and noted the effect on transition. His results showed that small amounts of roughness can increase the transition Reynolds number by some 20%; it was not until large roughness elements were used that a significant reduction in transition Reynolds number occurred.

End-of-transition data, as estimated from James' report are presented in Figure 3-52. The estimates are based on Figures 13, 14, and 19 of Reference 12. The smooth body data are reproduced from Figure 3-51 for comparison. As shown in Figure 3-52, James ultimately obtained reductions in the transition Reynolds number of 30 to 60% with large-scale roughnesses. However, it is apparent that roughness is not a good means of introducing small disturbances into a supersonic laminar boundary layer; rather, small roughnesses apparently distort the laminar boundary layer into a more stable configuration. It was comparisons such as this one, and the results reported by Korkegi that led to the use of mass injection tripping in the present investigation.

Comparing James' data with the Figure 3-48 curve, it is seen that his end of transition data are about a factor of two higher than the Figure 3-48 curve which was interpreted as approximately the beginning of transition. It will be recalled that this is about equal to the factor relating the beginning and end of natural transition; hence it would appear that the lowest attainable transition Reynolds numbers by the two tripping methods are about the same.

Irrespective of geometry effects, all of the hypersonic data show the same Mach number effect. It is interesting to note that a very similar trend has been observed in wake transition data. Figures 3-53 and 3-54, reproduced from References 45 and 46, illustrate the observed trends in wake data. The curves of Figure 3-53 are seen to also exhibit an exponential increase with free-stream Mach number

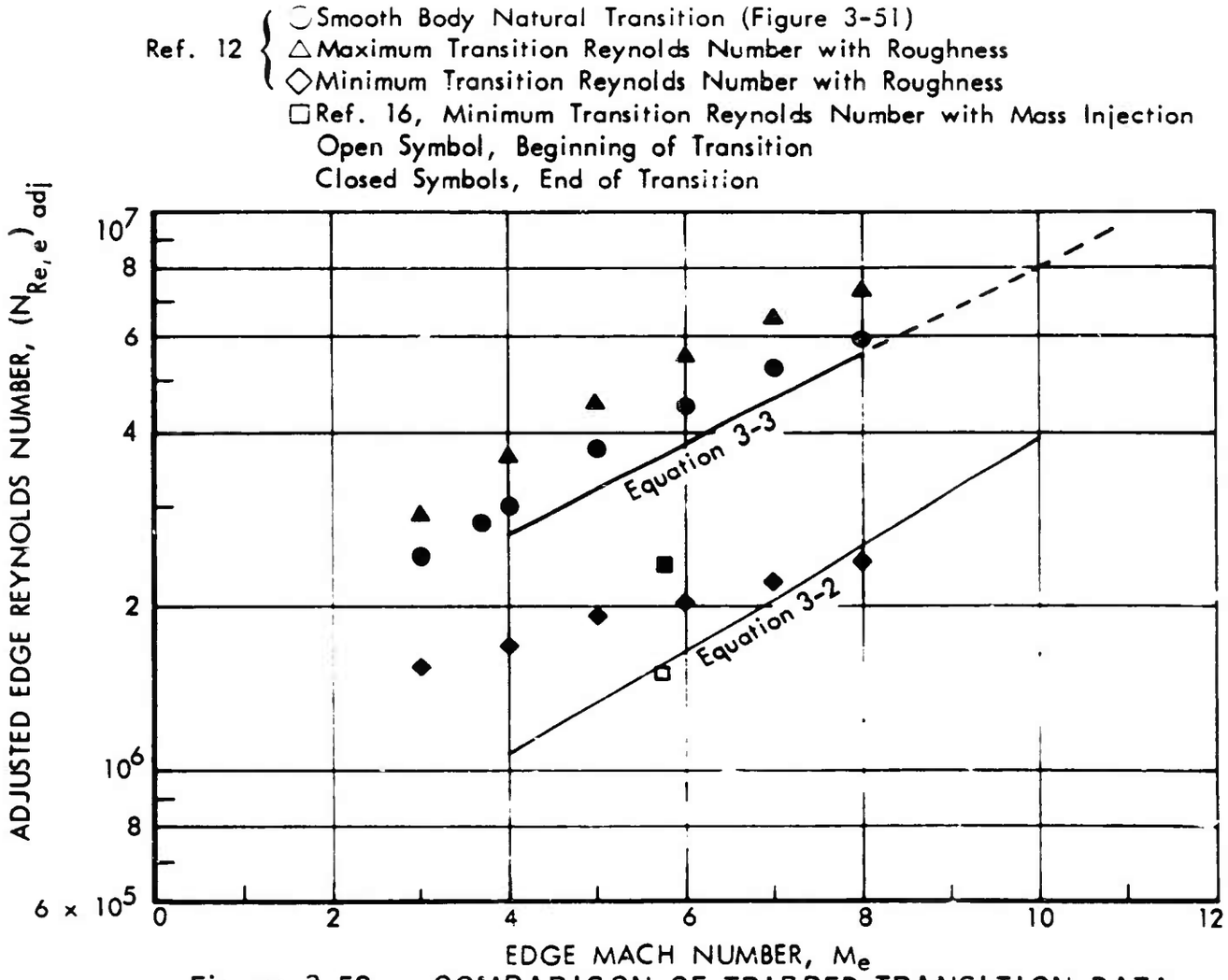

Figure 3-52: COMPARISON OF TRIPPED TRANSITION DATA

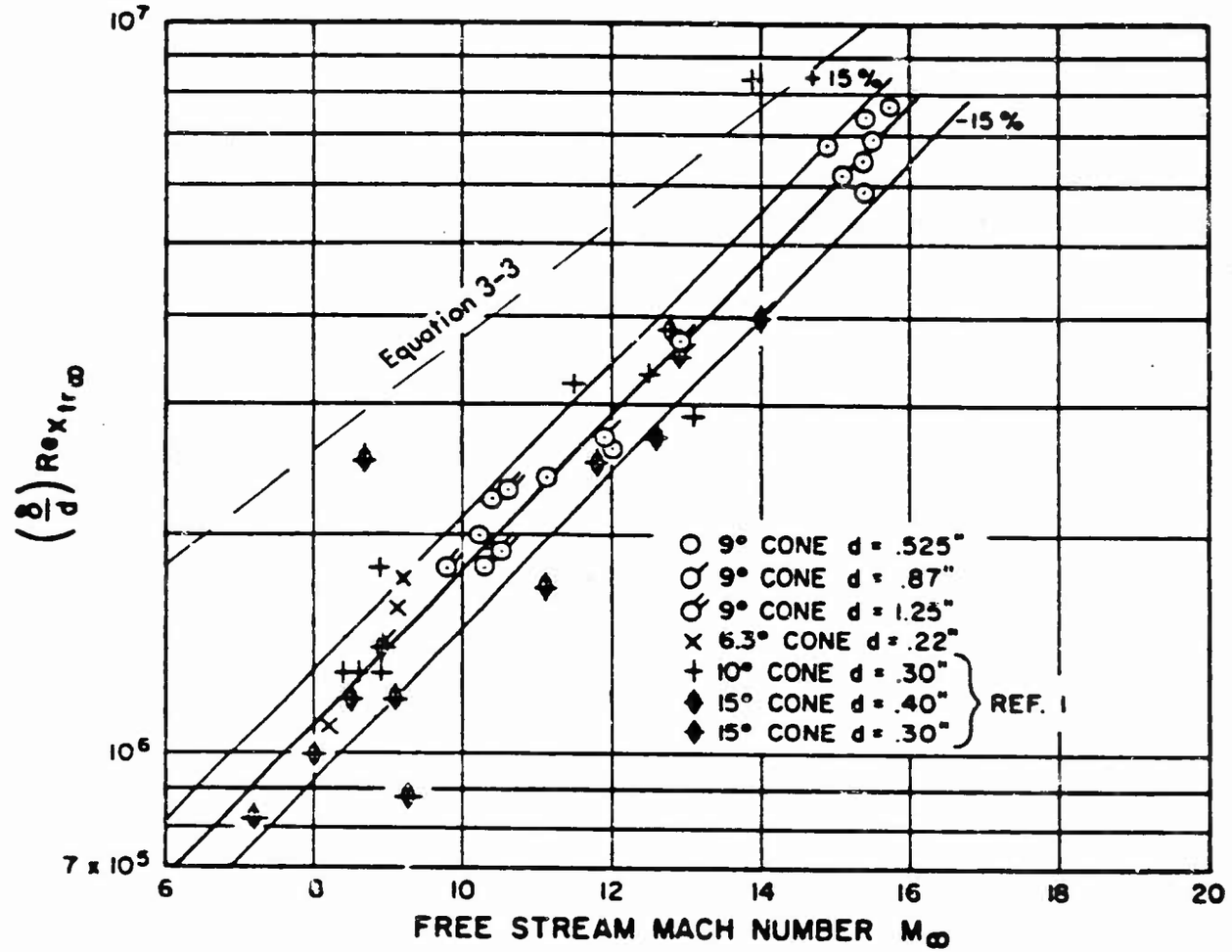

Fig. 4 Correlation of wake transition data.

Figure 3-53: COMPARISON OF PRESENT DATA WITH WAKE TRANSITION CORRELATION OF REFERENCE 45

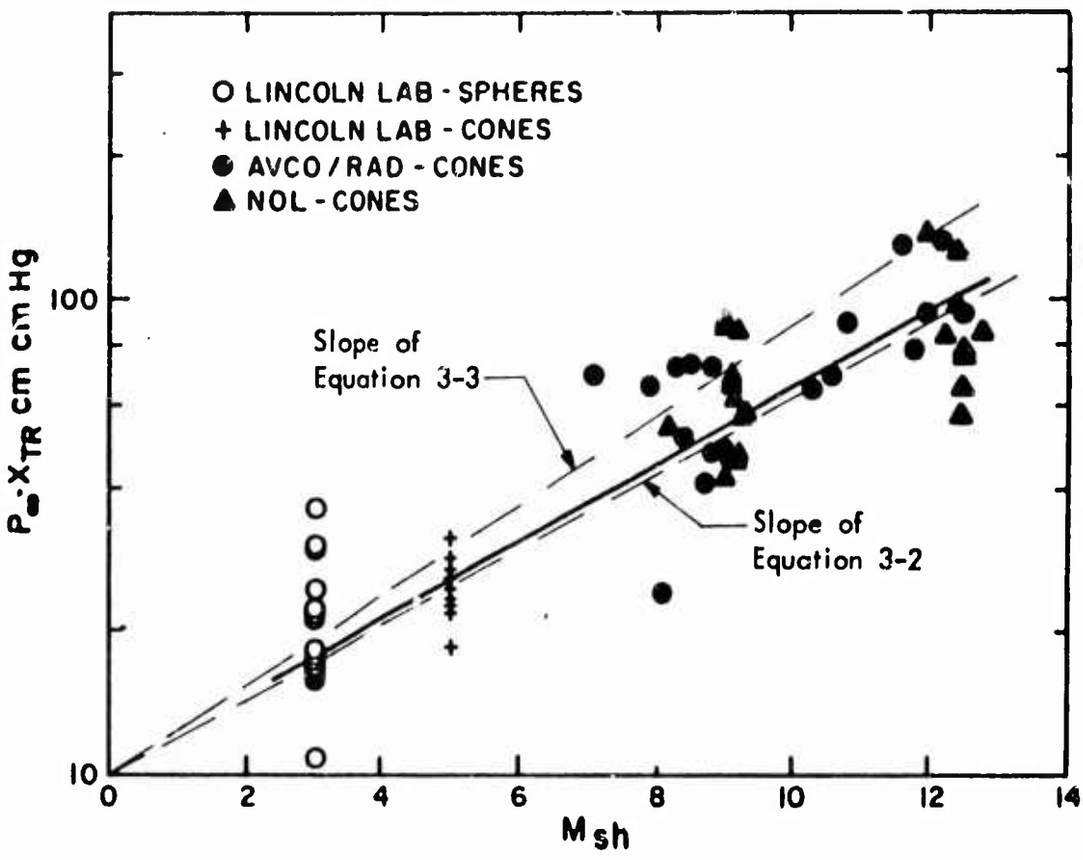

Fig. 3 $p_\infty \cdot X_{TR}$ **vs** M_{shoulder}.

Figure 3-54: COMPARISON OF PRESENT DATA WITH WAKE TRANSITION CORRELATION OF REFERENCE 46

up to a Mach number of almost 16. Waldbusser, in Reference 45, has adjusted his data by the factor δ/d (δ is the wake width and d is the body diameter), but this adjustment does not appear to alter the Mach number trend. His use of free-stream Reynolds numbers and Mach numbers is more likely to affect the plotted results, but presumably wake "edge" conditions would not be greatly different from free-stream conditions. However, the Mach number effect found in Reference 45 is very similar to that shown in the present boundary layer data, as may be seen from the Equation 3-3 curve.

Goldburg, in Reference 46, has taken the Mach number at the body shoulder as being more representative of the local Mach number. The transition length is scaled by the free-stream pressure, which, for constant free-stream temperature is equivalent to Reynolds number scaling. Direct comparison with the present results is of course not possible, but it is seen that the Mach number trend (indicated by the slope of Equations 3-2 and 3-3) follow the trend of the data very well. The slope of Equation 3-2 almost exactly matches that of the fairing given by the author of Reference 46.

Of course, much more careful comparisons must be made before any relation between wake transition and boundary layer transition could be established, but the similarity in the qualitative trends suggests that a simple relation may exist.

IV

COMPARISON OF ANALYTIC RESULTS WITH EXPERIMENTAL DATA

As stated previously, the objective of the present analytic study was the development of a new method for calculating laminar flow stability having sufficient generality to be extended to treat the nonlinear effects that occur in the transition region. Development of the method has been described; it is now appropriate to consider its implications regarding transition.

It is, of course, not to be expected that transition will occur upstream of the point of minimum critical Reynolds number because distrubances are not amplified in that region. The analysis also shows that, even downstream of the critical point, disturbances will be damped initially. It is not until the disturbance has developed into a characteristic profile that any amplification will be observed. Conversely, it may be possible to trip the boundary layer by introducing disturbances upstream of the critical point. Although the disturbance will be damped initially, it will spread downstream beyond the critical point, after which amplification will occur. With the present method, it is possible to examine these effects in more detail than with previous methods because any initial disturbance can be applied and its subsequent behavior calculated. By relating distance to time through the stream velocity, the calculated time history can be regarded as a streamwise variation. For the present, all calculations must be carried out at a constant Reynolds number, however, so that the calculation is not exactly equivalent to following the disturbance growth in a streamwise direction. By selecting a mean Reynolds number over the transition region, an indication of the early behavior should be obtained, however.

Some typical results are presented in Figure 4-1. In all cases the initial disturbance was a streamwise velocity pulse introduced at a point in the boundary layer. Initially the amplitude diminishes rapidly, even though the flow is well above the critical Reynolds number. This behavior was already shown in more detail in Figure 2-15. At Mach 7 it is seen that the flow progresses about 20 boundary layer thicknesses before the amplitude begins to increase, and that it is only after more than 100 boundary layer thicknesses that the amplitude is equal to that of the original pulse. In terms of streamwise distance from the point of disturbance, the disturbance is smaller than the initial pulse for a distance that is about one half of the original leading edge distance. Of course, the subsequent growth will be much more rapid.

Figure 4-2 summarizes the results of the analytic studies, the experimental data, and their relation to each other. The analytic results for the critical Reynolds number are represented by the faired curve, which is taken from Figure 2-25.

Experimental data from the present program are indicated by curves that are derived from the faired curves of Figure 3-33 and 3-48. Also shown are data from

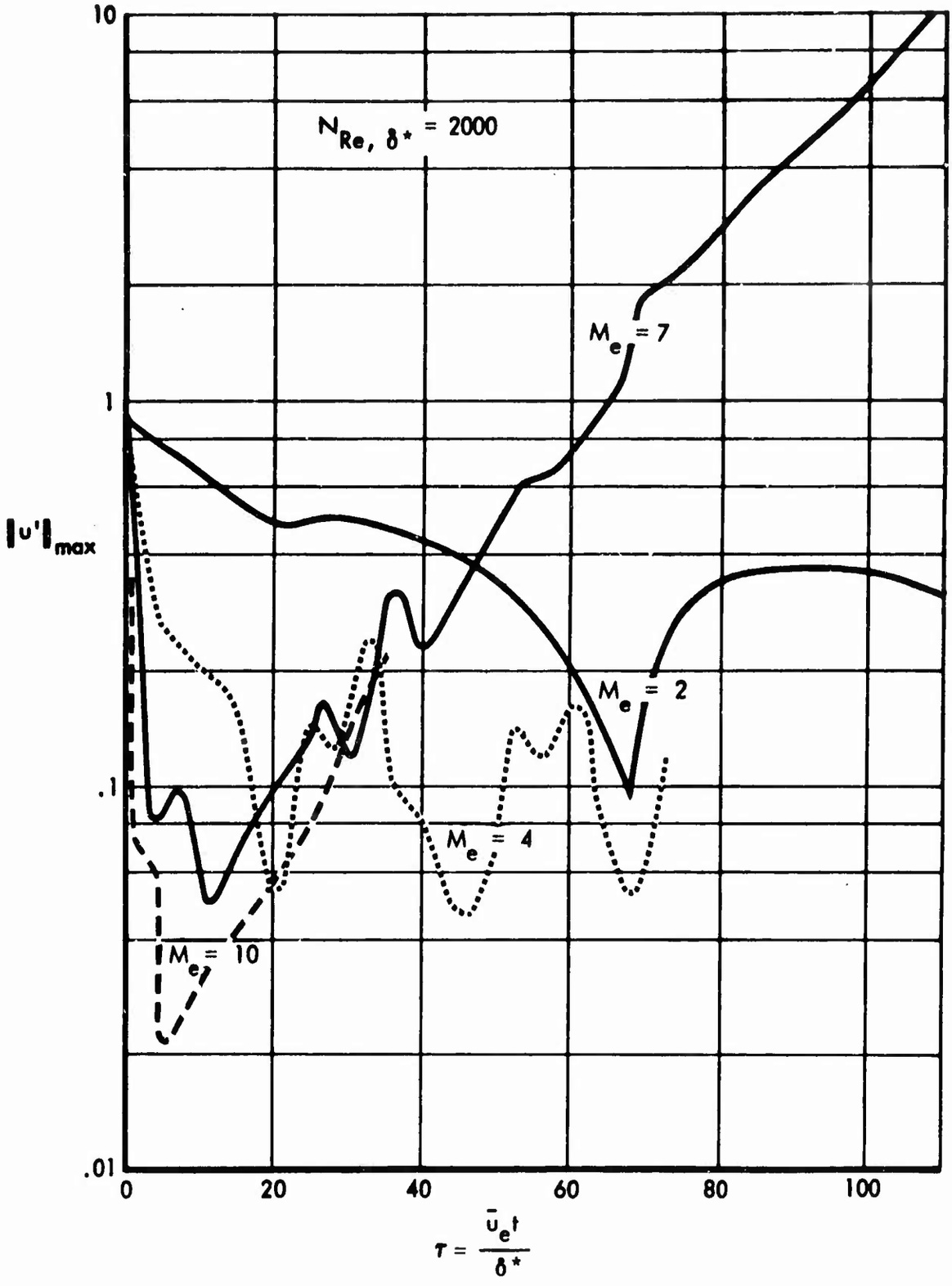

Figure 4-1: HISTORY OF DISTURBANCE AMPLITUDES

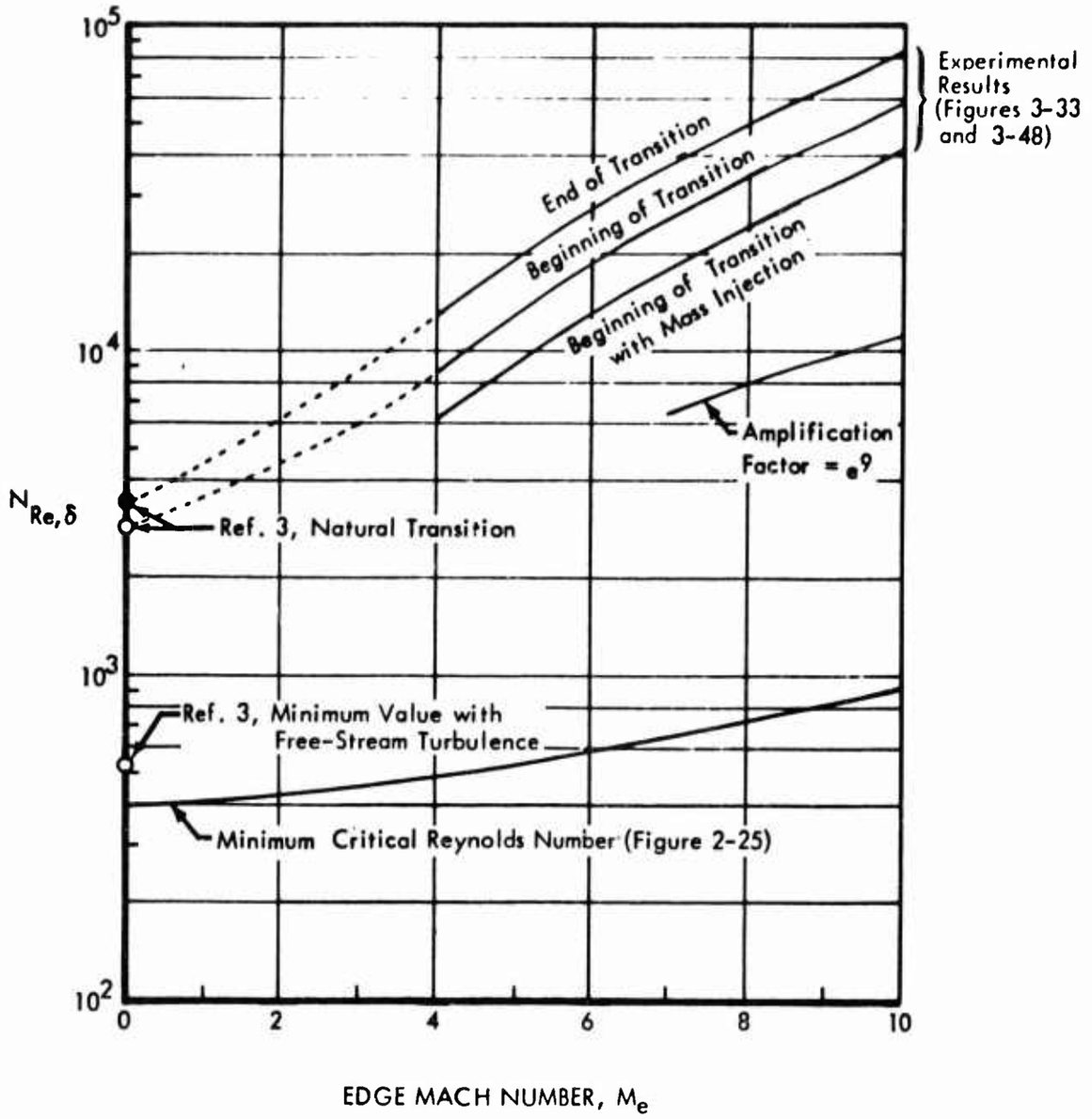

Figure 4-2: COMPARISON ON ANALYTIC AND EXPERIMENTAL DATA

Reference 3, which is seen to fair in well with the present data, thus providing an empirical transition Reynolds number over the entire speed range.

The experimental natural transition data are well above the critical Reynolds number as expected. The transition Reynolds number is reduced somewhat by mass injection, but is still well above the critical Reynolds number. In contrast, it is seen that the effect of free-stream turbulence reported in Reference 3 reduced the transition Reynolds number to only slightly above the critical value. Thus it appears that either mass injection is an ineffective tripping method, or that the supersonic boundary layer is much more difficult to trip.

As described in Chapter 17 of Reference 17, subsonic transition has been related to amplification by the empirical rule that transition occurs when the integrated amplification equals e^9, or about 8,000. Applying that rule in the supersonic case using the amplification rates illustrated by Figure 4-1 would predict transition at 100 to 200 boundary layer thicknesses further downstream. A curve has been added to Figure 4-2 showing the Reynolds number at which an amplification of e^9 will have occurred, based on Figure 4-1 . It is seen that the present data are well above the curve so obtained. Of course, the factor e^9 is purely empirical and based on subsonic flow data. It is not surprising that better agreement was not obtained. On the basis of the present data an empirical factor could be determined, but this has not yet been done. The computer program should first be modified to vary the Reynolds number during the calculation, an extension of which is beyond the scope of the present study.

It is noted, however, that the calculated transition line has about the same trend as the experimental data, suggesting that there may exist a simple rule relating the stability theory results to transition. It is fortunate that the amplification factor is related to transition rather than the minimum critical Reynolds number. From the results given in Section II it may be seen that the precise determination of the critical Reynolds number is often difficult; the calculation of integrated amplification factors is less difficult with the present method.

V

CONCLUDING REMARKS

ANALYTIC PROGRAM

The analytic investigation centered about the development of a new method for calculating laminar flow stability based on numerical integration of the complete Navier-Stokes equations. A number of preliminary results have been obtained, and it is believed that the fundamental problems associated with the development of the new method have been overcome. The numerical stability of the system of equations has been investigated and an integration scheme devised that has apparently satisfactory characteristics. A means has also been found for simulating the boundary conditions at infinity that appears to be satisfactory. By restricting the calculations to a specific disturbance wavelength, the amount of computer time required for calculation was greatly reduced with improvements in accuracy and detail of the numerical results. Even when restricted to a specific wavelength, the method is more general than previous stability calculations, and makes possible the analysis of arbitrary initial disturbances.

Calculations with arbitrary initial disturbances show that in general the initial disturbance decreases in amplitude until certain characteristic profiles develop. It was found that, by the time the characteristic profiles had developed, the flow would have traveled the equivalent of many boundary layer thicknesses. Once the characteristic profiles have developed, the amplitude then increases if the Reynolds number is greater than a critical value; however, the equivalent of many more boundary layer thicknesses of flow are required before the disturbance regains its initial amplitude, even where the Reynolds number was several times greater than the critical value. These results show that transition is not to be expected for some considerable distance downstream of the critical point (critical Reynolds number location) and that calculated amplification factors are much more useful as a guide to transition than is the critical Reynolds number itself. With the present method the amplification factor is also more easily obtained than is the critical Reynolds number.

The analytic program should be continued. There are many obvious and important improvements that could be made. Among these would be an extension of Stuart's (Ref. 18) energy method that would allow the direct calculation of the critical Reynolds number and wavelength without the laborious double parameter search technique that is now required. Concurrently, equations should be developed to calculate the distortion of the steady laminar flow due to Reynolds stresses. These additions involve no major changes to the method as it now stands; rather, they involve only operating algebraically upon the results already calculated. It is, however, necessary to derive the correct formulae as they are not yet available.

All of the results presented are for two-dimensional flow with calculations carried out at two streamwise locations in the flow field. Three-dimensional perturbations could be calculated (with the restriction of discrete wavelength) by the addition of a single z-location (z is normal to the main flow and tangent to the surface). Considering the extra terms that would be involved, it appears that the work required for such a calculation would be about double that for the present two-dimensional calculation. The transverse wavelength would also introduce at least one additional parameter that would have to be searched (along with α and N_{Re}) to find the most critical case. The aforementioned energy method should therefore be developed before three-dimensional calculations are attempted.

All of the results shown herein are based on linearized equations. Although the nonlinear terms are easily included (as, in fact, some calculations were made with nonlinear equations) it is felt that the study of nonlinear effects should await a better understanding of the present results. It is believed that the most important nonlinear effects will be associated with the (as yet unincorporated) three-dimensional and Reynolds stress terms.

EXPERIMENTAL PROGRAM

The test program extended previous transition knowledge by obtaining data that show angle-of-attack effects on blunt and sharp leading edge flat plates, sharp leading edge delta wing planform effects, and mass-injection effects. In spite of numerous difficulties encountered in the experimental program, the results obtained show remarkable consistency and close agreement with results of a previous investigation reported in Reference 15. The data presented here depend on qualitative trends rather than on absolute values, which to some extent minimized the effect of experimental errors. While the known deficiencies in the data preclude drawing firm conclusions, several significant trends are strongly suggested, particularly by the end-of-transition data, which are also believed to be least affected by the probe system deficiencies. The authors feel that the following trends are indicated with sufficient probability and are of sufficient probability and are of sufficient importance to justify further experimental work:

1) For sharp tip cones at zero angle of attack, and for sharp flat plates at angle of attack, natural transition Reynolds numbers depend only on local flow properties; there is no effect of angle of attack or cone angle, as such.

2) At zero angle of attack, natural transition Reynolds numbers on a cone are about 1/3 greater than on a flat plate.

3) The effect of unit Reynolds number on natural transition is much less for a highly swept, sharp delta wing than for flat plates, cones, or flow-aligned hollow cylinders. The effect is the same for the latter three geometries.

4) Natural transition Reynolds numbers at hypersonic speeds increase exponentially with the Mach number, as does the length of the transition region. The effect of Mach number is the same for sharp tip, flat plates, cones, hollow cylinders, and delta wings.

5) On a sharp-leading-edge delta wing the local Reynolds number at transition decreases slightly with angle of attack.

If these trends are verified by future experimental work, some important conclusions would seem to follow. From the first statement, it would appear that the unit Reynolds effect on natural transition is not spurious, as has been suggested by several authors, but is an unexplained fluid mechanic effect not associated with any particular model or test facility. If the effect originated from disturbances outside the shock layer, angle of attack, or cone angle would seem to change the relative magnitude of that disturbance and hence the effect on transition. If the unit Reynolds number effect originates from some spurious influence within the shock envelope, the model or support system must be at fault. However, since many tests involving many different models (and at least three different geometries) have shown the same effect, it is clearly not associated with either a particular model or its support.

The second observation supports the hypothesis that the eruption of turbulent spots assumed by the Emmons-Bryson calculation (Ref. 44) is the phenomenon that determines the transition location, and that the eruption rate is about the same for cones as for flat plates. This implication is somewhat obscured by the apparent existence of higher transition Reynolds numbers on a hollow cylinder than on a flat plate. No effect would be predicted by the Emmons-Bryson calculation except as possibly the result from disturbances caused by the corners of the plate. Further cone and hollow-cylinder experiments would be of great value, but it does appear that cone transition Reynolds numbers are not three times higher than flat plate values, as suggested by stability theory. The prediction of the stability theory that the length of stable laminar flow on a cone is three times greater than on a flat plate is probably correct, but the length of stable laminar flow is so small compared to the transition distance that no effect is observed. However, the absence of a large factor between flat plate and cone transition Reynolds numbers does indicate that the rate of turbulent spot production is not controlled by the boundary layer thickness Reynolds number. If the rate of spot production is assumed to depend only on the local unit Reynolds number it could be possible to explain both the ratio of cone to flat plate transition Reynolds numbers, and the existence of a unit Reynolds number trend. An examination of this possibility, particularly in light of observation Number 3 above should lead to a much better understanding of the unit Reynolds number effect and its significance in making transition predictions for atmospheric flight.

The hypersonic exponential dependence of the transition Reynolds number on the local Mach number is evident in the data for both the sharp flat plate and the sharp delta wing. Data from other sources for cones and cylinders show the same trend. Wake transition data of Reference 45 also exhibit an exponential Mach number effect suggesting that the Mach-number effect may be a universal function.

It was also noted that no great reduction in transition Reynolds number was obtained with the mass injection trips. This results suggests that perhaps an empirical lower bound on transition could be obtained that would be applicable in actual flight by a systematic study with many types of tripping devices.

APPENDIX

BOUNDARY-LAYER STABILITY PROGRAM

This appendix provides a complete description of the computer program that was used to obtain the analytic results presented in Section II. Included are definitions of symbols, flow charts, and important useful instructions. The material is presented in six sections as follows:

A-1 PHYSICAL AND NUMERICAL CONSTANTS

Symbol			
Math	Fortran	Definition	Units
C_p	CP	Specific heat at constant pressure	ft^2/sec^2 - °R
N_{Re}	REYN	Reynolds number	none
R	GR	Gas constant	ft^2/sec^2 - °R
T_R	TR	Arbitrary reference temperature (see μ_R)	°R
α	ALPHA	$2\pi/\lambda$	1/ft
γ	GAMMA	Ratio of specific heats	none
δ^*	DELTAS	Boundary layer displacement thickness	ft
Δy	DY	Value of y increment	ft
Δx	DX	Value of x increment	ft
λ	QLAMDA	Perturbation wavelength	ft
μ_R	XMUR	Reference viscosity coefficient corresponding to T_R $\mu = \mu_R \left(\frac{T}{T_R}\right)^{3/2} \left(\frac{T_R + 198.6}{T + 198.6}\right)$	lb-sec/ft^2
π	PI	3.14159...	none

A-2 PHYSICAL AND PROGRAM VARIABLES

Symbol			
Math	Fortran	Definition	Units
H	HT	Steady-state enthalpy	ft^2/sec^2
H'	HTP	Perturbation enthalpy	ft^2/sec^2
$\hat{H}'$	HTPA	Average of H'	ft^2/sec^2
$\partial H'/\partial x$	HTPX	Perturbation enthalpy 1st x-deriv.	ft/sec^2
$\partial^2 H'/\partial x^2$	HTPXX	Perturbation enthalpy 2nd x-deriv.	$1/sec^2$
$\partial H/\partial y$	HTY	Steady-state enthalpy 1st y-deriv.	ft/sec^2
$\partial^2 H/\partial y^2$	HTYY	Steady-state enthalpy 2nd y-deriv.	$1/sec^2$
H_∞	H8	Free-stream enthalpy (steady state)	ft^2/sec^2
$\partial H'/\partial t$	DHPDT	Perturbation enthalpy time derivative (partial)	ft^2/sec^3
$\frac{(N_{Re})_{new}}{(N_{Re})_{previous}}$	REEYN	Ratio of Reynolds numbers	none
P	P	Steady-state pressure	lbs/ft^2
P'	PP	Perturbation pressure	lbs/ft^2
$\hat{P}'$	PPA	Average of P'	lbs/ft^2
$\partial P'/\partial x$	PPX	1st x-deriv. of P'	lbs/ft^3
$(P'_L)^2 + (P'_R)^2$	PPSQ	P' amplitude	lbs^2/ft^4
T	T	Steady-state temperature	°R
T'	TP	Perturbation temperature	°R
$\hat{T}'$	TPA	Average perturbation temperature (Eq. 2-52)	°R
$\bar{u}$	U	Steady-state x-velocity	ft/sec
u'	UP	Perturbation x-velocity	ft/sec
$\partial u'/\partial t$	DUPDT	Time derivative of u' (partial)	ft/sec^2
u'_{ave}	UPA	Ave. of perturbation x-velocity	ft/sec
u'_L	UPLT	Left value of u' (at x = 0)	ft/sec
u'_R	UPRT	Right value of u' (at $x = \lambda/4$)	ft/sec
$\partial u'/\partial x$	UPX	Perturbation vel. 1st x-deriv.	1/sec
$\partial^2 u'/\partial x^2$	UPXX	Perturbation vel. 2nd x-deriv.	1/sec - ft

$\partial\bar{u}/\partial y$	UY	Steady-state 1st y-deriv. of $\bar{u}$	1/sec
$\partial\bar{u}/\partial y^2$	UYY	Steady-state 2nd y-deriv. of $\bar{u}$	1/sec - ft
$\partial^2 u'/\partial x \partial y$	UPXDY	Mixed partials of u'	1/sec - ft
$(u'_L)^2 + (u'_R)^2$	UPSQ	Sum of squares of u'	ft^2/sec^2
$\|u'\|$	UPSQRT	Square root of UPSQ	ft/sec
$\|u'\|_{max}$	UMAX	Maximum value of UPSQRT	ft/sec
u_∞	U8	Free-stream velocity (steady state)	ft/sec
$\bar{v}$	V	Steady-state y-velocity	ft/sec
v'	VP	Perturbation y-velocity	ft/sec
v'_{ave}	VPA	Average of v'	ft/sec
$\partial v'/\partial t$	DVPDT	Time deriv. of v' (partial)	ft/sec^2
$\partial v'/\partial x$	VPX	1st x-deriv. of v'	1/sec
$\partial^2 v'/\partial x^2$	VPXX	2nd x-deriv. of v'	1/sec - ft
$\partial^2 v'/\partial x \partial y$	VPXDY	Mixed partials of v'	1/sec - ft
$(v'_L)^2 + (v'_R)^2$	VPSQ	Sum of squares of v'	ft^2/sec^2
x	X	Abscissa in x-y plane	ft
y	Y	Ordinate in x-y plane	ft
μ	XMU	Steady-state viscosity	lbs - sec/ft^2
μ'	XMUP	Perturbation viscosity	lbs - sec/ft^2
$\hat{\mu}'$	XMUPA	Ave. of perturbation viscosity	lbs - sec/ft^2
$\partial\mu/\partial y$	XMUY	Steady-state viscosity 1st y-deriv.	lbs - sec/ft^3
ρ	RHO	Steady-state density	$slugs/ft^3$
ρ'	RHPO	Perturbation density	$slugs/ft^3$
$\hat{\rho}'$	RHOPA	Ave. of perturbation density	$slugs/ft^3$
$\partial\rho/\partial y$	RHOY	Steady-state density 1st y-deriv.	$slugs/ft^4$
$\partial\rho'/\partial x$	RHOPX	1st x-deriv. of perturbation density	$slugs/ft^4$
$\partial\rho'/\partial t$	DRPDT	Time deriv. of ρ' (partial)	$slugs/ft^3$ - sec
ω'	WP	Acoustical energy density	slugs/ft - sec^2 = lbs/ft^2

Fortran	Definition
MIL	Lower "I" index limit (x)
MIR	Upper "I" index limit (x)
MJW	Lower "J" index limit (y)
MJF	Upper "J" index limit (y)
MJK	1st limit for printout (upper)
MJKK	2nd limit for printout (lower)
NPLOT	No. of points to be plotted
MJ8	Appropriate "J" value corresponding to outer boundary
MJ9	MJ8 + 1
MPUT	1st value of y for 2-pt input
MSTART	MPUT + 3
MAXY	Maximum y value in program
NIT	Number of iterations to be run
LPLT	(See input form)
LBDY	(See input form)
LTP	Not used at present
MDECAY	Value of y from which decaying takes place
LDECAY	Iteration period between smoothing
KRP	(See input form)
KSAVE	(See input form)
NTAPE	Tape number unit on which output is to be stored
KARR	Word string for plot annotation
WORDS	Word string for title description
ITER	Number of iterations completed

A-3 BOUNDARY-LAYER STABILITY PROGRAM FLOW CHART

The boundary-layer stability program flow chart is presented in Figures A-1 through A-3. The main program is given in A-1; subroutines are given in A-1 and A-3.

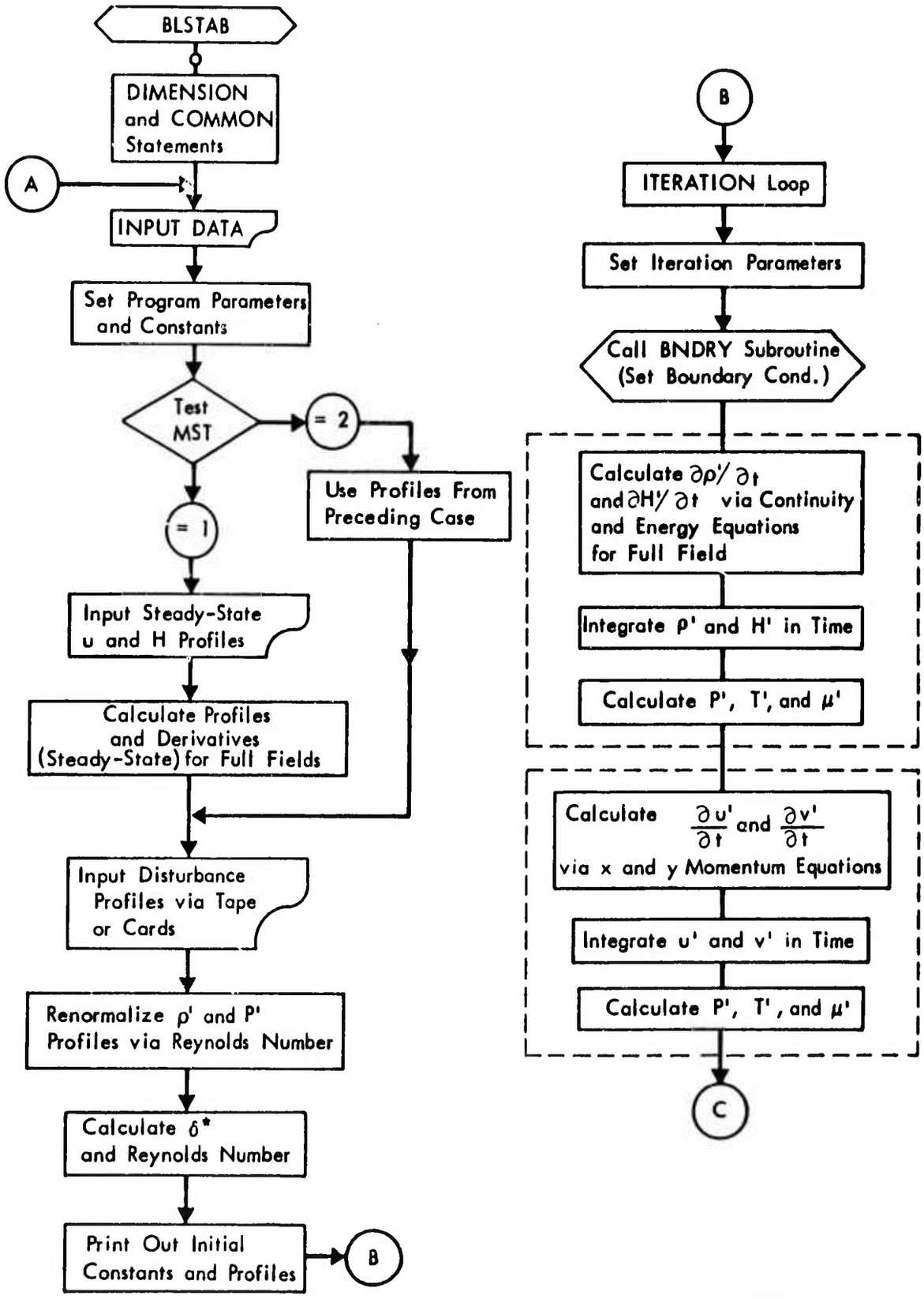

Figure A-1: BOUNDARY-LAYER STABILITY PROGRAM FLOW CHART

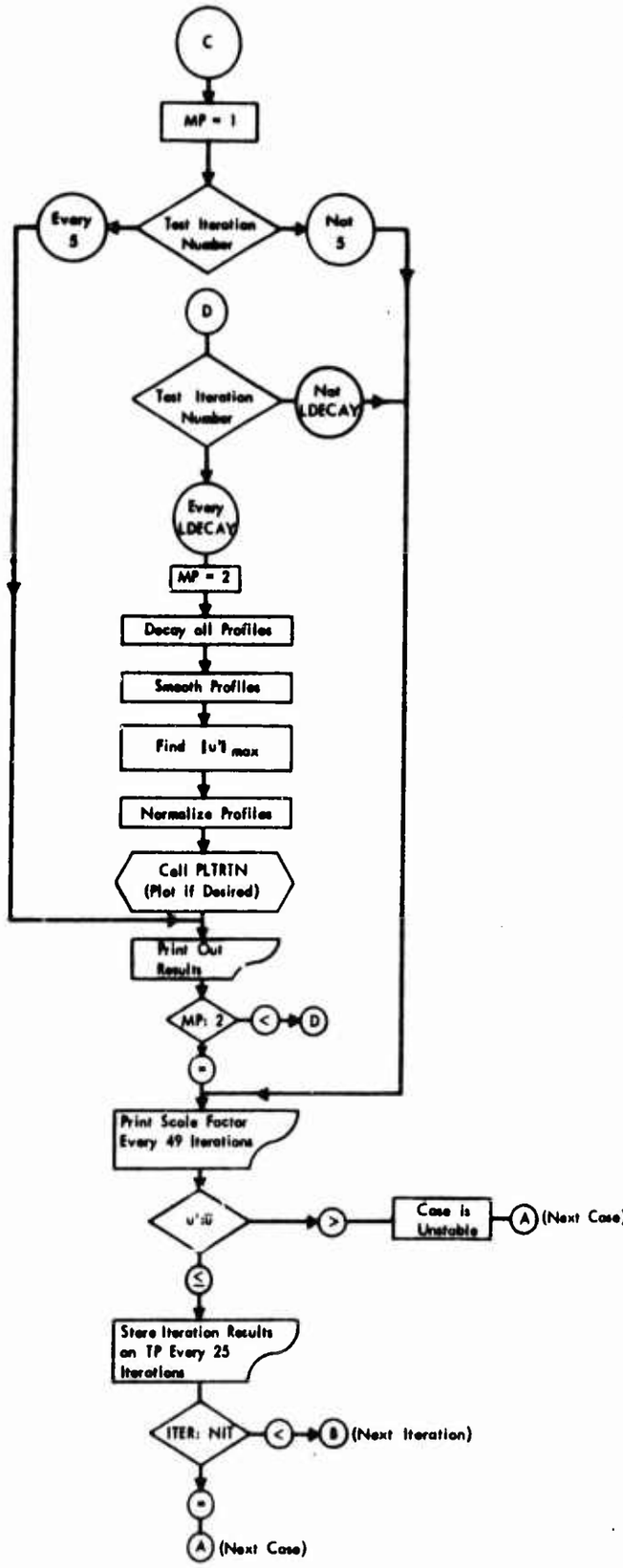

Figure A-1: BOUNDARY LAYER STABILITY PROGRAM FLOW CHART (Continued)

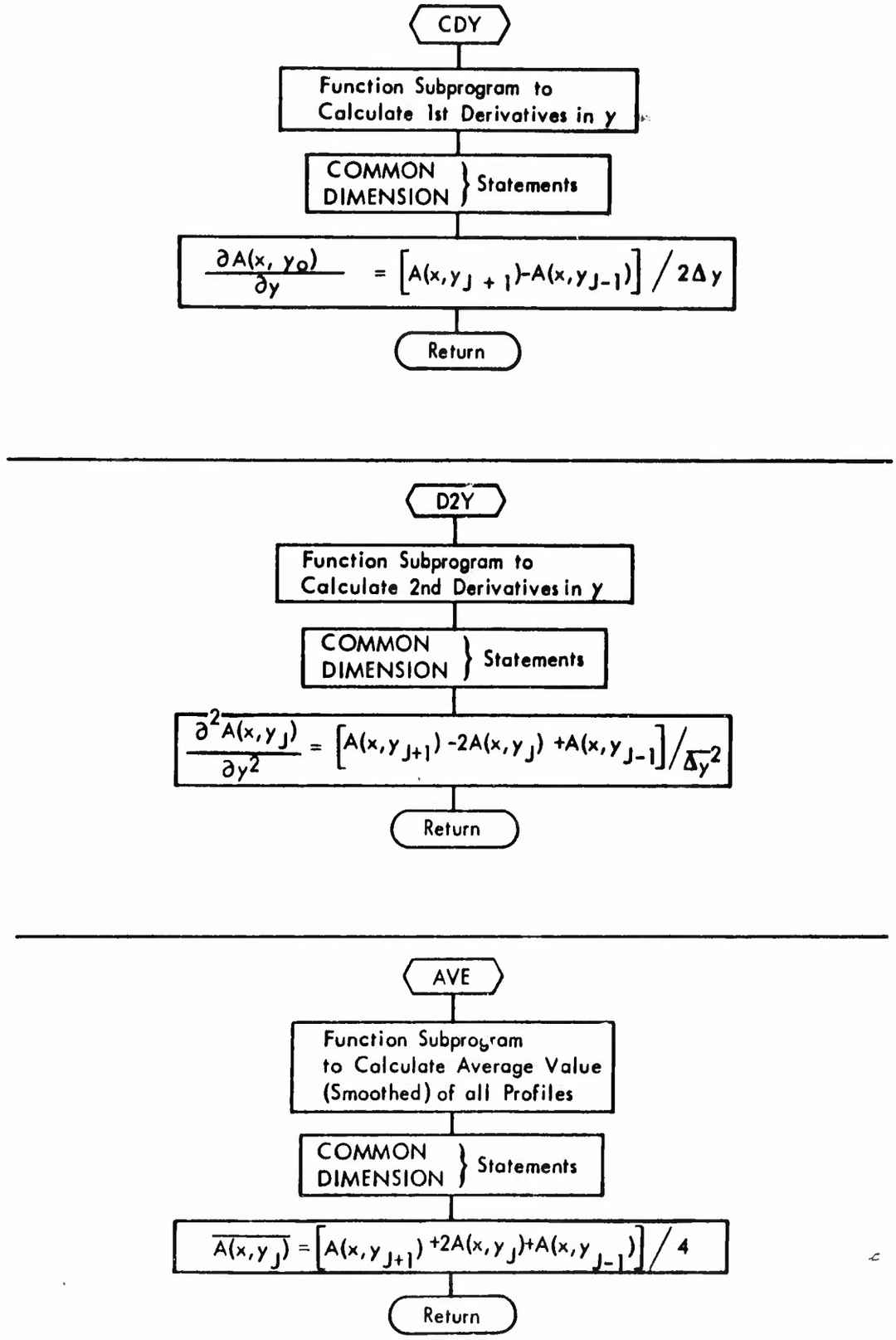

Figure A-2: BOUNDARY LAYER STABILITY PROGRAM FUNCTION SUBPROGRAMS

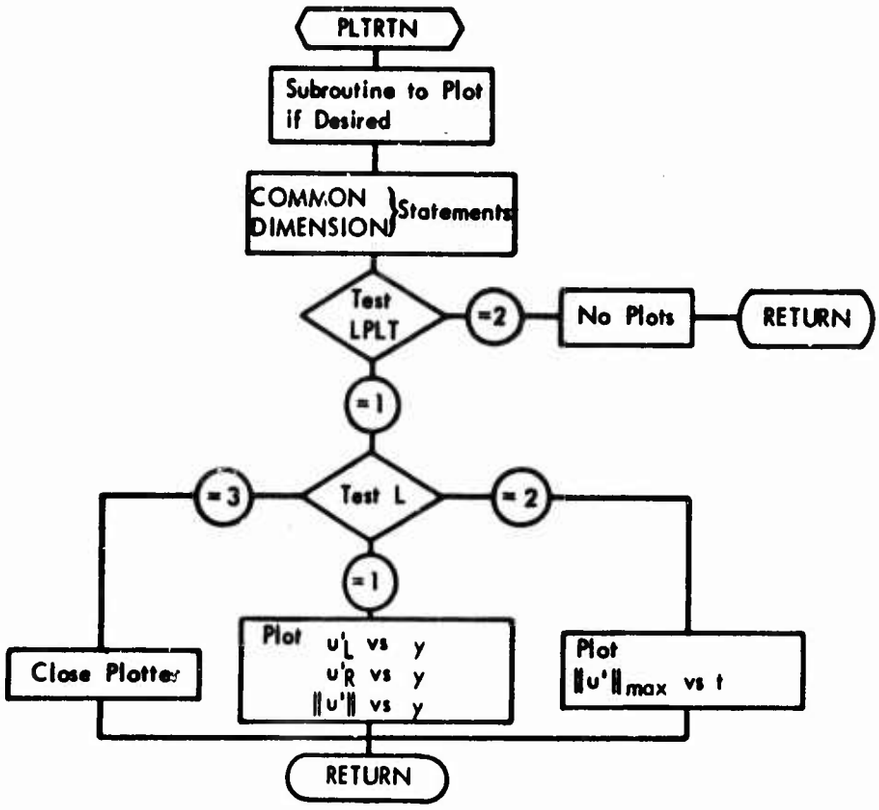

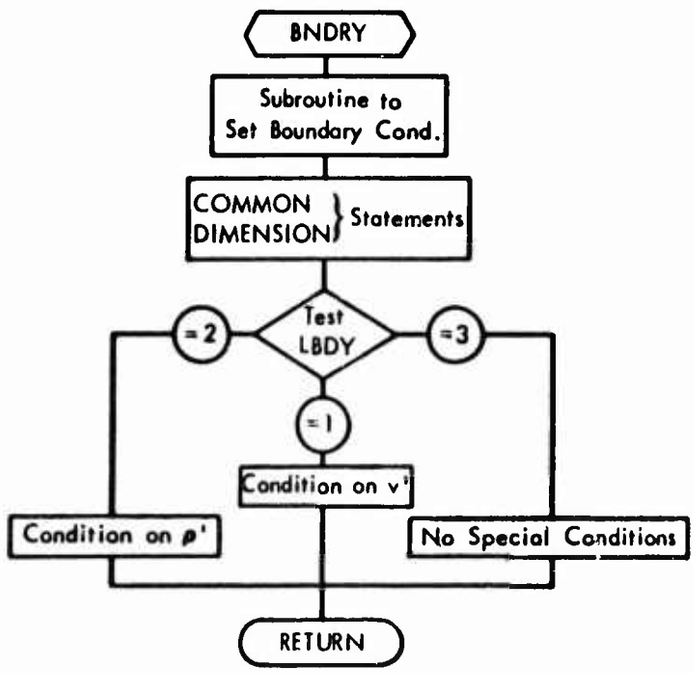

Figure A-3: BOUNDARY LAYER STABILITY SUBROUTINE SUBPROGRAMS

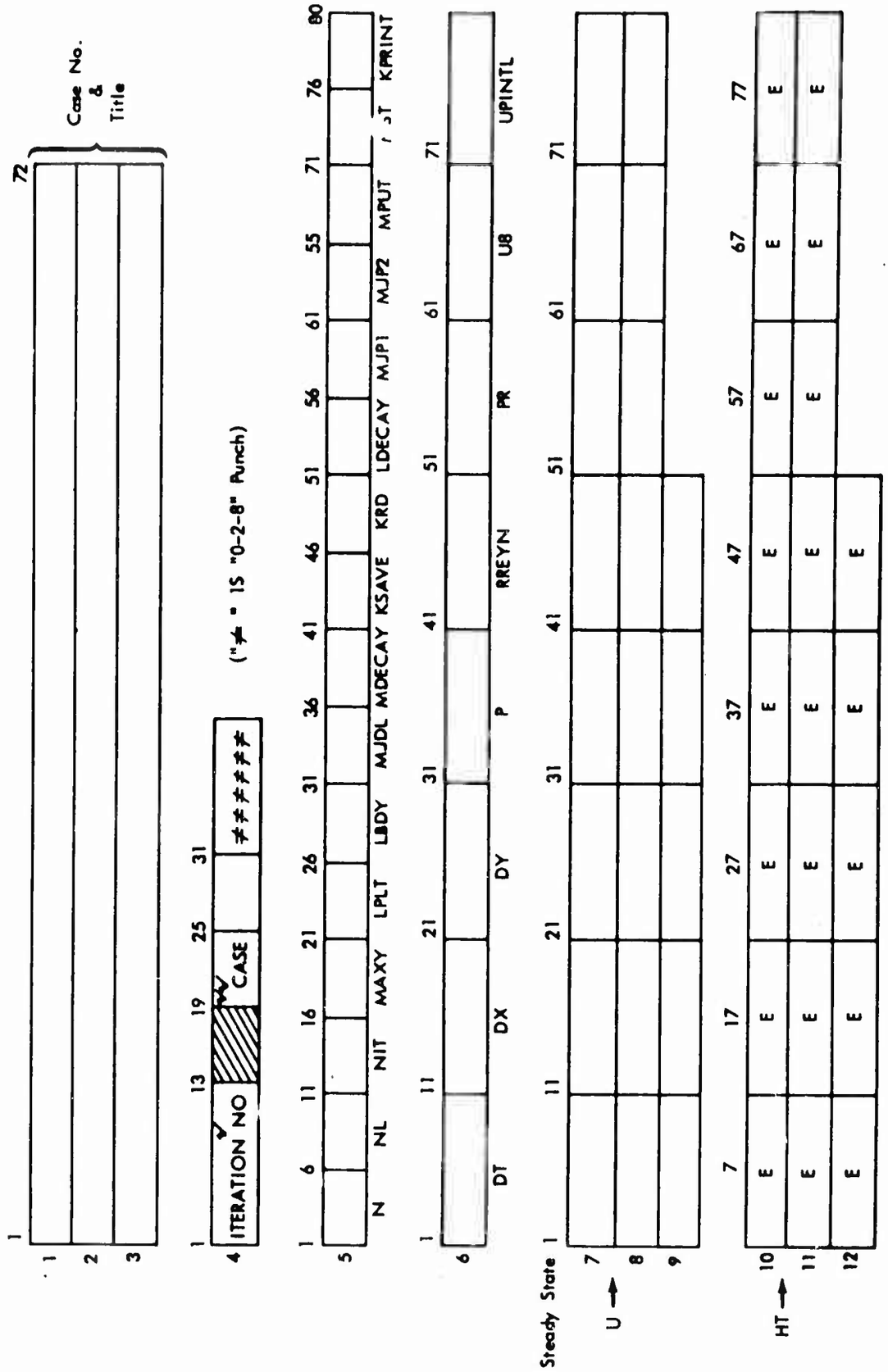

Figure A-4: BOUNDARY LAYER STABILITY PROGRAM — KEYPUNCH FORM

A-4 INPUT AND OUTPUT DESCRIPTION

Input Preparation

The input data deck may be coded using the keypunch form included with this appendix (Figure A-4). Explanation of the input deck follows:

Cards 1, 2, 3
Format (12A6)
WORDS

Alphameric characters used for case designation and description. These three lines of input will be printed out along with the initial constants.

Card 4
Format (12A6)
KARR

This line of alphameric characters will be used to annotate the plots with the case number and iteration number. Insert case number in columns 25 to 30. This card must be included in the data deck whether plots are desired or not.

Card 5
Format (16I5)

All values must be right adjusted in each 5-column field.

- N - Number of x-values (usually two)
- NL - Number of y-positions stored on input tape, if a tape is used for the initial disturbance profile.
- NIT - Number of iterations desired.
- MAXY - Value of maximum y for case (194 is upper limit).
- LPLT - LPLT = 1 if plots desired;
  LPLT = 2 if no plots desired.
- LBDY - LBDY = 1 if v' boundary condition desired (ref: BNDRY);
  LBDY = 2 if ρ' boundary condition desired;
  LBDY = 3 if no special boundary conditions desired.
- MJDL - Number of input steady-state velocity (or enthalpy) values.
- MDECAY - y_0 value from which decaying begins.
- KSAVE - KSAVE = 1 if results are to be stored on tape;
  KSAVE = 2 if results are not to be stored on tape.
- KRD - KRD = 1 if disturbance profiles are tape input;
  KRD = 2 if disturbance profile is two-point input.
- LDECAY - Set equal to iteration period for which decaying is to occur.
- MJP1 - Printout profiles are generated by two distinct WRITE statements. MJP1 is upper y-limit for first printout statement.

MJP2 - MJP2 is lower y-limit for second printout statement. If all y-stations are to be printed out, set MJP2 = MJP1+1.

MPUT - Set equal to the first y-value for which the first of the two-point inputs occurs.

MST - MST = 1 if the steady-state u' and H profiles are to be read in;
MST = 2 if the steady-state profiles from the previous case are to be used.

KPRINT - KPRINT = 1 if other cases follow on same run;
KPRINT = 2 if no cases follow.

Card 6
Format (8F10.0)

DT - Value of time increment.

DX - Value of x increment.

DY - Value of y increment.

P - Value of free-stream pressure.

RREYN - If the input profile was generated by a previous case, set RREYN = $(REYN)_{new}$ /$(REYN)_{previous}$

If input profile is generated by this case, set RREYN = 1.0.

PR - Value of Prandtl number.

U8 - Value of free-stream x-velocity.

UPINTL - Value of initial disturbance profile (2 points).

Cards 7, 8, 9
Format (8F10.0) Values of steady-state velocity profile from y = 0 to y = free-stream value. Number of input values should correspond to the value of MJDL.

NOTE: If MST = 2, do not submit cards 7, 8, 9.

Cards 10, 11, 12
Format (8E10.4) Values of steady-state enthalpy profile from y = 0 to y = free-stream value. Number of input values should correspond to the value of MJDL.

NOTE: If MST = 2, do not submit cards 10, 11, 12.

Output

The printout consists of a three-line description of the case, a list of the initial free-stream inputs, the input and calculated steady-state profiles, and the initial disturbance profiles.

Every five iterations, the iteration number and computed time are printed with the values of the disturbance profiles.

When decaying, smoothing, and normalizing occurs, the disturbance profiles are printed out twice, once before and once after reinitialization occurs.

Also printed out is the scale factor:

$$\text{SCALE} = (\text{SCALE}) * \left(\|u'\|\right)_{\max.}$$

The Fortran Variable Names are used as profile column headings.

A-5 PROGRAM USAGE

The boundary-layer stability program consists of one Fortran deck with the appropriate control cards and data deck. The program deck contains the main program, BLSTAB, two subroutine subprograms, PLTRTN and BNDRY, and three function subprograms, CDY, D2Y, and AVE.

The program may also be stored as relocatable on a PCF tape. This should be mounted on Physical Unit F.

If the initial disturbance profile is read in from tape, this input tape should be mounted on Physical Unit E.

If output tapes are desired, up to four may be saved, beginning with Unit A, B, C, D.

The CDY subprogram is used to calculate the first y-derivative using the three-point central-difference formula:

$$\frac{\partial A(x, y_0)}{\partial y} = \left[A(x, y_{j+1}) - A(x, y_{j-1})\right] \Big/ (2\Delta y)$$

The D2Y subprogram is used to calculate the second y-derivative, using the three-point central-difference formula:

$$\frac{\partial^2 A(x, y_j)}{\partial y^2} = \left[A(x, y_{j+1}) - 2\,A(x, y_j) + A(x, y_{j-1})\right] \Big/ \overline{\Delta y}^2$$

The AVE subprogram is used to smooth the disturbance profiles, using the average formula:

$$\overline{A(x, y_j)} = \left[A(x, y_{j+1}) + 2\,A(x, y_j) + A(x, y_{j-1})\right]/4$$

The BNDRY subroutine is used to fix the upper and lower boundary conditions for each iteration. At present, three options exist within this subroutine; the particular one chosen is dependent on the input parameter LBDY.

If LBDY = 1, then

$$v'(y_{max}+1) = v'(y_{max})$$

If LBDY = 2, then

$$\rho'(x,0) = \left[4\,P'(x,1) - P'(x,2)\right]/\left[5148\,T(x,1)\right]$$

If LBDY = 3, then all disturbance values remain at zero for $y = 0$, and $y = y_{max}+1$.

The PLTRTN subroutine is used to plot the results of the u' profile calculations. Based on the MACRO-PLOT system, this routine will cause Tally plots to be generated, providing that the input parameter LPLT is set to 1, and that the run-request card indicates a scratch tape as well as the statement "PLOT-MACROS".

At present this routine will periodically (every "LDECAY" iterations, with LDECAY an input parameter) plot the u' profile vs. y, and the $\|u'\|$ profile vs. y.

At the completion of each case, the maximum value of $\|u'\|$ based on the previous plots, will be plotted against time.

Estimated Run Time and Printout

On the 1107 computer, program execution will be about 10 minutes for a 600-iteration case without plotting. Plotting will add from 5 to 10 minutes to the execution time.

On the 1108, execution time will be from one-third to one-half that of the 1107.

A 600-iteration case will generate about 150 pages of output.

Control Cards

The following control cards are necessary when the boundary-layer stability program is used with the Boeing SRU system:

Run Request Card for the 1107 or 1108.

Run card

Tape ASG cards

CUR control cards if PCF tape is read in

FOR card for main program and subprograms

CUR cards if program is to be stored on tape

XQT card

FIN card

A-6 BOUNDARY-LAYER STABILITY PROGRAM LISTING

The complete Fortran deck listing of the boundary-layer stability program is given on the following pages.

```
- XQT CUR                                                                1417 001
  INALT 40                                                               1417 002
  INALT 21                                                               1417 003
- MLIB PLTRTN                                                            1417 004
      SUBROUTINE PLTRTN(L)                                               1417 005
      DIMENSION UPLT(200), UPRT(200), UPSQRT(200), Y(200), KARR(6),      1417 006
     1PTIME2(90), UMAX(100)                                              1417 007
      COMMON/DRAW/KARR,NPLOT,Y,UPSQRT,UPLT,UPRT,IPP2,PTIME2,             1417 008
     1UMAX,LTP                                                           1417 009
      GO TO (50 ,400),LTP                                                1417 010
   50 CONTINUE                                                           1417 011
      GO TO (100,200,300),L                                              1417 012
  100 CONTINUE                                                           1417 013
      CURVE SIZE/NPLOT,NPLOT,NPLOT                                       1417 014
      PLOT ON TALLY/LINEAR/Y,UPSQRT,Y,UPLT,Y,UPRT                        1417 015
      TITLE/UP RESULTANT VS.Y., UP LEFT VS. Y, UPRIGHT VS. Y.            1417 016
      TITLE ARRAY/KARR                                                   1417 017
      RETURN                                                             1417 018
  200 CONTINUE                                                           1417 019
      CURVE SIZE/IPP2                                                    1417 020
      PLOT ON TALLY/LINEAR/PTIME2,UMAX                                   1417 021
      TITLE/                                                             1417 022
     1UP MAX. VS. TIME                                                   1417 023
      RETURN                                                             1417 024
  300 CONTINUE                                                           1417 025
      CLOSE TALLY PLOTTER                                                1417 026
  400 CONTINUE                                                           1417 027
      RETUR                                                              1417 028
      END                                                                1417 029
- FOR,* PL                                                               1417 030
```

```
- FOR BNDRY                                                          1417 031
      SUBROUTINE BNDRY(L)                                           1417 032
C SUBROUTINE TO CALCULATE SPECIAL BOUNDARY CONDITIONS.              1417 033
      DIMENSION UP(2,200), VP(2,200), RHOP(2,200), HTP(2,200),      1417 034
     1PP(2,200),TP(2,200), T(2,200), XMUP(2,200)                    1417 035
      COMMON/BN/UP,VP,RHOP,HTP,PP,TP,T,XMUP,MJW,MJF,MIL,MIR         1417 036
      GO TO (100,200,900),L                                         1417 037
  100 CONTINUE                                                      1417 038
C BOUNDARY CONDITION ON VP.                                         1417 039
      VP(MIL,MJF+1)=VP(MIL,MJF)                                     1417 040
      VP(MIR,MJF+1)=VP(MIR,MJF)                                     1417 041
      RETURN                                                        1417 042
  200 CONTINUE                                                      1417 043
C BOUNDARY CONDITION ON RHOP.                                       1417 044
      DO 210 I=MIL,MIR                                              1417 045
      RHOP(I,MJW-1) = (4.*PP(I,MJW)-PP(I,MJW+1))/(5148.*T(I,MJW))   1417 046
  210 CONTINUE                                                      1417 047
      RETURN                                                        1417 048
  900 CONTINUE                                                      1417 049
C *** SORRY ***   NO SPECIAL BOUNDARY CONDITIONS THIS TIME.         1417 050
      RETURN                                                        1417 051
      END                                                           1417 052
```

```
- FOR CDY                                                          1417 053
      FUNCTION CDY(A,I,J,D)                                        1417 054
      DIMENSION A(2,200)                                           1417 055
      COMMON/SAM/MJW,MJ5,MJ6,MJF,KQQ                               1417 056
    6 CONTINUE                                                     1417 057
    7 CDY = (A(I,J+1) - A(I,J-1))/(2.*D)                           1417 058
  390 CONTINUE                                                     1417 059
      RETURN                                                       1417 060
       END                                                         1417 061

- FOR D2Y                                                          1417 062
      FUNCTION D2Y(A,I,J,D)                                        1417 063
      DIMENSION A(2,200)                                           1417 064
      COMMON/SAM/MJW,MJ5,MJ6,MJF,KQQ                               1417 065
    6 CONTINUE                                                     1417 066
      D2Y = (A(I,J+1)-2.*A(I,J)+A(I,J-1))/D **2                    1417 067
    7 CONTINUE                                                     1417 068
      RETURN                                                       1417 069
       END                                                         1417 070

- FOR AVE                                                          1417 071
      FUNCTION AVE(Q,I,J)                                          1417 072
      COMMON/PETE/MJF2                                             1417 073
      DIMENSION Q(2,200)                                           1417 074
      AVE = (Q(I,J+1)+Q(I,J-1)  + 2.*Q(I,J))/4.                    1417 075
    8 CONTINUE                                                     1417 076
      RETURN                                                       1417 077
      END                                                          1417 078
```

```
- FOR B) STAR                                                          1417 079
C BOUNDARY LAYER TRANSITION                                           1417 080
C      RESEQUENCED N.S. PERTURBATION EQUATIONS                        1417 081
C HYPERSONIC FLOW FIELD.                                              1417 082
C RECTANGULAR ARRAY                                                   1417 083
C ******      BLASIUS PROFILE INPUT FOR X-VELOCITY      ******        1417 084
C BLASIUS PROFILE WITH NUMERICAL DERIVATIVES                          1417 085
C 3-POINT DERIVATIVE ROUTINES                                         1417 086
      DIMENSION KARR(6)                                               1417 087
      DIMENSION WORDS(36)                                             1417 088
      DIMENSION TPA(2,200), XMUPA(2,200), U(2,200), V(2,200), HT(2,200),1417 089
     1UP(2,200), VP(2,200), RHOP(2,200), HTP(2,200), PP(2,200), X(2),  1417 090
     2Y(200),DRPDT(2,200), DUPDT(2,200), DVPDT(2,200), DHPDT(2,200),   1417 091
     3UPA(2,200), VPA(2,200), RHOPA(2,200), HTPA(2,200), PPA(2,200),   1417 092
     4UPSQ(200), PPSQ(200), WP(200), UPSQRT(200), UPX(2,200), VPSQ(200),1417 093
     5UPXX(2,200), VPX(2,200), TP(2,200), VPXX(2,200), RHOPX(2,200),   1417 094
     6PPX(2,200), HTPX(2,200), HTPXX(2,200), T(2,200), RHO(2,200),XMU(2,1417 095
     62001, XMUP(2,200),UY(2,200),UYY(2,200),HTY(2,200),HTYY(2,200),   1417 096
     7RHOY(2,200),XMUY(2,200),VPXDY(2,200), UPXDY(2,200), XMUPX(2,200), 1417 097
     8UPLT(200), UPRT(200),UMAX(100), PTIME2(90), SC(100)              1417 098
      COMMON/PETF/MJF2                                                1417 099
      COMMON/SAM/MJWS,MJ5,MJ6,MJFS,KQQ                                1417 100
      COMMON/BN/UP,VP,RHOP,HTP,PP,TP,T,XMUP,MJW,MJF,MIL,              1417 101
     1MIR,MJWI,ALPHA,DY,U,DELTAS,X,RHO,UY,LTP                         1417 102
      COMMON/DRAW/KARR,NPLOT,Y,UPSQRT,UPLT,UPRT,IPP2,PTIME2,UMAX,LPLT 1417 103
      NTAPE=0                                                         1417 104
      DATA KRD,MIL,MIR,MJW,SCALE/1,1,2,4,1.0/,MIRM,PI,                1417 105
     1XMUR,GR,CP,TR/1.3,1416,3.7452E-7,1716.5,6006.0,520./            1417 106
  100 CONTINUE                                                        1417 107
      READ(5,9) (WORDS(I),I=1,36)                                     1417 108
      READ(5,9) (KARR(I),I=1,6)                                       1417 109
      READ(5,11) N,NL,NIT,MAXY,LPLT,LBDY,MJDL,MDECAY,KSAVE,KRP,LDECAY,1417 110
     1MJP1,MJP2,MPUT,MST,KPRINT                                       1417 111
      READ(5,10) DT,DX,DY,P,RREYN,PR,U8,UPINTL                        1417 112
      KK=1                                                            1417 113
      MJW1 = MJW-1                                                    1417 114
      MJ8=MJW1+(MJDL-1)                                               1417 115
      MJ9=MJ8+1                                                       1417 116
C     INITIAL CONSTANTS                                               1417 117
      MJF=MAXY+3                                                      1417 118
      MJWS=MJW                                                        1417 119
      MSTART = MPUT+3                                                 1417 120
      MJFS=MJF                                                        1417 121
      MJW14=MDECAY+3                                                  1417 122
      NYP2=MAXY+6                                                     1417 123
      MJK=MJP1+3                                                      1417 124
      MJKK=MJP2+3                                                     1417 125
      MJF1=MJF+1                                                      1417 126
      MJN1=MJK+1                                                      1417 127
      MJN2=MJKK-1                                                     1417 128
      MJ20=MJW+20                                                     1417 129
      MJF2 = MJF-1                                                    1417 130
      ITERQ = 0.                                                      1417 131
```

```
      MJF4 = MJF-3                                                      1417 132
      MJ5=MJW+1                                                         1417 133
      MJ6=MJW+2                                                         1417 134
      MJ7=MJW+3                                                         1417 135
      MJF1=MJF+1                                                        1417 136
      GAMMA = CP/(CP-GR)                                                1417 137
      GAMMA1 = GAMMA-1.                                                 1417 138
      GAMMA2=GAMMA1/GAMMA                                               1417 139
      DT SAVE=DT                                                        1417 140
      QLAMDA = 4.*DX                                                    1417 141
      ALPHA = 2.*PI/QLAMDA                                              1417 142
      ALPHA2=ALPHA**2                                                   1417 143
      NITS=NIT                                                          1417 144
C*****************************************************************************1417 145
      GO TO (102,104),MST                                               1417 146
  102 CONTINUE                                                          1417 147
C INITIAL STEADY-STATE FIELD VALUES                                     1417 148
      READ(5,10) (U(MIL,J),J=MJW1,MJ8)                                  1417 149
      READ(5,43) (HT(MIL,J), J=MJW1,MJ8)                                1417 150
      DO 110 J=MJ9,NYP2                                                 1417 151
      U(MIL,J) = U(MIL,MJ8)                                             1417 152
      HT(MIL,J) = HT(MIL,MJ8)                                           1417 153
  110 CONTINUE                                                          1417 154
      DO 120 J=MJW1,NYP2                                                1417 155
      U(MIR,J) = U(MIL,J)                                               1417 156
      HT(MIR,J) = HT(MIL,J)                                             1417 157
  120 CONTINUE                                                          1417 158
      DO 130 I=1,N                                                      1417 159
      DO 130 J=1,NYP2                                                   1417 160
      V(I,J) = 0.0                                                      1417 161
      T(I,J) = (HT(I,J)-U(I,J)**2/2.)/CP                                1417 162
      XMU(I,J) = XMUR*(TR+216.)/(T(I,J)+216.)*(T(I,J)/TR)**1.5          1417 163
  130 CONTINUE                                                          1417 164
      U8 = U(MIL,MJ9)                                                   1417 165
      H8 = HT(MIL,MJ9)                                                  1417 166
C                                                                       1417 167
      DO 138 I=MIL,MIR                                                  1417 168
      DO 138 J=MJW,MJF                                                  1417 169
      IF(U(I,J)-U8) 135,136,136                                         1417 170
  135 CONTINUE                                                          1417 171
      KQQ=1                                                             1417 172
      UY(I,J) = CDY(U,I,J,DY)                                           1417 173
      UYY(I,J) = D2Y(U,I,J,DY)                                          1417 174
      HTY(I,J) = CDY(HT,I,J,DY)                                         1417 175
      HTYY(I,J) = D2Y(HT,I,J,DY)                                        1417 176
      XMUY(I,J) = CDY(XMU,I,J,DY)                                       1417 177
      GO TO 137                                                         1417 178
  136 CONTINUE                                                          1417 179
      UY(I,J) = 0.                                                      1417 180
      UYY(I,J) = 0.                                                     1417 181
      HTY(I,J) = 0.                                                     1417 182
      RHOY(I,J) = 0.                                                    1417 183
      XMUY(I,J) = 0.                                                    1417 184
      HTYY(I,J) = 0.                                                    1417 185
```

```
  137 CONTINUE                                                          1417 186
  138 CONTINUE                                                          1417 187
  139 CONTINUE                                                          1417 188
  104 CONTINUE                                                          1417 189
      NTAPE = NTAPE+1                                                   1417 190
      IF(NTAPE-5)205,200,200                                            1417 191
  200 CONTINUE                                                          1417 192
      CALL EXIT                                                         1417 193
  205 CONTINUE                                                          1417 194
C                                                                       1417 195
C DEFINE THE RECTANGLE.                                                 1417 196
      DO 140 I = 1,N                                                    1417 197
      X(I) = FLOAT(I-11)*DX                                             1417 198
  140 CONTINUE                                                          1417 199
C                                                                       1417 200
      DO 145 J = 1,NYP2                                                 1417 201
      Y(J) = FLOAT(J-3)*DY                                              1417 202
  145 CONTINUE                                                          1417 203
C                                                                       1417 204
C RE-INITIALIZE PERTURBATION VALUES TO ZERO                             1417 205
      DO 210 I=MIL,MIR                                                  1417 206
      DO 210 J=1,NYP2                                                   1417 207
      UP(I,J)=0.0                                                       1417 208
      VP(I,J)=0.0                                                       1417 209
      RHOP(I,J)=0.0                                                     1417 210
      HTP(I,J)=0.0                                                      1417 211
      PP(I,J)=0.0                                                       1417 212
      XMUP(I,J)=0.                                                      1417 213
      DRPDT(I,J)=0.                                                     1417 214
      DHPDT(I,J)=0.                                                     1417 215
      DUPDT(I,J)=0.                                                     1417 216
      DVPDT(I,J)=0.                                                     1417 217
  210 CONTINUE                                                          1417 218
C INITIALIZE INPUT PERTURBATION                                         1417 219
      GO TO (220,230),KRP                                               1417 220
  220 CONTINUE                                                          1417 221
      REWIND 15                                                         1417 222
      READ TAPE 15, ITER,NL,TIME, ((UP(I,J),VP(I,J),RHOP(I,J),         1417 223
     1PP(I,J),HTP(I,J),XMUP(I,J), TP(I,J),DHPDT(I,J),DRPDT(I,J),       1417 224
     2DUPDT(I,J),DVPDT(I,J),J=1,NL),I=MIL,MIR)                          1417 225
      REWIND 15                                                         1417 226
      MJF3=MJF+3                                                        1417 227
      DO 225 I=MIL,MIR                                                  1417 228
      DO 225 J=MJF1,MJF3                                                1417 229
      UP(I,J)  =0.                                                      1417 230
      VP(I,J)  =0.                                                      1417 231
      RHOP(I,J)=0.                                                      1417 232
      HTP(I,J) =0.                                                      1417 233
      PP(I,J)  =0.                                                      1417 234
      XMUP(I,J)=0.                                                      1417 235
      DRPDT(I,J)=0.                                                     1417 236
      DHPDT(I,J)=0.                                                     1417 237
      DUPDT(I,J)=0.                                                     1417 238
      DVPDT(I,J)=0.                                                     1417 239
```

```
  225 CONTINUE                                                          1417 240
      GO TO 235                                                         1417 241
  230 CONTINUE                                                          1417 242
      UP(MIL,MSTART)   = UPINTL                                         1417 243
      UP(MIL,MSTART+1) = UPINTL                                         1417 244
  235 CONTINUE                                                          1417 245
      ITER =0                                                           1417 246
      TIME = 0.0                                                        1417 247
      IPP=1                                                             1417 248
      IPP2 = 1                                                          1417 249
C RE-NORMALIZE RHP AND PP.                                              1417 250
      DO 300 I=MIL,MIR                                                  1417 251
      DO 300 J=MJW1,MJF                                                 1417 252
      RHOP(I,J) = RREYN*RHOP(I,J)                                       1417 253
      PP(I,J) = PREYN*PP(I,J)                                           1417 254
      RHO(I,J) = P/(GR*T(I,J))                                          1417 255
  300 CONTINUE                                                          1417 256
      I=MIL                                                             1417 257
      SUM5 = 0.                                                         1417 258
      DO 310 J=MJW1,MJ8                                                 1417 259
      SUM5=SUM5+( 1.-(RHO(I,J)*U(I,J)+RHO(I,J+1)*U(I,J+1)) /(2.*RHO(MIL,1417 260
     1MJ9)*U8))*DY                                                      1417 261
  310 CONTINUE                                                          1417 262
      KT6=1                                                             1417 263
      DELTAS = SUM5                                                     1417 264
      REYN = U8*RHO(MIL,MJF)*DELTAS/XMU(MIL,MJF)                        1417 265
C PRINT OUT THE INITIAL CONSTANTS.                                      1417 266
      WRITE (6,50)                                                      1417 267
      WRITE(6,53) (WORDS(I),I=1,36)                                     1417 268
      WRITE(6,52) RHO(MIL,MJF),REYN,T(MIL,MJF),P,XMU(MIL,MJF),QLAMDA,   1417 269
     1ALPHA,DX,DY,DT,PR                                                 1417 270
      WRITE(6,57) (X(I),I=MIL,MIR)                                      1417 271
      WRITE(6,58) (Y(J),(U(I,J),HT(I,J),T(I,J),RHO(I,J),XMU(I,J),I=MIL, 1417 272
     1MIR),Y(J),J=MJW1,MJ9,KRD)                                         1417 273
C PRINT OUT THE INITIAL INPUT PROFILE.                                  1417 274
      WRITE(6,40)ITER,TIME                                              1417 275
      WRITE(6,45) (X(I),I=MIL,MIR)                                      1417 276
      WRITE(6,42) (Y(J),(UP(I,J),VP(I,J),PP(I,J),I=MIL,MIR),            1417 277
     1Y(J),J=MJW1,MJK,KRD)                                              1417 278
      WRITE(6,42) (Y(J),(UP(I,J),VP(I,J),PP(I,J),I=MIL,MIR),            1417 279
     1Y(J),J=MJKK,MJF,KRD)                                              1417 280
  400 CONTINUE                                                          1417 281
      ITER=ITER+1                                                       1417 282
      TIME = TIME + DT                                                  1417 283
C INTERMEDIATE PRINT-CONTROL PARAMETERS.                                1417 284
      KT1 = MOD(ITER,LDECAY)                                            1417 285
      KT2 = MOD(KT1,5)                                                  1417 286
      KT3 = MOD(ITER,20)                                                1417 287
C                                                                       1417 288
      CALL BNDRY(LBDY)                                                  1417 289
      DO 410 J=MJW,MJF                                                  1417 290
C CALCULATE X-DERIVATIVES.                                              1417 291
      UPX(MIL,J) = +ALPHA*UP(MIR,J)                                     1417 292
      UPX(MIR,J) = -ALPHA*UP(MIL,J)                                     1417 293
```

```
      VPX(MIL,J) = +ALPHA*VP(MIR,J)                                     1417 294
      VPX(MIR,J) = -ALPHA*VP(MIL,J)                                     1417 295
      RHOPX(MIL,J) = +ALPHA*RHOP(MIR,J)                                 1417 296
      RHOPX(MIR,J) = -ALPHA*RHOP(MIL,J)                                 1417 297
      HTPX(MIL,J) = ALPHA*HTP(MIR,J)                                    1417 298
      HTPX(MIR,J) = -ALPHA*HTP(MIL,J)                                   1417 299
      XMUPX(MIL,J) = +ALPHA*XMUP(MIR,J)                                 1417 300
      XMUPX(MIR,J) = -ALPHA*XMUP(MIL,J)                                 1417 301
  410 CONTINUE                                                          1417 302
      DO 422 I=MIL,MIR                                                  1417 303
      DO 420 J=MJW,MJF                                                  1417 304
      RHOY(I,J) = CDY(RHO,I,J,DY)                                       1417 305
      UAUP      = U(I,J) + UP(I,J)                                      1417 306
      VAVP      = V(I,J) + VP(I,J)                                      1417 307
      ROAROP = RHO(I,J) + RHOP(I,J)                                     1417 308
      HTAHTP      = HT(I,J) + HTP(I,J)                                  1417 309
      PAPP = P + PP(I,J)                                                1417 310
      UPXX(I,J) = -ALPHA2*UP(I,J)                                       1417 311
      VPXX(I,J) = -ALPHA2*VP(I,J)                                       1417 312
      HTPXX(I,J) = -ALPHA2*HTP(I,J)                                     1417 313
      UPXDY(I,J) = CDY(UPX,I,J,DY)                                      1417 314
      VPXDY(I,J) = CDY(VPX,I,J,DY)                                      1417 315
C CONTINUITY EQUATION                                                   1417 316
C     ITERATE RHO                                                       1417 317
      EN1 = CDY(VP,I,J,DY)                                              1417 318
      CB1 = RHO(I,J)*UPX(I,J)                                           1417 319
      CB2 = U(I,J)*RHOPX(I,J)                                           1417 320
      CB3 = RHO(I,J)*EN1                                                1417 321
      CB4 = VP(I,J)*RHOY(I,J)                                           1417 322
      DRPDT(I,J) = -(CB1+CB2+CB3+CB4)                                   1417 323
C ENERGY EQUATION                                                       1417 324
      EN2 = GAMMA*P*DRPDT(I,J)/(ROAROP**2)                              1417 325
      EN3 = GAMMA1*U(I,J)*DUPDT(I,J)                                    1417 326
      EN4 = GAMMA*(U(I,J)*HTPX(I,J)+VP(I,J)*HTY(I,J))                   1417 327
      EN5 = XMU(I,J)*(HTPXX(I,J)+D2Y(HTP,I,J,DY))                       1417 328
      EN6 = XMUP(I,J)*HTYY(I,J)                                         1417 329
      EN7 = XMUY(I,J)*CDY(HTP,I,J,DY)+CDY(XMUP,I,J,DY)*HTY(I,J)         1417 330
      EN8 = (EN5+EN6+EN7)/PR                                            1417 331
      EN9 = XMU(I,J)*(.3333*U(I,J)*(UPXX(I,J)+VPXDY(I,J))+2.*VPX(I,J)*  1417 332
     1UY(I,J))                                                          1417 333
      EN10 = XMUY(I,J)*U(I,J)*VPX(I,J)                                  1417 334
      EN11 = XMU(I,J)*(U(I,J)*(D2Y(UP,I,J,DY)+UPXX(I,J))+UP(I,J)*       1417 335
     1UYY(I,J))                                                         1417 336
      EN13 = XMUP(I,J)*(U(I,J)*UYY(I,J)+UY(I,J)**2)                     1417 337
      EN12 =2.*XMU(I,J)*UY(I,J)*CDY(UP,I,J,DY)                          1417 338
      EN14 = XMUY(I,J)*(UP(I,J)*UY(I,J)+U(I,J)*CDY(UP,I,J,DY))          1417 339
      EN15 = CDY(XMUP,I,J,DY)*U(I,J)*UY(I,J)                            1417 340
      EN16 = (1.-1./PR)*(EN11+EN12+EN13+EN14+EN15)                      1417 341
      EN17 = (GAMMA/ROAROP)*(EN8+EN9+EN10+EN16)                         1417 342
      DHPDT(I,J) = EN2-EN3-EN4+EN17                                     1417 343
  420 CONTINUE                                                          1417 344
      DRPDT(I,MJW1) = -(RHO(I,MJW1)+RHOP(I,MJW1))*(VP(I,MJW)/DY-.375*   1417 345
     1(RHOP(I,MJW)-RHOP(I,MJW1))/XMU(I,MJW1))                           1417 346
  422 CONTINUE                                                          1417 347
```

```
      DO 432 I=MIL,MIR                                                  1417 348
      DO 430 J=MJW,MJF                                                  1417 349
C CALCULATE NEW PERTURBATION VALUES                                     1417 350
      RHOP(I,J) = RHOP(I,J) + DRPDT(I,J)*DT                             1417 351
      HTP(I,J) = HTP(I,J) + DHPDT(I,J)*DT                               1417 352
C AUXILIARY EQUATIONS                                                   1417 353
      PP(I,J) = GAMMA2*RHO(I,J)*(HTP(I,J)-(UP(I,J)**2+VP(I,J)**2)/2.   1417 354
     1-U(I,J)*UP(I,J)) + P*RHOP(I,J)/RHO(I,J)                           1417 355
      TP(I,J) = (HTP(I,J)-U(I,J)*UP(I,J))/CP                            1417 356
      XMUP(I,J) = TP(I,J)*XMU(I,J)*((.5*T(I,J)+316.)/(T(I,J)*(T(I,J)+   1417 357
     1216.)))                                                           1417 358
  430 CONTINUE                                                          1417 359
      RHOP(I,MJW-1) = RHOP(I,MJW-1) + DRPDT(I,MJW-1)*DT                 1417 360
      PP(I,MJW-1) = P*RHOP(I,MJW-1)/RHO(I,MJW-1)                        1417 361
  432 CONTINUE                                                          1417 362
C*********************************************************************1417 363
      DO 500 J=MJW,MJF                                                  1417 364
      UPX(MIL,J) = +ALPHA*UP(MIR,J)                                     1417 365
      UPX(MIR,J) = -ALPHA*UP(MIL,J)                                     1417 366
      VPX(MIL,J) = +ALPHA*VP(MIR,J)                                     1417 367
      VPX(MIR,J) = -ALPHA*VP(MIL,J)                                     1417 368
      PPX(MIL,J) = +ALPHA*PP(MIR,J)                                     1417 369
      PPX(MIR,J) = -ALPHA*PP(MIL,J)                                     1417 370
      XMUPX(MIL,J) = +ALPHA*XMUP(MIR,J)                                 1417 371
      XMUPX(MIR,J) = -ALPHA*XMUP(MIL,J)                                 1417 372
  500 CONTINUE                                                          1417 373
      DO 512 I=MIL,MIR                                                  1417 374
      DO 510 J=MJW,MJF                                                  1417 375
      UAUP       = U(I,J) + UP(I,J)                                     1417 376
      VAVP       = V(I,J) + VP(I,J)                                     1417 377
      ROAROP = RHO(I,J) + RHOP(I,J)                                     1417 378
      UPXX(I,J) = -ALPHA2*UP(I,J)                                       1417 379
      VPXX(I,J) = -ALPHA2*VP(I,J)                                       1417 380
      UPXDY(I,J) = CDY(UPX,I,J,DY)                                      1417 381
      VPXDY(I,J) = CDY(VPX,I,J,DY)                                      1417 382
      XM1 = U(I,J)*UPX(I,J)                                             1417 383
      XM2 = VP(I,J)*UY(I,J)                                             1417 384
      XM3 = PPX(I,J)                                                    1417 385
      XM4 = XMU(I,J)*(1.333*UPXX(I,J) + D2Y(UP,I,J,DY) + VPXDY(I,J)/3.) 1417 386
      XM5 = XMUP(I,J)*UYY(I,J)                                          1417 387
      XM6 = XMUY(I,J)*(VPX(I,J)+CDY(UP,I,J,DY))                         1417 388
      XM7 = CDY(XMUP,I,J,DY)*UY(I,J)                                    1417 389
      DUPDT(I,J) = -XM1-XM2 + (-XM3+XM4+XM5+XM6+XM7)/ROAROP             1417 390
      YM1 = U(I,J)*VPX(I,J)                                             1417 391
      YM2=0.                                                            1417 392
      YM3 = CDY(PP,I,J,DY)                                              1417 393
      YM4 = XMU(I,J)*(1.333*D2Y(VP,I,J,DY) + .333*UPXDY(I,J) + VPXX(I,J)1417 394
     1)                                                                 1417 395
      YM5 = XMUPX(I,J)*UY(I,J)                                          1417 396
      YM6 = XMUY(I,J)*(1.333*CDY(VP,I,J,DY)-.667*UPX(I,J))              1417 397
      DVPDT(I,J) = -YM1-YM2+(-YM3+YM4+YM5+YM6)/ROAROP                   1417 398
  510 CONTINUE                                                          1417 399
  512 CONTINUE                                                          1417 400
      DO 516 I=MIL,MIR                                                  1417 401
```

```
      DO 515 J=MJW,MJF                                                  1417 402
C CALCULATE NEW PERTURBATION VALUES                                     1417 403
      UP(I,J) = UP(I,J) + DUPDT(I,J)*DT                                 1417 404
      VP(I,J) = VP(I,J) + DVPDT(I,J)*DT                                 1417 405
C AUXILIARY EQUATIONS                                                   1417 406
      PP(I,J) = GAMMA2*RHO(I,J)*(HTP(I,J)-(UP(I,J)**2+VP(I,J)**2)/2.    1417 407
     1-U(I,J)*UP(I,J)) + P*RHOP(I,J)/RHO(I,J)                           1417 408
      TP(I,J) = (HTP(I,J)-U(I,J)*UP(I,J))/CP                            1417 409
      XMUP(I,J) = TP(I,J)*XMU(I,J)*((.5*T(I,J)+316.)/(T(I,J)*(T(I,J)+   1417 410
     1216.)))                                                           1417 411
  515 CONTINUE                                                          1417 412
  516 CONTINUE                                                          1417 413
C*****************************************************************    1417 414
C PRINT OUT THE RESULTS OF EACH INTERATION                              1417 415
      MP=1                                                              1417 416
      IF(KT2) 700,570,700                                               1417 417
  520 CONTINUE                                                          1417 418
      IF(KT1) 1422,523,1422                                             1417 419
C*****************************************************************    1417 420
  523 CONTINUE                                                          1417 421
      MP=2                                                              1417 422
      WRITE(6,31)                                                       1417 423
      WRITE(0,8) ITER                                                   1417 424
      READ(0,9) KARR(3)                                                 1417 425
CALCULATE THE EXPONENTIAL DECAY OF ALL PROFILES.                        1417 426
      DO 530 I=MIL,MIR                                                  1417 427
      DO 530 J=MJW14,MJF                                                1417 428
      ARG = ALPHA*(Y(J)-Y(MJW14))                                       1417 429
      EX = EXP(-ARG)                                                    1417 430
      UP(I,J) = UP(I,MJW14)*EX                                          1417 431
      VP(I,J) = VP(I,MJW14)*EX                                          1417 432
      PP(I,J) = PP(I,MJW14)*EX                                          1417 433
      HTP(I,J) = HTP(I,MJW14)*EX                                        1417 434
      TP(I,J) = TP(I,MJW14)*EX                                          1417 435
      XMUP(I,J) = XMUP(I,MJW14)*EX                                      1417 436
  530 CONTINUE                                                          1417 437
CALCULATE THE AVERAGES OF ALL PROFILES.                                 1417 438
      DO 542 I=MIL,MIR                                                  1417 439
      DO 540 J=MJW,MJF                                                  1417 440
      RHOPA(I,J) = AVE(RHOP,I,J)                                        1417 441
      HTPA(I,J) = AVE(HTP,I,J)                                          1417 442
      UPA(I,J) = AVE(UP,I,J)                                            1417 443
      VPA(I,J) = AVE(VP,I,J)                                            1417 444
      PPA(I,J) = AVE(PP,I,J)                                            1417 445
      TPA(I,J) = AVE(TP,I,J)                                            1417 446
      XMUPA(I,J) = AVE(XMUP,I,J)                                        1417 447
  540 CONTINUE                                                          1417 448
      RHOPA(I,MJW1) = .5*(RHOP(I,MJW1)+RHOP(I,MJW))                     1417 449
      PPA(I,MJW1) = .5*(PP(I,MJW1)+PP(I,MJW))                           1417 450
  542 CONTINUE                                                          1417 451
CALCULATE THE UP RESULTANT PROFILE AND FIND THE MAXIMUM.                1417 452
      TRY=0.                                                            1417 453
      DO 550 J=MJW1,MJF                                                 1417 454
      UPSQ(J) =UPA(MIL,J)**2 +UPA(MIR,J)**2                             1417 455
```

```
      UPSQRT(J) = SQRT(UPSQ(J))                                          1417 456
      TRY=AMAX1(UPSQRT(J),TRY)                                           1417 457
  550 CONTINUE                                                           1417 458
C SUBSTITUTE THE SMOOTHED PROFILE DIVIDED BY UP RES. MAX.                1417 459
      IPP2 = IPP2+1                                                      1417 460
      UMAX(IPP2) = TRY                                                   1417 461
      PTIME2(IPP2) = TIME                                                1417 462
      SC(IPP2) = SCALE                                                   1417 463
      ISTOP=IPP2                                                         1417 464
      DO 587 I=MIL,MIR                                                   1417 465
      DO 587 J=MJW1,MJF,KRD                                              1417 466
      RHOP(I,J) = RHOPA(I,J)/TRY                                         1417 467
      HTP(I,J) = HTPA(I,J)/TRY                                           1417 468
      UP(I,J) = UPA(I,J)/TRY                                             1417 469
      VP(I,J) = VPA(I,J)/TRY                                             1417 470
      PP(I,J) = PPA(I,J)/TRY                                             1417 471
      TP(I,J) = TPA(I,J)/TRY                                             1417 472
      XMUP(I,J) = XMUPA(I,J)/TRY                                         1417 473
      IG=1                                                               1417 474
      GO TO (590,592),IG                                                 1417 475
  590 CONTINUE                                                           1417 476
      UPLT(J) = UP(I,J)                                                  1417 477
      GO TO 594                                                          1417 478
  592 CONTINUE                                                           1417 479
      UPRT(J) = UP(I,J)                                                  1417 480
  594 CONTINUE                                                           1417 481
  587 CONTINUE                                                           1417 482
C*************************************************************************1417 483
  588 CONTINUE                                                           1417 484
C*****PREPARE TALLY PLOT.*****                                           1417 485
      WRITE(0,8) ITER                                                    1417 486
      READ(0,9) KARR(3)                                                  1417 487
      NPLOT = MJF                                                        1417 488
      CALL PLTRTN(1)                                                     1417 489
      WRITE(6,29) TRY                                                    1417 490
  581 CONTINUE                                                           1417 491
C*************************************************************************1417 492
C*************************************************************************1417 493
  570 CONTINUE                                                           1417 494
  518 CONTINUE                                                           1417 495
      SUM=0.                                                             1417 496
      DO 600 J=MJW1,MJK                                                  1417 497
      UPSQ(J) = UP(MIL,J)**2 + UP(MIR,J)**2                              1417 498
      PPSQ(J) = PP(MIL,J)**2 + PP(MIR,J)**2                              1417 499
      VPSQ(J) = VP(MIL,J)**2 + VP(MIR,J)**2                              1417 500
      UPSQRT(J) = SQRT(UPSQ(J))                                          1417 501
C CALCULATE THE ACOUSTICAL ENERGY DENSITY.                               1417 502
      WP(J) = RHO(I,J)*(UPSQ(J)+VPSQ(J))/2. + .2786*PPSQ(J)/P            1417 503
      SUM=SUM+WP(J)                                                      1417 504
  600 CONTINUE                                                           1417 505
      SUM1 = 0.                                                          1417 506
      DO 619 J=MJKK,MJF,KRD                                              1417 507
      UPSQ(J) = UP(MIL,J)**2 + UP(MIR,J)**2                              1417 508
      PPSQ(J) = PP(MIL,J)**2 + PP(MIR,J)**2                              1417 509
```

```
      VPSQ(J) = VP(MIL,J)**2 + VP(MIR,J)**2                              1417 510
      UPSQRT(J) = SQRT(UPSQ(J))                                          1417 511
C CALCULATE THE ACOUSTICAL ENERGY DENSITY.                               1417 512
      WP(J) = RHO(I,J)*(UPSQ(J)+VPSQ(J))/2. + .2786*PPSQ(J)/P            1417 513
      SUM1= SUM1+ WP(J)                                                  1417 514
  619 CONTINUE                                                           1417 515
      WRITE (6,32) ITER,TIME,(X(I),I=MIL,MIR)                            1417 516
      WRITE(6,33) (Y(J),(UP(I,J),VP(I,J),RHOP(I,J),PP(I,J),HTP(I,J),I=MI1417 517
     1L,MIR),UPSQRT(J),WP(J),J=MJW1,MJK)                                 1417 518
      WRITE(6,33) (Y(J),(UP(I,J),VP(I,J),RHOP(I,J),PP(I,J),HTP(I,J),I=   1417 519
     1MIL,MIR),UPSQRT(J),WP(J),J=MJKK,MJF)                               1417 520
      WRITE(6,55) Y(MJW1),Y(MJK),SUM                                     1417 521
      WRITE(6,55)Y(MJKK),Y(MJF),SUM1                                     1417 522
      GO TO (520,700),MP                                                 1417 523
C*************************************************************************1417 524
  700 CONTINUE                                                           1417 525
 1422 CONTINUE                                                           1417 526
      IF(KT1.EQ.(LDECAY-1)) GO TO 710                                    1417 527
      GO TO 720                                                          1417 528
  710 CONTINUE                                                           1417 529
      TRY1 = 0                                                           1417 530
      DO 715 J=MJW1,MJK                                                  1417 531
      UPSQ(J) = UP(MIL,J)**2 + UP(MIR,J)**2                              1417 532
      UPSQRT(J) = SQRT(UPSQ(J))                                          1417 533
      TRY1 = AMAX1(UPSQRT(J),TRY1)                                       1417 534
  715 CONTINUE                                                           1417 535
      SCALE = SCALE*TRY1                                                 1417 536
      WRITE(6,28) SCALE                                                  1417 537
  720 CONTINUE                                                           1417 538
      I=MIL                                                              1417 539
      TEST1=UP(MIL,MJW1+2)                                               1417 540
      TEST2=U(MIL,MJ8)                                                   1417 541
      IF(ABS(TEST1)-ABS(TEST2)) 735,733,733                              1417 542
  733 CONTINUE                                                           1417 543
      WRITE(6,30)                                                        1417 544
      GO TO 900                                                          1417 545
  735 CONTINUE                                                           1417 546
C*************************************************************************1417 547
      IF(ITER/25.EQ.KK) GO TO 800                                        1417 548
      IF(ITER-NIT) 400,800,800                                           1417 549
  800 CONTINUE                                                           1417 550
      GO TO (840,841),KSAVE                                              1417 551
  840 CONTINUE                                                           1417 552
C STORE THE RESULTS ON TAPE.                                             1417 553
      KK=KK+1                                                            1417 554
      REWIND NTAPE                                                       1417 555
      NL=NYP2                                                            1417 556
      WRITE TAPE NTAPE,ITER,NL,TIME, ((UP(I,J),VP(I,J),RHOP(I,J),PP(I,J)1417 557
     1HTP(I,J),XMUP(I,J),TP(I,J),DHPDT(I,J),DRPDT(I,J),DUPDT(I,J),       1417 558
     2DVPDT(I,J), J=1,NYP2),I=MIL,MIR)                                   1417 559
  841 CONTINUE                                                           1417 560
      IF(ITER-NIT) 400,860,860                                           1417 561
  860 CONTINUE                                                           1417 562
      CALL PLTRTN(2)                                                     1417 563
```

```
      WRITE(6,17) (PTIME2(KI),SC(KI),UMAX(KI), KI=1,ISTOP)                1417 564
      GO TO (870,872),KSAVE                                               1417 565
  870 CONTINUE                                                            1417 566
      CALL UNLOWD(NTAPE)                                                  1417 567
      WRITE(6,12)NTAPE                                                    1417 568
  872 CONTINUE                                                            1417 569
  900 CONTINUE                                                            1417 570
      GO TO (100,999),KPRINT                                              1417 571
  999 CONTINUE                                                            1417 572
      CALL PLTRTN(3)                                                      1417 573
      WRITE (6,69)                                                        1417 574
C*************************************************************************1417 575
    8 FORMAT(10I6)                                                        1417 576
    9 FORMAT(12A6)                                                        1417 577
   10 FORMAT(8F10.0)                                                      1417 578
   11 FORMAT(16I5)                                                        1417 579
   12 FORMAT(1H0//25X,36HTHE ABOVE CASE IS STORED ON TAPE NO.,I2)         1417 580
   13 FORMAT(4E20.6)                                                      1417 581
   17 FORMAT(1H1,5X,4HTIME,3X,12HSCALE FACTOR,8X,4HUMAX/(1H ,3E12.4))     1417 582
   28 FORMAT(1H ,14HSCALE FACTOR =,E10.4)                                 1417 583
   29 FORMAT(1H0,15X,18HUP RESULTANT MAX =,E12.4)                         1417 584
   30 FORMAT(1H0///1H0,17HCASE IS UNSTABLE.)                              1417 585
   31 FORMAT(1H0,25X,31HAFTER RE-INITIALIZING PROFILES.)                  1417 586
   32 FORMAT(1H,10X,13HITERATION NO.,I4,5X,6HTIME =F6.4/13X,3HX =F4.0,511417 587
     1X,3HX =F4.0,31X,9HRESULTANT,5X,6HENERGY/1H ,2X,1HY,7X,2HUP,8X,2HVP1417 588
     2,8X,3HRHP,7X,2HPP,8X,2HHP,9X,2HUP,8X,2HVP,8X,3HRHP,7X,2HPP,8X,2HHP1417 589
     3,11X,2HUP,8X,2HWP)                                                1417 590
   33 FORMAT(1H ,F4.1,1X,5E10.4,1X,5E10.4,3X,2E10.4)                      1417 591
   34 FORMAT(1H0,11HMASS FLOW =,E12.4)                                    1417 592
   35 FORMAT(1H0,20X,9HRESULTANT/(10E12.4))                               1417 593
   36 FORMAT(1H ,F4.1,E10.4,10X,E10.4,12X,E10.4,10X,E10.4,18X,E10.4,3X, 1417 594
     1E10.4)                                                            1417 595
   40 FORMAT(1H0,13HITERATION NO.I4,5X,6HTIME =F5.4)                      1417 596
   41 FORMAT(1H0,35X,16HPRIMITIVE VALUES/1H ,25X,3HX =F4.0,40X,3HX =F4.01417 597
     1/1H ,2X,1HY,9X,4HRHOP,8X,3HHTP,9X,2HPP,15X,4HRHOP,8X,3HHTP,9X,2HPP1417 598
     2,8X,1HY)                                                          1417 599
   42 FORMAT(1H ,F4.1,3X,3E12.4,5X,3E12.4,2X,F4.1)                        1417 600
   43 FORMAT(8E10.5)                                                      1417 601
   44 FORMAT(1H, 8HUPINTL =F4.1/1H ,10HRHOPINTL =F4.1/1H ,9HHTPINTL =F4.1417 602
     11)                                                                1417 603
   45 FORMAT(1H0,35X,16HPRIMITIVE VALUES/1H ,25X,3HX =F4.0,40X,3HX =F4.01417 604
     1/1H ,2X,1HY,9X,2HUP,10X,2HVP,10X,2HPP,15X,2HUP,10X,2HVP,10X,2HPP,81417 605
     2X,1HY)                                                            1417 606
   46 FORMAT(1H0//35X,15HAVERAGED VALUES/1H ,25X,3HX =F4.0,50X,3HX =F4.01417 607
     1/1H ,2X,1HY,5X,2HUP,8X,2HVP,8X,4HRHOP,6X,3HHTP,7X,2HPP,10X,2HUP,8X1417 608
     2,2HVP,8X,4HRHOP,6X,3HHTP,7X,2HPP,7X,1HY)                          1417 609
   47 FORMAT(1H ,F4.1,5E10.4,2X,5E10.4,F4.1)                              1417 610
   48 FORMAT(1H0,10X,13HITERATION NO.I3,5X,6HTIME =F6.4/13X,3HX =F4.0,341417 611
     1X,3HX =F4.0,36X,9HRESULTANT,5X,6HENERGY/1H ,2X,1HY,7X,2HUP,8X,  1417 612
     23HUPA,7X,2HVP,8X,3HVPA,9X,2HUP,8X,3HUPA,7X,2HVP,8X,3HVPA,       1417 613
     3    13X,2HUP,12X,2HWP)                                            1417 614
   49 FORMAT(1H ,F4.1,4E10.4,2X,4E10.4,8X,E10.4,3X,E10.4)                 1417 615
   50 FORMAT(1H1,49X,31HBOUNDARY LAYER TRANSITION STUDY/////1H0,47HINITI1417 616
     1AL STEADY-STATE FIELD CONSTANTS AND INPUTS,19H AT THE FREE STREAM/1417 617
```

```
     2/)                                                                    1417 618
  52 FORMAT(1H ,10HDENSITY  =E10.3/1H ,15HREYNOLDS NO.  =E10.3/1H ,14HT1417 619
    1EMPERATURE  =F5.1/1H ,11HPRESSURE  =E10.3/1H ,12HVISCOSITY  =E10.31417 620
    2/1H ,13HWAVELENGTH  =F7.2/1H ,8HALPHA  =F10.3/1H ,5HDX  =F6.1/1H ,1417 621
    35HDY  = F4.1/1H ,5HDT  =F10.2/1H ,13HPRANDTL NO. =F4.2////)        1417 622
  53 FORMAT(1H0////(2X,12A6))                                           1417 623
  54 FORMAT(1H ,6HTIME =F10.8,6X,13HITERATION NO.I3/1H ,10X,3HY =,      1417 624
    1F5.2,11(F10.2)                                                     1417 625
  55 FORMAT(1H0,15X,18HSUM OF WP FROM Y =,F4.0,7H TO Y =,F4.0,3X,E10.4)1417 626
  56 FORMAT (1H0,3HX =,   12F10.2)                                      1417 627
  57 FORMAT(1H0,45X,21HSTEADY STATE PROFILES/1H0,25X,3HX =F4.1,48X,3HX  1417 628
    1=F4.1 1H ,1X,1HY,5X,1HU,9X,2HHT,10X,1HT,8X,3HRHO,8X,3HXMU,12X,1HU,1417 629
    29X,2HHT,10X,1HT,8X,3HRHO,8X,3HXMU,5X,1HY)                          1417 630
  58 FORMAT(1H ,F4.1,1X,5F10.4,8X,5E10.4,F5.1)                          1417 631
  59 FORMAT(I5,F10.5/(6E12.4))                                          1417 632
  60 FORMAT(1H0,2F4.0,9E10.4/(11E10.4))                                 1417 633
  61 FORMAT(1H0,25X,22HSTEADY STATE T PROFILE/(1H ,10E12.4))            1417 634
  62 FORMAT(1H0,25X,24HSTEADY STATE RHO PROFILE/(1H ,10E12.4))          1417 635
  63 FORMAT (1H ,2I4,6F13.4)                                            1417 636
  64 FORMAT(1H0,25X,24HSTEADY STATE XMU PROFILE/(1H ,10E12.4))          1417 637
  65 FORMAT(1H0///1H0,13HITERATION NO.I4,5X,6HTIME =F5.4)               1417 638
  67 FORMAT(1H0,15X,78HSQUARE ROOT OF THE SUM OF THE SQUARES OF THE AVE1417 639
    1RAGED VELOCITIES AT EACH LAYER//1H ,7X,3HY =,10F10.4/1H ,9X,2HUP) 1417 640
  68 FORMAT(1H ,E10.4,8X,I3,10X,E10.4,11X,E10.4,13X,E10.4)              1417 641
  69 FORMAT (1H1,22H1107 PRINTOUT COMPLETE)                             1417 642
  70 FORMAT(1H0,28HRESULTANT AND ENERGY DENSITY/1H ,2X,1HY,8X,3HUPA,7X,1417 643
    12HWP)                                                              1417 644
  75 FORMAT(1H1)                                                        1417 645
  78 FORMAT(1H ,F4.1,2X,2E10.4)                                         1417 646
  99 FORMAT(1X///1H0,40HTOTAL TIME ELAPSED FOR ALL ITERATIONS = ,2A6)   1417 647
     END                                                                1417 648
- XQT CUR                                                               1417 649
  TRW F                                                                 1417 650
  OUT F                                                                 1417 651
  TEF F                                                                 1417 652
  TRI F                                                                 1417 653
- XQT BLSTAB                                                            1417 654
SUBSONIC CASE RX-1.  INPUT TP.4062. (R-17).
REYN. NO. 16,000.  MACH .4
DECAY EVERY 25.

    2   56 2000   75    2     3   21   50    1    1   25   20   21    1    1    2
.001      92.0      1.0       2.016     1.0      .7       400.      1.
.00       53.11     105.9     157.5     206.7    251.9    291.6     324.6
350.4     369.3     382.2     390.3     395.1    397.7    399.0     399.6
399.8     399.9     400.0     400.0     400.0
.2498 E+07 .25  E+07 .2504E+07 .2511E+07 .2520E+07.2530 E+07 .2541E+07 .2551E+07
 .256 E+07 .2567E+07 .2572E+07 .2575E+07 .2577E+07 .2578E+07 .2578E+07 .2578E+07
 .2578E+07 .2578E+07 .2578E+07 .2578E+07 .2578E+07
```

000677

REFERENCES

1. Reynolds, O., Phil. Trans. Roy. Soc. (1883) or Collected Papers, II, 51.

2. Tollmien, W., "Asymptotische Integration der Störungsdifferentialgleichung ebener laminarer Strömungen bei höhen Reynoldsschen Zählen," ZMM, 25/27, 33, 1947.

3. Schubauer, G.B., and H.K. Skramstad, "Laminar Boundary Layer Oscillations and Stability of Laminar Flow," Journal of Aeronautical Sciences, Vol. 14, No. 7, p. 69, 1947.

4. Low, G.M., "Boundary Layer Transition at Supersonic Speeds," NACA RM E56E10, August 1956.

5. Moeckel, W.E., "Some Effects of Bluntness on Boundary Layer Transition and Heat Transfer at Supersonic Speeds," NACA Report 1312, 1957.

6. Brinich, P.F., "Effect of Leading-Edge Geometry on Boundary-Layer Transition at Mach 3.1," NACA TN 3659, March 1956.

7. Brinich, P.F., "A Study of Boundary-Layer Transition and Surface Temperature Distributions at Mach 3.12," NACA TN 3509, July 1955.

8. Brinich, P.F., "Boundary-Layer Transition at Mach 3.12 With and Without Single Roughness Elements," NACA TN 3267, December 1954.

9. Brinich, P.F., "Boundary-Layer Transition on an Open-Nose Cone at Mach 3.1," NACA TN 4212, February 1958.

10. Brinich, P.F., and N. Sands, "Effect of Bluntness on Transition for a Cone and a Hollow Cylinder at Mach 3.1," NACA TN 3979, May 1957.

11. Rogers, R., "Boundary-Layer Development in Supersonic Shear Flow," AGARD Report No. 269, April 1960.

12. James, C.S., "Boundary-Layer Transition on Hollow Cylinders in Supersonic Free Flight as Affected by Mach Number and a Screw Thread Type of Surface Roughness," NASA Memorandum 1-20-59A, February 1959.

13. Potter, J.L., and J.D. Whitfield, "The Relation Between Wall Temperature and the Effect of Roughness on Boundary-Layer Transition," Journal of the Aerospace Sciences, Vol. 29, No. 8, August 1961.

14. Potter, J.L., and J. D. Whitfield," Boundary-Layer Transition Under Hypersonic Conditions," No publication date.

15. Deem, R.E., C.R. Erickson, and J.S. Murphy, "Flat-Plate Boundary-Layer Transition at Hypersonic Speeds," Technical Documentary Report FDL-TDR-64-129, October 1964.

16. Korkegi, R.H., "Transition Studies and Skin Friction Measurements on an Insulated Flat Plate at a Hypersonic Mach Number," California Institute of Technology, GALCIT Hypersonic Wind Tunnel Memo No. 17, July 1954.

17. Schlichting, H. Dr., "Boundary Layer Theory," Pergamon Press, New York, London, Paris, 1955.

18. Stuart, J.T., "On the Effects of the Reynolds Stress on Hydrodynamic Stability," Z. angew. Math. Mech. Sonderheft, 532-38, 1956.

19. DeSanto, D.F., and H.B. Keller, "Numerical Studies of Transition from Laminar to Turbulent Flow over a Flat Plate," J. Soc. Indust. Appl. Math. Vol. 10, No. 4, December 1962.

20. Reshotko, E., "Stability of the Compressible Laminar Boundary Layer," GALCIT Memorandum No. 52, January 1960.

21. Brown, W.B., "Exact Numerical Solution of the Complete Linearized Equations for the Stability of Compressible Boundary Layers," Northrop Corporation, Norair Division, Report No. NOR-6215 (BLC-137), January 1962.

22. Dunn, D. W., and C. C. Lin, "On the Stability of the Laminar Boundary Layer in Compressible Fluids," Journal of the Aeronautical Sciences, Vol. 22 (1955), p. 455.

23. Mack, L. M., "Numerical Calculation of the Stability of the Compressible Laminar Boundary Layer," J.P.L. Report No. 20-122, May 1960.

24. Mack, L. M., "The Stability of the Compressible Laminar Boundary Layer According to a Direct Numerical Solution," Space Programs Summary, No. 37-16, Vol. IV, J.P.L., August 1962.

25. Mack, L.M., "The Stability of the Compressible Laminar Boundary Layer According to a Direct Numerical Solution," AGARD Specialists Meeting, Naples, Italy, May 10-14, 1965.

26. Jaeck, C., and W. Jackson, " Non-Similar Boundary Layer — Real Gas Computer Program (Deck AS 1188)," Boeing Document D2-81296, August 1964.

27. Lin, C.C., "Theory of Hydrodynamic Stability," Cambridge University Press, 1955.

28. Pretsch, J., "Die Stäbilitat der Laminarströmung bei Drückgefälle und Drückansteig," Forschungbereicht Nr. 1343, Deutsche Luftfahftforchung Göttengen, 1941.

29. Performance and Aerothermodynamics Organization," Aerodynamics and Aerothermodynamics," Boeing Document D2-23951-1, October 1964 to March 1965.

30. Tani, I., and H. Komoda, "Boundary-Layer Transition in the Presence of Streamwise Vortices," Journal of the Aerospace Sciences, Vol. 29, No. 4, April 1962.

31. Moore, F.K., (Editor), "Theory of Laminar Flows," Princeton University Press, Vol. IV, High-Speed Aerodynamics and Jet Propulsion, 1964.

32. Schlichting, H., Dr., "Boundary Layer Theory," Pergamon Press, New York, London, Paris, 1950.

33. Lees, L., "The Stability of the Laminar Boundary Layer in a Compressible Fluid," NACA Report 876, 1947.

34. Lees, L., and E. Reshotko, "Stability of the Compressible Laminar Boundary Layer," J. Fluid Mech. 12, 550-590, 1962.

35. "Test Facilities Handbook," Arnold Engineering Development Center.

36. Matthews, R.K., and L.L. Trimmer, " Operating Conditions and Flow Parameters for the VKF Hypersonic Wind Tunnel," VKF/LR-HS-28, September 2, 1965.

37. "Repair of Wind Tunnel Test Model," AF33(615)-3182, July 1, 1965.

38. Liepmann, H.W., and A. Roshko, "Elements of Gasdynamics."

39. Nagel, A. L., H. D. Fitzsimmons, and L. B. Doyle, "Analysis of Hypersonic Pressure and Heat-Transfer Tests on Delta Wings with Laminar and Turbulent Boundary Layers," NASA Contractor Report CR-535, 1966.

40. Morkovin, M. V., "On Transition Experiments at Moderate Supersonic Speeds," Journal of the Aeronautical Sciences, Vol. 24, pp. 480-486 (1957).

41. Coles, Donald, "Measurements of Turbulent Friction on a Smooth Flat Plate in Supersonic Flow," Journal of the Aeronautical Sciences, Vol. 21, pp. 433-448 (1954).

42. Van Driest, E. R. and W. D. McCauley, "Boundary-Layer Transition on a 10-Degree Cone at Mach Number 2.81 as Affected by Extreme Cooling," Journal of Aeronautical Sciences, April (1960).

43. Sanator, R. J., J. P. De Carlo, and D. T. Torrillo, "Hypersonic Boundary-Layer Transition for a Cold-Wall Slender Cone," AIAA Journal, Vol. 3, No. 4, p. 1758 (1965).

44. Emmons, H. W., and A. E. Bryson, "The Laminar-Turbulent Transition in a Boundary Layer," Proceedings of the First U.S. National Congress of Theoretical and Applied Mechanics, June 11-16, 1951, American Society of Mechanical Engineers, New York, N.Y., 1952.

45. Waldbusser, E., "Relationship of Laminar Wake Width to Wake Transition Distance," AIAA Journal, Vol. 3, No. 10, p. 1965 (1965)

46. Goldburg, A., "A Hypersonic Wake Transition Map," AIAA Journal, Vol. 3, No. 11, p. 2170 (1965).

UNCLASSIFIED
Security Classification

DOCUMENT CONTROL DATA - R&D

(Security classification of title, body of abstract and indexing annotation must be entered when the overall report is classified)

1 ORIGINATING ACTIVITY (Corporate author)
The Boeing Company
Seattle, Washington

2a REPORT SECURITY CLASSIFICATION
Unclassified

2b GROUP

3 REPORT TITLE
Investigation of Boundary Layer Transition in Hypersonic Flow at Angle of Attack

4 DESCRIPTIVE NOTES (type of report and inclusive dates)
Final Report 7/64 - 8/66

5 AUTHOR(S) (Last name, first name, initial)
Nagel, A. L.
Savage, R. T. Wanner, R.

6 REPORT DATE	7a TOTAL NO. OF PAGES	7b NO. OF REFS
June 1966	190	46

8a CONTRACT OR GRANT NO.	9a ORIGINATOR'S REPORT NUMBER(S)
AF 33(615)-2011	D2-113089-1
b PROJECT NO. 1366	
c Tasks: 136606 and 136615	9b OTHER REPORT NO(S) (Any other numbers that may be assigned this report)
d	AFFDL-TR-66-122

10 AVAILABILITY/LIMITATION NOTICES
This document is subject to special export controls, and each transmittal to foreign governments or foreign nationals may be made only with prior approval of the AF Flight Dynamics Laboratory (FDMG).

11 SUPPLEMENTARY NOTES	12 SPONSORING MILITARY ACTIVITY
	AF Flight Dynamics Laboratory Research & Technology Division Wright-Patterson AFB, Ohio

13 ABSTRACT

An analytical and experimental investigation has been made of boundary layer transition at angle of attack in hypersonic flow. A new method of calculating laminar flow stability has been developed that is more general than previous methods. The method employs the timewise integration of perturbation equations derived from the complete Navier-Stokes equations for two-dimensional flow of a compressible fluid with variable transport properties. The present calculations are for perturbations about a known steady flow. The perturbations are assumed to be sinusoidal in the streamwise direction, but no restriction is known that would prevent the streamwise wave form from being arbitrary, as are the vertical distributions and the time variations. The sinusoidal wave assumption greatly reduces the amount of computer time required and simplifies the interpretation of the results. Nonlinear terms are easily retained with the present method, but nonlinear calculations are not physically correct when perturbations are required to be sinusoidal. For this reason, nonlinear terms were deleted for all calculations presented.

The experimental program was conducted in Arnold Center tunnels B and C at Mach numbers of 6, 8, and 10. The models included blunt and sharp flat plates and a 75-degree swept delta wing with sharp leading edges. The results are somewhat questionable due to probe interferences and leakages that are now known to have occurred during the tests. However, the results are self-consistent (continued)

DD FORM 1 JAN 64 1473
U3 4802 1030 REV. 4/65
PART 1 OF 2

UNCLASSIFIED
Security Classification

13 Abstract (continued)

and consistent with the results of previous investigations. Natural transition data for the sharp flat plate at angles of attack up to 15 degrees agree with previous results for zero angle of attack when compared on the basis of local flow properties. Transition Reynolds numbers on the sharp flat plate were found to increase as the 0.4 power of the unit Reynolds number, but the effect on the sharp delta wing centerline data was much smaller. The independence of this effect of angle of attack, and the dependence on the model geometry suggest that the unit Reynolds number trend is not produced by model or wind tunnel disturbances, but is an authentic fluid mechanical effect that will occur in free flight as well. However, no explanation of the unit Reynolds number effect was found in the analytic studies.

When corrected to a common unit Reynolds number, the transition Reynolds number was found to increase exponentially with Mach number, for Mach numbers from 4 to 10.

Attempts were made to trip the boundary layer by mass injection to verify the analytic prediction that the boundary layer could not be tripped below a certain critical Reynolds number. These attempts were successful to the extent that tripping did not occur below, nor even near the calculated critical Reynolds numbers. However, other tripping techniques should be investigated before any conclusions are formed.

14 KEY WORDS	LINK A		LINK B		LINK C	
	ROLE	WT	ROLE	WT	ROLE	WT
Boundary Layer Transition Hypersonic Flow Reference Reynolds Number Unit Reynolds Number Boundary Layer Stability Pilot Probe Techniques						

INSTRUCTIONS

1. ORIGINATING ACTIVITY: Enter the name and address of the contractor, subcontractor, grantee, Department of Defense activity or other organization (corporate author) issuing the report.

2a. REPORT SECURITY CLASSIFICATION: Enter the overall security classification of the report. Indicate whether "Restricted Data" is included. Marking is to be in accordance with appropriate security regulations.

2b. GROUP: Automatic downgrading is specified in DoD Directive 5200.10 and Armed Forces Industrial Manual. Enter the group number. Also, when applicable, show that optional markings have been used for Group 3 and Group 4 as authorized.

3. REPORT TITLE: Enter the complete report title in all capital letters. Titles in all cases should be unclassified. If a meaningful title cannot be selected without classification, show title classification in all capitals in parenthesis immediately following the title.

4. DESCRIPTIVE NOTES: If appropriate, enter the type of report, e.g., interim, progress, summary, annual, or final. Give the inclusive dates when a specific reporting period is covered.

5. AUTHOR(S): Enter the name(s) of author(s) as shown on or in the report. Enter last name, first name, middle initial. If military, show rank and branch of service. The name of the principal author is an absolute minimum requirement.

6. REPORT DATE: Enter the date of the report as day, month, year, or month, year. If more than one date appears on the report, use date of publication.

7. TOTAL NUMBER OF PAGES: The total page count should follow normal pagination procedures, i.e., enter the number of pages containing information.

7b. NUMBER OF REFERENCES: Enter the total number of references cited in the report.

8a. CONTRACT OR GRANT NUMBER: If appropriate, enter the applicable number of the contract or grant under which the report was written.

8b, 8c, & 8d. PROJECT NUMBER: Enter the appropriate military department identification, such as project number, subproject number, system numbers, task number, etc.

9a. ORIGINATOR'S REPORT NUMBER(S): Enter the official report number by which the document will be identified and controlled by the originating activity. This number must be unique to this report.

9b. OTHER REPORT NUMBER(S): If the report has been assigned any other report numbers (either by the originator or by the sponsor), also enter this number(s).

10. AVAILABILITY/LIMITATION NOTICES: Enter any limitations on further dissemination of the report, other than those imposed by security classification, using standard statements such as:

(1) "Qualified requesters may obtain copies of this report from DDC."

(2) "Foreign announcement and dissemination of this report by DDC is not authorized."

(3) "U.S. Government agencies may obtain copies of this report directly from DDC. Other qualified DDC users shall request through _____."

(4) "U.S. military agencies may obtain copies of this report directly from DDC. Other qualified users shall request through _____."

(5) "All distribution of this report is controlled. Qualified DDC users shall request through _____."

If the report has been furnished to the Office of Technical Services, Department of Commerce, for sale to the public, indicate this fact and enter the price, if known.

11. SUPPLEMENTARY NOTES: Use for additional explanatory notes.

12. SPONSORING MILITARY ACTIVITY: Enter the name of the departmental project office or laboratory sponsoring (paying for) the research and development. Include address.

13. ABSTRACT: Enter an abstract giving a brief and factual summary of the document indicative of the report, even though it may also appear elsewhere in the body of the technical report. If additional space is required, a continuation sheet shall be attached.

It is highly desirable that the abstract of classified reports be unclassified. Each paragraph of the abstract shall end with an indication of the military security classification of the information in the paragraph, represented as (TS), (S), (C), or (U).

There is no limitation on the length of the abstract. However, the suggested length is from 150 to 225 words.

14. KEY WORDS: Key words are technically meaningful terms or short phrases that characterize a report and may be used as index entries for cataloging the report. Key words must be selected so that no security classification is required. Identifiers, such as equipment model designation, trade name, military project code name, geographic location, may be used as key words but will be followed by an indication of technical context. The assignment of links, roles, and weights is optional.